Investigating interactions between influenza A virus and respiratory syncytial virus during coinfection

Joanne Haney

Submitted in fulfilment for the degree of Doctor of Philosophy in Virology

MRC-University of Glasgow Centre for Virus Research

Institute of Infection Immunity and Inflammation

College of Medical, Veterinary and Life Sciences

Oilthigh Ghlaschu – University of Glasgow

December 2021

Abstract

Respiratory viruses are the cause of significant disease burden and coinfections with more than one virus constitute between 10-30% of viral respiratory infections. Interactions among respiratory viruses are recognised for their importance in influencing viral dynamics, however direct virus-virus interactions are poorly understood. Influenza A virus (IAV) and respiratory syncytial virus (RSV) are important respiratory pathogens that share epidemiological characteristics, including timing of seasonal peaks of infections, and biological characteristics, including cellular tropism within the respiratory tract.

To characterise interactions between IAV and RSV during coinfection, we developed an *in vitro* model in A549 cells, a cell line derived from the human lung. Analysis of viral growth kinetics and viral dynamics by live cell imaging showed that, while IAV replication appears unaffected by coinfection with RSV, RSV replication is significantly decreased in coinfection. Imaging of coinfected cells stained for IAV and RSV nucleoproteins and glycoproteins show that they localise to the same regions of the plasma membrane, suggesting there may be opportunity for viral interactions during viral assembly. To further explore this hypothesis, virus particles budding from coinfected cells were examined using super-resolution confocal microscopy. Filamentous structures extended from coinfected cells, that incorporated glycoproteins from both viruses in distinct patches along the filament. The ultra-structure of these filaments, determined by cryo-electron tomography, revealed the formation of chimeric viral particles (CVPs) that contained genomes and structural features from both IAV and RSV. Additionally, coinfection by IAV and RSV generated pseudotyped RSV filaments that incorporate IAV glycoproteins. Functional assays using a sialidase showed that CVPs can facilitate entry of IAV into cells that were stripped of IAV entry receptors, demonstrating CVPs possess expanded receptor tropism.

To determine the likelihood for CVP formation in the airway epithelium, we coinfected primary differentiated human bronchial epithelial cell (hBEC) cultures at air-liquid interface. We observed that IAV and RSV infect ciliated epithelial cells and identified foci of coinfection. IAV and RSV proteins both localised at the apical surface of coinfected cells, providing opportunity for interactions to occur during viral assembly. Additionally, IAV and RSV replication kinetics and cytopathic effect in

hBEC cultures reflected trends observed in the *in vitro* cell model, suggesting that viral interactions may be conserved between simplified and representative airway models.

Overall, this project characterises interactions between IAV and RSV during coinfection and we show that coinfection by IAV and RSV results in formation of a novel class of viral particles. By expanding viral tropism, formation of CVPs may alter viral dissemination within the respiratory tract, potentially impacting disease outcomes for a coinfected individual. Further, by defining a previously unknown source of viral interaction with implications on viral structure, we contribute more widely to the understanding of the properties of IAV and RSV, and their infection biology as a whole.

Table of Contents

List of Abbreviations

A549	Human alveolar adenocarcinoma cell line
AdV	Adenovirus
ALI	Air-liquid interface
ALRI	Acute lower respiratory tract infection
ARDS	Acute respiratory distress syndrome
AU	Arbitrary units
BSA	Bovine serum albumin
BX795	Inhibitor of the innate immune response
CC3	Cleaved caspase 3
CLEM	Correlative light and electron microscopy
CoV	Coronavirus
CPE	Cytopathic effect
Cryo-EM	Cryo-electron microscopy
Cryo-ET	Cryo-electron tomography
CVP	Chimeric viral particle
CX_3CR1	CX3C-chemokine receptor 1
DAPI	4′,6-diamidino-2-phenylindole
DMEM	Dulbecco's minimum essential media
DNA	Deoxyribonucleic acid
DPBS	Dulbecco's phosphate buffered solution
ds	Double stranded
ECL	Erythrina Cristagalli Lectin
EGFR	Epidermal growth factor receptor
eIF4F	Eukaryotic initiation factor 4F
ER	Endoplasmic Reticulum
F	Respiratory Syncytial Virus fusion glycoprotein
FBS	Foetal bovine serum
FFPE	Formalin fixed paraffin embedded
FIB	Focused ion beam
G	RSV attachment glycoprotein
GFP	Green fluorescent protein
H&E	Hematoxylin and eosin
HA	Influenza A virus haemagglutinin
hBEC	Human bronchial epithelial cells
hBoV	Human bocavirus
HEp-2	Human Epithelial cell line
HIV-1	Human immunodeficiency virus 1
HMPV	Human metapneumovirus
hpi	Hours post infection
IAV	Influenza A Virus
IBV	Influenza B virus
ICAM-1	Intracellular adhesion molecule 1
ICV	Influenza C virus
IDV	Influenza D virus
IFIT	Interferon-induced protein with the tetratricopeptide
IFN	Interferon
IGRF	Insulin-like growth factor receptor

IRF7	Interferon regulatory factor 7
LRT	Lower respiratory tract
M	RSV matrix protein
M1	IAV matrix protein 1
MALII	Maackia Amurensis Lectin II
MAVS	mitochondrial antiviral signalling protein
MDA-5	Melanoma differentiation-associated gene 5
MDCK	Madin Darby canine kidney cells
MEM	Minimum essential media
MOI	Multiplicity of infection
mRNA	Messenger ribonucleic acid
MxA	Myxovirus resistance protein
N	Respiratory syncytial virus nucleoprotein
NA	Influenza A virus neuraminidase
NF-κB	Nuclear Factor κB
NP	Influenza A virus Nucleoprotein
NS1	Non-structural protein 1
pfu	plaque forming units
PIV	Parainfluenza viruses
PR8	A/Puerto Rico/8/34
PRR	Pattern recognition receptor
PV	Pseudotyped particle
qPCR	Quantitative polymerase chain reaction
RdRP	RNA dependent RNA polymerase
RIG-I	Retinoic acid inducible gene I
RNA	Ribonucleic acid
RNP	Ribonucleoprotein
RSV	Respiratory Syncytial Virus
RV	Human Rhinovirus
SARS-CoV-2	Severe acute respiratory syndrome virus 2
SD	Standard deviation
SEM	Scanning electron microscopy
SEM	Standard error of the mean
ss	Single stranded
STAT	Signal Transducer and Activator of Transcription
TEM	Transmission electron microscopy
TPCK	Tosylsulfonyl Phenylalanyl Chloromethyl Ketone
TRIM25	Tripartite Motif Containing 25
UK	United Kingdom
v/v	Volume/volume
vRNA	Genomic viral RNA

List of Figures and Tables

Acknowledgements

First, I'd like to thank my supervisors, Pablo Murcia and Swetha Vijayakrishnan, for their continued support and guidance throughout my PhD. I'd like to say a huge thank you to Pablo for your ongoing encouragement and advice. I truly appreciate the time you spent discussing my project and ideas and everything you did to help me develop as an independent scientist. I'd also like to say a massive thank you to Swetha for all your excellent advice throughout my PhD. Thank you for the time you spent training and guiding me, and for introducing me to the beauty of cryo-ET!

Thank you to all involved in MRC Precision Medicine DTP for giving me the opportunity to take on my PhD and for all the training provided. Thank you also to my PhD assessors Sheila Graham, Massimo Palmarini and George Baillie for your advice and support as my PhD progressed.

An enormous thank you to everyone at the CVR who has helped me along the way and more generally, thank you for making the CVR a fantastic environment to learn and develop as a scientist – I feel very lucky to have started my virology career here.

A hugely important thank you goes to the people who have seen me through my PhD journey. Daniel, Julien and Kieran thank you for the advice about my project, but much more importantly, thank you for being excellent friends. To all other past and present members of the Murcia group, I can't thank you enough for all your help and support.

Thank you to my family for supporting me always, regardless of what direction I take. And to my friends, thank you for always being there.

My final and biggest thank you goes to my husband Sam, thank you for everything.

Author Declaration

I, Joanne Haney, declare that, except where explicit reference is made to the contribution of others, this thesis is the result of my own work and has not been submitted for any other degree at the University of Glasgow or any other institution. This project was supported by the Precision Medicine Doctoral Training Program funded by the Medical Research Council.

Signature:

Printed name: Joanne Haney

Chapter 1

Introduction

1.1 The global impact of respiratory viral infections

Respiratory viral infections represent a major ongoing pressure on human public health and are the cause of substantial morbidity and mortality worldwide. Acute lower respiratory tract infection (ALRI) is the leading cause of mortality in children under five years worldwide and many of these cases can be attributed to viral infections (GBD 2016 Causes of Death Collaborators et al., 2017). The burden of mortality is disproportionally high in low and middle income countries, where lack of access to intensive health care facilities and comorbidities are important risk factors for severe disease (Geoghegan et al., 2017). In high income countries, respiratory infections cause substantial economic losses. A report commissioned by the British Lung Foundation estimated that cost of upper and lower respiratory tract infections in the United Kingdom (UK) was 1.74 billion GBP in 2014 (Trueman et al., 2014). In recent years, the potential of a pandemic influenza outbreak was identified as the greatest risk to the population of the UK (United Kingdom Cabinet Office, 2019), emphasising the lack of preparedness for dealing with emerging infectious disease, in countries of all economic status. This was realized upon the emergence of the pandemic severe acute respiratory syndrome virus 2 (SARS-CoV-2). The unforeseen magnitude of pandemic has so far resulted in massive global morbidity and mortality, as well as severe economic damage due to country-wide lock downs (Harari, Keep and Brien, 2020; Pinilla *et al.*, 2021)

1.2 General epidemiology of co-circulating respiratory viruses

A taxonomically diverse range of respiratory viruses co-circulate within human populations, including orthomyxoviruses: influenza A (IAV) and B (IBV) viruses; picornavirus: human rhinovirus (RV); pneumoviruses: respiratory syncytial virus (RSV) and human metapneumovirus (HMPV); pandemic (SARS-CoV-2) and seasonal (OC43, NL63 and 229E) coronaviruses (CoV), adenovirus (AdV), and paramyxoviruses: parainfluenza viruses 1-4 (PIV). These genetically diverse viruses share a common tropism for cells within the human respiratory tract and are all transmitted via the respiratory secretions of an infected host through direct contact, fomite transmission, formation of respiratory droplets or aerosol transmission (Reviewed by [Leung, 2021]).

1.2.1 Seasonality of respiratory viral infections

In temperate climates, many respiratory viruses show some degree of seasonal oscillation in infection peaks. IAV and RSV are important winter peaking viruses, account for significant healthcare burden during the winter months. IAV infection peaks typically range from November to March (Tamerius et al., 2011; Nickbakhsh et al., 2016), while RSV peaks from October to March (Broberg et al., 2018). Seasonal coronaviruses, OC43, 229E and NL-63, typically peak slightly later in the winter season, between January to March (Nickbakhsh et al., 2020). Other respiratory viruses, including RV, PIVs, AdV and HMPV, are detected throughout the year, with inconsistent timing in epidemic peaks (Price et al., 2019).

The reasons for the seasonality of respiratory viruses continue to confound researchers and multiple factors have been proposed to contribute toward seasonality. Physical factors including temperature and humidity (Lowen et al., 2007) during winter months have been proposed to prolong IAV stability and enhance transmission. Sociological factors including the propensity to mix indoors with low ventilation during colder months (Lapeña et al., 2005; Yang and Marr, 2011). Host factors such as vitamin D deficiency have also been proposed to enhance host susceptibility (Cannell et al., 2006) and therefore increase viral transmission. Viral interference has also been proposed to influence seasonality (Linde et al., 2009; J.S. Casalegno et al., 2010; Nickbakhsh et al., 2019) and is discussed in greater detail in section 1.4.3. Interestingly, in tropical climates, IAV does not appear to exhibit a specific seasonality, while RSV retains a distinct seasonal pattern of infection (Bloom-Feshbach et al., 2013; Wang et al., 2020). In Bangladesh, Guatemala and Thailand, peaks in RSV infection were correlated with increased rainfall and humidity during rainy seasons (Haynes et al., 2013; Thongpan et al., 2020). Cross-immunity between co-circulating paramyxoviruses has also been suggested to explain seasonal oscillations (Bhattacharyya et al., 2015).

1.2.2 Age related patterns in respiratory viral infections

Disease burdens for all respiratory viruses are predominantly associated with young children and elderly populations. The highest prevalence of acute respiratory infections (ARIs) are detected in children (Yang, Chan, Lorna K.P. Suen, et al.,

2015; Ramaekers et al., 2017) and viral coinfections are most frequently detected in children (Nickbakhsh et al., 2016). RV infection occurs early in infancy, with the average age of first RV infection between 4-6 months (Regamey et al., 2008). RSV is a well described paediatric virus and RSV seroprevalence is over 95% in children under the age of 2 (Andeweg et al., 2021). Transmission of IAV has been associated with school age children in multiple studies (Cauchemez et al., 2008; Hens et al., 2009; Ali et al., 2013). IAV transmission was shown to be reduced in children by up to 29% during school holidays, but no reduction was observed in adult populations during the same period (Cauchemez et al., 2008). In healthy adult populations, the observed prevalence of respiratory viral infections is lower. Detection of respiratory viral infection most often relies on individuals accessing medical services or hospitalisations. Therefore, the true prevalence of respiratory viral infections, particularly in adult populations, is unclear, as asymptomatic and subclinical infections are not reported. In elderly populations, the burden associated with respiratory viral infections is high and represents an unmet clinical need, which is increasing in demand due to aging populations (Watson and Wilkinson, 2021). The vast majority of mortality associated with SARS-CoV-2 infection occurred in elderly populations in the first wave of the pandemic in Europe, with over 50% of COVID-related deaths in the UK occurring in patients over 80 years (Docherty et al., 2020). Hospitalisation associated with respiratory viral infection is considered to be underestimated, with the majority of primary diagnoses listed as another factor, including dehydration or a fall, despite having laboratory confirmed viral infection (Datta et al., 2017). Respiratory viral infection can also exacerbate chronic health conditions (Flamaing et al., 2003), contributing further to the burden of morbidity.

1.3 Respiratory viral coinfections

Until relatively recently, respiratory viruses have predominantly been considered in isolation, with diagnostic laboratory tests designed to detect a single virus. The application of multiplex qPCR testing for respiratory screening for diagnostic and research purposes has enabled huge advancements in detection of multi-virus coinfections (Brittain-Long et al., 2012). Respiratory viral coinfections occur frequently and therefore may contribute substantially to the dynamics of respiratory

viral infections and the pathogenesis of disease. In recent years, research into viral coinfections has rapidly increased.

1.3.1 Prevalence of coinfections

The prevalence of coinfection by more than one respiratory virus is relatively high, estimated between 10-30% of respiratory viral infections detected (Martin et al., 2012; Zhang et al., 2014; Goka et al., 2015; Nickbakhsh et al., 2016; Kim et al., 2020; Góes et al., 2020).

Children are an important driver of respiratory viral dynamics, so as expected, child populations have the highest coinfection prevalence compared to adult groups (Mandelia et al., 2021) and high observed coinfection in children has been supported by multiple independent studies (Peng et al., 2009; Martin et al., 2012; Góes et al., 2020). In a large-scale study, the proportion of coinfections within virus positive patients was found to be 35% in children under 5 years old, compared with only 5.8% in adults (Mandelia et al., 2021). Further, there appears to be a difference in likelihood of coinfection between older and younger children. In a sample of over 9500 patients positive for at least one virus by multiplex qPCR screen, viral coinfection was detected in 18% of children under 5, compared to 7% of patients over 5 years, with the most common viruses detected being RV, RSV, AdV and CoVs (Nickbakhsh et al., 2016). Studies assessing respiratory viral prevalence among children living in high density populated urban slums reported high coinfection prevalence of just under 30% in children under 5 years (Breiman et al., 2015; Góes et al., 2020). Further, coinfections with more than two viruses are detected in children, with triple and quadruple coinfections detected, albeit at relatively low frequency (Zhang et al., 2014; Danis et al., 2020; Mandelia et al., 2021).

Most coinfection studies are based on respiratory diagnostic screens, which are collected when an individual presents at a hospital or primary healthcare setting with respiratory symptoms. The limitation of these datasets is that they may not accurately reflect the prevalence of coinfection within the general population when also accounting for asymptomatic or subclinical infections. Rates of coinfection in studies looking at asymptomatic infections are generally lower (up to 10%) (Galanti

et al., 2019). Birger *et al.* tested 2,685 asymptomatic adults and of the 6.2% infected, no coinfections were identified (Birger et al., 2018). The reduced detection of coinfections in asymptomatic individuals suggests that coinfection may more likely to be associated with clinical symptoms.

RV, AdV and seasonal CoVs are most frequently detected in coinfections with other viruses (Martin et al., 2012; Goka et al., 2015; Nickbakhsh et al., 2016; Mandelia et al., 2021), while IAV and RSV are detected less frequently in coinfection (Tanner et al., 2012; Nickbakhsh et al., 2016; Meskill et al., 2017). Epidemiological studies have observed that pairs of taxonomically different viruses were found in coinfection together at a higher or lower frequency compared to individual virus prevalence. IAV and RV were shown to negatively interact, whilst positive interactions were identified with RSV coinfection with IBV, AdV and RV, and AdV with RV (Tanner et al., 2012; Nickbakhsh et al., 2019). Similarly, Meskill *et al.* observed that coinfections by IAV and RSV were found 6-7 times less frequently than expected, based on the individual prevalence of each virus (Meskill et al., 2017).

Martin *et al.* described patterns in viral load during coinfection. Some viruses: RSV, IAV, HMPV and PIV3, had high viral loads in both single infection and coinfection, while AdV and PIV1 had lower viral loads in coinfection, compared to single infection. Further, the majority (82%) of coinfections comprised of a virus in the high viral load group and the virus in the variable viral load group (Martin et al., 2012), which provides an interesting insight to the potential within host-dynamics of coinfections.

1.3.2 Clinical impact of coinfections

The clinical impact of coinfection on disease severity is unclear. While some studies report an increase in disease severity (Marcos et al., 2011; Zhang et al., 2014), other studies report that coinfection results in less severe or similar clinical outcomes to single virus infections (Martin et al., 2012; Asner et al., 2014; Asner et al., 2015).

Coinfection with RSV and HMPV was strongly associated with the development of bronchiolitis and resulted in a 10-fold increased risk of need for mechanical ventilation in paediatric intensive care (Semple et al., 2005). This is supported by Stempel *et al.* who found that coinfection with RSV and a secondary virus may be a

risk factor for bronchiolitis (Stempel et al., 2009). Coinfection with AdV and RSV was associated with particularly severe disease outcomes and fatalities (Tristram et al., 1988). RSV coinfection with RV or human bocavirus (hBoV) was not associated with more severe disease than RSV single infected patients, but disease severity and length of hospital stay was substantially increased compared to RV or hBoV single infected patients (Calvo et al., 2015).

The causal relationship between IAV infection and secondary bacterial coinfection is well characterised and results in increased disease severity and complications including bacterial pneumonia (Chertow and Memoli, 2013). IAV infection induces tissue damage and virions interact with bacteria within the respiratory tract, facilitating colonization by bacteria, primarily *Staphylococcus aureus, Streptococcus pyogenes* and *Streptococcus pneumoniae*, that normally reside in the healthy respiratory microbiome (Okamoto et al., 2003; Plotkowski et al., 2015; Rowe et al., 2019). Due to this interaction's strong association with enhanced disease severity (MacIntyre et al., 2018), IAV coinfections have been of particular research interest, to determine if virus-virus interactions with IAV may result in similar outcomes. Zhang *et al.* report more severe clinical outcomes in patients coinfected with IAV and RSV, compared to single infection by either virus (Zhang et al., 2014). Clinical outcome may depend on the coinfecting virus, as RV coinfection with H1N1 IAV was shown to reduce symptom severity, while coinfection with non-RV viruses, particularly CoVs resulted in more severe disease outcomes (Esper et al., 2011).

1.3.3 **Experimental coinfections in animals**

The relative frequency of coinfection demonstrates that respiratory viral infections do not occur in isolation. The clinical outcomes of coinfections are variable, but a substantial number of clinical studies do support the role of coinfections in altered viral pathogenesis or more severe disease outcomes. The interactions occurring between coinfecting viruses and the host are poorly understood and thus warrant further study using experimental systems. In recent years, an increasing number of experimental coinfection studies have been published, many of which used animal challenge models. *In vivo* studies are important for determining the impact of coinfection on disease progression, viral pathogenesis and host immune response.

Due to their high clinical importance and potential for interference interactions, coinfections between IAV and RSV have been extensively studied using animal models. Chan *et al.* used a ferret model to determine the role of viral interference interactions between IAV and RSV. Ferrets inoculated with 2009 pandemic H1N1 IAV were protected from subsequent infection by RSV for 7 days. However, when challenged at 11 days post IAV infection, RSV infection was able to establish. Conversely, primary infection with RSV did not prevent infection by IAV at any time interval, but did reduce morbidity (weight loss) following IAV infection (Chan et al., 2018). Similarly, Ayegbusi *et al.* observed that in mice coinfected with RSV and IAV H3N2, correlates of disease pathology were reduced, compared to singly infected animals (Ayegbusi et al., 2019). Drori *et al.* established a temporal pattern in IAV induced interference of RSV infection. Mice were infected with IAV up to 12 days prior to secondary RSV infection, and it was found that mice were refractory to RSV infection when inoculated 1-3, or 8-10 days post IAV infection, but RSV infection could establish when inoculated between 4-7 days post IAV infection. This was linked to a two-wave expression of anti-viral proteins, induced by the primary infection by IAV (Drori et al., 2020). Conversely, Georges *et al.* observed an exacerbation in disease severity following sequential coinfection with IAV and RSV (IAV followed by RSV and RSV followed by IAV) and detected a higher IAV viral load (George et al., 2021).

IAV coinfection with other (non-RSV) viruses has also been studied. Gonzalez *et al.* demonstrated that sequential challenge with RV or a mouse CoV (MHV-1), followed by challenge with IAV, did not alter the replication of IAV, but did result in disease attenuation and faster viral clearance (Gonzalez et al., 2018). Multiple studies demonstrate that experimental coinfection with SARS-CoV-2 and IAV results in enhanced disease severity and both Bai *et al.* and Achdout *et al.* reported that IAV coinfection actually results in increased replication of SARS-CoV-2 (Zhang et al., 2020; Bai et al., 2021; Achdout et al., 2021). Li et al showed that IAV shedding is also increased in coinfection with SARS-CoV-2 (H. Li et al., 2021).

1.4 Virus-virus interactions

Viral interactions between respiratory viruses have been described at multiple scales, from the population level, to the individual coinfected cell (Figure 1-1).

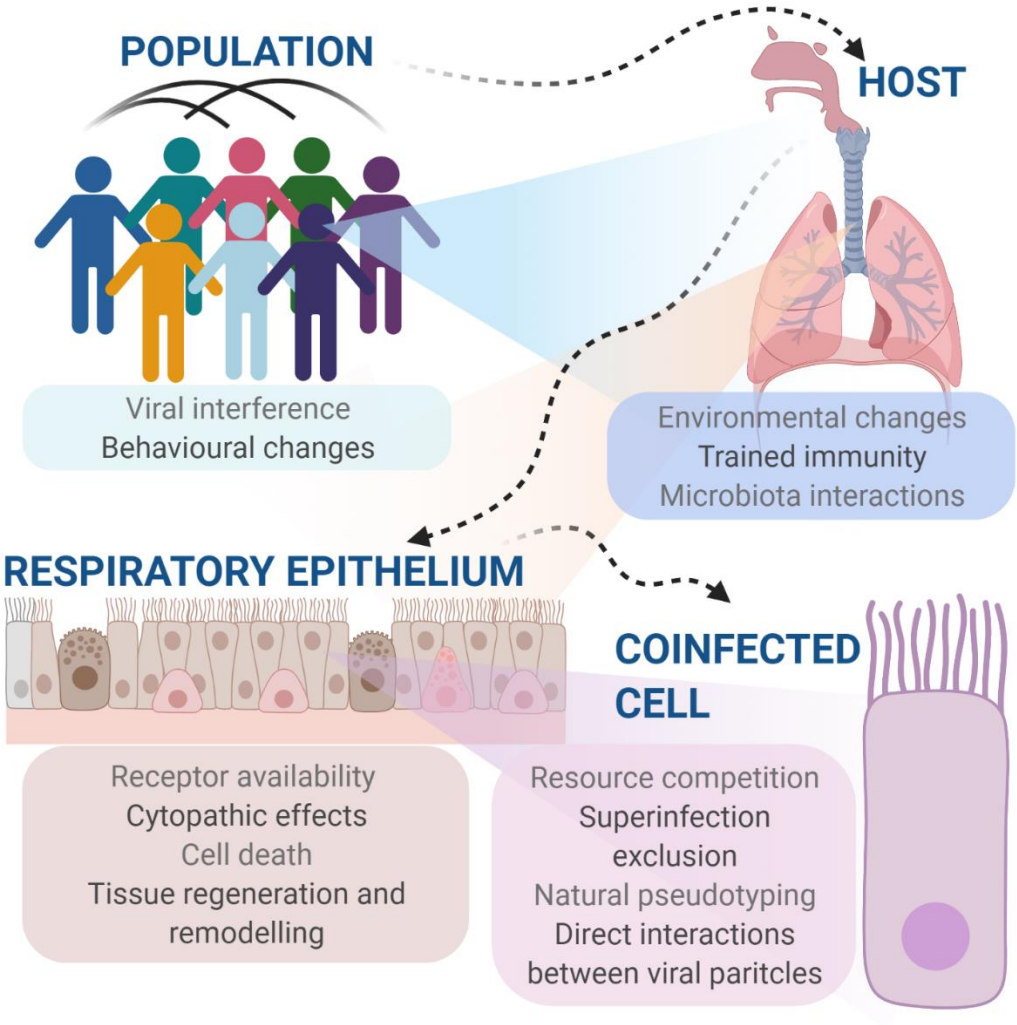

Figure 1-1: Respiratory virus-virus interactions occur across multiple scales. Viral interactions that influence respiratory viral dynamics can occur from the population level to the individual coinfected cell.

1.4.1 Population and host level interactions

At the population level, positive and negative relationships have been observed between taxonomically different viruses that cocirculate in shared populations (Nickbakhsh et al., 2019). An analysis of over 44000 cases of respiratory illness found evidence to support statistically significant positive interactions between non-

influenza viruses and negative interactions between influenza and non-influenza viruses, when controlling for age and seasonality (Nickbakhsh et al., 2019). A growing body of evidence supports the existence of interactions between influenza A virus and rhinovirus A (Linde et al., 2009; J S Casalegno et al., 2010; Ånestad, Gabriel, Nordbø, 2011; Nickbakhsh et al., 2019). Nickbakhsh et al., identified a negative or antagonistic, relationship between IAV and RV, where reductions in RV prevalence coincided with IAV seasonal peaks over an 11-year time period (Nickbakhsh et al., 2019). This negative interaction was conserved at the host level.

1.4.2 Viral Interference

Negative interactions at the host and population level interactions between viruses have been described for decades, much which has been attributed to viral interference – a phenomenon where infection with one virus is proposed to provide short-lived non-specific protection against subsequent viral infection, mediated by host immunity. Viral interference was first described in plants in 1929 (McKinney, 1929), and these interactions have since been recognised in insect (Baidaliuk et al., 2019), mammalian and avian (Rim et al., 2019) systems. Viral interference is understood to explain viral dynamics observed during the 2009-10 H1N1 IAV pandemic (Anestad and Nordbo, 2009; J. S. Casalegno et al., 2010; Ånestad, Gabriel, Nordbø, 2011). Interference induced by prior rhinovirus epidemics was thought to delay and reduce the severity of the influenza pandemic in several European countries (Linde et al., 2009; Anestad and Nordbo, 2009; J. S. Casalegno et al., 2010; Ånestad, Gabriel, Nordbø, 2011). In turn, the first wave of the influenza epidemic was proposed to cause the seasonal peak of RSV to be unusually delayed (J S Casalegno et al., 2010; Yang, Chan, Lorna K. P. Suen, et al., 2015; van Asten et al., 2016). Nickbakhsh *et al.* used mathematical simulations to model viral interference and found that introducing a short refractory period of just two days post influenza infection, in which a host is insusceptible to secondary infection by a common-cold like illness, was enough to reduce incidence of common-cold infection by nearly one quarter (Nickbakhsh et al., 2019). Further, interference induced by RV was mathematically modelled based on experimental coinfections in primary differentiated human bronchial epithelial cells (hBEC). Dee *et al.* showed that an RV-induced interference interaction prevent exponential growth of SARS-CoV-2 infections in the population (Dee et al., 2021). A reduction in infection of this scale

could contribute heavily to the dynamics of infection at the population level, demonstrating that host level interactions are of importance, as amplification of these effects results in population-wide effects. Mak *et al.* analysed incidence of a panel of respiratory viruses in Hong Kong and observed that the infection trends of several non-influenza respiratory viruses, including RV, RSV, PIV and AdV, were abnormal in the months following the 2009 H1N1 IAV pandemic. These observations were proposed to be a result of a lack of normal viral interference interactions, that result in cyclical patterns of infection by respiratory viruses (Mak et al., 2012).

The underlying mechanisms driving viral interference interactions are not fully elucidated and tissue level interactions including competition for receptors and resources within host tissues proposed to contribute. Immune mediated interactions have, however, been demonstrated to play a primary role in driving dynamics and this is considered to be a key mediator of viral interference between taxonomically diverse respiratory viruses.

1.4.3 **Mechanisms of viral interference**

The immunological mechanisms of viral interference have been explored in multiple studies. In a differentiated model of the airway epithelium, Dee *et al.* demonstrated RV infection peaked quickly and induced a widespread antiviral response, resulting in high levels of expression of anti-viral protein MxA. In the same culture system, SARS-CoV-2 replicated more slowly and induced a comparatively low interferon (IFN) response, with antiviral signalling contained to foci of infection. In coinfection, RV-induced antiviral signalling blocks the replication of SARS-CoV-2. In the presence of BX795, an inhibitor of the innate immune response, SARS-CoV-2 replication was restored to the level of single infection, despite the presence of RV. The recovery of SARS-CoV-2 replication in the presence of the inhibitor demonstrates that it is immune signalling, not resource competition that limits the replication of SARS-CoV-2 in coinfection (Dee et al., 2021). Similarly, Wu *et al.* demonstrated that IAV replication is inhibited following infection by RV, in an immune-mediated manner. Treatment with BX795 resulted in the recovery of IAV replication in coinfection with RV (Wu et al., 2020). Geiser *et al.* showed that HMPV replication was reduced in coinfection with RSV in an air-liquid interface model of

the airway epithelium, but the inhibitory effect was partially alleviated in the presence of IFN type I and III neutralising antibodies (Geiser et al., 2021). These experimental studies support the idea that viral interference is driven by the innate immune response and that viruses that induce a strong IFN response can block infection by a secondary virus. Essaidi-Lassiozi *et al.* showed that replication of IAV and RSV was unaffected by pre-treatment by IFNλ in *ex vivo* respiratory cultures, while RV infection was substantially reduced. All three viruses were sensitive to IFNα, but a lower level of inhibition was observed for IAV and RSV, compared to RV (Essaidi-Laziosi et al., 2020). IAV and RSV encode potent anti-viral proteins, that engage with multiple components of the innate immune pathways, to supress host innate immune signalling (Nogalez et al., 2018; Thornhill and Verhoeven, 2020). The varying sensitivity to IFN suggests some viruses may be better equipped to overcome interference interactions induced by a coinfecting virus, while other viruses cannot.

Drori *et al.* demonstrated that temporal patterns in interference were driven by distinct waves of anti-viral signalling. Mass spectrometry analysis of cells infected with IAV revealed a subset of ten proteins that exhibited a distinct two-wave pattern of upregulation, peaking between days 1-3 and 8-12 post IAV infection. Members of the interferon-induced protein with the tetratricopeptide (IFIT) family of proteins were specifically enriched in the subset (Drori et al., 2020) and these proteins have been shown to restrict RSV and CoV replication by binding to the 5' end of viral RNA, therefore occluding interactions with translational initiation factor eIF4F (Kumar et al., 2014). IFIT proteins do not restrict IAV replication, likely because IAV uses cap-snatching mechanisms that make the 5' end of IAV RNA indistinguishable from host-cell RNA (Pinto et al., 2015).

Ayegbusi *et al.* analysed the T cell response to single infection or coinfection with IAV H3N2 and RSV. They found that coinfection by both viruses simultaneously resulted in a reduction of CD11c+ dendritic cells, however also resulted in significantly higher activation of natural killer T cells and CD4+ helper T cells. There was a significant reduction in CD8+ cytotoxic T cells in coinfection (Ayegbusi et al., 2019).

1.4.4 **Trained immunity**

Viral interference has been demonstrated experimentally to occur due to transient immune mediated interactions, that cause the respiratory epithelium to become refractory to infection by a secondary virus. However, longer-lived heterologous interference interactions have also been described. Trained immunity describes a process in which innate immune cells display characteristics of memory in response to an initial infection or vaccine administration, and thus can induce a non-specific protective effect upon rechallenge (Netea et al., 2020). Infection memory is generated through a combination of metabolic reprogramming and epigenetic changes within innate immune cells in response to a primary infection. Upregulation of metabolic processes results in activation of factors involved in chromatin remodelling, which ultimately results in histone modifications to selected genes involved in innate immunity. Upon secondary exposure to a pathogen, the modifications to chromatin structure allow upregulation of the epigenetically modified genes to a greater extent, resulting in an immune response of greater magnitude than the initial infection (Netea et al., 2020). This phenomenon is not specific to viral infection: Kleinnijenhuis *et al.* demonstrated that up to 3 months following the BCG vaccine, T cells collected from human volunteers exhibited enhanced IFNγ and TNFα response to unrelated bacterial pathogens, compared to unvaccinated individuals (Kleinnijenhuis et al., 2012).

Cross-reactive immunity between related viruses has been well described. Cross immunity from seasonal CoVs is proposed to play a role in reducing of disease severity induced by SARS-CoV-2 infection (Yaqinuddin, 2020), while others suggest it may enhance immunopathology (Beretta et al., 2020). Additionally, protective heterosubtypic T cell responses to IAVs are well characterised (Schulman and Kilbourne, 1965; Slütter et al., 2017). However, cross reactive immune interactions between unrelated viruses are less well described and trained immunity may play an important role here. The formalin-inactivated RSV vaccine caused severe enhancement of disease and excess mortality following natural infection by RSV during the 1960s, but infection by RSV prior to vaccination alleviated the severe immune reaction. Walzl *et al.* showed that prior infection with IAV also exerts a protective effect against subsequent infection by RSV, therefore demonstrating that heterologous immune interactions induced by unrelated viruses play a role in determining clinical outcomes (Walzl et al., 2000).

1.5 Cellular level viral interactions

1.5.1 Applying social interactions to virus-virus interactions

At the individual host level, many respiratory viruses share tropism for specific regions and cell types in the respiratory tract. Therefore, they can be considered to occupy the same ecological niche. As with all biological systems, the community interactions within the respiratory tract will impact on the dynamics of other organisms co-existing within the same ecological niche and alter environmental factors to which the organisms depend.

Díaz-Muñoz *et al.* used the term Sociovirology to describe a framework in which the diverse range of virus-virus interactions that occur during the course of infection can be understood, using principles of social evolution theory (Díaz-Muñoz et al., 2017). The application of social principles to study viruses has previously been overlooked, as these principles assume a level of complex behavior, which viruses, as obligate entities, cannot display. However, using this framework can clarify and direct our understanding of evolved traits or interactions between coinfecting viruses.

Ecological interactions have been used to describe interactions in other multi-pathogen systems, including virus-bacteria interactions of the respiratory tract, but virus-virus interactions have been overlooked by this framework. At all stages of viral infection there are opportunities for classical ecological interactions that are well described in higher order systems (Lang and Benbow, 2013). The most obvious interaction is competition, between coinfecting viruses for host resources, cellular machinery, and space within a coinfected cell. It has been demonstrated that facilitative, mutualistic and altruistic interactions also occur during viral infections (Domingo-Calap et al., 2019). DaPalma *et al.* grouped virus-virus interactions into three broad categories: indirect interactions driven by host immunological responses, indirect interactions driven by environmental changes and direct interactions between viral gene products (DaPalma et al., 2010).

It is important to make the distinction between different classes of virus interactions. Viral infection is established by a dynamic population of non-identical variants, each varying degrees of fitness. Resource competition between non-identical variants drives viral evolution and influences the course of infection, while cooperative interactions between variants maintain genetic diversity. The extent of interactions

between related subspecies of viruses may depend on the relatedness of the two viruses or the context of coinfection. Interactions between taxonomically distinct, unrelated viruses are the most poorly characterised, and the factors influencing such interactions are unclear.

1.5.2 **Direct interaction between virus particles**

Virus particles can aggregate to form large, structured assemblies of viral particles, with a total size that is considerably larger than a single viral particle, containing multiple genomes. Aggregation of influenza virions has been demonstrated to promote multiplicity reactivation (Hirst and Pons, 1973). Viral aggregates can provide additional advantageous traits, including enhanced resistance to neutralising antibodies and inactivation in the environment. Cuevas *et al.* demonstrated that free VSV virions can spontaneously aggregate, forming multi-virion bodies. These bodies facilitate delivery of multiple genomes into the same cell, thereby maintaining genetic diversity. This interaction is favoured in bodily fluids such as saliva, compared to tissue culture media, therefore this suggests that direct interactions between virions maybe an evolved advantageous trait within the respiratory tract (Cuevas et al., 2017). Andreu-Moreno *et al.* demonstrated that although these aggregates provide a transient advantage for inter-cell transmission, it comes at a fitness cost to the virus as it drives the production of defective interfering particles (Andreu-Moreno and Sanjuán, 2020). It is possible that aggregates composed of unrelated viruses during coinfection could provide the same benefits, by promoting extracellular stability.

1.5.3 **Resource competition**

Resource competition has been demonstrated to drive the outcome of coinfection in bacterial and parasite coinfection systems (Kinnula et al., 2017; Budischak et al., 2018; Rovenolt and Tate, 2021). However, no experimental laboratory studies have attempted to quantify resource competition between coinfecting viruses. The energy cost of producing new viral particles is substantial (Mahmoudabadi et al., 2017), therefore it is plausible to assume that limitations of finite resources within a

coinfected cell or tissue will ultimately drive competition between co-replicating viruses. On a simplified level, the most essential resource for viral replication is the availability of susceptible cells. Mathematical simulations of coinfections based on the *in vitro* growth parameters of multiple respiratory viruses shows that faster growing viruses outcompete slower growing viruses by consuming more resources, in the form of susceptible cells (Pinky and Dobrovolny, 2016). This was supported by a recent study, which showed that the length of the viral life cycle was the primary factor driving competition, and was more important than timing of infection (Vafadar et al., 2021). These models are an over-simplification of the complexity of respiratory viral infection, but do highlight that the kinetics of viral replication, which varies between co-circulating viruses, can impact access to cellular resources.

1.5.4 **Superinfection exclusion**

Superinfection exclusion describes the process in which a virus prevents secondary infection of the same cell or tissue by a related virus. Superinfection exclusion has been demonstrated for a diverse range of viruses including orthomyxoviruses (Huang et al., 2008; Sun and Brooke, 2018), paramyxoviruses (Morrison and McGinnes, 1989; Horga et al., 2000), retroviruses (Barnard et al., 2006), flaviviruses (Tscherne et al., 2007; Blitvich and Firth, 2015), pestiviruses (Lee et al., 2005) and alphaviruses (Karpf et al., 1997).

Interference with cellular entry is a key mechanism to mediate superinfection exclusion. Laliberte *et al.* demonstrated that poxviruses can induce superinfection exclusion by interfering with membrane fusion process during viral entry, therefore blocking entry of a second virus (Laliberte and Moss, 2014). Other viruses target cellular entry receptors and this is a is a key mechanism to mediate superinfection exclusion (Geleziunas et al., 1994; Horga et al., 2000; Huang et al., 2008). Human immunodeficiency virus type I (HIV1) depletes its receptor CD4 from the cell surface, by triggering its internalization, via the viral encoded *nef* protein (Geleziunas et al., 1994). The haemagglutinin-neuraminidase glycoprotein of PIV3 cleaves sialic acid (its cellular entry receptor) from the cellular surface, thereby preventing subsequent infection (Horga et al., 2000). Similarly, IAV neuraminidase (NA) removes sialic acids from the surface of cells producing IAV virions. Huang *et al.* showed that N1 from A/Puerto Rico/8/34 could restrict the entry of retroviral pseudotypes expressing

a range of haemagglutinins. Further, they showed that superinfection exclusion was correlated with a loss of sialic acids on the cell surface (Huang et al., 2008).

Equally, for IAVs, coinfection is an important event for the delivery of a viral genome, as the majority of IAV particles produced do not contain a complete viral genome (Brooke et al., 2013). Complementation reactivation is the process whereby more than one semi-infectious virus infects the same cell, each bringing components to make a complete infectious genome, therefore enabling viral replication. Sun *et al.* showed that semi-infectious influenza particles are more likely to coinfect the same cell, whereas IAV particles with complete genomes potently inhibit superinfection (Cannell et al., 2006; Sun and Brooke, 2018). This suggests that the mechanism of superinfection exclusion relies on a fully infectious particle, whose infectious progeny mediates superinfection exclusion on release from infected cells, by NA cleavage of receptors.

Relatedness between viruses is an important factor to the extent to which superinfection exclusion occurs. Studies demonstrate that only viruses of the same strain or closely related viruses are sensitive to superinfection exclusion (Folimonova, 2012; Laliberte and Moss, 2014). It is unclear whether superinfection exclusion interactions occur between unrelated viruses, however based on known mechanisms of exclusion, it seems unlikely. Unrelated respiratory viruses have been shown to coinfect individual cells experimental studies. (Shinjoh et al., 2000; Geiser et al., 2021), therefore, immune-mediated viral interference that prevents coinfection of the same tissues, rather than cellular superinfection exclusion may play a more important role in respiratory viral dynamics. A recent pre-print by Czerkies *et al.* showed that in a mixed infection, immune-mediated interference induced by RSV actually promotes coinfection, over infection of bystander cells (Czerkies et al., 2021).

1.5.5 **Natural pseudotyping**

Pseudotyping, or phenotypic mixing, is an interaction that occurs between enveloped viruses and describes the process in which virions containing the internal core proteins of one virus incorporate the envelope proteins of a different virus. The interaction has been widely adopted in molecular virology research. Non-

pathogenic, replication incompetent viral pseudotypes can be flexibly developed through using lentivirus and vesicular stomatitis virus (VSV) vectors, containing structural proteins and enzymes from the vector, whilst expressing the glycoproteins of interest from unrelated viruses.

Pseudotyping between RNA viruses was demonstrated in early coinfection studies (Zavada, 1982) and has been demonstrated between respiratory viruses IAV and Newcastle Disease Virus (Granoff and Hirst, 1954). Components from morphologically different viruses were also demonstrated to result in infectious pseudotyped virions. Filamentous parainfluenza virus SV5 and spherical VSV produced pseudotyped virions that contain VSV nucleocapsid and SV5 membrane proteins (Choppin and Compans, 1970). RNA virus VSV was also shown to incorporate glycoproteins from DNA virus, herpes simplex virus 1 (HSV1), demonstrating that highly genetically diverse viruses are structurally compatible in the formation of pseudotyped virions (Huang et al., 1974). Natural pseudotyping can result in functional changes to the biological properties of viruses (Granoff and Hirst, 1954; Choppin Atn and Compans, 1970). Pseudotyping between human immunodeficiency virus 1 (HIV-1) with gammaretrovirus, xenotropic murine leukemia virus-related virus, was demonstrated to facilitate evasion of neutralising antibodies and expansion cellular receptor tropism (Tang et al., 2014).

Natural pseudotyping between taxonomically distinct respiratory viruses raises questions surrounding the structural compatibility of envelope proteins with internal structural proteins of unrelated viruses. Zavada *et al.* proposed that evolutionarily conserved structural features in the interacting regions between viral glycoproteins and matrix proteins may facilitate pseudotype formation (Zavada, 1982).

Heng *et al.* described a more complex interaction, which resulted in structural changes to virions generated in coinfection with HIV-1 and HSV-1, identified by electron microscopy. In skin biopsies from acquired immunodeficiency syndrome (AIDS) patients with coinfected with HSV-1 and HIV-1, particles were identified within coinfected cells that were larger in size than each virus alone, with an irregular morphology. Additionally, the cellular tropism of both viruses was altered in coinfection: HIV-1 was identified in keratinocytes, which lack CD4 receptor, whilst the proportion of macrophages positive for HSV-1 was significantly higher in coinfected patients compared to those negative for HIV-1 (Heng et al., 1994). This observation has not been described with other viruses during coinfection but

suggests some viruses may be compatible to produce hybrid viral progeny during coinfection. The fact that this interaction was identified in human biopsies shows the potential for virus-virus interactions that result in changes to viral progeny in coinfected individuals, particularly immunocompromised patients, where viral load may be high.

1.6 **Influenza A Virus**

1.6.1 **Clinical impact**

Influenza virus replication peaks around 48 hours after infection and viral shedding lasts for between 6-8 days (Carrat et al., 2008). Influenza infection predominantly results in uncomplicated illness, with classical influenza disease including fever, headache, muscle pain, runny nose, cough and sore throat (Carrat et al., 2008). Gastro-intestinal symptoms can also manifest and appear more common in a strain dependent manner (Palese and Shaw, 2013). In the elderly, influenza infection can present without respiratory symptoms, with symptoms including fatigue and confusion being more prevalent. In children, symptoms are similar to adults but with some differences. Fevers can be more severe and result in a higher burden of illness (Jané et al., 2019). Also, infection and inflammation of the inner ear (otitis media) can occur, which potentially results in permanent hearing loss (Short et al., 2013). Influenza infection can also be an important cause of Croup in infants, which can result in more severe disease outcomes.

Severe disease outcomes and mortality associated with influenza infection are due to influenza induced inflammation in the lung, which can develop into acute respiratory distress syndrome (ARDS) (Kalil and Thomas, 2019). Complications due to secondary bacterial infection contribute towards adverse disease outcomes. Pneumonia resulting from bacterial coinfection, predominantly with *Staphylococcus pneumoniae*, was estimated to account for up to 90% of mortality associated with the 1918 H1N1 IAV pandemic, which resulted in over 50 million deaths worldwide (Morens and Fauci, 2007).

1.6.2 **Therapeutic Interventions**

Influenza vaccines are offered in the UK prior to the winter season. Live attenuated vaccine is administered predominantly to children, while adult populations receive the inactivated vaccine. Both vaccines are composed of four seasonal IAV strains: two IAVs (H3N2 and pandemic H1N1) and two IBVs, one each from the Yamagata and Victoria lineages. The components of the vaccine are updated annually based on recommendations from the Global Influenza Surveillance and Response System and different strains are incorporated to reflect circulating influenza virus in the northern and southern hemispheres. Due to the antigenic drift and emergence of new IAV strains, prediction for vaccine strains can result in mismatch, where the vaccine strains do not match those circulating in the population, therefore the vaccine does not provide protection against infection by these strains (Flannery et al., 2020; Tenforde et al., 2020). Overall vaccine effectiveness is variable, with typical effectiveness ranging between 40-60% (Public Heath England, 2020).

Small molecule antivirals are licensed to treat influenza virus infection, with neuraminidase inhibitors, Oseltamivir and Zanamivir, being the front line treatment. Oseltamivir resistance is a significant challenge, with high rates of resistance detected. During the 2009-10 H1N1 pandemic, greater than 90% of seasonal strains detected in multiple countries including the UK (Lackenby et al., 2011). Due to this high level of resistance, many small molecule inhibitors targeting different aspects of the influenza life cycle are in development, a few of which have been licensed for clinical use. Favipiravir inhibits the RNA dependent RNA polymerase (RdRP) and is licensed for used in Japan under strict clinical use (Shiraki and Daikoku, 2020). Baloxavir Marboxil is licensed for use in the USA and Japan. It is a pro-drug that is converted to active from, Baloxavir acid. This inhibits IAV replication by inhibiting the cap-dependent endonuclease activity of PA (Shirley, 2020).

1.6.3 **Influenza virus Classification**

Influenza viruses are categorized within the family Orthomyxovirus. Four distinct influenza virus genera have been identified: Influenza A, B, C and D.

Influenza B viruses (IBV) have a segmented genome composed of eight segments. IBVs have important distinctions from IAVs. They encode an additional membrane protein NB, which has a transcriptional start site upstream of NA. Additionally they lack PB-F2 and have other important differences in length of proteins and non-coding regions (reviewed by [Palese and Shaw, 2013]). IBVs are separated into two distinct linages: B/Victoria and B/Yamagata (Rota et al., 1990). IBVs have no known animal reservoir and circulate predominantly in human populations, therefore there is little risk of the emergence of pandemic IBVs. While IBVs do not present a pandemic risk, they contribute substantially to the global burden of disease, representing the dominant seasonal influenza strain approximately every third year (Lin et al., 2004), therefore the seasonal influenza vaccine contains an IBV from both lineages.

Influenza C viruses (ICV) contain seven genome segments. In contrast to IAVs and IBVs, ICV only encodes one surface protein: haemagglutinin-esterase function protein, which forms a lattice structure across the surface of the virion (Halldorsson et al., 2021). This protein combines the roles of HA and NA, mediating receptor binding (Rogers et al., 1986), destruction of receptors (Herrler et al., 1985) and membrane fusion (Ohuchi et al., 1982). ICV circulates in human populations and predominantly causes mild upper respiratory tract infection, although some infections progress to more severe lower respiratory tract infections (Matsuzaki et al., 2006). Despite not receiving as much clinical attention as IAV or IBV, seroprevalence for ICV in children has been reported as high as 90% (Homma et al., 1982).

Influenza D viruses (IDV) were first identified in 2011, from pigs (Hause et al., 2013; Hause et al., 2014) and have since been isolated from cattle, which is believed to be the main reservoir for this virus (Ducatez et al., 2015). IDVs are closest related to ICVs with a similar genome organisation, but cannot recombine with ICVs to produce viable progeny (Hause et al., 2014). Seropositivity in humans has been identified (Eckard, 2016) and IDV grows well in physiological temperatures and conditions similar to the human respiratory tract (Hause et al., 2013). Therefore, IDV has zoonotic potential, however it is likely to cause mild disease so may be of low public health priority.

1.6.4 **Influenza A subtypes**

IAVs have a characteristically wide host range and have been detected in a diverse range of mammalian and avian species. IAV diversity is greatest in wild aquatic birds, therefore this is considered to be the reservoir. Due to this expansive host range, species cross over and viral reassortment, resulting in novel emergent strains is possible, which presents a considerable ongoing threat to human health.

IAVs can be divided into subtypes depending on the type of antigenic proteins on the virion surface: haemagglutinin (HA) and neuraminidase (NA). There are at least 18 known HA subtypes (H1 to H18) and 11 NA (N1 to N11) subtypes. IAV H1N1 and H3N2 co-circulate in human populations and cause seasonal IAV infections. IAVs are further classified into individual virus isolates by the nomenclature: genus, species from which the virus was isolated, location of isolation, the number of the isolation and the year of the isolation (Palese and Shaw, 2013).

1.6.5 **Influenza A virus genome organisation**

Influenza A virus has a negative sense, single stranded RNA genome, with a total size of approximately 13.5 kb (Ghedin et al., 2005). It contains a segmented genome composed of eight individually packaged gene segments, encoding ten core proteins that are essential for viral replication and a number of additional accessory proteins. Gene segments are referred to in order of size, ranging from 2.3kb to 0.89 kb (Ghedin et al., 2005), with segment one being the largest, encoding basic polymerase protein 2 (PB2), followed by basic polymerase protein 1 (PB1), acidic polymerase protein (PA), HA, nucleoprotein (NP), NA, matrix proteins (M1 and M2), and the smallest genome segment, NS. Segments 1 (PB2), 3 (PA), 4 (HA), 5 (NP) and 6 (NA) encode a single core protein (plus additional accessory proteins), while segment 7 encodes core proteins M1 and M2; and segment 8 encodes core proteins NS1 and nuclear export protein (NEP)/nonstructural protein 2 (NS2) (Figure 1-2A). Expression of a number of accessory proteins is facilitated by overlapping open reading frames and alternative splicing of gene segments. Of these the most important include PB1-F2, encoded on segment two, and PA-X, encoded on segment three (Figure 1-2A). While the functional role of many of these accessory

proteins remains unclear, many interact with antiviral pathways (reviewed by [Pinto *et al.*, 2020]).

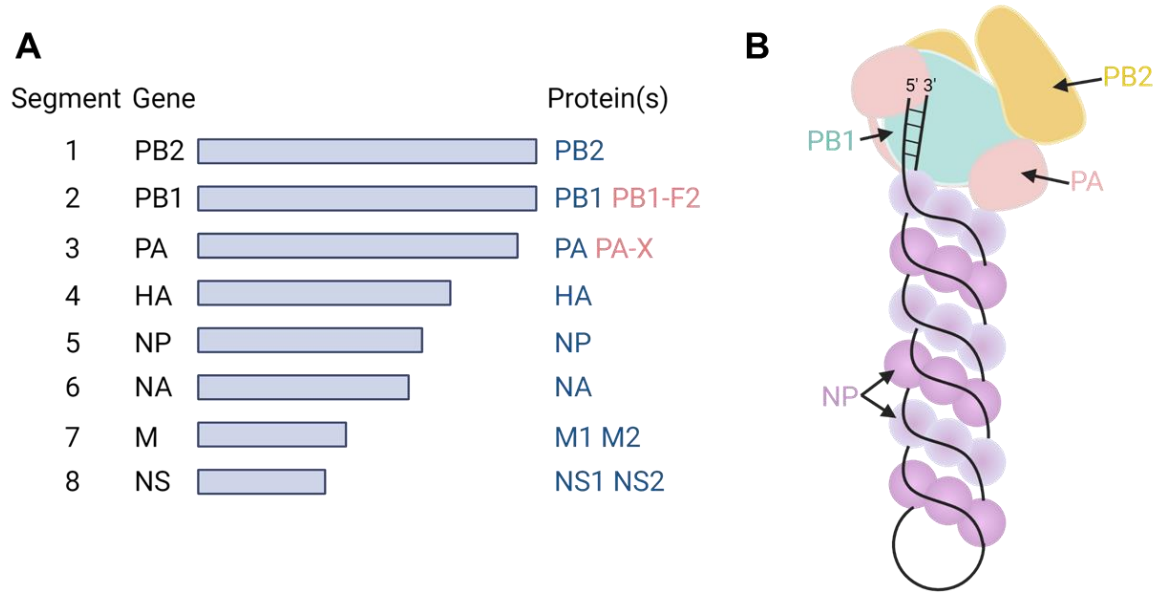

Figure 1-2: Influenza A virus genome structure. (A) Influenza A virus genome segments labelled with gene names and corresponding core proteins (blue) and accessory proteins (red). Blue bars are scaled to size to demonstrate relative gene size from 3.34 kb to 0.89 kb. (B) Schematic of RNP structure. vRNA genome (black line) is packaged in a helical arrangement with nucleoproteins. Genome wraps around and both 5' and 3' ends are associated with the polymerase complex, consisting of PB1, PA (pink) and PB2 (yellow).

1.6.6 **Virion composition and structure**

IAV is highly pleiomorphic, exhibiting spherical, bacilliform and filamentous morphologies. The spherical morphology is associated with laboratory adapted strains, while filamentous virions are more frequent in viral isolates (Seladi-Schulman et al., 2014a). Spherical virions are approximately 120nm in diameter, while filament widths average between 70-100nm (Harris et al., 2006; Dadonaite et al., 2016). Influenza filaments can extend to many microns in length (Elleman and Barclay, 2004). Long filaments tend to be thinner in diameter, while smaller bacilliform particles are widths closer to 90-100nm (Vijayakrishnan et al., 2013).

IAV virions consist of an envelope derived from the host cell. Embedded within this envelope and protruding from the virion surface are glycoprotein spikes, HA and NA. Spikes have a close irregular arrangement, with an average spacing of 11 nm between spikes (Harris et al., 2006). The distribution of NA is clustered (Harris et al., 2006) and on filamentous virions it is typically polarised to one end, with studies presenting conflicting evidence as to whether NA is enriched at the end containing genome (Vahey and Fletcher, 2019) or the opposite end (Calder et al., 2010).The viral envelope also contains proton channels composed of transmembrane protein, M2. M2 is incorporated at 10-100 fold lower abundance to HA (Zebedee and Lamb, 1988).

The viral membrane is derived from host membranes, but it has a different composition. Ivanova *et al.* showed that viral membranes are enriched in phosphatidylethanolamine, a lipid that induces membrane curvature, while the main structural component of cell membranes, phosphatidylcholine, is depleted (Ivanova et al., 2015). Hutchinson *et al.* identified a substantial collection of host-derived proteins within IAV virions. Of these, tetraspanin proteins, CD9 and UPK-1B, were abundant in mammalian and avian derived virus particles respectively (Hutchinson et al., 2014). Tetraspanins have been shown to enhance membrane fusion and extracellular vesicle formation (Andreu and Yáñez-Mó, 2014), therefore active incorporation of CD9 and UPK-1B by IAVs may provide a functional benefit.

Under the membrane is the matrix layer composed on M1 arranged in a helical structure, to which the viral envelope is closely associated (Figure 1-3A). M1 proteins assemble into polymers in linear strands, which wrap with parallel strands to form a helical structure (Calder et al., 2010; Peukes et al., 2020). The sequential assembly of monomers to the polymeric strands, followed by the assembly of polymeric strands to helical assemblies provides the conformational changes and free energy requirements to promote virion assembly (Peukes et al., 2020). The cytoplasmic tails of both HA and NA interact with M1 and this interaction is critical to promote virion assembly (Zhang and Lamb, 1996). Matrix is absent in regions where there are gaps in glycoprotein expression (Harris et al., 2006). The hydrophobic N-terminal domains of M1 interact with both the RNA and protein components of ribonucleoprotein (RNP) complexes within virions (Ye et al., 1999).

Genomic viral RNA (vRNA) is packaged into individual RNPs (Figure 1-2B). vRNA associates with nucleoprotein (NP) to form a coiled rod-like structure. This is bound

to the heterotrimeric polymerase complex, consisting of PB1, PB2 and PA (Figure 1-2B). Each NP associates with approximately 24 bases of vRNA, without sequence specificity. NP binds to the vRNA backbone, leaving bases exposed to facilitate transcription without the requirement for dissociation of the complex (Baudin et al., 1994; Elton et al., 1999). The vRNA has a closed conformation, with both 5' and 3' ends interacting with the polymerase complex. NP and vRNA arranges into a helical structure, where the NP-vRNA strand loops around and parallel and anti-parallel strands interact to provide stability (Arranz et al., 2012; Moeller et al., 2012). vRNA in RNP complexes forms distinct secondary structures, which engage in intra- and inter-segment interactions. These interactions drive co-segregation of virions and dictate compatibility of genome segments during reassortment (Dadonaite et al., 2019).

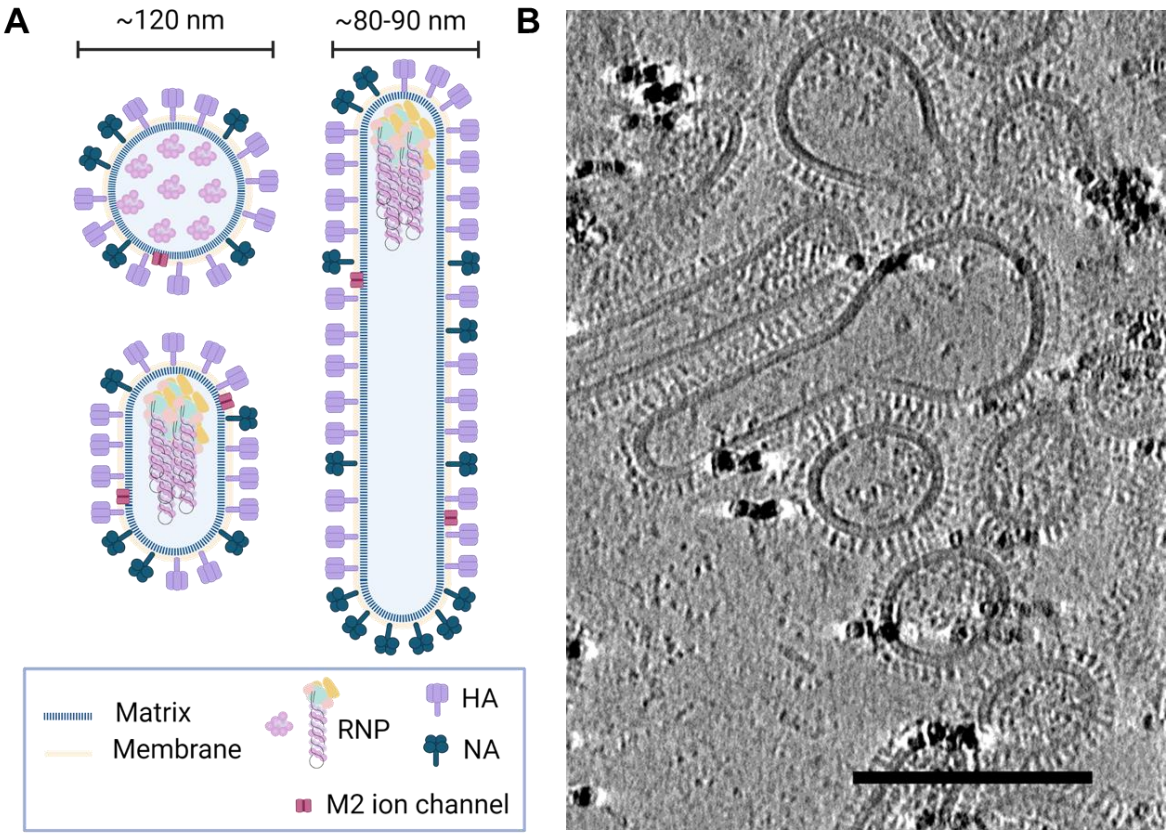

Figure 1-3: Influenza A virion structure and morphologies. (A) Schematic showing influenza A virus virion structure and pleomorphic particles. (B) Image collected by cryo-electron tomography showing pleomorphic IAV virions. Scale bar indicates 200 nm.

The IAV genome is packaged in a structured arrangement within virions, with a 7+1 arrangement of RNPs (Figure 1-3A), with a central RNP surrounded by the seven other genome segments (Noda et al., 2006; Harris et al., 2006). This 7+1 arrangement is conserved across IAVs and Noda *et al.* showed that viruses lacking the HA segment, incorporate 18S and 28S ribosomal RNA to maintain the eight segment arrangement (Noda et al., 2018). RNPs are packaged toward the distal tip of a budding virus, with an orientation perpendicular to the budding membrane (Noda et al., 2006). In filamentous virions, packaging of RNPs is polarised to one end (Figure 1-3) (Calder et al., 2010; Vijayakrishnan et al., 2013; Vahey and Fletcher, 2019), although some filamentous virions lack RNPs completely (Vijayakrishnan et al., 2013).

1.6.7 **Influenza replication cycle**

Influenza virus is transmitted through respiratory droplets, aerosolized droplets and contact transmission (Killingley and Nguyen-Van-Tam, 2013). Once inside the respiratory tract, influenza virions move through the mucus layer to reach the cells of respiratory epithelium. Influenza cellular tropism is discussed in more detail in Chapter 5. Below describes the life cycle of IAV from attachment to a host cell, to release of infectious progeny.

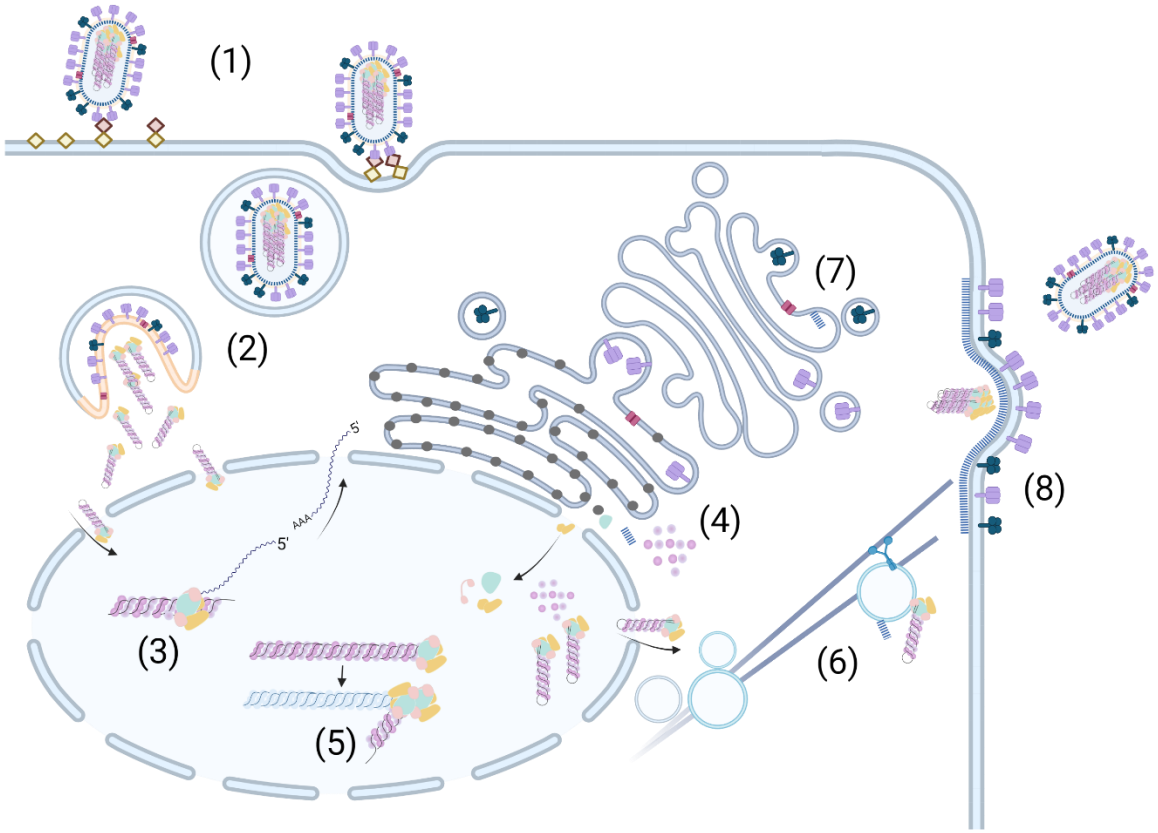

Figure 1-4: Influenza A virus replication cycle. IAV attaches to the cell via interactions between HA and sialic acids on the cell surface, before internalisation, via clathrin mediated endocyotosis or macropinocytosis (1). Endosomal acidification results in conformational changes within the virion that trigger fusion of endosomal and viral membranes, facilitating release of IAV RNPs into the cytoplasm (2). RNPs are transported into the nucleus, where transcription of viral genes is mediated by the IAV polymerase complex (3). Viral mRNAs are translated in the endoplasmic reticulum or by free ribosomes in the cytoplasm. Newly translated NP, PB1, PB2 and PA are transported back into the nucleus for assembly of new RNPs, while envelope proteins progress into the secretory system (4). Replication of viral genomes occurs via a cRNA intermediate (5). Newly synthesized RNPs are transported out of the nucleus and trafficked to the plasma membrane via Rab11 mediated pathways (6). Viral envelope proteins are inserted into the membrane in the ER and processed within the Golgi apparatus, before transport to the plasma membrane via the secretory system (7). Viral components concentrate in lipid raft regions of the plasma membrane. Virion budding and elongation is mediated by polymerisation of the matrix and membrane scission is carried out in a process mediated by M2 (8).

1.6.7.1 Attachment, Entry & Uncoating

IAV virions attach to the cell surface via HA interactions with the terminal sialic acids of carbohydrate chains of glycoproteins or glycolipids (Weis et al., 1988; Takemoto et al., 1996; Gambaryan et al., 1997). The receptor binding site for HA was identified in 1981 and is a conserved binding pocket within the head region of HA, which contains a number of specifically conserved residues and structures facilitating engagement with sialic acids (Rogers et al., 1983; Weis et al., 1988). Specificity for sialic acid structures vary, with avian IAVs typically displaying a preference for α-2,3-gal linkages, which are predominant in the avian gut (Ito et al., 1998), whereas mammalian IAVs preferentially engage with α-2,6-gal linkages, which predominate the human respiratory tract (Matrosovich et al., 2004).

Once attached, using a combination of HA-mediated binding activity and NA-mediated enzymatic cleavage of sialic acids, virions can traverse the surface of the cell (Figure 1-4). This movement has been demonstrated to result in a higher rate of internalization, so suggests that virions move around the cell surface until they encounter the optimum region for internalization, for example regions with endocytic machinery (Sakai et al., 2017). Influenza virions are internalised in two ways. First, clathrin-mediated endocytosis can occur (Rust et al., 2004) and assembly of clathrin coated pits is mediated by the adaptor protein Epsin-1 (Chen and Zhuang, 2008). This is thought to be the primary route of endocytosis for IAVs (Rust et al., 2004). It was also demonstrated that virions can be internalised independently of clathrin, by micropinocytosis (Sieczkarski and Whittaker, 2002; de Vries et al., 2011). Macropinocytosis is required to internalise virions of larger bacilliform or filamentous morphologies (Rossman et al., 2012).

Once internalised into an endosome, IAV undergoes a stepwise uncoating process that relies on both viral induced physiological changes and those induced by the host cell in endosome maturation (Figure 1-4). Within the early endosome, IAV activates M2 ion channels, that allow an influx of protons to the virion. This induces conformational changes in M1 that destablise the matrix layer and disrupt its interactions with HA cytoplasmic tails, the lipid envelope and packaged RNPs (Li et al., 2014; Stauffer et al., 2014). As the endosome matures, concentration of potassium ions increases, which destabilises further interactions between RNPs (Stauffer et al., 2014).

As the endosome matures into a late endosome, with an acidic pH between 5-5.5, HA undergoes conformational changes, that bring the virion membrane and the endosome membrane into extremely close proximity (Benhaim et al., 2020). For this to occur, HA must first have been cleaved from its inactivated conformation (HA_0) to two functional components: the receptor binding domain (HA1) and the fusion domain (HA2). This is described in section 1.6.7.3. Cleavage of HA allows exposure of the fusion peptide on the N-terminus of HA2. The fusion peptide inserts itself into the endosomal membrane, while the C-terminal domain of HA2 is anchored within the viral membrane. HA2 then folds to form a hairpin, which brings together viral and endosomal membranes (Carr et al., 1997; Garcia et al., 2015; Das et al., 2018). Further conformational change brings the two membranes into even closer proximity, initiating membrane fusion. After membrane fusion, RNPs are released into the cytoplasm (Figure 1-4). To aid in capsid disassembly and RNP release, Histone Deacetylase 6 and Transportin 1 interact with M1 to destablise the interactions between the matrix and the RNPs (Banerjee et al., 2014; Miyake et al., 2019). After release, RNPs de-bundle within the cytoplasm and the individual RNPs traffic to the nucleus (Qin et al., 2019).

1.6.7.2 Nuclear import, transcription and genome replication

Influenza virus replication occurs in the nucleus, which allows the virus access to necessary cellular machinery. IAV RNPs are too large to enter the nucleus via passive diffusion, so require active import through the nuclear pore complex. Whilst all components of the RNP complex contain nuclear localisation signals (NLS), it is the NLS on NP that primarily mediate RNP transport into the nucleus (Bullido et al., 2000; Cros et al., 2005; Ozawa et al., 2007). NLS on NP are recognised by importin-α (also known as karyopherin-α) (O'Neill et al., 1995). Importin-α then recruits importin-β, which mediates transport of RNPs through the nuclear pore complex and into the nuclear sub-compartment.

Transcription of viral genes occurs upon entry to the nucleus. Influenza polymerases lack the ability to produce 5' mRNA caps, therefore IAV utilizes a process of cap-snatching, whereby the 5' cap from host mRNA is removed and transferred to viral mRNA. The 5' end of the vRNA strand is bound to PB1, which induces conformational changes in PB2, allowing it to recognise and bind the 5' cap structure

of a cellular mRNA (Guilligay et al., 2008). Next, the 3' end of the vRNA strand binds within PB1 and base pairs with the 5' end. This activates the endonuclease activity of PA, which cleaves the 5' cap from the cellular mRNA (Dias et al., 2009). The snatched region of capped RNA then serves as a primer, annealing to the 3' end of the vRNA (Reich et al., 2014). RNA elongation is catalyzed by PB1 and continues until the polymerase reaches a polyU sequence near the 5' end of vRNA. Steric hindrance, due to the fact the that the 5' end is bound to PB1, causes the polymerase to stutter, resulting in the addition of a poly-adenylated tail (Pritlove et al., 1999). This mechanism of polyadenylation allows IAV to forego cellular polyadenylation machinery, which is down regulated in NS1 induced host shutoff (Nemeroff et al., 1998).

IAVs expand the coding capabilities of their genome by utilizing splicing machinery within the nucleus (reviewed by [Dubois, Terrier and Rosa-Calatrava, 2014]). Alternative splicing of segment 7 mRNA and segment 8 mRNA is required to produce core proteins M2 and NS2/NEP respectively (Lamb and Choppin, 1979; Inglis and Brown, 1981).

Replication of the negative sense viral genome is also carried out by the polymerase complex, in a process independent to transcription. De novo replication of the vRNA results in a full-length copy, complementary to the vRNA (cRNA). The cRNA is assembled into an RNP like structure (cRNP), from which then serves as a template for production of copies of the vRNA genome (Fodor and Velthuis, 2020). The resident polymerase complex on the cRNP forms a dimer with another soluble polymerase complex (Fan et al., 2019). The interaction is stabilised by host protein ANP32A, which binds at the interface between the two heterotrimeric polymerase complexes (Carrique et al., 2020). The resident polymerase complex serves as the replicase and catalyzes the polymerisation of the nascent RNA strand in a primer independent process, while the soluble polymerase regulates the co-replicative assembly of RNPs by encapsulating the newly formed RNA strand with NP (Figure 1-4) (Carrique et al., 2020).

1.6.7.3 Translation, maturation and trafficking of viral proteins

Viral mRNA is exported from the nucleus for translation by cellular translational machinery. PB1, PB2, PA, NP, NS1, NS2, and M1 are translated by cytoplasmic ribosomes, while translation of membrane proteins HA, NA and M2 occurs in the rough endoplasmic reticulum (ER) (Figure 1-4). Protein components of the RNP complex are imported back into the nucleus after translation. PB2 and NP are transported via importin-α and importin-β (Cros et al., 2005; Tarendeau et al., 2007), while PB1 and PA form a heterodimer in the cytoplasm, prior to transport into the nucleus via β-importin Ran binding protein 5 (Deng et al., 2006).

Translation of membrane proteins is mediated by ribosomes associated with the ER. After initiation of translation, hydrophobic signals on the nascent polypeptides are recognised by the signal recognition particle (Daniels et al., 2004; Dou et al., 2014). This directs the ribosome-mRNA complex to sec61, a translocon on the ER membrane (Görlich et al., 1992), that facilitates the translocation of the newly forming polypeptide chain into the ER lumen and partitioning of hydrophobic α-helix transmembrane domains into the lipid bilayer (Hessa et al., 2007) of the ER membrane. Folding of N-terminal domains of HA and NA are promoted with the addition of N-linked glycans (Daniels et al., 2004) and the recruitment of chaperone proteins (Hebert et al., 1997). HA, NA and M2 monomers are then oligomerized in the ER before transport through the Golgi apparatus (Figure 1-4).

HA is translated as inactivated precursor HA0. To become activated, the protein must be cleaved to active subunits HA1 and HA2 (Klenk et al., 1975), via a monobasic or polybasic cleavage site. For highly pathogenic avian IAVs with multi-basic cleavage sites, this cleavage is mediated in the Golgi apparatus by protease furin (Stieneke-Grober et al., 1992). For human IAVs and low pathogenic avian IAVs, with monobasic cleavage sites, cleavage has been shown to occur via transmembrane protease serine S-1 member 2 (TMPRSS2) or human airway trypsin-like protease (Böttcher et al., 2006; Chaipan et al., 2009). Both have been shown to localise to the plasma membrane in human epithelial cells (Böttcher et al., 2006).

1.6.7.4 Egress, Assembly and Budding

Nuclear export of newly formed RNPs is mediated by M1 and NEP/NS2. The C-terminal domain M1 binds to NP in RNPs, while its N-terminal domain interacts with NEP/NS2. NEP/NS2, in turn, interacts with Chromosomal Maintenance 1 (CRM1) via two nuclear export signals. CRM1 is a nuclear export protein which, in association with Ran GTPase, mediates the transport of the RNPs through the nuclear pore complex and out of the nucleus (Reviewed by [Paterson and Fodor, 2012]). M1 ensures the transport of RNPs is unidirectional, by blocking the nuclear localisation signals on NP (Bui et al., 1996). Transport of RNPs to the plasma membrane is dependent on GTPase Rab11 (Bruce et al., 2010; Momose et al., 2011; Eisfeld et al., 2011; De Castro Martin et al., 2017), but the source of the endosomes is debated. Amorim *et al.* showed that newly exported RNPs are concentrated at the recycling endosome, near the microtubule organizing centre, via interactions proposed between PB2 and Rab11 (Amorim et al., 2011). Here, the RNPs associate with Rab11 positive vesicles, which then move along the microtubule network to the periphery of the cell (Figure 1-4) (Amorim et al., 2011; Bhagwat et al., 2020). M1 is also proposed to remain associated with the RNP complexes for transport to the plasma membrane via the microtubule network (Avalos et al., 1997). By contrast, Martin *et al.* demonstrated that RNPs are transported to the ER after nuclear export, where they associate with Rab11 positive irregularly coated vesicles derived from the ER which mediate their transport to the plasma membrane (De Castro Martin et al., 2017). After maturation in the ER and Golgi apparatus, viral membrane proteins are transported to the plasma membrane via their apical localisation signals through the trans-Golgi network secretory pathway. Some studies suggest that M1 can also associate with HA and NA here and progress through the trans-Golgi network to the plasma membrane (Zhang and Lamb, 1996; Ali et al., 2000).

Concentration of viral proteins occurs at lipid raft regions of the plasma membrane, enriched in cholesterol and sphingolipids (Gerl et al., 2012). HA and NA contain raft-targeting motifs within their transmembrane domains, which facilitates their concentration within these regions (Lin et al., 1998; Barman and Nayak, 2000). M1 then assembles a matrix layer underneath the membrane, via interactions with the cytoplasmic tails of HA and NA (Figure 1-4) (Zhang et al., 2000; Chen et al., 2007; Leser and Lamb, 2017). RNPs are recruited via interactions between NP and M1

(Noton et al., 2007). M2 is excluded from lipid raft regions (Leser and Lamb, 2017), but accumulates at the edges of raft regions, ready to mediate scission of newly formed viral particles (Rossman et al., 2010).

Once all the components have been assembled, membrane curvature must be induced to enable budding of new viral particles. This is thought to be achieved by a number of complementary mechanisms (reviewed by [Rossman and Lamb, 2011]). First, accumulation of HA and NA on the external face of the membrane drives the membrane outward (Chlanda et al., 2015). Second, assembly of M1 to a helical matrix layer drives curvature (Chlanda et al., 2015) and subsequently extension of the virion (Peukes et al., 2020). Third, accumulation of curvature inducing lipids into one leaflet of the membrane (Jarsch et al., 2016). Finally, the actin cytoskeleton contributes to the extension of budding virions. This is evidenced by the detection of actin microfibrils within IAV particles by cryo-electron tomography and proteomic analysis (Vijayakrishnan et al., 2013; Hutchinson et al., 2014).

Membrane scission is initiated by the M1-mediated recruitment of M2 to budding virions (Chen et al., 2007; Rossman et al., 2010). This process is independent of the endosomal sorting complex required for transport (ESCRT) machinery. Instead, insertion of an amphipathic helix from the M2 cytoplasmic tail into the membrane causes disruption to membrane curvature, mediating scission and therefore release of IAV particles (Figure 1-4) (Rossman et al., 2010).

1.6.7.5 The role of NS1 and Immune antagonism

NS1 is an essential viral protein, whose main function is to antagonize the cellular innate immune system, predominantly the IFN response, therefore allowing IAV to replicate (García-Sastre et al., 1998). NS1 functions at multiple stages during the replication cycle.

NS1 inhibits the expression of type I IFN. Within the cytoplasm, NS1 interferes with the actions of pattern recognition receptor retinoic acid inducible gene I (RIG-I) by a number of mechanisms. NS1 forms a complex with RIG-I either directly or via an intermediary protein (Jureka et al., 2015). Additionally, NS1 associates with and inhibits positive regulators of RIG-I, including Tripartite Motif Containing 25 (TRIM25) (Koliopoulos et al., 2018). This prevents TRIM25-mediated ubiquitination

of the RIG-I caspase activation and recruitment domain (CARD), which prevents its dimerization with the CARD on Mitochondrial antiviral-signaling protein (MAVS) (Jureka et al., 2020) and subsequent activation of the MAVS-dependent signaling pathway. This prevents phosphorylation of interferon regulatory factor 3 (IRF3), blocking its dimerization and translocation to the nucleus where it would activate expression of IFNβ. NS1 can also directly bind to RIG-I's substrate, dsRNA, therefore sequestering it from recognition by RIG-I (Hatada and Fukuda, 1992). By a similar mechanism, NS1 also inhibits the action of interferon-induced protein 2, 5, -oligoadenylate synthetase (OAS), which is a cytoplasmic PRR that recognises dsRNA structures (Min and Krug, 2006).

One of the most essential roles of NS1 is in inducing shutoff of cellular mRNA translation. This mechanism, combined with cap-snatching which results in the degradation of cellular mRNA, enables efficient shutoff of host cell translation, and allows IAV access to host translational machinery without competition from cellular mRNAs. In addition, it prevents the expression of antiviral proteins. NS1 binds to and inhibits cellular cleavage and polyadenylation factor 30 (CPSF30), which is essential for 3' polyadenylation and export of mRNAs from the nucleus (Nemeroff et al., 1998). Accessory protein, PA-X further contributes to host shutoff by degrading cytoplasmic mRNAs (Khaperskyy and McCormick, 2015). Binding of NS1 to dsRNA also blocks the dsRNA-dependent serine/threonine protein kinase R (PKR), that plays an autoinhibitory role in blocking translation initiation factor eIF2a (Lu et al., 1995). Further, NS1 was demonstrated to bind directly to eukaryotic initiation factor 2a (eIF2a) (Enami et al., 1994), which may promote the selective assembly of translation initiation complexes on viral mRNA. Combined, these data show that NS1 plays a multi-faceted role in host shutoff, by preventing processing of cellular mRNA and selectively promoting the translation of viral mRNA.

NS1 also modulates cell growth, survival, and cell death pathways. NS1 activates phosphatidylinositol 3-kinase (PI3K) and downstream effector Akt/protein kinase B (PKB) (Ehrhardt et al., 2007). The PI3K-Akt signaling pathway has important roles in metabolic regulation, proliferation and cell survival (reviewed by [Hemmings and Restuccia, 2012]). Activation of this pathway is thought to prevent premature apoptosis of infected cells, allowing completion of replication and release of viral progeny (Ehrhardt et al., 2007). This contradicts with other studies that demonstrate viral factors are associated with inducing apoptosis. NA and PB1-F2 have both been

demonstrated to induce apoptosis (Chen et al., 2001). Zhirnov *et al.* shows that induction of anti- or pro- apoptotic signals are induced in a temporal manner. During early infection, NS1-mediated activation of PI3K-Akt signaling prevents apoptosis, but later, as the concentration of viral proteins within the cell increases, pro-apoptotic signaling pathways, mediated by upregulation of p53, tip the balance and ultimately result in IAV-induced apoptosis (Zhirnov and Klenk, 2007).

1.7 **Respiratory Syncytial Virus**

1.7.1 **Clinical impact**

RSV is hugely important respiratory virus and a leading cause of respiratory disease worldwide. The estimated rate of hospitalisation due to RSV infection in infants in western countries is approximately between 6-18% (Deshpande and Northern, 2003; Hall et al., 2009). This presents a high burden of disease, considering approximately 40-69% of infants are infected for RSV by the age of one (Glezen et al., 1986; Andeweg et al., 2021), which rises to 90% by the age two (Andeweg et al., 2021). However, 99% of the disease burden and mortality associated with RSV infection occurs in developing countries (Nair et al., 2010), where RSV infection is the leading cause of mortality associated with lower respiratory tract infection (Lozano et al., 2012; Shi et al., 2017).

In adults, RSV is a substantial cause of disease and in high income countries, RSV related mortality is predominantly associated with elderly, rather than infant, populations. In the UK, RSV infection results in over 8000 deaths, while in the USA this number rises to over 17000, with the vast majority of these deaths in adults over the age of 65 (Thompson et al., 2003; Fleming et al., 2015).

RSV infection initiates in the nasopharynx, where it causes upper respiratory tract symptoms including runny nose, sneezing and fever. Progression of infection to lower respiratory tract tissue occurs in approximately one third of infections (Glezen et al., 1986). Lower respiratory tract infection (LRTI) manifests as bronchiolitis and pneumonia. Mild LRTI symptoms include coughing and wheezing, that self-resolve within days. In infants, progression of disease is characterised by shallow, rapid breathing, resulting in hypoxia. If hypoxia becomes more severe, respiratory failure

can occur (Collins and Karron, 2013). Respiratory symptoms may be more severe in infants due to the higher likelihood of obstruction due to narrow airways by inflammatory cells or sloughed cells of the respiratory epithelium.

1.7.2 **Therapeutic interventions**

Despite the devastating toll on infant health worldwide, there are currently no licensed vaccines against RSV. Enhanced respiratory disease following a trial of formalin-inactivated RSV vaccine in the 1960s (Kim et al., 1969) has presented ongoing challenges to vaccine design and trial procedures. There are a number of vaccine approaches under development - including live attenuated vaccines, mRNA vaccines, adenoviral vaccines, nanoparticle-based vaccines – many of which are in late-stage development or clinical trials (Swanson et al., 2020; Williams et al., 2020; Aliprantis et al., 2021; Karron et al., 2021). Vaccination strategies include targeting of both infants and individuals during pregnancy (Madhi et al., 2020). Vaccination during pregnancy was projected to prevent up to 355 thousand deaths over a 12 year period if a vaccine is developed with 60% efficacy (Baral et al., 2020). RSV is a challenging target for vaccination due to transient immunity, and frequent reinfection rates (Glezen et al., 1986; Hall et al., 1991) and late phase clinical trials have failed to meet clinical endpoints (Madhi et al., 2020). Further, the understanding of correlates of protection against RSV is still relatively limited and there are currently no clearly defined biomarkers for severe RSV disease. The World Health Organisation has developed a roadmap to accelerate development of RSV vaccines and guide the work of academic researchers and funders, alongside biotechnology and pharmaceutical industry to achieve this goal (Vekemans et al., 2019).

Palivizumab is the only licensed therapeutic targeted specifically to treat RSV infection. It is a humanized monoclonal antibody, targeting the fusion glycoprotein. Palivizumab is administered to high-risk infants as a prophylactic measure, to severe disease following RSV infection (Luna et al., 2020). It has been demonstrated to reduce hospitalisations by up to 50%, however, mutations conferring Palivizumab resistance have been identified (Adams et al., 2010; Hashimoto and Hosoya, 2017). Further prophylactic antibody therapies are currently undergoing clinical trials (Griffin et al., 2020).

A wide range of small molecule antivirals, predominantly targeting the fusion glycoprotein or polymerase protein, are also under development or clinical trials. Compounds with a range of inhibitory actions have been developed, including stabilizing the pre-fusion conformation of the F glycoprotein (Roymans et al., 2017) and inhibition of the polymerase L protein via nucleotide analogues or non-nucleoside inhibitors (Wang et al., 2015; Noton et al., 2015; Coates et al., 2017).

1.7.3 **Taxonomy and subtypes**

Respiratory syncytial virus (RSV) is an enveloped virus, containing a single stranded negative sense RNA genome and belongs to the family, Pneumoviridae. This includes two genera: Pneumovirus, to which RSV belongs, and Metapneumovirus, to which HMPV belongs (Collins and Karron, 2013). Pneumoviridae are closely related to the Paramyxoviridae family, which is a large viral family that includes important human viruses transmitted via the respiratory tract, parainfluenza viruses (Respiroviruses), mumps virus (Rubullavirus) and measles virus (Morbillivirus). Additionally this family includes emerging viruses Hendra virus and Nipah virus (Plemper and Lamb, 2021).

RSV is divided into two antigenic subtypes: RSV A and RSV B, defined by the reactivity with F and G glycoproteins with neutralising antibodies (Mufson et al., 1985; T. Li et al., 2021). The two subtypes co-circulate within the human population, but often one subtype dominates in a given season. It is unclear if there is a difference in the clinical severity of infection between the two subtypes, with some studies reporting more severe disease with RSV A (McConnochie et al., 1990; Walsh et al., 1997; Papadopoulos et al., 2004), while others report no difference (Kneyber et al., 1996; Fodha et al., 2007).

1.7.4 **Genome Organisation**

RSV has a negative sense RNA genome, approximately 15.2 kb in size (Collins et al., 1986). It is a single strand of RNA that is not capped at the 5’ end or polyadenylated. It contains 10 genes, encoding 11 core proteins. The genes are in the following order from the 3’ end: NS1, NS2, N, P, M, SH, G, F, M2, L (Figure 1-

5) (Collins et al., 1986). Each gene encodes for a single protein, with the exception of M2, which contains two open reading frames, encoding M2-1 and M2-2 (Gould and Easton, 2007). Each gene contains a highly conserved 9 nucleotide gene start sequence, and ends with a 12-14 nucleotide termination sequence, which contains a polyU sequence to enable polyadenylation (Kuo et al., 1997). NS1 to F genes are separated by short intergenic sequences with no obvious conservation, while the last two genes M2 and L contain a short overlapping region. The 3' and 5' ends of the genome contain extragenic regions, named the leader and trailer regions respectively (Figure 1-5) (Collins et al., 1986).

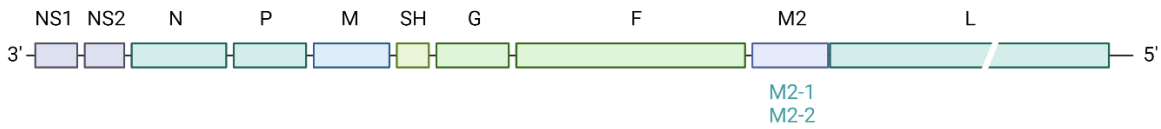

Figure 1-5: Respiratory syncytial virus genome organisation. RSV contains a single stranded, negative sense RNA genome, containing 10 genes. Each box represents an individual gene and boxes are scaled to show relative size of each gene.

The genes encoding structural proteins N, nucleoprotein; P, phosphoprotein; M, matrix protein; SH, small hydrophobic protein; G, attachment glycoprotein; F, fusion glycoprotein; and L, RNA dependent RNA polymerase, are conserved among all paramyxoviruses. NS1, non-structural protein 1 and NS2, non-structural protein 2 and M2, are specific to pneumoviruses (Huang et al., 1985).

1.7.5 **Virus structure**

RSV is pleiomorphic virus, characterised by the formation of large spherical membrane bound virions, asymmetric shaped virions and filamentous virions (Liljeroos et al., 2013; Kiss et al., 2014). RSV filaments are approximately 120-200nm in width and can extend for many microns in length (Liljeroos et al., 2013; Kiss et al., 2014; Ke et al., 2018). Despite containing genome, the infectivity of spherical virions is substantially less than filamentous virions, suggesting spherical virions may be the result of collapsed or defective virions. Freeze-thawing results in

a higher proportion of spherical virions, coupled with a loss of infectivity (Liljeroos et al., 2013).

The surface of the virion is coated in the fusion glycoprotein (F) and attachment glycoprotein (G) (Figure 1-6A). Glycoproteins are arranged in a helical array, which is mediated by the matrix layer (Conley et al., 2021). Glycoproteins also appear to cluster into pairs, which may reflect functional pairing of F and G (Conley et al., 2021). Infectivity is driven by the conformation of the F protein. F can exist in pre-fusion or post-fusion conformations. Ke *et al.* demonstrated that on filaments, F is predominantly in the pre-fusion conformation, while on spherical particles it is predominantly post-fusion (Ke et al., 2018). Liljeroos *et al.* however identified filaments with both pre- and post- fusion conformations (Liljeroos et al., 2013). Formalin inactivated virions have been shown to contain F in the post-fusion conformation (Killikelly et al., 2016). The transition from pre-post fusion is irreversible and on infectious virions mediates membrane fusion (described in section 1.7.6.1). Therefore, virions predominantly containing F in the post-fusion have a substantial loss in infectivity. The RSV envelope also contains pentameric ion channels consisting of SH protein (Gan et al., 2012). SH is expressed in much lower abundancy than F and G.

The viral envelope is derived from the host cell membrane. RSV infection was demonstrated to alter the lipid content of host cells, therefore composition of RSV envelopes may be altered compared to the host plasma membrane. RSV incorporates integral membrane protein Caveolin-1 in distinct clusters within mature virions (Brown et al., 2002).

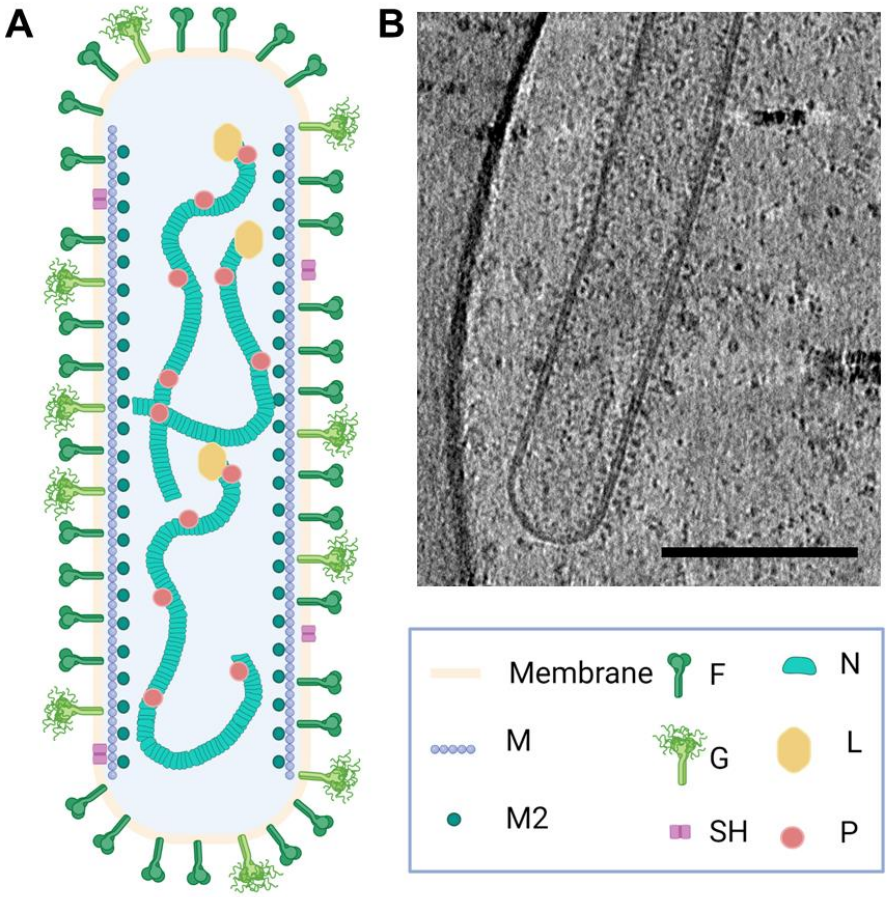

Figure 1-6: Structure of respiratory syncytial virus. (A) Schematic of the structure of an RSV filament showing organisation of glycoproteins, matrix layer, M2-1 and RNPs. (B) Image of an RSV filament generated by cryo-electron tomography. Scale bar indicates 200 nm.

The matrix layer sits approximately 5 nm underneath the viral envelope (Liljeroos et al., 2013; Kiss et al., 2014). Matrix (M) protein monomers dimerize to their biologically active form (Förster et al., 2015), before oligomerizing into curved sheets (Conley et al., 2021). This results in a helically ordered assembly of M protein (Conley et al., 2021), that forms a tubular structure in filamentous virions (Liljeroos et al., 2013). The coverage of the matrix layer varies between virus morphologies, with filamentous viruses having the greatest amount of matrix, while spherical particles only have around 25% of membrane associated with matrix (Kiss et al., 2014). In filaments, the matrix layer does not extend to the tip of the filament (Liljeroos et al., 2013). Underneath the M matrix layer is a second, less ordered layer composed of M2-1 protein (Figure 1-6A) (Kiss et al., 2014; Ke et al., 2018). The M2-1 protein acts as a linker, between the N-terminal domain of M in the matrix

layer (Li et al., 2008) and the RNA genome in the RNP complex (Cuesta et al., 2000).

The RSV RNA genome is packaged with nucleoprotein (N) to form a ribonucleoprotein (RNP) complex (Figure 1-6A). The RNA-N complex forms a flexible left-handed helical nucleocapsid structure (Liljeroos et al., 2013; Bakker et al., 2013), that has a characteristic herringbone appearance by TEM (Bhella et al., 2002b). Nucleocapsid ring structures have also been detected within RSV filaments and may represent transverse cross sections through larger RNP assemblies or may be products of aborted replication cycles (Bhella et al., 2002b; Conley et al., 2021). The RdRP L protein and the phosphoprotein (P) also associate with the RNP to form the RNP complex (Cao et al., 2020). RSV virions, along with other paramyxoviruses, are polyploid, therefore multiple copies of the RSV genome packaged into nucleocapsids are incorporated into virions (Figure 1-6A) (Loney et al., 2009). Genome copies appear to be incorporated in the same direction, suggesting that there may be an interaction between the RNP and the tip of budding filament or M2-1 layer that directs directional packaging (Liljeroos et al., 2013).

1.7.6 **Replication cycle**

RSV preferentially infects ciliated cells in the upper respiratory tract and type I pneumocytes in the lung (Johnson et al., 2006). RSV tropism is further discussed in Chapter 5. The replication cycle of RSV is described in the following section (Figure 1-7).

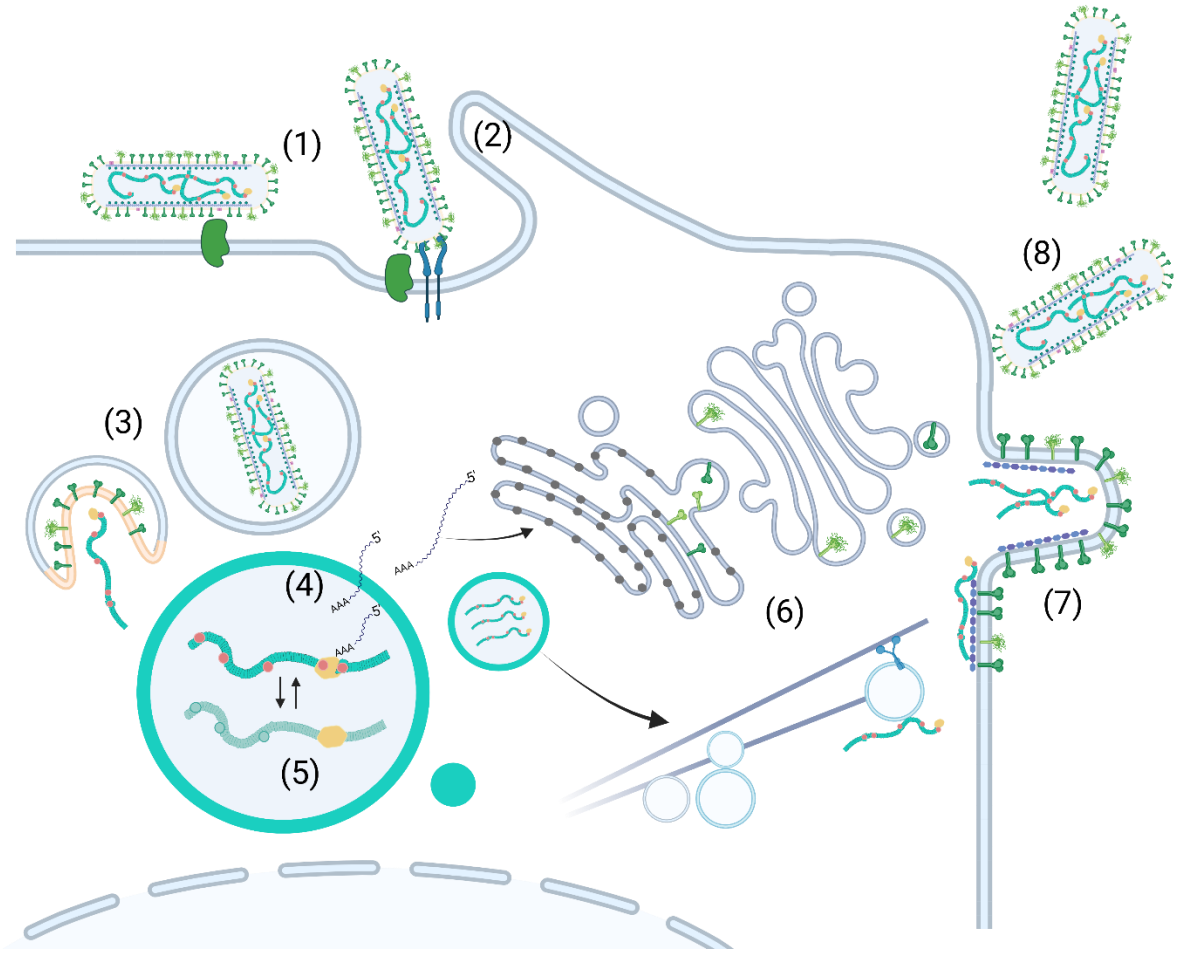

Figure 1-7: Respiratory syncytial virus replication cycle. Attachment glycoprotein, G, engages with receptors on the cell surface and fusion glycoprotein, F, engages with IGFR-1, which activates a signaling cascade that results in upregulation of co-receptor nucleolin at the cell surface (1). RSV virions are internalised by micropinocytosis, or fusion between viral and cellular membrane occurs directly at the plasma membrane (2). Conformational changes in the F protein induce fusion between viral and cellular membranes, allowing release of RSV RNPs into the cytoplasm (3). Transcription of viral genes occurs in the cytoplasm and is mediated by the RSV polymerase. Viral mRNAs are transported to the endoplasmic reticulum for translation. As N and P proteins accumulate within the cell, inclusion bodies are formed, which function as concentrated sites for transcription and replication. Sequential transcription of viral genes starts at the 3' end of the genome and production of individual mRNAs are regulated by gene start and end sequences (4). Replication of the viral genome occurs within cytoplasmic inclusion bodies. Replication is mediated by the viral polymerase, via an anti-sense genome copy intermediate (5). Newly synthesized RNPs are trafficked to the membrane via Rab11 mediated pathways. Envelope proteins G and F are folded

and glycosylated within the Golgi apparatus, before transport to the plasma membrane via the secretory system (6). Viral proteins concentrate in lipid raft regions of the plasma membrane, in a process coordinated by F. Matrix polymerisation and interactions with F actin drive filament assembly and elongation (7). Some RSV virions are released and many remain cell associated (8).

1.7.6.1 Attachment, Entry & Uncoating

RSV attaches to respiratory epithelial cells via G, the attachment glycoprotein (Figure 1-7) (Levine et al., 1987). The outward facing domain of the G protein is composed of two large mucin like region and a heparin binding region. In cell culture systems, the heparin binding domain of G mediates interactions with glycosaminoglycans (GAGs) on the surface on membrane proteins (Feldman et al., 1999). Heparin sulphate was identified as an important attachment factor for RSV infection (Krusat and Streckert, 1997), however, the abundance of heparin sulphate in the airway epithelium is unclear and this finding may be a reflection of the in vitro cell culture system (Zhang et al., 2005; Johnson et al., 2015). CX3C-chemokine receptor 1 (CX3CR1) was also identified as an attachment factor (Tripp et al., 2001; Johnson et al., 2015), and studies in primary differentiated models of the airway epithelium show that RSV colocalizes with CX3CR1 in a G-dependent manner (Jeong et al., 2015).

Once attached to the cell, the F glycoprotein binds to receptor, insulin-like growth factor 1 receptor (IGF1R) (Figure 1-7). This initiates a signaling cascade, activating Protein Kinase C zeta (PKCζ), which facilitates the recruitment on nucleolin from the nucleus to the cell surface (Griffiths et al., 2020). The F1 subunit binds to nucleolin, which acts as a co-receptor, facilitating membrane fusion and entry to the cell (Tayyari et al., 2011)). The location of the fusion event is unclear. Studies report that fusion occurs in cholesterol rich regions of the plasma membrane (San-Juan-Vergara et al., 2012), while a two-step process involving the endocytic pathway has also been described (Krzyzaniak et al., 2013). Krzyzaniak *et al.* describes the internalisation of RSV by macropinocytosis. Following internalisation, proteolytic cleavage of the F protein by a Furin-like protease induces the conformational change in F, inducing fusion of the viral and endosomal membranes (Figure 1-7) (Krzyzaniak et al., 2013). This cleavage event replaces the requirement for the

endosome to become acidified before fusion can occur. It is possible the RSV utlises both pathways to mediate entry, depending on the situation.

On infectious virions, the majority of F proteins adopt the pre-fusion conformation. The pre-fusion conformation is unstable however, and a low energy barrier is required for it to irreversibly re-fold into the post fusion conformation (Liljeroos et al., 2013). The trigger for conformational change when the virion comes into close contact with a target membrane is not full elucidated. The F protein is a trimer, which contains two fusion peptides per monomer that are buried in the centre of the protein in the pre-fusion conformation. On refolding, the trimer of F1 subunits of F refold into an α-helix bundle and the fusion peptides extend and insert into the proximal membrane. The F1 domain then continues to refold into trimer of hairpins motif, that brings the membranes close enough together for fusion to occur (Zhao et al., 2000). Once fusion of the membranes has occurred, RSV RNP is released into the cytoplasm.

1.7.6.2 Transcription and genome replication

Transcription and replication occur in the cytoplasm (Figure 1-7). Both processes are carried out by the RdRP complex, composed of polymerase (L) and cofactor (P). As well as ribonucleotide polymerisation, L mediates 5' capping and cap methylation (Liuzzi et al., 2005; Cao et al., 2020). The P protein binds to L and induces conformational changes to bring together L protein domains into a closed conformation (Cao et al., 2020), which changes again to the open conformation once the RNA-nucleocapsid genome have been recruited. The P protein also acts as a tether, to join the L protein to the RNA-nucleocapsid genome and also binds to M2-1 (Selvaraj et al., 2018), which is required for RdRP transcriptase activity, but not for replicase activity (Yu et al., 1995; Fearns and Collins, 1999).

Transcription is initiated at the promoter in the 3' leader region of the genome (Tremaglio et al., 2013). This is the only promoter therefore transcription can only be initiated at this site. The RdRP complex carries out transcription of viral genes using a stop-start process, guided by the gene start and gene end signals flanking each gene (Kuo et al., 1997). When the polymerase reaches the gene start sequence of a gene it begins transcription. The complementary sequence to the

gene start signal on the nascent RNA is signal for 5' capping and methylation by the L protein (Sutto-Ortiz et al., 2021), this process is essential for mRNA elongation (Liuzzi et al., 2005). M2-1 prevents premature termination of transcription, facilitating the transcription of full-length mRNAs (Fearns and Collins, 1999). When the RdRP complex reaches the gene end signal, it encounters a polyU signal, which causes polymerase stuttering and the polyadenylation of the 3' end of the transcript (Kuo et al., 1997). The capped and polyadenylated mRNA transcript is then released and the polymerase complex continues to the next gene.

Genome replication is also carried out by the RdRP complex, but without the requirement for M2-1 (Yu et al., 1995). In genome replication, the polymerase complex does not respond to gene start or gene end sequences, producing a full-length anti-sense copy of the genome. The nascent anti-sense genome strand is encapsulated by nucleoprotein as replication progresses. Accumulation of low abundance protein, M2-2 (Bermingham and Collins, 1999); the binding of free nucleoprotein to P (Cao et al., 2020); and the association of matrix protein (M) to inclusion bodies (Ghildyal et al., 2002) are all proposed to be the mechanisms to induce switching between transcriptase and replicase activity. Once the anti-sense nucleocapsid has been produced, this serves as a template for production of new copies of the negative sense viral genome, which is encapsulated by newly translated nucleoprotein as replication progresses to form new viral RNPs.

Transcription and replication occur within cytoplasmic inclusion bodies (Figure 1-7) (Lahaye et al., 2009). These are generated early during the infection cycle and the assembly of N and P were shown to be the minimal elements required for their formation (Galloux et al., 2020). These cytoplasmic bodies become factories of viral replication, to which other factors are recruited at different stages in the replication cycle, including host proteins involved in translation (Rincheval et al., 2017) and control of immune responses (Lifland et al., 2012).

1.7.6.3 Translation, maturation and trafficking of viral components

Viral proteins are translated in the ER (Figure 1-7). Unlike IAV, RSV does not induce host shutoff by degrading host mRNAs. Instead, RSV uses a number of mechanisms involving different viral proteins. RSV manipulates the ER stress

response to generate cytoplasmic stress granules that are distinct from viral inclusion bodies (Cervantes-Ortiz et al., 2016). Accumulation of SH in the Golgi apparatus has been implicated in this process (Triantafilou et al., 2013; Cervantes-Ortiz et al., 2016). Inclusion body associated granules (IBAGs) are also formed during replication. These granules are positive for M2-1 and viral mRNA, but negative for N, P and L (Rincheval et al., 2017). It has been proposed that the formation of stress granules and IBAGs function as mRNA sorting stations within the cell, that may help to improve efficiency of translation of viral mRNAs (Rincheval et al., 2017). However, the function of stress granule formation in RSV infection is yet to be fully established. Non-structural protein 1 (NS1) has also been demonstrated to down-regulate transcription of host genes, by binding to regulatory elements on regions of chromatin near genes that are differentially regulated during RSV infection, including antiviral IFIT-family proteins (Pei et al., 2021). Additionally, M localises to the nucleus during the early stages of infection (Ghildyal et al., 2003), where it likely disrupts nuclear export of host mRNAs by binding to components of the nuclear pore complex (Faria et al., 2005).

Transmembrane proteins F, G and SH are inserted into the membrane and folded in the ER before post-translational modifications are carried out in the Golgi apparatus (Figure 1-7) (Collins and Karron, 2013). G is highly glycosylated with N- and O-linked glycans and glycosylation occurs within the trans-Golgi network (Collins and Mottet, 1992). Membrane proteins are targeted to the apical plasma membrane via the trans Golgi network secretory pathway.

Similar to IAV, the Rab11 mediated trafficking through the endosomal recycling pathway has been implicated in the transport of viral components to the plasma membrane (Figure 1-7) (Brock et al., 2003). Rab11-FIP2 mediates RSV transport within the apical recycling system and is involved in viral budding (Utley et al., 2008). To coordinate trafficking and assembly of both viral RNPs, comprised of the vRNA genome, N, L, P and M2-1, and envelope proteins, F, G and SH, the matrix protein, M, is recruited to both inclusion bodies (Ghildyal et al., 2002) and lipid raft regions of the plasma membrane (Marty et al., 2004). M coordinates the transport of RNPs from inclusion bodies to the plasma membrane, and the absence of M results in accumulation RNP in inclusion bodies. Mitra *et al.* demonstrated that in M null-mutant cells, localisation of N, G and F is diffuse and not targeted to viral filaments,

indicating that M plays an essential role in both coordinating trafficking of viral proteins, and formation of filamentous particles (Mitra et al., 2012).

1.7.6.4 Assembly and Budding

Assembly of viral components preferentially occurs in lipid raft regions of the plasma membrane (Figure 1-7) (McCurdy and Graham, 2003; Fleming et al., 2006; Chang et al., 2012). The transmembrane domain and cytoplasmic tail of F have been implicated in its concentration to lipid raft microdomains at the apical surface of cells (Oomens et al., 2006). F is proposed to play a role in coordinating viral assembly at the plasma membrane as it independently localises to budding regions while other proteins do not (Henderson et al., 2002; Oomens et al., 2003; Fleming et al., 2006).

RSV assembly is also proposed to occur within the cytoplasm. Vanover *et al.* suggest that assembly of filaments occurs within the cytoplasm, in endosomal compartments. Vesicles containing RSV glycoproteins go through a process of extension, mediated by dynein and the microtubule network. These extended vesicles then fuse to vesicles containing the RNP complex and M protein, before finally fusing with the plasma membrane, where particle elongation occurs (Vanover et al., 2017).

Ke *et al.* used cryo-electron tomography to visualize RSV budding sites and showed that assembly initiates at the plasma membrane, where first virion components assemble at the plasma membrane, before the virion elongates and protrudes from the membrane (Ke et al., 2018). RSV filaments have been demonstrated to incorporate F actin, suggesting a role for actin in driving filament assembly or elongation (Jeffree et al., 2007; Liljeroos et al., 2013). Dimerization of M1 is essential for the budding of viral filaments, and mutagenesis of the dimer interface blocks filament formation (Förster et al., 2015). Polymerisation of M dimers into a helical lattice then drives filament elongation (Mitra et al., 2012; Förster et al., 2015; Conley et al., 2021). Finally, membrane scission occurs independently of the ESCRT complex and Vsp4, in a process involving Rab11-FIP2 (Utley et al., 2008).

1.7.6.5 Immune antagonism

RSV encodes two specific proteins that antagonize the host innate immune system: NS1 and NS2 (Chatterjee et al., 2017; Pei et al., 2021). These genes are positioned at the 3' end of the genome, meaning they are quickly transcribed upon infection (Collins et al., 1986). Additionally, structural proteins have also been shown to contribute to immune evasion (Ghildyal et al., 2003; Bukreyev et al., 2008; Lifland et al., 2012).

NS1 and NS2 prevent the induction of interferon signaling. NS1 interferes with the pattern recognition receptor RIG-I indirectly, by targeting down-stream effectors. NS1 directly interacts with MAVs to block its interaction with RIG-I (Boyapalle et al., 2012). It also interacts with TRIM25, to prevent ubiquitination of RIG-I (Ban et al., 2018). NS2 directly interacts with the N-terminal domain itself, which prevents its association with MAVS (Ling et al., 2009). RSV also sequesters melanoma differentiation-associated gene 5 (MDA5) and MAVs, but not RIG-I, within RSV inclusion bodies via interactions with N (Lifland et al., 2012) NS1 and NS2 prevent the transcription of type I and II interferons by blocking transcriptional regulators. NS1 and NS2 prevent nuclear translocation of IRF3 and NS2 inhibits Nuclear Factor κB (NF-κB) (Spann et al., 2003).

NS1 and NS2 also block the induction of a response to interferon. As described in section 1.7.6.3, NS1 induces host shut off by binding directly to chromatin. Many of the regions that NS1 interacts with are enhancer sequences proximal to genes involved in the interferon response (Pei et al., 2021). NS1 induces the expression of a micro-RNA, which downregulates the expression of interferon alpha/beta receptor 1 (IFNAR1), thus reducing the sensitivity of cells to interferon (Zhang et al., 2016). NS1 and NS2 have been implicated regulation of the Signal Transducer and Activator of Transcription (STAT) proteins by multiple mechanisms. NS1 has E3 ligase activity, which targets STAT2 for degradation (Elliott et al., 2007). NS2 reduces phosphorylation, and therefore activation, of STAT1 (Ramaswamy et al., 2006). NS1 also prevents nuclear translocation of STAT2 proteins (Lo et al., 2005).

RSV also produces a soluble G protein from an alternative translational start codon within the transmembrane domain (Roberts et al., 1995). Soluble G is produced in abundance during early infection and secreted from cells, where it acts as decoy antigen for antibodies, allowing virions to evade neutralisation (Bukreyev et al.,

2008). Further, a fractalkine-like motif on the membrane bound G has been demonstrated to reduce the influx of CX3CR1 positive leukocytes, including NK cells and T lymphocytes (Harcourt et al., 2006).

1.8 Scope of project

A diverse group of respiratory viruses cocirculate in human populations and occupy a shared ecological niche. Virus-virus interactions have been demonstrated to occur at the individual host level and impact observable outcomes including viral dynamics at the population scale and clinical outcomes of infections. Coinfection occurs quite frequently, however the biological mechanisms underpinning viral interactions at the host level remain poorly characterised, and this represents a substantial gap in our understanding of respiratory viral biology. It is currently unknown how unrelated respiratory viruses interact if both are replicating within the same respiratory tissue of a coinfected host. Additionally, the extent to which cellular coinfection occurs during natural infection is unclear and the implications of cellular coinfection are unknown. Further, within a coinfected cell, the potential points of interaction between viruses are yet to be elucidated.

In this project, I sought to address some of these gaps in our understanding of viral interactions, by carrying out fundamental coinfection experiments to examine features of coinfected cells that may help identify specific points of viral interaction between taxonomically unrelated respiratory viruses. IAV and RSV were selected as model viruses for these experiments for a number of reasons. Firstly, these viruses are of extremely high clinical importance and contribute significantly to the global burden of respiratory disease. IAV and RSV have shared epidemiological features: the prevalence of both viruses peak during the winter season in temperate climates, and both viruses have a propensity to infect children and elderly populations. IAV and RSV also share tropism for cell types within the respiratory tract, so there is potential for direct contact between IAV and RSV infectious foci. Therefore, using a model of IAV and RSV coinfection, the overarching aim of this research project was to further the understanding of the biological mechanisms underpinning virus-virus interactions within coinfected cells and contribute to the understanding of the possibility of these events occurring during coinfection in the respiratory tract.

Chapter 2

Materials and Methods

2.1 Materials

2.1.1 Cell lines

Human alveolar adenocarcinoma cell line (A549) cells (American Type Culture Collection [ATCC], CCL-185), Madin Darby canine kidney (MDCK) cells (ATCC, CCL-34) and HEp-2 (ATCC, CCL-23) cells were cultured in Dulbecco's minimum essential media (DMEM), high glycose GlucoMAX with 10% foetal bovine serum (FBS). Cells were maintained at 37˚c, 5% CO_2 in a humidified incubator.

2.1.2 Primary cells

Human bronchial epithelial cells (hBEC) (Epithelix) were cultured in Epithelix human airway epithelial cell medium (Epithelix; EP09AM) 37˚c, 5% CO_2 in a humidified incubator. Cells were cultured in tissue culture flasks until 80% confluent. At this point, cells were trypsinised and seeded at $2x10^4$ cells/transwell onto transwell inserts for 24-well plate with 0.4 µm pore size with a pore density of $1.6x10^6$ pores per cm^2 (Falcon, 734-0036). When cells were fully confluent on transwell membranes, apical media was removed to initiated air-liquid interface (ALI). Basal media was replaced with Pneumacult-ALI media (STEMCELL Technologies, 05001). Basal media was replenished every 2-3 days. When cultures began producing mucus (approximately 20 days post ALI initiation), the apical surface of cultures was washed twice weekly with serum free DMEM.

2.1.3 Viruses

H1N1 influenza A/Puerto Rico/8/34 was rescued using an 8-plasmid rescue system in 293T cells and virus stocks were propagated in MDCK cells. 'Color-flu' virus A/Peurto Rico/8/34 with mCherry reporter insert in the NS1 gene open reading frame (Fukuyama et al., 2015) were kindly provided by Dr Edward Hutchinson and Dr Jack Hirst. RSV strain A2 (American Type Culture Collection, VR-1540) was grown in HEp-2 cells. RSV strain A2 containing GFP reporter gene was kindly provided by Professor Massimo Palmarini.

2.1.4 Antibodies

2.1.4.1 Table 2-1: List of primary antibodies

Target	Supplier	Catalogue number	Species	Working dilution
RSV nucleoprotein	Abcam	AB22501	Mouse monoclonal	1/1500
RSV fusion protein	Abcam	AB24011	Mouse monoclonal	1/1000
RSV (whole virus)	Abcam	AB20745	Goat polyclonal	1/500
IAV nucleoprotein	European Veterinary Society (EVS)	EVS238	Mouse monoclonal	IF: 1/1000 Plaque assay: 1/3000
IAV haemagglutinin	National Institute of Biological Standards and Controls (NIBSC)	03/242	Sheep polyclonal	1/1000
IAV haemagglutinin	Sinobiological	11684-MM03	Mouse monoclonal	1/500
Myxovirus resistance protein (MxA)	Kindly provided by Georg Kochs	M143	Mouse monoclonal	1/1000
Cleaved caspase 3 (CC-3)	R&D Systems	AF835	Rabbit	1/1000

2.1.4.2 Table 2-2: List of secondary antibodies

Target	Conjugate	Supplier	Catalogue number	Species	Working dilution
Mouse IgG	Alexafluor-488	Sigma Aldrich	SAB4600056	Rabbit	1/1000
Mouse IgG	Alexafluor-594	Abcam	AB150108	Donkey	1/1500
Mouse IgG	Horse radish peroxidase (HRP)	Cell Signalling	7076S	Horse	1/1500
Sheep IgG	Alexafluor-594	Thermo Fisher	A-11016	Donkey	1/1000
Goat IgG	Alexa	Abcam	AB175704	Donkey	1/500

2.2 General Methods

2.2.1 Preparation of IAV stocks

IAV stocks were propagated in MDCK cells. MDCK cells were seeded to achieve 100% confluency on the day of infection. Flasks were inoculated with 10-100 pfu of low passage IAV stock for 1 hour, resulting in an MOI of approximately $1x10^{-5}$. After this, inoculum was removed and replaced with serum free DMEM with 1µg/ml trypsin-TPCK. Flasks were incubated 37˚c, 5% CO_2 for 1-2 days until 90% cells had detached from the flask. Fluorescent reporter virus stocks were also monitored for fluorescence using a widefield fluorescent microscope. Media was collected from the flask and centrifuged at 1500 rpm for 10 minutes. Supernatant was retained and aliquoted, and stocks were stored at -80˚c.

2.2.2 Preparation of RSV stocks

RSV stocks were propagated in HEp-2 cells. HEp-2 cells were seeded in tissue culture flasks to achieve 70% confluency on the day of infection. Flasks were inoculated with low passage RSV stock at multiplicity of infection (MOI) 0.01 for 1.5 hours. After this, inoculum was removed and cells were washed once with Dulbecco's phosphate buffered solution (DPBS), before replacing with DMEM with 5% FBS. Flasks were incubated for 3-5 days at 37˚c, 5% CO_2 until approximately 80-90% cytopathic effect was observed. RSV-GFP virus stocks were monitored for fluorescence using a widefield fluorescent microscope. For harvesting viral stocks, half of the volume of the media was retained, and cells were scraped and combined with this media in a falcon tube. Sterile glass beads were added to the falcon and stocks were vortexed for 1 minute to destroy cells and release cell associated virus particles. Stocks were then centrifuged at 1500-3000 rpm for 10 minutes, and supernatant was aliquoted to individual vials. Stocks were flash frozen on dry ice before transfer to -80˚c.

2.2.3 Titration of IAV stocks

Ten-fold serial dilutions of virus were prepared in MEM with 1µg/ml trypsin TPCK, 1µg/ml penicillin/streptomycin. Confluent MDCK cell monolayers were inoculated with sample dilutions and at 37°c for 1 hour, before overlay with infection media containing 0.6% Avicel. Plates were incubated at 37°c for 48 hours, followed by fixation with 4% formaldehyde and staining with 10% coomasie blue solution. Plaques were counted from duplicate wells and the mean count used to calculate titre in plaque forming units per millilitre (pfu/ml).

For titration in A549 cells, serial dilutions were prepared in MEM, with 1% FBS, 1µg/ml trypsin TPCK and 1µg/ml penicillin/streptomycin. Cell monolayers were inoculated with serial dilutions for 1 hour before overlay with infection media containing 0.6% Avicel. Plates were incubated for 72-96 hours, followed by fixation with 4% formaldehyde. Infectious foci were detected by immunostaining for IAV nucleoprotein. Monolayers were permeablised with 0.1% triton X100 for 10 minutes, followed by blocking in 2% bovine serum albumin (BSA) in PBS for 30 minutes. Primary antibody mouse anti-IAV nucleoprotein (NP) (European Veterinary Society, EVS238, 1/3000) was applied for 1 hour at room temperature, followed by washing with PBS. Secondary antibody rabbit anti-mouse IgG conjugated to horse radish peroxidase (HRP) (Cell Signalling, 7076S, 1/1500) was applied for 1 hour. Trueblue substrate (KPL, 5510-0050) was applied for 10 minutes, or until sufficient blue signal was detected. Foci were counted from duplicate wells and the mean count used to calculate titre in pfu/ml.

2.2.4 Titration of RSV stocks

Ten-fold serial dilutions of virus were prepared in DMEM with 5% FBS, 1µg/ml penicillin/streptomycin. Confluent HEp-2 cell monolayers were inoculated with sample dilutions and at 37°c for 1.5 hours, before overlay with infection media containing 0.6% Avicel. Plates were incubated at 37°c for 4-5 days, followed by fixation with 4% formaldehyde and staining with 10% coomasie blue solution. Plaques were counted from duplicate wells and the mean count used to calculate titre in pfu/ml.

2.2.5 Infection of A549 cells

A549 cells were seeded at $1x10^5$ cells per well in a 24-well plate, with or without 13mm glass coverslips depending on the output of the experiment. Infections were carried out when cells were approximately 80% confluent. Inoculum was prepared by diluting virus stocks in DMEM containing 2% FBS and 1µg/ml trypsin TPCK to the correct concentration to achieve the desired MOI for the experiment. For mixed infections, IAV and RSV were diluted within the same media, to produce a single inoculum volume containing both viruses. Cell monolayers were washed once with DPBS before the inoculum volume was added. Plates were incubated with inoculum at 37˚c for 1.5 hrs. Following this, the inoculum was removed, cells were washed once with DPBS and overlaid with DMEM containing 2% FBS and 1µg/ml trypsin TPCK.

2.2.6 Immunofluorescence for formalin fixed cells

Monolayers were permeablised with 0.1% triton X100 for 10 minutes, followed by blocking in 2% BSA in PBS for 30 minutes. Primary antibodies were diluted in 2% BSA in PBS and applied for 1 hour at room temperature, followed by washing with PBS. Secondary antibodies were diluted in 2% BSA in PBS and were applied for 1 hour at room temperature. Coverslips were mounted onto glass slides with Prolong Gold mounting media containing DAPI (Invitrogen, P36392). Cells in plates were incubated with 1 µg/ml Hoescht 33342 solution for 10 minutes to stain nuclei, prior to storage at 2-8˚c in DPBS.

2.2.7 Statistical analysis and data visualisation

Statistical analysis was carried out using Graphpad Prism version 9.1.0 or RStudio version 4.0.2. Statistical tests are described where applicable in the relevant method sections and figure legends within results chapters. Data was visualised using Graphpad Prism version 9.1.0 or RStudio version 4.0.2 using ggplot2 package. Figures were created in Adobe Illustrator and Biorender.com.

2.3 Chapter 3 specific methods

2.3.1 Growth curves in A549 cells

A549 cells were seeded at $2x10^4$ cells per well in a 48-well plate. A549 cells were infected with IAV, RSV or synchronously infected with a mixed inoculum of IAV and RSV, diluted in DMEM, with 2% FBS and 1µg/ml trypsin TPCK. Single infections were carried out with RSV at a multiplicity of infection (MOI) of 4 and IAV at an MOI of 4, 0.4 or 0.04. Mixed infections were carried out with RSV MOI, combined with IAV MOI 4, 0.4 or 0.04. Triplicate wells containing A549 cells were inoculated in 48-well plates and incubated at 37˚C, 5% CO_2 for 1.5 hours, before the inoculum was removed and replaced with DMEM, with 2% FBS and 1µg/ml trypsin TPCK. Cells were incubated at 37˚C, 5% CO_2 and supernatant from each infection was collected at 24, 48 and 72 hours post infection and stored at -80˚C prior to titration by plaque assay. Infectious titre was determined by plaque assay in MDCK cells or HEp-2 cells for IAV and RSV, respectively. Statistical significance was determined by Mann Witney test, * $p<0.05$, ** $p<0.01$, *** $p<0.001$, ns $p>0.05$. Infections were carried out in technical triplicate and three independent experiments were carried out.

2.3.2 Mixed infections with IAV at staggered timepoints

A549 cells were seeded at $1x10^5$ cells per well in 24-well plates. Inoculum was prepared in DMEM, with 2% FBS and 1µg/ml trypsin TPCK. Cells were infected in triplicate with RSV at MOI 4 for 1.5 hours, followed by replacement of inoculum with DMEM, with 2% FBS and 1µg/ml trypsin TPCK. Cells were the incubated at 37˚C, 5% CO_2 for 6, 16 or 24 hours, before media was removed and replaced with inoculum containing IAV at MOI 0.04. Inoculum was applied for 1.5 hours, before removal and replacement with DMEM, with 2% FBS and 1µg/ml trypsin TPCK. A synchronous (0 hours) mixed infection was also carried out using a mixed inoculum of RSV at MOI 4 and IAV at MOI 0.04. At 24 hours post IAV infection, media was collected from each well and frozen at -80˚c, prior to determination of IAV infectious titre by plaque assay in MDCK cells. Experiments were carried out in technical triplicate and two independent experiments were carried out.

To determine the level of RSV infection at each experimental timepoint, A549 cells were seeded at $1x10^5$ cells per well on 13 mm glass coverslips in 24-well plates. Cells were infected with RSV at MOI 4 for 1.5 hours and then incubated at 37˚C, 5% CO_2 for 0, 6, 16 or 24 hours. Following incubation, plates were washed with PBS and fixed with 4% formaldehyde. Cells were stained according to the protocol detailed in section 2.2.6, using primary antibody mouse anti-RSV nucleoprotein (Abcam, AB22501, 1/1500) and secondary antibody rabbit anti-mouse IgG conjugated to alexafluor 488 (Sigma-Aldrich, SAB4600056, 1/1000). Confocal microscopy was carried out using Zeiss LSM880 AxioObserver microscope (ZEISS, Germany). Standard images were collected using GaAsP detector with 405 nm and 488 nm excitation lasers, using 40x/1.4 plan-apochromat oil DIC M27 objective.

2.3.3 Determining proportions of infected A549 cells

A549 cells were seeded at $1x10^5$ cells per well on 13 mm glass coverslips in 24-well plates. A549 cells were infected with IAV, RSV or synchronously infected with a mixed inoculum of IAV and RSV, diluted in DMEM, with 2% FBS and 1µg/ml trypsin TPCK. Single infections were carried out with RSV at a multiplicity of infection (MOI) of 4 and IAV at an MOI of 4, 0.4 or 0.04. Mixed infections were carried out with RSV MOI, combined with IAV MOI 4, 0.4 or 0.04. Virus was incubated on cells for 1.5 hours at 37˚C, 5% CO_2, before replacement with DMEM, with 2% FBS and 1µg/ml trypsin TPCK. Plates were incubated at 37˚C, 5% CO_2 for 8 hours or 24 hours, prior to washing once with DBPS and fixation with 4% formaldehyde.

Infected cells were detected by immunostaining using the protocol described in section 2.2.6, using primary antibodies sheep anti-IAV haemagglutinin (HA) (National Institute of Biological Standards and Controls [NIBSC], 03/242, 1/1000) and mouse anti-RSV nucleoprotein (Abcam, AB22501, 1/1500) and secondary antibodies donkey anti-sheep IgG conjugated alexafluor 594 (Thermo Fisher, A-11016, 1/1500) and rabbit anti-mouse IgG conjugated to alexafluor 488 (Sigma-Aldrich, SAB4600056, 1/1000). Confocal microscopy was carried out using Zeiss LSM880 AxioObserver microscope (ZEISS, Germany). Standard images were collected using GaAsP detector with 405nm, 488nm and 598nm excitation lasers, using 40x/1.4 plan-apochromat oil DIC M27 objectives. Images were collected as a 3 x 3 tile scan and stitched together on Zeiss Zen Black software. Three tile scans

per coverslip were collected and areas were selected based on cell density using the DAPI channel. Images were processed using ImageJ version 1.53c. Window and level adjustments were made using the auto threshold, before colour channels were combined. Cells were counted manually using the cell counter plugin. Data was analysed in Graphpad Prism version 9.1.0. Statistical significance determined by Mann Witney test, * $p<0.05$, ** $p<0.01$, *** $p<0.001$, ns $p>0.05$. Infections were carried out in technical triplicate and three independent experiments were carried out.

2.3.4 Immunofluorescence of Viral Proteins

A549 cells were seeded at $1x10^5$ cells per well on 13 mm glass coverslips in 24-well plates. Cells were infected with RSV MOI 4, IAV MOI 1 or a mixed inoculum of both viruses for 1.5 hours before media was replaced with DMEM, with 2% FBS and 1µg/ml trypsin TPCK. At 24 hpi, cells were washed with DPBS and fixed with 4% formaldehyde.

For co-staining with IAV NP and RSV N primary antibodies, coverslips were blocked with neat rabbit serum (Gentex, USA, GTX73221) for 30 minutes, followed by washing with PBS. Mouse anti-RSV N primary antibody (Abcam, AB22501, 1/1500) was diluted in 2% BSA in PBS and applied to coverslips for 1 hour at room temperature, followed by washing with PBS. Next, rabbit anti-mouse secondary antibody was diluted in 2% BSA in PBS and applied to coverslips for 1 hour, followed by washing with PBS. Samples were then subjected to a secondary blocking step in neat donkey serum (Gentex, USA, GTX73205), followed by staining with mouse anti-IAV NP primary antibody (European Veterinary Society, EVS238, 1/1000) and donkey anti-mouse IgG (Abcam, ab150108, 1/1000) as described in primary staining step. Slides were mounted with Prolong Gold mounting media with DAPI.

For co-staining with IAV HA and RSV F, the general immunofluorescence protocol described in section 2.2.6 was used. Coverslips were stained with primary antibodies sheep anti-IAV haemagglutinin (HA) (NIBSC, 03/242, 1/1000) and mouse anti-RSV F (Abcam, ab24011, 1/1000), followed secondary antibodies donkey anti-sheep IgG conjugated alexafluor 594 (Thermo Fisher, A-11016, 1/1500) and rabbit anti-mouse IgG conjugated to alexafluor 488 (Sigma-Aldrich, SAB4600056, 1/1000).

Confocal microscopy was carried out using Zeiss LSM880 AxioObserver microscope (ZEISS, Germany). Standard images were collected using GaAsP detector with 405 nm, 598 nm and 488 nm excitation lasers, using 40x/1.4 or 63x/1.4 plan-apochromat oil DIC M27 objective. Images were processed using FIJI, version 1.53c. Imaging experiments were carried out at least twice independently.

2.3.5 Live cell Imaging

A549 cells were seeded at $1x10^5$ cells per well in 24-well plates. Triplicate wells were infected with PR8-mcherry at MOI 1, RSV-GFP at MOI 1, a mixed inoculum of both viruses or mock infected with DMEM for 1.5 hours, before media was replaced with DMEM, with 2% FBS and 1µg/ml trypsin TPCK, containing 1µg/ml Hoescht 33342 solution (Thermo Fisher Scientific, 62249) to stain nuclei. Plates were then transferred to a humidified chamber at 37˚c, 5% CO_2 attached to Zeiss Live cell observer microscope. The plane of focus was registered for each well manually before imaging was started. Images were collected from three positions in each well every 15 minutes for 64 hours.

Raw image data was processed to time series using Zen Blue software version 2.6. Fluorescent signal area was quantified using ImageJ version 1.53c. Time series were imported to FIJI as an image sequence and split to individual image channels. Window and level were adjusted using the zero hours image as a threshold for fluorescent signal and applied to the whole time series. Fluorescent signal was then binarized using the auto threshold command. The following macro was developed to select fluorescent signal as a region of interest and measure fluorescent area in pixels for in each individual timepoint image and collate data into a single results file.

```
Run("Set Measurements…", "area redirect=None decimal=3");
For (n=1; n <=258; n++)
{ setSlice(n);
Run("Create Selection");
Run("ROI Manager…");
roiManager("Add") }
roiManager("Measure");
selectWindow("Results")
```

To measure timing of cell death, ten cells were selected at random from the first frame of each timeseries for all infection conditions. Cells were manually tracked through the timeseries until they underwent cell death, identified by morphological changes indicating cell destruction. The frame at which cells were detected to have undergone cell death was recorded and converted to time post infection.

2.4 Chapter 4 specific methods

2.4.1 Super resolution confocal imaging

A549 cells were seeded at $1x10^5$ cells per well on 13 mm glass coverslips in 24-well plates. Cells were infected with RSV MOI 4, IAV MOI 1 or a mixed inoculum of both viruses for 1.5 hours before media was replaced with DMEM, with 2% FBS and 1µg/ml trypsin TPCK. At 24 hpi, cells were washed with DPBS and fixed with 4% formaldehyde. The general immunofluorescence protocol described in section 2.2.6 was used. Coverslips were stained with primary antibodies sheep anti-IAV HA (NIBSC, 03/242, 1/1000) and mouse anti-RSV F (Abcam, ab24011, 1/1000), followed secondary antibodies donkey anti-sheep IgG conjugated alexafluor 594 (Thermo Fisher, ab150108, 1/1500) and rabbit anti-mouse IgG conjugated to alexafluor 488 (Sigma Aldrich, SABA00046, 1/1000).

For live cell staining, cells were seeded at $1x10^5$ cells per dish in 35 mm glass bottom dishes. Thirty minutes prior to initiating staining, cell culture media was replaced with DMEM containing 1 µg/ml Hoescht 33342 solution (Thermo Fisher Scientific, 62249). Cells were maintained on ice throughout the staining protocol. Cells were washed with PBS prior to incubation with primary antibodies targeting IAV HA and RSV F as described above, for 5 minutes on ice. Cells were washed with PBS, followed by incubation with anti-sheep IgG and anti-mouse IgG secondary antibodies as described above for 5 minutes on ice. Cells were washed with PBS and kept in cold PBS on ice. Following staining, samples were immediately imaged by confocal microscopy.

Super resolution confocal microscopy was carried out using Zeiss LSM880 AxioObserver microscope (ZEISS). Images were collected using the airyscan detector with 405 nm, 598 nm and 488 nm excitation lasers, using 63x/1.4 plan-apochromat oil DIC M27 objective. Z stacks were collected at 100 nm intervals.

2.4.2 Image processing and analysis

Images were processed using ImageJ, version 1.53c. Z stacks were visualised using Zen Blue version 2.6, using the cut function to generate a two-dimensional image. Three dimensional images were visualised in Imaris viewer version 9.8.0. Imaging experiments were carried out at least twice independently.

Fluorescence intensity profiles along filaments were collected in Zen Blue version 2.6, using the profile function. All filaments within the selected region were measured by using the line tool to draw a line along the length of the filament from which fluorescence intensity profiles were generated.

2.4.3 Scanning electron microscopy

Cells were seeded at $2x10^5$ cells/ml on 13 mm glass coverslips in 24-well plates. Cells were infected with IAV at MOI 4, RSV at MOI 4, or a mixed inoculum of both viruses for 1.5 hours, before media was replaced with DMEM, with 2% FBS and 1µg/ml trypsin TPCK. Cells were then incubated for 24 hours at 37˚c, 5% CO_2. At 24 hpi, cells were fixed with 1.5% Glutaraldehyde in 0.1M sodium cacodylate buffer for 1 hour. Following this, samples were washed 3 times for 5 minutes each with 0.1M sodium cacodylate buffer, before incubation with 1% osmium tetroxide for 1 hour. Next, samples were stained with aqueous 0.5% Uranyl Acetate for 1 hour and further dehydrated through an ethanol series. Samples were then subjected to critical point drying using an Autosamdri-815 Critical Point Dryer (Tousimis, USA), before mounting and coating in 20nm Gold/Palladium using a Quorum Q150T ES High vacuum coating system (Quorum Technologies, UK). Images were collected using JEOL IT100 SEM at 20kV, with InTouch Scope software, version 1.05 (JEOL USA Inc., USA). Two independent experiments were carried out.

Filament width measurements were carried out in ImageJ version 1.53c. Fifty measurements were collected from filaments across five images for each infection condition. Data was visualised in RStudio using the ggplot2 package.

2.4.4 Cryo-electron Tomography

Gold 200 mesh TEM grids with holey carbon support film (Quantifoil micro tools GmbH) were placed in 35 mm glass bottom dishes. Grids were coated with 1:10 v/v laminin solution for a minimum of 6 hours prior to cell seeding. A549 cells were seeded at $4x10^4$ cells per dish, to achieve an approximate density of 1-2 cells per grid square at 24 hours post cell seeding. Cells were infected with a mixed inoculum of IAV at MOI 1 and RSV at MOI 4 for 1.5 hours, after which the media was replaced with DMEM, with 2% FBS and 1µg/ml trypsin TPCK. Cells were then incubated for 24 hours at 37˚c 5% CO_2. Prior to plunge freezing, 5 µl of 15 nm colloidal gold (British Biocell International) was added at a ratio of 1:10 v/v in DMEM. Grids were then blotted for 7 seconds from the back (no cell side) and plunge frozen into liquid ethane using the Leica EM GP 2 (Leica Microsystems).

Grids were screened on the JEOL F200 (Jeol Ltd) for quality prior to imaging for data collection. Tilt series were collected using the JEOL CRYO ARM 300 (JEOL Ltd) with an energy filter and DE64 detector (Direct Electron). Tilt series were acquired with the following parameters: voltage 300 KV, energy filter 30eV slit, 1.921 Å/pixel pixelsize, 30000x magnification, -6 µm defocus, -60˚ to +60˚ tilt with a 3˚ increment, total dose of ~92 e/ Å2 per tilt series. Tilt series were collected using a dose symmetric scheme starting at 0˚ implemented in SerialEM.

2.4.5 Tomogram construction and processing

Tilt series were aligned using alignframes module in IMOD (Kremer et al., 1996). Tomograms were then reconstructed, ctf-corrected using CTFFIND (Rohou and Grigorieff, 2015) and visualised by weighted back projection using IMOD. To aid interpretation and visualisation, tomograms were binned by a factor of four and then denoised using Topaz (Bepler et al., 2020).

2.4.6 Tomogram analysis

Filament width and glycoprotein distance was calculated using the imodinfo module in IMOD (Kremer et al., 1996). Denoised tomograms were averaged between 5-10 slices to improve contrast and glycoproteins were viewed from top down. Distances

were measured between the centres of pairs of adjacent glycoproteins. For IAV and RSV controls, spike measurements were collected from 11 individual tomograms for each virus (n=326 for IAV, n=236 for IAV). For pseudotyped virus, spike measurements were collected from each particle, from 4 individual tomograms (n=50 measurements per tomogram). Statistical difference between groups was determined by unpaired t-test.

2.4.7 Viral entry assay in sialidase treated cells

A549 cells were seeded at $1x10^5$ cells per well in 24-well plates. Cells were infected with IAV at MOI 1, RSV at MOI 4 or mixed inoculum of both viruses for 1.5 hours, before media was replaced with DMEM, with 2% FBS and 1µg/ml trypsin TPCK. Infected cells were incubated for 24 hours at 37˚c 5% CO_2. Following incubation, supernatant, containing released virus, was collected. The remaining cell monolayers were scraped and collected in suspension in DMEM. Cell suspensions were vortexed briefly to dislodge virus attached to cell fragments. Next, supernatant samples and cell suspension samples were centrifuged at 1500 rpm for 5 minutes to remove cell debris. Supernatant was retained as released and cell associated virus samples and used fresh (no freezing) in the neuraminidase assay.

Neuraminidase from *Clostridium perfringens* (Sigma-Aldrich, N2876) was prepared by reconstituting in d.H_2O to generate a 10 units/ml stock, followed by filtration through 0.45 µm sterile PES filter. The stock was stored in aliquots at -20˚c.

For the neuraminidase assay, cells were seeded at $1x10^4$ cells per well in 96-well plates 48 hours before the assay. Neuraminidase was diluted in DMEM 1mU/µl and cells were treated with 50mU neuraminidase for 2 hours. To confirm removal of sialic acids, neuraminidase treated cells and control cells were stained with biotinylated Maackia Amurensis Lectin II (MAL II) (Vector Laboratories, B-1265-1), followed by fluorescein conjugated streptavidin (Vector Laboratories, SA-5001-1) or Erythrina Cristagalli Lectin (ECL) conjugated to fluorescein (Vector Laboratories, FL-1141-5). Fresh released and cell associated virus stock were transferred neat (25 µl per well) into wells in triplicate containing neuraminidase treated or untreated cells, and plates were incubated for 1.5 hours. Following this, monolayers were washed with PBS, and media was replaced with DMEM, with 2% FBS. Fresh virus stocks were also transferred to neuraminidase treated cells on coverslips. Cells were incubated for

12 hours at 37˚c 5% CO_2. 96-well plates were then fixed and immunostained using the protocol detailed in section 2.2.6 for IAV or RSV nucleoprotein, followed by rabbit anti-mouse 488 (Sigma Aldrich, USA, SABA4600056) secondary antibody. Infected cells were counted using Celigo automated cytometer (Nexcelom Bioscience), using two target expression analysis to detect NP signal and nuclei. Coverslips were fixed and stained for IAV HA and RSV F as described in section 2.2.6 and imaged using Zeiss LSM880 with airyscan detector. Viral entry experiments were carried out three times independently, confocal microscopy imaging was carried out once. Statistical difference between conditions was determined by unpaired t-test.

2.4.8 Neutralisation assay

Anti-IAV HA serum (NIBSC, 03/242) was titrated in 2-fold dilution series starting at 1/100 dilution, against 10^4 pfu of IAV A/Peurto Rico/8/34 and RSV A2 stock to determine the working dilution range for IAV neutralisation and check cross-reactivity with RSV.

To generate virus stocks for the neutralisation experiment, A549 cells were seeded at $1x10^5$ cells per well in 24-well plates. Cells were infected with IAV at MOI 1, RSV at MOI 4 or mixed inoculum of both viruses for 1.5 hours, before media was replaced with DMEM, with 2% FBS and 1µg/ml trypsin TPCK. Infected cells were incubated for 24 hours at 37˚c 5% CO_2. Following incubation, supernatant, containing released virus, was collected. The remaining cell monolayers were scraped and collected in suspension in DMEM. Cell suspensions were vortexed briefly to dislodge virus attached to cell fragments. Next, supernatant samples and cell suspension samples were centrifuged at 1500 rpm for 5 minutes to remove cell debris. Supernatant was retained as released and cell associated virus samples and used fresh (no freezing) in the neutralisation assay.

For the neutralisation assay, cells were seeded at $1x10^4$ cells per well in 96-well plates 48 hours before the assay. Serum was diluted 1/100 in DMEM into triplicate wells in 96-well plates (50 µl per well). Serum-free wells were set up in parallel containing DMEM only. Fresh virus stocks containing released or cell associated virus were transferred neat (50 µl per well) to triplicate serum or control wells. Wells were mixed thoroughly by pipetting and the plate was stored at 4˚c for 2 hours.

Following incubation, samples were transferred using a multichannel pipette to wells containing A549 cells. Plates were incubated for 1.5 hours 37˚c 5% CO_2. Following this, monolayers were washed with PBS, and media was replaced with DMEM, with 2% FBS. Cells were incubated for 24 hours at 37˚c 5% CO_2. Cells were then fixed and immunostained for IAV nucleoprotein, followed by rabbit anti-mouse 488 (Sigma Aldrich, USA, SABA4600056) secondary antibody. Infected cells were counted using Celigo automated cytometer (Nexcelom Bioscience), using two target expression analysis to detect NP signal and nuclei. Neutralisation in wells that contained serum was calculated as a percentage of the mean of the positive cell count in the control wells for each virus sample. Wells were also imaged by wide field fluorescence using the EVOS FL microscope using 20x objective. Experiments were carried out three times independently. Statistical difference between conditions was determined by unpaired t-test.

2.5 Chapter 5 specific methods

2.5.1 Viral Infections in hBEC cultures

HBEC cultures were infected no earlier than 35 days post ALI initiation. The apical surface of cultures was washed with DMEM 24 hours prior to infection by applying pre-warmed DMEM to the apical surface of cultures and incubating at 37˚c, 5% CO_2 in a humidified incubator for 20 minutes, followed by removal. This washing step was repeated immediately before infection. Inoculum containing 10^5 pfu of IAV, RSV or a mixed inoculum of both viruses (10^5 pfu of each virus) was prepared in DMEM. Cultures were incubated with inoculum for 2 hours at 37˚c 5% CO_2, after which the inoculum was removed and cultures were washed once with DMEM as described. Inoculum was back titrated back plaque assay to confirm virus input and served as the zero hours time point for growth curves. Two cultures were infected per infection and time point. Samples were collected from the apical surface of cultures at 24, 48 and 72 hpi, by incubating with DMEM for 30 minutes. Sample were then removed and stored at -80˚c, prior to titration by IAV or RSV plaque assay. Transwells were then fixed with 4% formaldehyde for 1 hour, before paraffin embedding or storage at 4˚c in PBS.

2.5.2 Processing of paraffin embedded tissue sections

After fixation, HBEC cultures were submitted to the University of Glasgow veterinary histology laboratory for processing. HBEC cultures were embedded in paraffin blocks, cut using a microtome to 2-3 µm thick sections and mounted on glass slides. Sections were stained with hematoxylin and eosin to confirm determine morphology.

2.5.3 Immunofluorescence staining of paraffin embedded sections

For immunofluorescence staining, sections were dewaxed by heating in an oven at 60˚c for 1 hour. Next, slides were washed four times with xylene, each for 10 minutes. Following this, sections were rehydrated via washes with 1:1 (v/v) Xylene:Isopropanol mixture, then 100%, 90%, 70% and 50% isopropyl alcohol solution each for five minutes. Sections were washed thoroughly with d.H_2O and PBS. For antigen retrieval, sections were treated with proteinase K solution (Dako, S3020) for 15 minutes.

Sections were mounted into humid chambers for immunostaining. Sections were permeablised with 1% triton X100 for 10 minutes, followed by three washes with PBS. Sections were blocked with 2% BSA in PBS for 30 minutes at room temperature. Primary antibodies, mouse monoclonal anti-IAV (A/Puerto Rico/8/34) HA (Sinobiological, 11684-MM03, 1/500), goat polyclonal anti-RSV (Abcam, AB20745, 1/500) or mouse monoclonal anti-MxA clone M143 kindly provided by Georg Kochs, were diluted in 2% BSA solution and applied to sections for two hours at room temperature, followed by washing with PBS. Secondary antibodies, rabbit anti-mouse IgG conjugated to alexafluor 488 (Sigma Aldrich, SABA00046, 1/1000) and donkey-anti goat IgG conjugated to alexafluor 568 (Abcam, ab175704) were diluted in 2% BSA solution and applied to sections for 1 hour in the dark at room temperature, followed washing with PBS and d.H_2O. Slides were mounted with Prolong Gold mounting media containing DAPI (Invitrogen, P36392).

2.5.4 Immunofluorescence staining of apical surface of transwells

For apical staining, cultures were retained in tranwells and all steps were applied from the apical and basal surfaces. Cultures were permeablised with 1% triton X100

for 10 minutes, followed by three washes with PBS. Cultures were blocked with 2% BSA in PBS for 30 minutes at room temperature. Primary antibodies were diluted in 2% BSA solution and applied to sections for one hour at room temperature, followed by four washes with PBS. Fluorophore conjugated secondary antibodies were diluted in 2% BSA solution, along with 2µg/ml hoescht 33342 nuclear staining solution (Thermo Fisher Scientific, 62249), and applied to sections for 1 hour in the dark at room temperature, followed by four washes with PBS and two washes with d.H_2O. Cultures were cut from transwell supports and transferred to glass slides. Slides were mounted to a coverslip using Prolong Gold mounting media (Invitrogen, P36392). Slides were imaged by confocal microscopy on Zeiss LSM880 AxioObserver microscope (ZEISS, Germany). Images were collected using GaAsP detector with 405 nm, 488 nm and 598 nm excitation lasers, using 40x/1.4 plan-apochromat oil DIC M27 objective.

Chapter 3

Characterising interactions between Influenza A virus and Respiratory Syncytial virus in an *in vitro* model of coinfection

3.1 Introduction

Respiratory viruses have evolved to infect the respiratory tract, an ecological niche populated with viral pathogens and commensal viruses, bacteria and other microbiota. Despite this, viruses are predominantly studied in isolated systems. Viral coinfections represent between 10-30% of the respiratory viral infections detected (Martin et al., 2012; Nickbakhsh et al., 2016; Kim et al., 2020; Góes et al., 2020), but experimental investigations into the consequences of coinfection remain sparse.

Animal challenge studies provide important insight into the complex interactions that occur during viral coinfection. Indirect interactions, where one virus renders the host refractory to infection by a secondary virus, are increasingly well characterised in the context of respiratory viral infections. Viral interference induced by IAV infection has been demonstrated to inhibit the replication of RSV in multiple challenge studies (Chan et al., 2018; Ayegbusi et al., 2019; Drori et al., 2020). Few studies, however, have attempted to identify and characterise direct interactions at the cellular level when viruses co-exist within the same tissue or coinfect the same cells.

Studies investigating direct interactions between coinfecting viruses at the cellular level remain limited, but IAV and RSV coinfections have been described using *in vitro* cell culture systems. Drori *et al.* infected HEp-2 cells with IAV, followed by RSV after a three-hour interval or vice versa. They found that, compared to RSV single infection, RSV replication in the presence of IAV was significantly reduced (Drori et al., 2020). Further, Shinjoh *et al.* coinfected MDCK cells with IAV and RSV. They found that, in simultaneous coinfections and staggered infections up to 8 hours post RSV infection, infection by IAV significantly reduced RSV replication, while IAV replication kinetics remained the same in the presence of RSV (Shinjoh et al., 2000). However, when cells were infected with IAV 12 hours post RSV infection, RSV replication was unaffected. Additionally, they found that expression of RSV matrix (M) protein, nucleoprotein (N) and phosphoprotein (P) were reduced in coinfection, so concluded that competitive interactions during translation of IAV and RSV viral proteins resulted in suppression of RSV growth (Shinjoh et al., 2000). Virus induced cytopathic effects can also impact replication dynamics in coinfection. Parainfluenza virus (PIV) 2 induced cell fusion was demonstrated to increase the spread of IAV in both Vero cells and primary cells derived from the human respiratory epithelium (Goto et al., 2016).

Despite lacking representative features of the respiratory epithelium, *in vitro* cell systems have provided the essential groundwork that enables our understanding of respiratory viruses. Our fundamental knowledge of the structure and molecular biology of both IAV and RSV was uncovered by *in vitro* experiments. This wealth of data allows for mathematical modelling to aid our understanding of the factors influencing coinfection. In a modelling study combining *in vitro* replication data from a wide range of respiratory viruses, viral growth rate was determined to be an important predictor of the outcome of coinfection, with faster growing viruses like rhinovirus (RV) able to outcompete slower growing PIVs (Pinky and Dobrovolny, 2016). However, when using a stochastic version of the same model that accounts for the likelihood of random events impacting early infection, it was found that slower growing viruses may outcompete faster viruses, if they establish infection in a greater number of cells initially (Pinky et al., 2019). The impact of other events including superinfection and tissue regeneration have been modelled and shown to contribute toward persistence in coinfection (Pinky et al., 2019). Whilst alone these models may not provide a comprehensive understanding of viral dynamics during coinfection, mathematical models using published experimental data can generate new biological insights to be validated by experimental methods. Given that there is a wealth of published data on the growth kinetics, cytopathology and host interactions induced by respiratory viral infections, mathematical modelling has an important place in understanding the impact of viral coinfection. This could be of particular importance in modelling more complex interactions within the respiratory tract, where experimental studies are limited by ethical considerations, technical challenges and expense.

This chapter describes the development of an in vitro model of coinfection using A549 cells, an adenocarcinoma cell line derived from the human lung (Giard et al., 1973). A549 cells recapitulate features of type II alveolar pneumocytes (Lieber et al., 1976; Balis et al., 1984) and therefore provide an important model of the human respiratory epithelium. A549 cells are permissive to infection by both IAV and RSV and are used frequently in respiratory virus research. Here, fundamental characteristics of the replication cycles of IAV and RSV in A549 cells have been characterised, comparing phenotypes in single virus and mixed infections to identify potential novel sources of viral interaction within coinfected cells.

The overall objectives of this chapter were to determine if IAV and RSV interact during coinfection and to identify measurable consequences of those interactions. To this end, I set out to address the following aims. Firstly, to establish a coinfection system whereby features of IAV and RSV replication cycles can be selectively measured in a population of coinfected cells. Secondly, to determine the replication kinetics of IAV and RSV in single virus infection and coinfection and assessed how factors such as timing of infection and viral input influence replication dynamics. Finally, to identify potential sources of viral interactions that could be avenues for more detailed mechanistic studies, using multi-modal imaging experiments to characterise features of coinfection.

3.2 Acknowledgements

I would like to thank the following individuals for their contributions to the work described in this chapter. David Anderson carried out the staggered infections described in section 1.2.4, as part of his undergraduate honours project, supervised by myself and Pablo Murcia. Jack Hirst rescued the IAV-mCherry stock used in live cell imaging experiments. Colin Loney provided training and assistance in setting up parameters for the live cell imaging experiment.

3.3 Results

3.3.1 IAV and RSV titres can be selectively quantified by plaque assay

In performing coinfection experiments, samples would be generated that contain a mixture of both IAV and RSV virions. Therefore, to determine the replication of IAV and RSV in a mixed infection, methods to selectively measure IAV and RSV infectivity had to be identified.

To this end, plaque assay protocols were optimised to allow selective detection of IAV or RSV plaques. MDCK cells are predominantly used to propagate IAV to high titre and titrate IAV, due to their plaque forming phenotype (Gaush and Smith, 1968). MDCK cells were infected with 100 pfu/well of IAV or RSV and wells were treated under IAV plaque assay conditions. Cells were immunostained for IAV nucleoprotein (NP) or RSV nucleoprotein (N) to visualize plaques. In MDCK cells, IAV formed large

plaques, while no plaques or evidence of infection was identified following infection of MDCK cells by RSV (Figure 3-1).

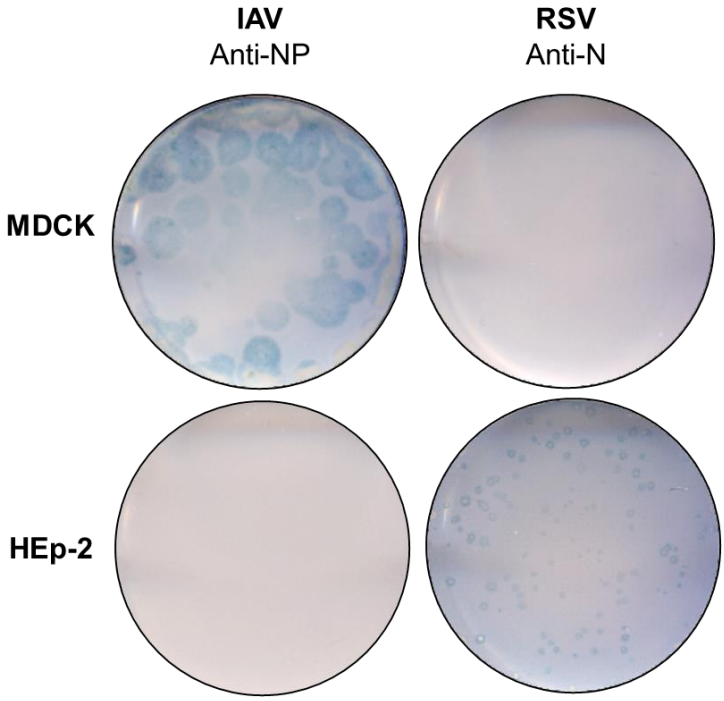

Figure 3-1: IAV and RSV can be selectively titrated by plaque assay by MDCK and HEp-2 cells. IAV and RSV were titrated in MDCK and HEp-2 cells under plaque assay conditions and immunostained to detect nucleoprotein (blue staining). IAV plaques were detected in MDCK cells but not in HEp-2 cells, whilst RSV plaques were detected in HEp-2 cells but not MDCK cells.

HEp-2 cells are predominantly used to titrate RSV. Therefore, the experiment described above was repeated, this time infecting HEp-2 cells with RSV or IAV under protocol conditions optimised for the RSV plaque assay. In HEp-2 cells, RSV forms small, uniform plaques identifiable by immunostaining for RSV N. No IAV plaques were detected in HEp-2s immunostaining for IAV NP (Figure 3-1).

These two cell lines are permissive to plaque formation by one virus, but not the other virus. Therefore, this provides a method to easily detect and quantify virus from a sample that contains both IAV and RSV infectious particles.

3.3.2 IAV replication kinetics are unchanged in mixed infection with RSV

To establish the growth kinetics of each virus in A549 cells viral replication was measured over a 72-hour time series. A549 cells were infected with IAV, RSV or a mixed inoculum of both viruses. Infections were carried out at high multiplicity of infection (MOI) (MOI=4) to facilitate a high degree of coinfection and to model high MOIs produced in advanced stages of infection, when IAV and RSV infectious foci may come into contact in the respiratory tract.

Replication of IAV was determined in single infection and mixed infection with RSV. In single infection, IAV replication peaked by 24 hours post infection (hpi) and plateaued for the remaining time course (Figure 3-2). In mixed infection with RSV, IAV replication was not inhibited by coinfection and IAV replicated to the same or marginally higher titres at 72 hpi.

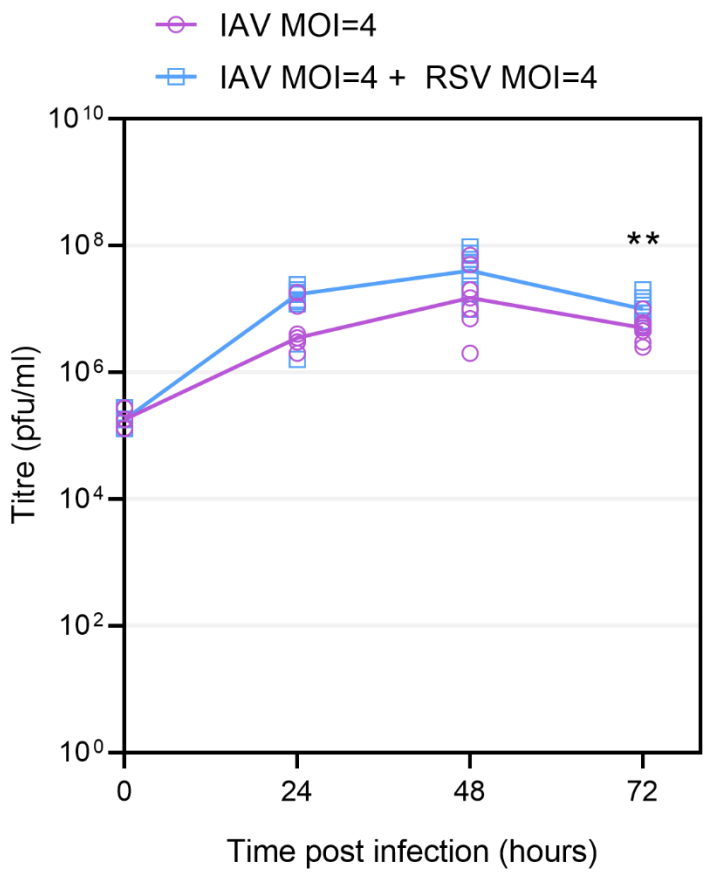

Figure 3-2: IAV replication unchanged during coinfection with RSV. A549 cells were infected with IAV alone at MOI 4 or in combination with RSV at MOI 4. Replication kinetics of IAV in single virus infection (magenta line, circle points) or mixed infection with RSV (blue line, square points). The zero hours timepoint is the

viral input in the inoculum. Lines connect medians of 9 replicate data points per time point, from 3 independent experiments. Statistical significance determined per timepoint by Mann Witney test, ** $p<0.01$, $p\geq0.05$ not indicated.

RSV replication in single infection increased between 24-48 hpi and started to plateau between 48-72 hpi. RSV titres reached 10^7 pfu/ml at 72 hpi, but the peak of replication was not captured within the time series measured. In coinfection with IAV, RSV replication was significantly reduced across all experimental time points and there was high variability in titre across replicate experiments (Figure 3-3).

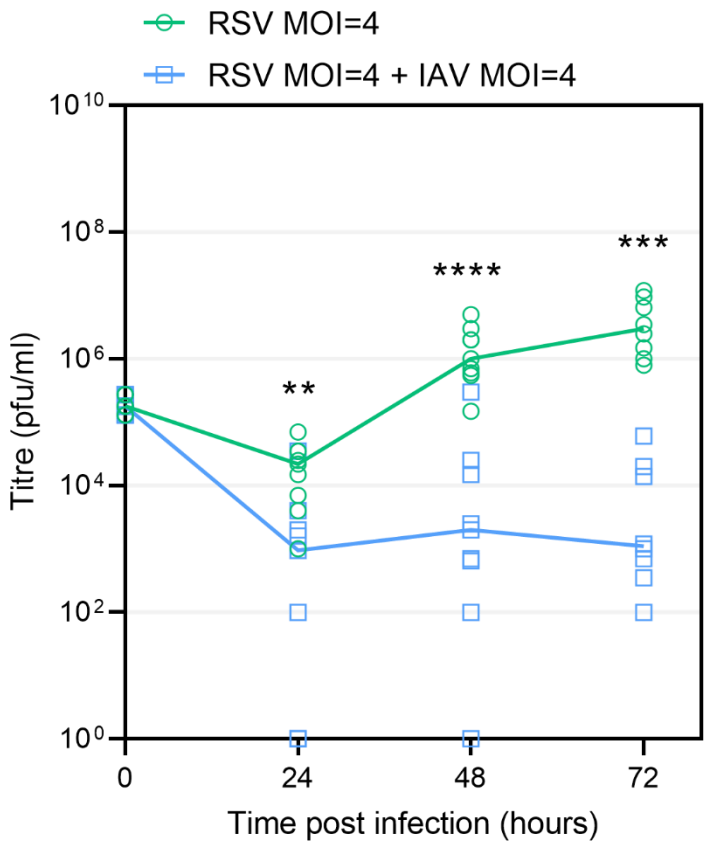

Figure 3-3: RSV replication is reduced during coinfection with IAV. A549 cells were infected with RSV alone at MOI 4 or in combination with IAV at MOI 4. Replication kinetics of RSV in single virus infection (green line, circle points) or mixed infection with IAV (blue line, square points). The zero hours timepoint is the viral input in the inoculum. Lines connect medians of 9 replicate data points per time

point, from 3 independent experiments. Statistical significance determined per timepoint by Mann Witney test, ** p<0.01, *** p<0.001, **** p<0.0001.

3.3.3 Reducing IAV input MOI relative to RSV input does not impact replication dynamics in coinfection

In infections at equivalent MOI, RSV was slower to reach its infection peak than IAV in single infection and replicated to significantly lower titres in mixed infection. Reducing IAV infectious input relative to RSV may therefore provide RSV with an advantage that might allow it to overcome the inhibition induced by IAV, while disadvantaging IAV, the faster growing virus. To test this, IAV input MOI was reduced 10-fold (MOI=0.4) or 100-fold relative (MOI=0.04) to RSV input (MOI=4).

Despite the reduction in input titre relative to RSV, IAV was still able to replicate to the same or greater titres in mixed infection compared to single IAV infection (Figure 3-4A and B). This implies that IAV may be tolerant to presence of RSV and is able to replicate as efficiently in its presence as alone. Conversely, RSV replication was negatively impacted by coinfection, regardless of IAV input, suggesting that IAV has a competitive advantage over RSV in the coinfection system (Figure 3-4C and D).

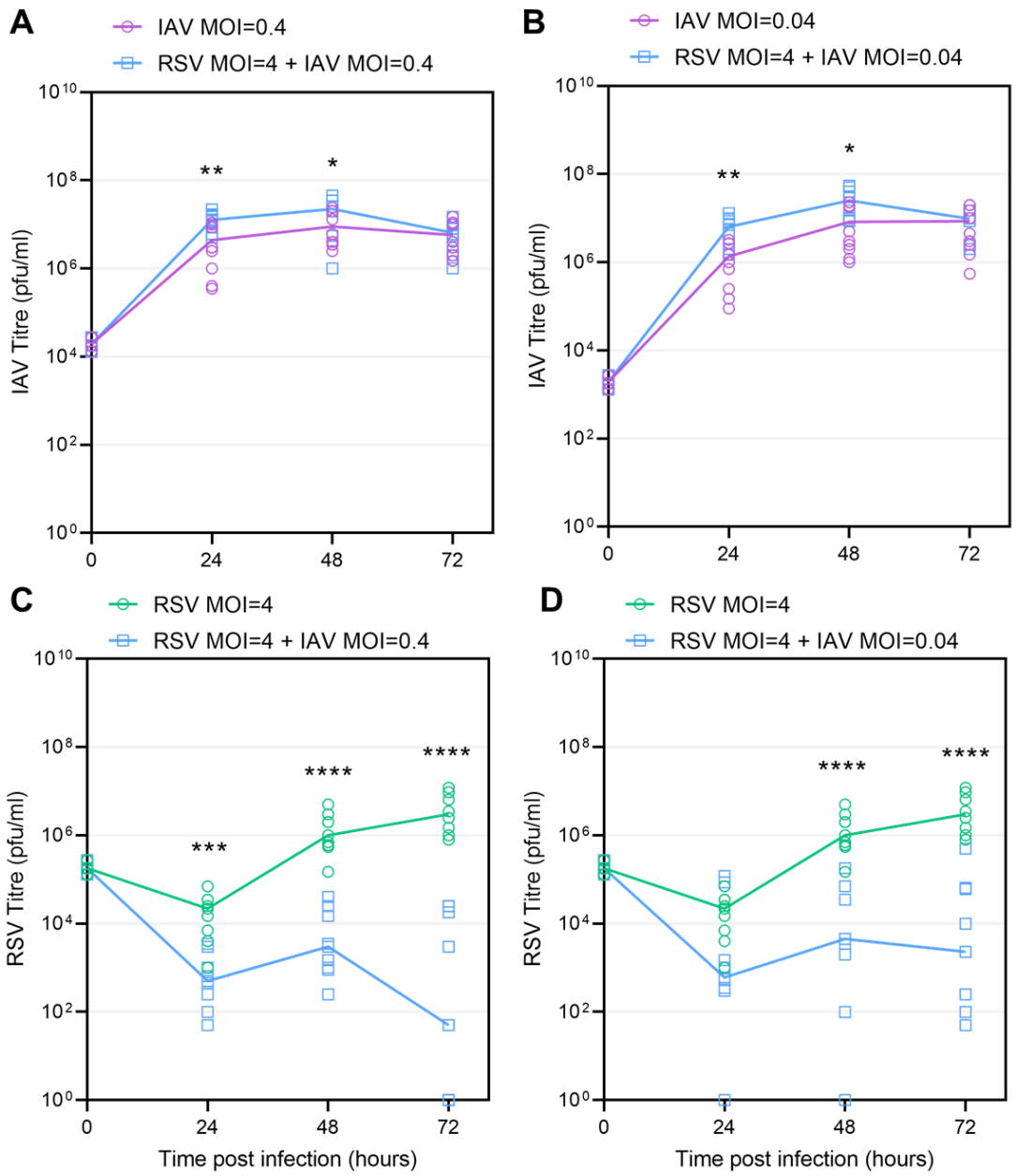

Figure 3-4: Reducing IAV input does not affect viral replication kinetics in coinfection. IAV replication in single infection (magenta line) or mixed infection with RSV MOI=4 (blue line), at (A) MOI=0.4 or (B) MOI=0.04. RSV replication in single infection (green line) or mixed infection (blue line) with IAV at (C) MOI=0.4 or (D) MOI=0.04. The zero hours timepoint is the viral input in the inoculum. Lines connect medians of 9 replicate data points per time point, from 3 independent experiments. Statistical significance determined per timepoint by Mann Witney test, * $p<0.05$, ** $p<0.01$, *** $p<0.001$, **** $p<0.0001$, $p>0.05$ not indicated.

3.3.4 Staggered infections show that IAV can superinfect and establish replication in cells prior infected with RSV

To determine if timing of infection could be a more important determining factor in the outcome of mixed infections, A549 cells were first infected with RSV at high MOI (MOI=4) or mock infected, followed by IAV at low MOI (MOI=0.04) at varying time intervals. This MOI combination was selected to represent the greatest challenge to IAV, as to overcome combined disadvantages of the time delay and the low input concentration, would require uninhibited IAV replication and spread in the RSV infected cell population to reach the same levels of IAV replication as in mock infected cells.

Time points for IAV staggered infection were selected to represent different stages of the RSV replication cycle. A six-hour time point represents a relatively early stage in RSV replication before release of new infectious RSV virions, while 16 hours and 24 hours represented time points where at least one replication cycle had been completed. A zero-hour timepoint was also included as a control. To determine the stage of replication, cells were infected with RSV and fixed at each experimental time point and stained for RSV nucleoprotein (N) (Figure 3-5A). No staining was observed at zero hours. At 6 hours, small cytoplasmic RSV inclusion bodies could be identified in cells, which are sites of genome replication and transcription of viral genes. At 16 hours diffuse N staining could be observed in infected cells, along with larger inclusion bodies. Diffuse staining was again observed at 24 hours, while other cells showed signs of the earlier stages of RSV replication, indicating multi cycle RSV replication (Figure 3-5A).

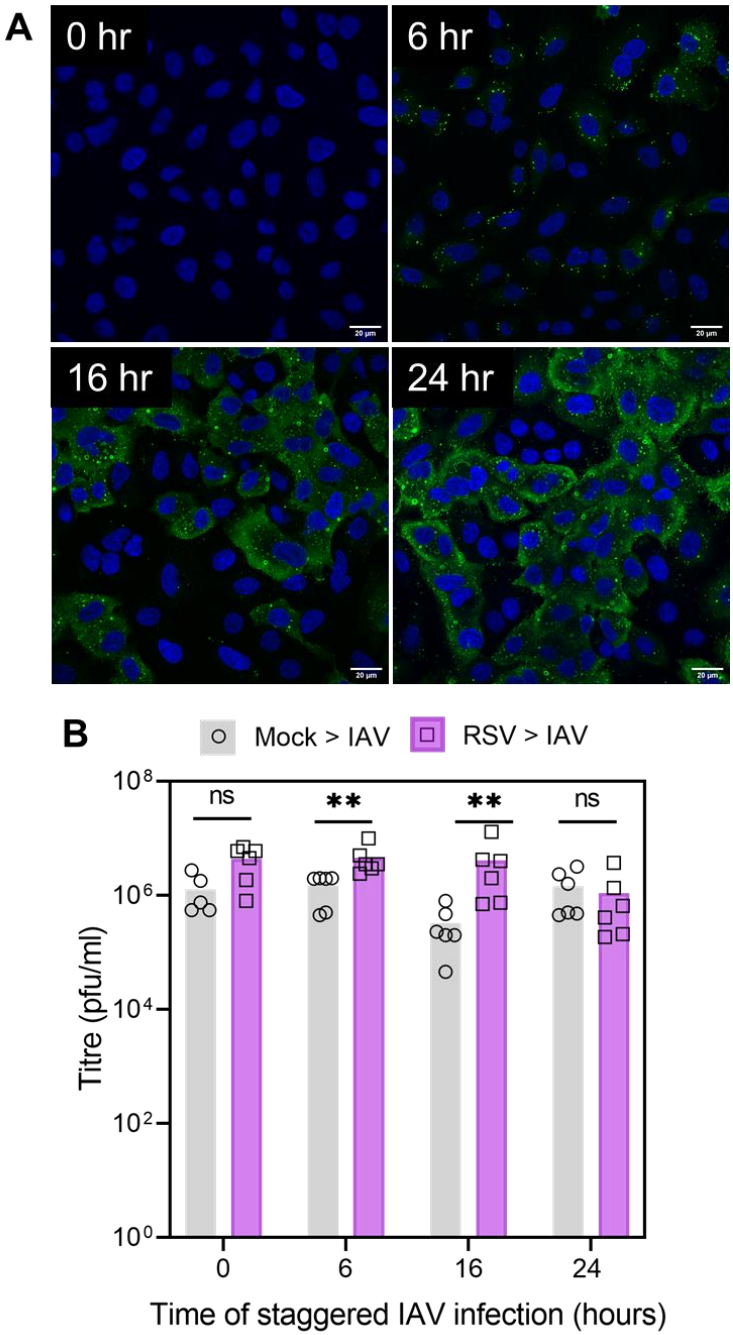

Figure 3-5: IAV can establish infection in cells previously infected with RSV and replicate to the same or higher titres. (**A**) Immunofluorescence staining for RSV nucleoprotein (green) at each timepoint shows RSV at different stages in the infection cycle. Scale bars indicate 20 µm. (**B**) IAV titre collected 24 hours after staggered infection with IAV (magenta bars) or mock infection (grey bars), at various times after the primary RSV infection. Data from two independent experiments, statistical significance determined by Mann Witney test, ** $p<0.01$, ns $p\geq0.05$.

Staggered infections were performed by infecting cells with RSV, or mock infecting, followed by infection with IAV at 0, 6, 16 or 24 hours post RSV infection. Cells were then incubated for a further 24 hours, then samples were collected for titration by IAV plaque assay. RSV titre was not measured in this experiment. Figure 3-5B shows IAV titres in staggered mixed infections or mock infected controls. IAV replicated to at least the same titre in all staggered infections with RSV, compared to mock primary infections. In fact, at 6 and 16 hours staggered timepoints, IAV replicated to significantly higher titres (6 hours $p=0.0022$, 16 hours $p=0.0087$ by Mann Witney test) in the RSV infected cultures compared to the mock infection. This indicates that IAV can superinfect a population of cells that were previously infected with RSV and can replicate to the same efficiency as in single IAV infection. Further, as demonstrated in simultaneous infections these experiments show that presence of RSV may provide an advantage for IAV replication, as IAV can replicate to slightly higher titres in mixed infections.

3.3.5 The proportions of cells infected with IAV and RSV was altered between single and mixed infections

Viral growth kinetics indicate that RSV replication was decreased in coinfection, while IAV replication was unaffected or even increased by the presence of RSV. However, experiments measuring viral replication do not provide information about what occurs at the individual cell level. It is possible that the interactions that result in the observed growth kinetics may be the result of altered cell-cell spread of IAV and RSV. Alternatively, the same number of cells may be infected, but they could have a different capacity to produce and release infectious virus.

To determine the status of infection of cells during single and mixed infection with IAV and RSV, cells were infected using the same MOI combinations used in replication experiments (Figures 3-2 to 3-4). Cells were fixed at 8 and 24 hpi and then immunostained for IAV haemagglutinin (HA) and RSV nucleoprotein (N) and imaged by confocal microscopy (Figure 3-6 and 3-7). Proportions of cells infected with each virus were quantified manually from images.

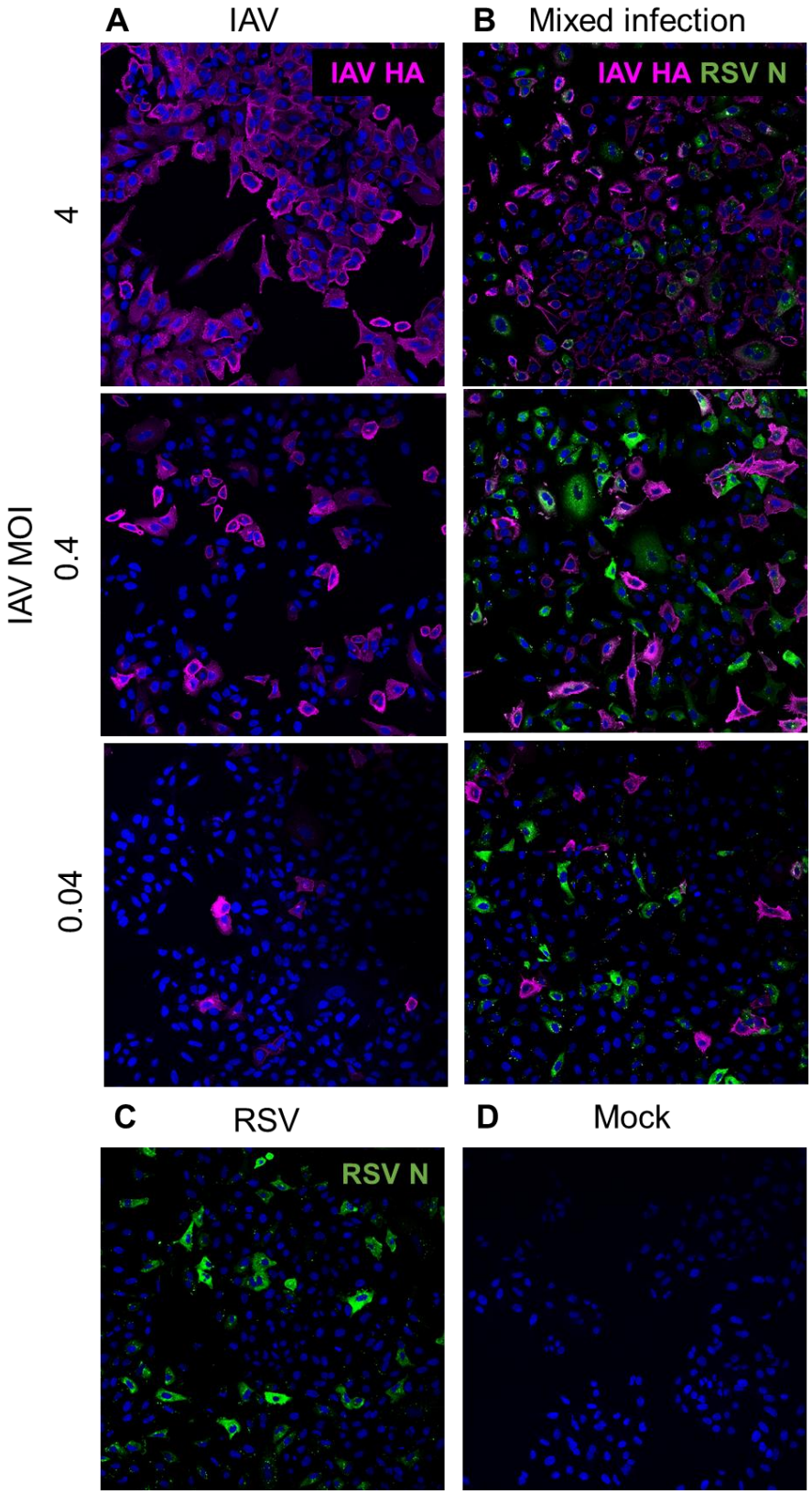

Figure 3-6: IAV and RSV infection in single and mixed infection at 8 hpi. Cells were infected with IAV and RSV, fixed at 8 hpi and all samples were stained for both IAV HA (magenta) and RSV NP (green) and DAPI (blue). (**A**) IAV infection at 8 hpi, following infection at MOI 4, 0.4 or 0.04. (**B**) Mixed infection with RSV at MOI 4 and IAV at MOI 4, 0.4 or 0.04. (**C**) RSV single infection at MOI 4. (**D**) Mock infected cells.

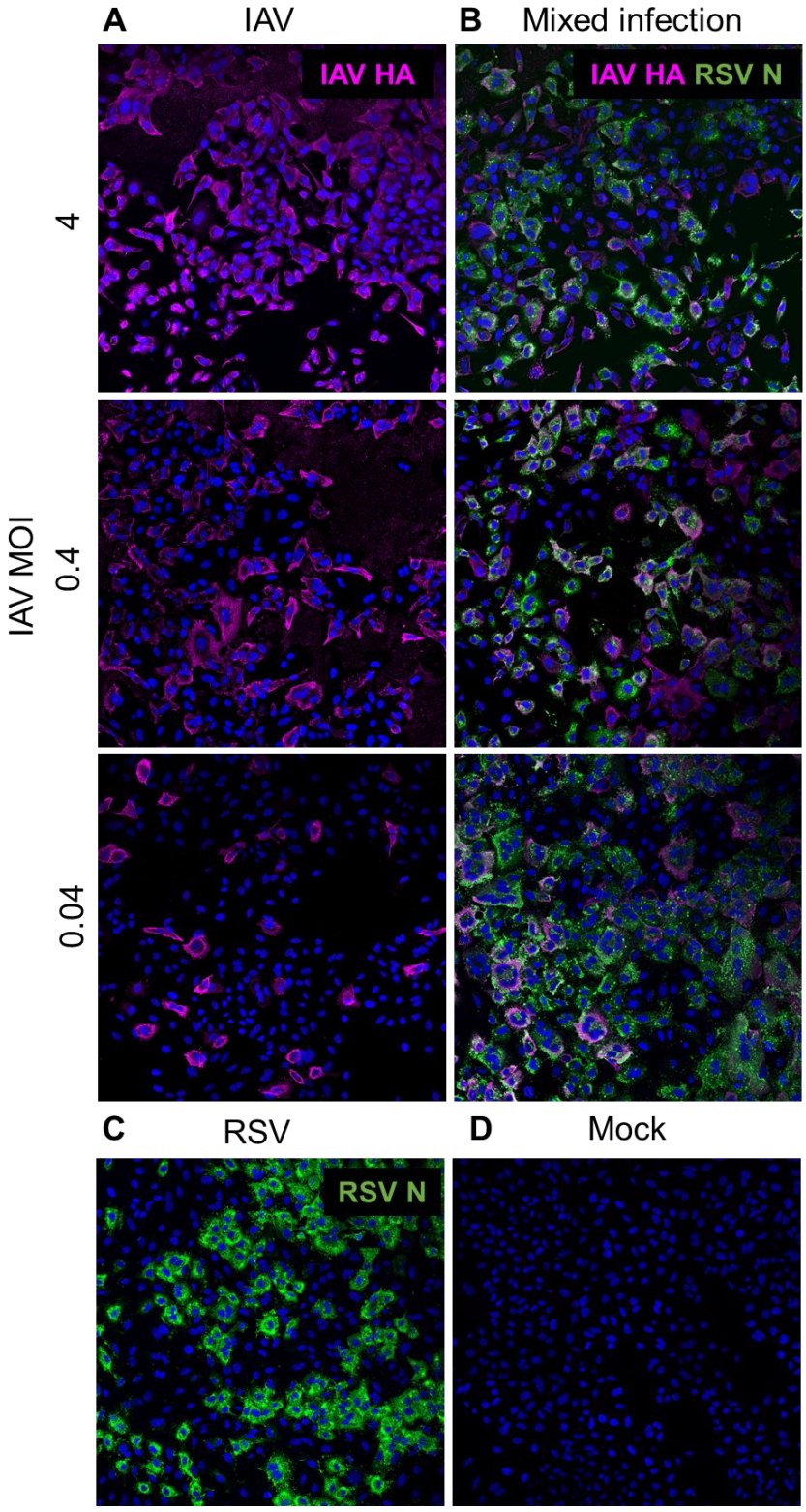

Figure 3-7: IAV and RSV infection in single and mixed infection at 24 hpi. Cells were infected with IAV and RSV, fixed at 24 hpi and all samples were stained for both IAV HA (magenta) and RSV NP (green). (A) IAV infection at 8 hpi, following infection at MOI 4, 0.4 or 0.04. (B) Mixed infection with RSV at MOI 4 and IAV at MOI 4, 0.4 or 0.04. (C) RSV single infection at MOI 4. (D) Mock infected cells.

At 8 hpi, a dose-dependent relationship was observed between cells positive for IAV HA and IAV input (Figure 3-8A), with 88% of cells positive for HA at 8 hpi following infection with IAV at MOI=4, compared to 7% at MOI=0.04 (Figure 3-8A). At 8 hpi, 37% of cells were positive for RSV N, despite infection at high MOI (MOI=4) (Figure 3-8A). In mixed infection at high MOI (both viruses MOI=4), half of cells were identified as coinfected. Interestingly, a greater proportion of cells were uninfected in the coinfection, compared to IAV only infection (Figure 3-8A).

At 24 hpi, a relationship between the proportion of IAV infected cells and IAV input MOI was still observed (Figure 3-8B), with fewer cells than expected positive for IAV at MOI=0.04 based on the replication kinetics described previously (Figure 3-4A). In single RSV infection, the proportion of cells infected with RSV rose to 65% (Figure 3-8B). In mixed infection, the majority of cells were coinfected with both IAV and RSV in infections with IAV at MOI=4 and MOI=0.4. This suggests that there was no barrier to infection of the same cell by both IAV and RSV. Surprisingly, only 20% of cells were coinfected by 24 hpi in mixed infection with IAV at MOI=0.04 (Figure 3-8B). This seems to contradict IAV replication kinetics at the IAV MOI=0.04, which show that by 24 hpi, IAV replication reaches comparable titres to infections starting with higher input MOI (Figure 3-4B).

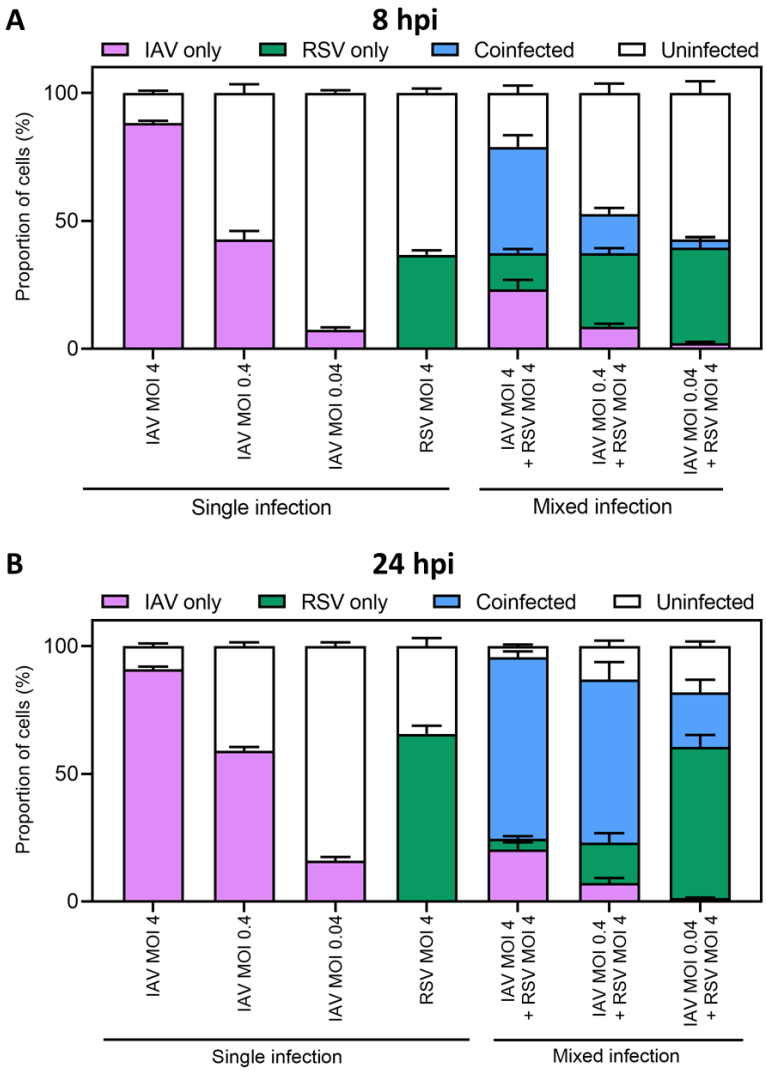

Figure 3-8: Total cell population stratified by infection status. Proportions of cells infected with IAV (magenta bars) or RSV (green bars), coinfected (blue bars) or uninfected (white bars). Data across single and mixed infection conditions shown for (A) 8 hpi and (B) 24 hpi. Bar shows mean proportion from 9 replicates from 3 independent experiments. Error bars indicate standard error of the mean (SEM).

The total number of cells positive for viral antigen was calculated (i.e., single infected plus coinfected) to determine the overall expression of viral proteins or spread of the viruses in coinfection. At 8 hpi, there was a significant reduction in the total number of cells positive for IAV in mixed infection at MOIs 4 ($p= 0.000166$ by Mann Witney test) and 0.4 ($p= 0.005567$ by Mann Witney test), compared to single infection at the corresponding MOIs (Figure 3-9A). This suggests that, during the initial round of replication, IAV infected less cells in mixed infection than in single infection. Alternatively, as expression of viral protein was measured, this finding could reflect

a delay in expression of IAV HA in coinfected cells. At 24 hpi there were no significant differences between the proportion of IAV infected cells detected in single or mixed infection (Figure 3-9A).

At 8 and 24 hpi, there was a significant increase in RSV positive cells detected in mixed infection compared to single RSV infection (Figure 3-9B). At 8 hpi, this effect appears to be dose dependent in relation to IAV MOI, so may reflect a positive interaction in coinfected cells to promote the expression of RSV proteins. There was no evidence of cytopathic effect or cell death at 8 hpi, so this is unlikely to impact the relative proportions of infected cells observed. At 24 hpi, the proportion of RSV infected cells was significantly greater in mixed compared to single infection across all MOI combinations (Figure 3-9B). This contrasts with replication data measuring released virus (Figures 3-3 and 3-4), which show a marked reduction in RSV titre 24 hpi in mixed infection.

Overall, cell spread is altered in mixed infection compared to single infection and the trends observed seem counter-intuitive compared to replication trends in mixed infection. This highlights the importance of understanding viral coinfection at the level of individual cells, as well as overall viral replication, to get a more comprehensive understanding of dynamics of viral infection.

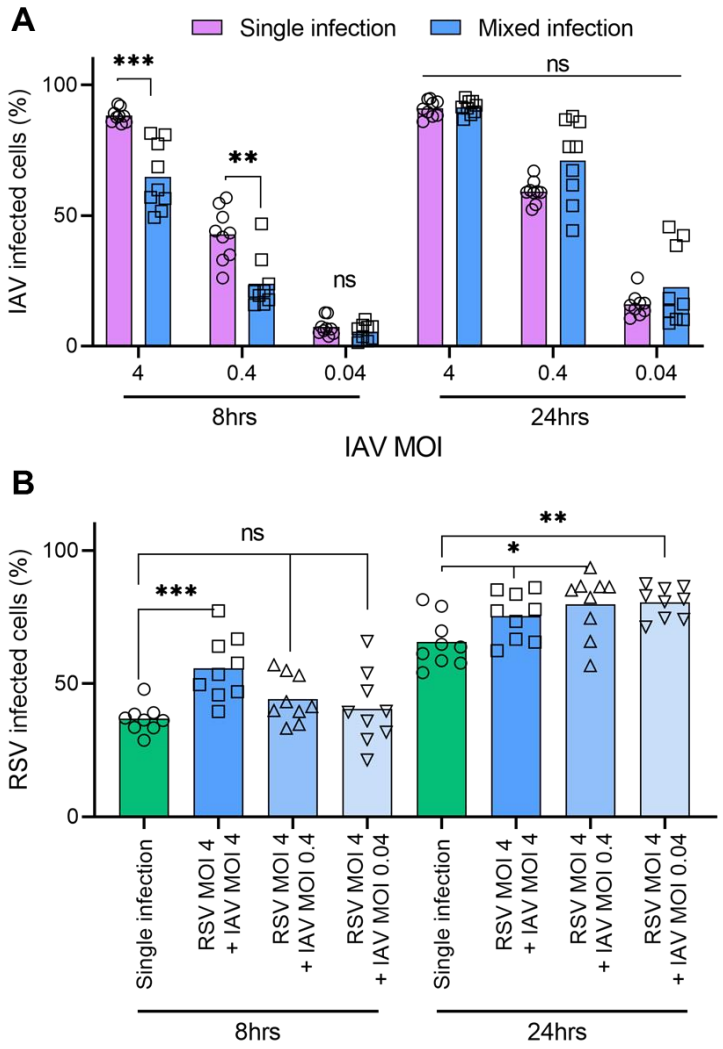

Figure 3-9: Total number of cells infected with IAV or RSV in single or mixed infection. (**A**) Comparison of total proportion of cells positive for IAV HA (infected with IAV-only or coinfected) in single IAV infection (magenta bars) or mixed infection (blue bars) at 8 and 24 hpi. (**B**) Comparison of total proportion of cells positive for RSV NP (infected with RSV-only or coinfected) in single RSV infection (green bars) or mixed infection with IAV MOI 4, 0.4 or 0.04 (blue bars) at 8 and 24 hpi. Statistical significance determined by Mann Witney test, * $p<0.05$, ** $p<0.01$, *** $p<0.001$, ns $p\geq0.05$.

3.3.6 Live cell imaging reveals kinetics of infection

Whilst analysis of static timepoints provides valuable insight, live cell imaging allows real-time analysis of infection spread, morphological changes and cell death. To visualise the kinetics of IAV and RSV coinfection more broadly, coinfections were carried out using fluorescently tagged viruses. Fukuyama *et al.* developed 'Color-flu', a tool kit of IAVs stably expressing fluorescent reporter proteins (Fukuyama et al., 2015). H1N1 A/Puerto Rico/8/34 encoding an mCherry fluorescent reporter protein in the NS1 open reading frame was used in our experiments. RSV A2 encoding a GFP fluorescent reporter was used to visualise RSV infection.

A549 cells were infected with IAV-mCherry, RSV-GFP or a mixed inoculum of both viruses at MOI=1 and transferred to the live cell microscope immediately to begin imaging. Infections were maintained within a humidified incubator through the duration of the experiment and images were collected automatically every 15 minutes from three positions on each well, for a total of 64 hours. Figure 3-10A shows images collected at timepoints across the experiment and fluorescent signal was quantified using an image analysis pipeline to quantify signal area per frame (Figure 3-10B and C).

Expression of mCherry was observed by 6 hpi in IAV single infections (Figure 3-10B) and peaked around 16 hpi. By 36 hpi, the mCherry signal had reduced, and then remained constant through the rest of the time course, which likely reflects virus induced cell death and residual mCherry signal, which could be visualised by the rounding of infected cells (Figure 3-10D). Expression of GFP in RSV single infections was detected at later timepoints, between 12-18 hpi, and slowly increased across the rest of the time series (Figure 3-10C). Wide-spread syncytia formation could be observed at late time points (Figure 3-10E). Whilst there was some cell death predominantly due to the collapse of syncytia, a high proportion of RSV infected cells remained alive at the end of the time series.

In the mixed infection, coinfected cells expressing both mCherry and GFP could be observed (Figure 3-10F). GFP expression in mixed infection was substantially reduced compared to RSV single infection (Figure 3-10C). By 36 hpi, GFP signal was almost entirely eliminated, which is was likely a consequence of cells expressing GFP undergoing cell death. In contrast, IAV-mCherry was observed widespread across wells in the mixed infection and the level of expression of

mCherry was unchanged between single IAV infection and mixed infection (Figure 3-10B).

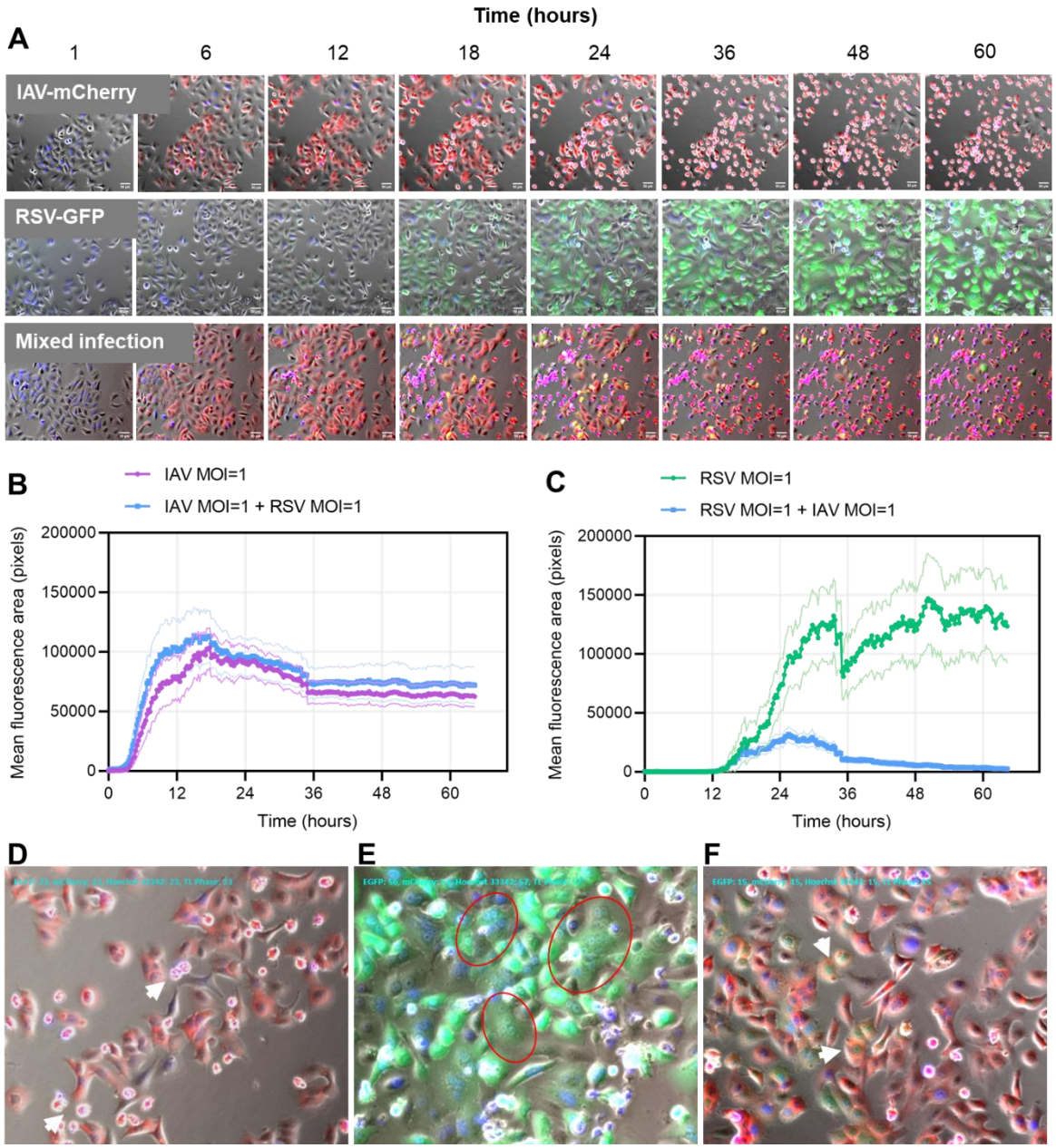

Figure 3-10: Live cell imaging shows dynamics of infection in single infection and coinfection. A549 cells were infected with IAV-mCherry, RSV-GFP or a mixed inoculum of both viruses and the infection was imaged by live cell microscopy for 63 hours. (**A**) Frames collected in single IAV-mCherry (red), RSV-GFP (green) or mixed infection at specified timepoints. (**B**) Mean fluorescence area over time shows kinetics of expression of IAV NS1 in single infection (magenta line) and coinfection (blue line). Standard deviation is shown by thin lines. (**C**) Fluorescence area shows RSV replication is substantially reduced in coinfection with IAV. Standard deviation is shown by thin lines. Figures (**D-F**) show features of each infection condition. (**D**)

Cells infected with IAV-mCherry at 23 hpi, showing some rounded dead cells, indicated by white arrows. (**E**) Cells infected with RSV-GFP at 57 hpi showing extensive syncytia formation, indicated by red ellipses. (**F**) Mixed infection showing coinfected cells producing both mCherry and GFP at 15 hpi, white arrows indicate coinfected cells.

A clear contrast between the cytopathic effects induced by IAV and RSV was shown through the live cell imaging. While cells infected with IAV rapidly underwent cell death, cells infected with RSV favoured cell survival and syncytia formation, with many infected cells remaining alive until the end of the time series. In the mixed infection, many infected cells underwent cell death, however some cells coinfected survived until the end of the time series. RSV has been demonstrated to induce pro-survival and anti-apoptotic signalling pathways (Bitko et al., 2007; Groskreutz et al., 2007). For this reason, cells coinfected with IAV and RSV, compared to cells infected with IAV alone, may be more likely to survive for a longer time post infection, due to RSV-mediated delay to induction of apoptosis. To determine if there was a difference in cell survival in single infected or coinfected cells, cells were randomly selected from the start of each imaging series (n=10 cells, from 8-9 replicate image series) and manually tracked through the frames, until they showed sign of infection via expression of fluorophores. They were tracked until they underwent cell death, at which point the timing of cell death was recorded, or if they didn't die, the time was recorded as 64 hours: the full length of the time series. Cells that did not show sign of infection were excluded in the dataset (Summarised in Figure 3-11A).

Figure 3-11B shows the differences in the kinetics of cell death between IAV-, RSV-infected or coinfected cells from single or mixed infection. In IAV single infection, the majority of tracked cells underwent cell death quickly with an average time of cell death of 30.4 hours post infection (Figure 3-11B). In contrast, RSV infection resulted in much longer cell survival times, with the mean time of cell death at 55.1 hours post infection, and many cells survived until the end of the time series (64 hours) (Figure 3-11B). In mixed infection, there was a significant increase in average cell survival time ($p<0.0001$ by unpaired t-test) between cells positive for both IAV and RSV (IAV+RSV+) compared cells infected with IAV only (IAV+), with mean survival times of 24.8 hours and 32.6 hours for IAV+ and IAV+RSV+ cells respectively (Figure 3-11B). This supports the hypothesis RSV induced pro-survival signalling

pathways may balance against pro-apoptotic pathways induced by IAV, allowing cells infected with both viruses to survive longer. This may provide a competitive advantage for IAV, by enabling each coinfected cell to have a longer productive infection period, potentially facilitating the assembly, release of more infectious virions before the cell undergoes cell death. Interestingly, IAV+ cells from the mixed infection also had a lower survival (p=0.0011 by unpaired t test) time than infected cells in the IAV single infection (Figure 3-11B), indicating that there may be other factors alongside infection status that impact cell survival, for example cytokine signalling in response to coinfection.

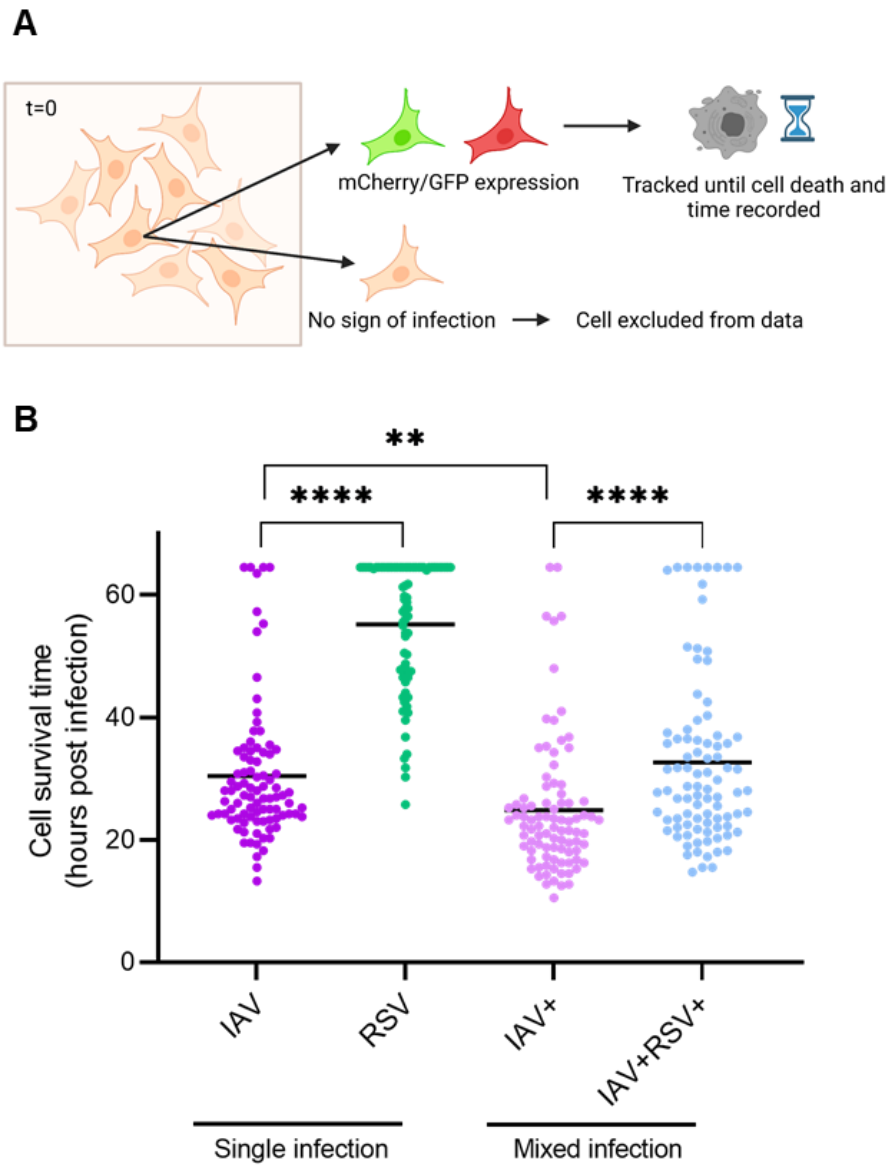

Figure 3-11: Cell survival is reduced following IAV infection compared to RSV infection. (A) Schematic depicting how cell survival was measured. **(B)** Timings of cell death in IAV (magenta, [n=90])) and RSV (green, [n=80]) single infection and

mixed infection (pink and blue). In mixed infection, cells were stratified to those infected only by IAV (pink, [n=90]) and coinfected cells, positive for IAV-mCherry and RSV-GFP (blue, [n=90]). Each point represents an individual cell that was tracked from the start of the time series to the time of cell death. Black lines show the median and statistical significance determined by unpaired t-test, ** p<0.01, **** p<0.0001.

3.3.7 IAV and RSV establish replication cycles in coinfected cells and localisation of nucleoproteins are similar to single virus infections

Analysis of replication dynamics, viral spread and live cell imaging of infected cell populations provides important information about the global impact of infection. However, to understand if viruses interact within cells, coinfected cells were analysed at the single cell level.

Cells on glass coverslips were infected with IAV (MOI=1) and RSV (MOI=4) to achieve a high degree of coinfection and fixed at 24 hpi. Cells were stained for the nucleoproteins of both viruses, IAV NP and RSV N. Due to the fact that both monoclonal antibodies were raised in mice, a sequential staining protocol was optimised to enable specific detection of both viruses. First, cells were blocked with rabbit serum, then incubated with the mouse monoclonal anti-IAV NP primary antibody, followed by incubation with an anti-mouse IgG secondary antibody raised in rabbit. Next, cells were blocked for a second time with donkey serum, followed by incubation with mouse monoclonal anti-RSV N primary antibody, then incubation with anti-mouse IgG secondary antibody raised in donkey. Figure 3-12 shows a panel of infections showing specific detection of IAV NP or RSV N in IAV or RSV single or mixed infections. Co-staining using a sequential staining protocol did not result in cross-staining between secondary antibodies, or background for either primary antibody (Figure 3-12).

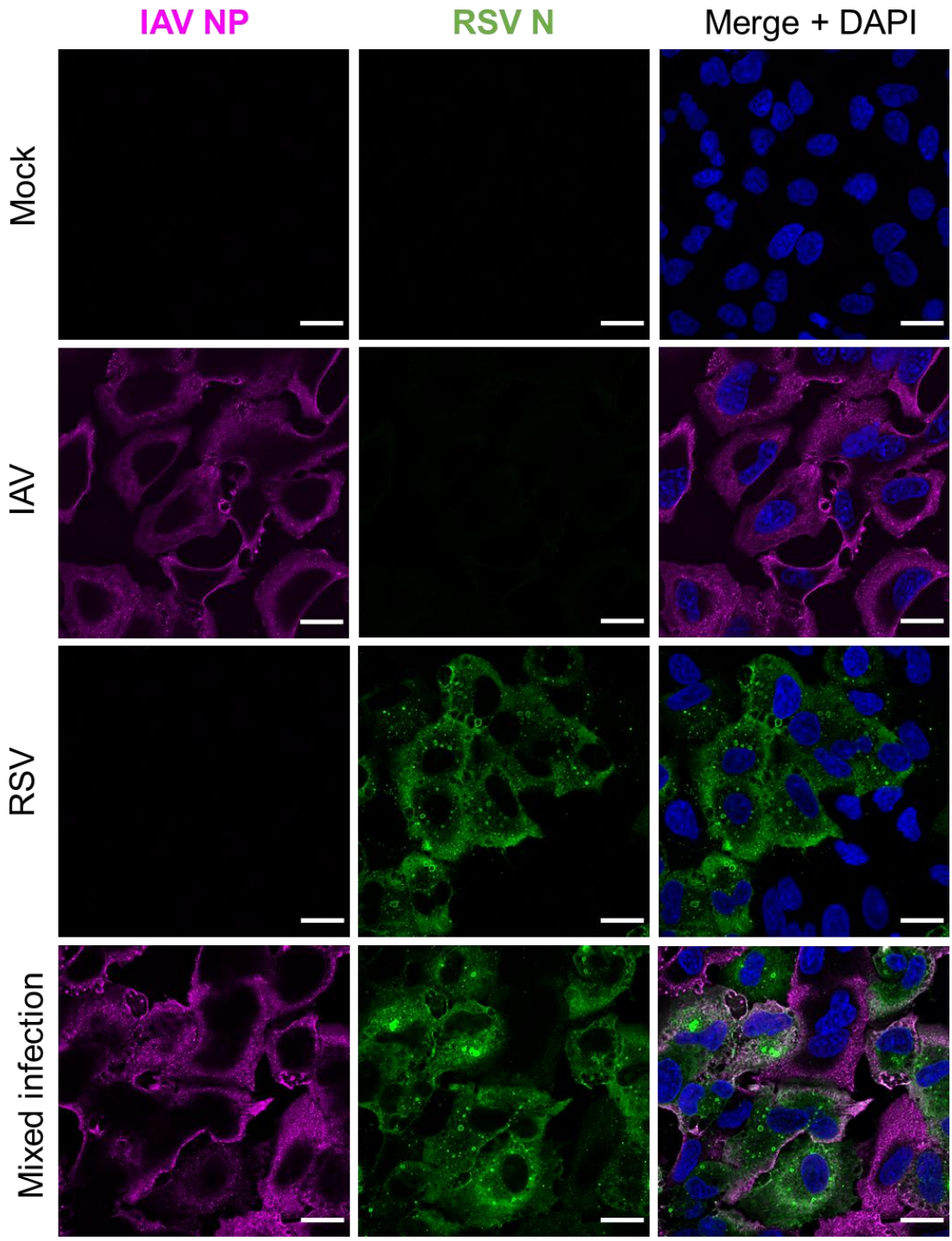

Figure 3-12: Nucleoprotein antibodies do not cross react using sequential staining protocol. A549 cells were infected with IAV (MOI=1) and RSV (MOI=4) for 24 hours, before fixation and staining for IAV and RSV nucleoprotein. Cells were imaged by confocal microscopy on Zeiss LSM880. IAV NP (magenta) and RSV N (green) antibodies both raised in mice do not exhibit cross reactivity and have no background signal. All samples were stained using the same protocol with both primary antibodies. Scale bars indicate 20 µm.

Using a combination of standard confocal microscopy and super-resolution confocal microscopy, nucleoprotein localisation was analysed with single infected and coinfected cells. The localisation of viral nucleoprotein in infected cells gives an indication of the status of infection and the progression of the viral replication cycle. IAV replicates its genome within the nucleus and as infection progresses, individual RNPs containing genome segments are trafficked out of the nucleus and towards the cell edges, therefore NP can be seen localised within the nucleus and diffuse throughout the cell or concentrated to the outer edges of the cell depending on the stage of infection (Figure 3-13A). In RSV infection, N assembles to cytoplasmic inclusion bodies, which are sites of genome replication and transcription (Lahaye et al., 2009; Galloux et al., 2020) (Figure 3-13B). In some cells, N assembles into filament shaped structures at the cell surface, which represents RNP packaged into budding RSV filaments extending from the cell (Figure 3-13B).

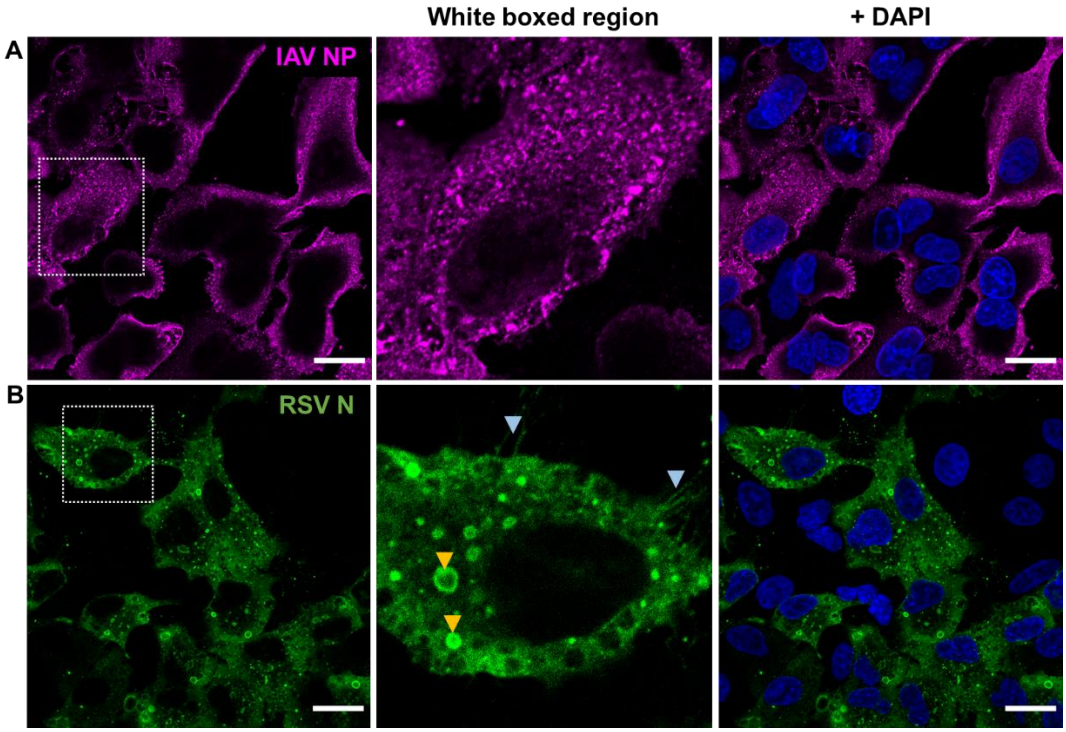

Figure 3-13: Localisation of IAV or RSV nucleoprotein in single infection. A549 cells were infected with IAV (MOI=1) and RSV (MOI=4) for 24 hours, before fixation and staining for IAV and RSV nucleoprotein. Cells imaged by confocal microscopy on Zeiss LSM880. (**A**) IAV NP staining (magenta) in single IAV infected cells at 24 hpi. Cytoplasmic NP staining is diffusely localised or localised towards cells. White box shows region magnified in central image, showing diffuse cytoplasmic NP staining, with some staining in nucleus. (**B**) RSV N staining (green) in single RSV infected cells at 24 hpi. White boxed region is magnified in central image. Staining

is cytoplasmic and inclusion bodies can be identified (yellow arrows) along with filamentous structures extending from the cell edge (pale blue arrows). Scale bars indicate 20 µm.

In coinfected cells, the features of the replication cycles of both viruses can be observed in varying stages of infection. IAV NP staining can be observed within the nucleus and the cytoplasm of coinfected cells alongside cytoplasmic RSV N positive inclusion bodies (Figure 3-14A).

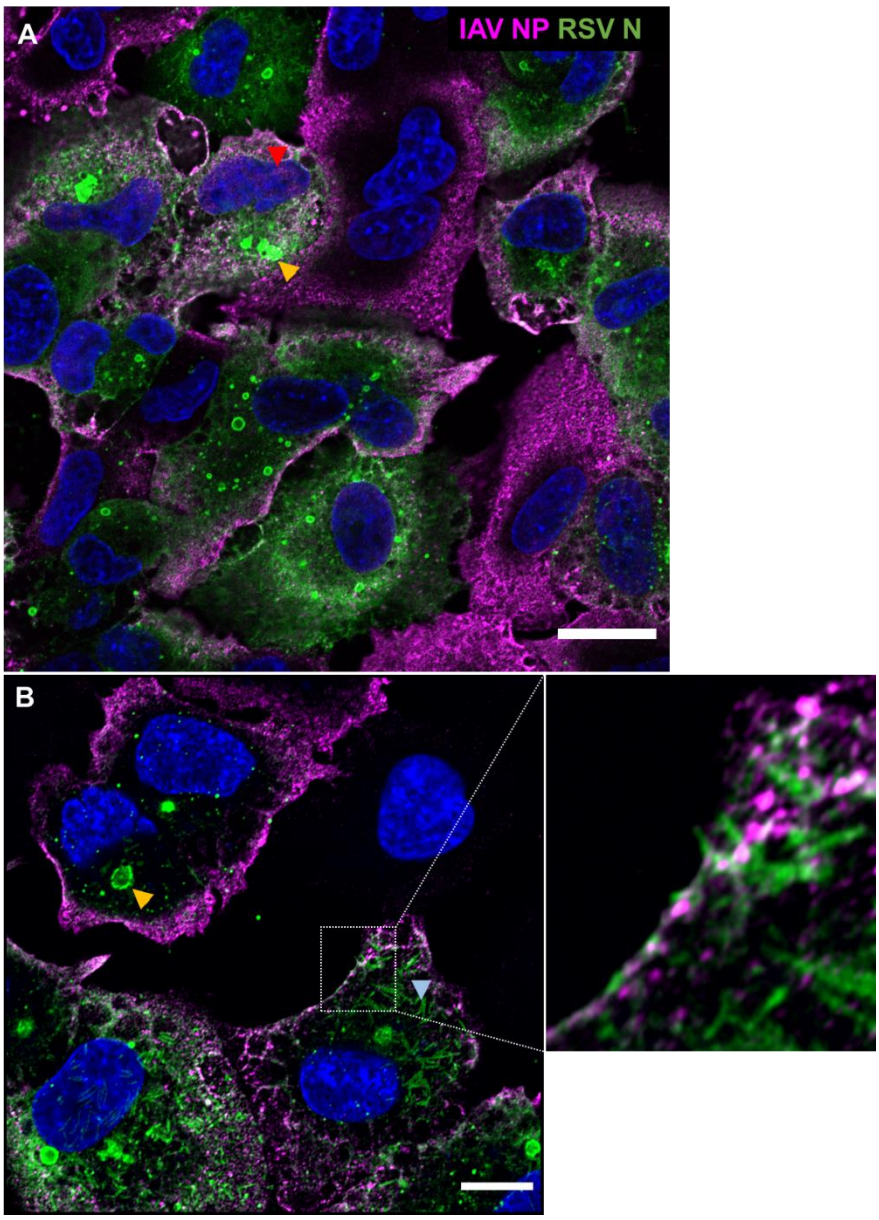

Figure 3-14: Localisation of IAV NP and RSV N in coinfected cells. A549 cells were infected with IAV (MOI=1) and RSV (MOI=4) for 24 hours, before fixation and staining for IAV and RSV nucleoprotein. (**A**) Coinfected cells displayed features of

the replication cycles of both IAV and RSV. RSV inclusion bodies are indicated by orange arrow, nuclear localisation of IAV NP is indicated by red arrow. Cells were imaged by confocal microscopy on Zeiss LSM880. Scale bar indicates 20 µm. (**B**) RSV N displayed features of late replication cycle and assembled into filamentous structures (light blue arrow). Inset of white boxed region shows IAV NP and RSV N localised in close proximity at plasma membrane. Cells were imaged by super-resolution confocal microscopy on Zeiss LSM880 with Airyscan detector. Scale bar indicates 10 µm.

Viral RNPs are trafficked to the cell membrane for assembly of new viral particles. In coinfected cells, IAV NP and RSV N can be observed localising to the same regions of the plasma membrane (Figure 3-14B inset). RSV N assembles to filamentous structures within the cytoplasm in some coinfected cells (Vanover et al., 2017) and some N positive structures can be observed extending from the cell edge (Figure 3-14B). This indicates that RSV can establish and progress its replication cycle in a cell coinfected with IAV and suggests both viruses may be tolerant to the presence of the coinfecting virus. This observation contrasts with replication data, which showed that the infectious titre of RSV released into the supernatant was significantly reduced in coinfection, particularly at later timepoints. The negative interaction between IAV and RSV may therefore be impacting assembly or release of infectious RSV, rather than earlier stages in the RSV replication cycle.

3.3.8 IAV and RSV glycoproteins localise to the plasma membrane in coinfected cells

IAV NP and RSV N localised to the same regions of the plasma membrane of coinfected cells, therefore it is reasonable to assume that these could be sites of viral assembly. To determine if other viral proteins also concentrate to the same regions of the plasma membrane, cells were stained for IAV and RSV glycoproteins. The major glycoproteins from each virus were selected: IAV HA and RSV fusion glycoprotein (F). There was no cross-reactivity detected between IAV HA (magenta) and RSV F (green) antibodies (Figure 3-15). Some background was observed in the mock and RSV-infected wells following staining for HA, although this appeared to

bind to cellular membrane structures, rather than cross-reacting with RSV proteins in infected cells (Figure 3-15).

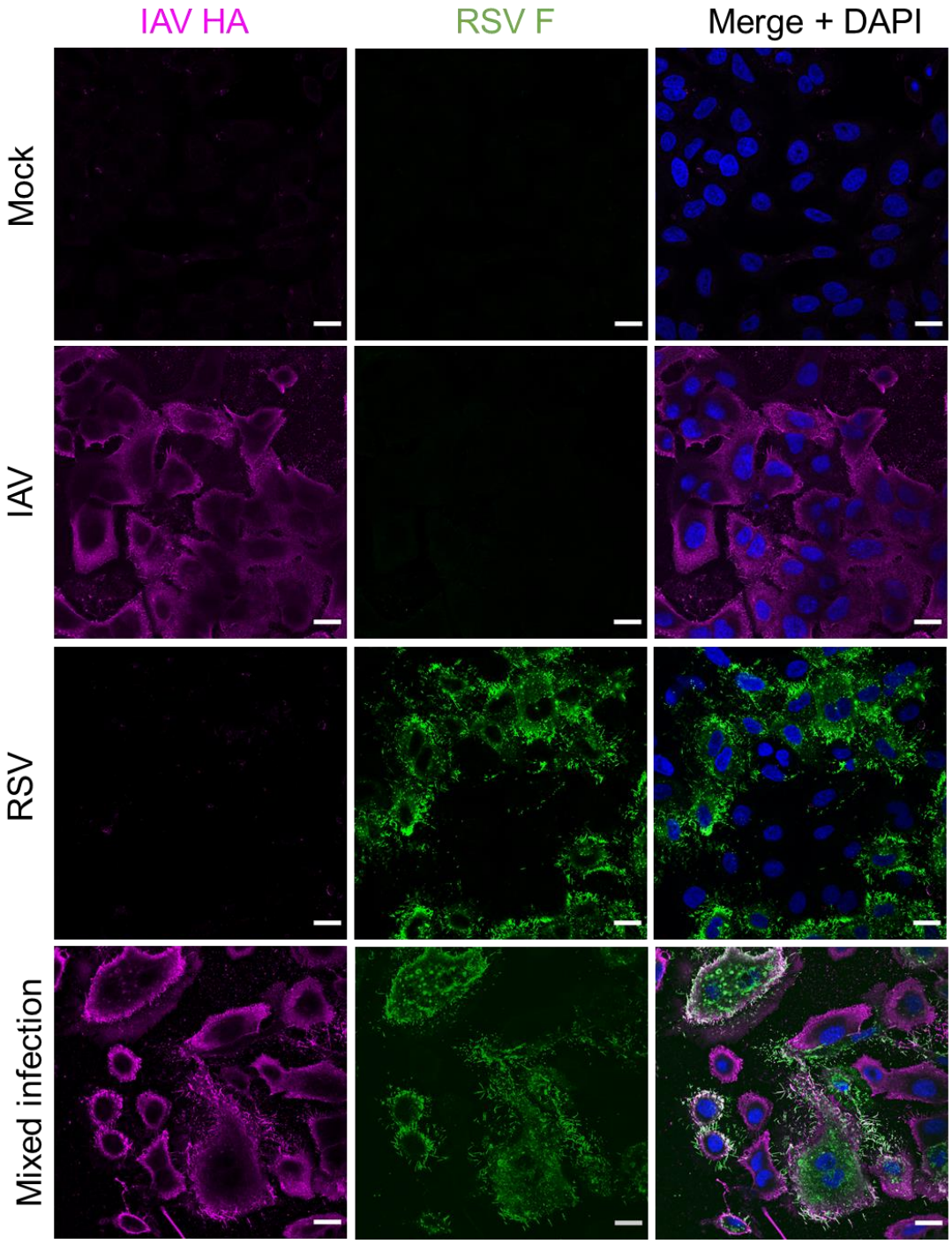

Figure 3-15: Panel of co-staining with IAV HA and RSV F. A549 cells were infected with IAV (MOI=1) and RSV (MOI=4) for 24 hours, before fixation and staining for IAV HA and RSV F. Cells were imaged by confocal microscopy on Zeiss LSM880. There was no cross-reactivity detected between IAV HA (magenta) and RSV F (green) antibodies. Colocalisation of proteins is shown by white signal. Scale bar indicates 20 µm.

In IAV single infected cells, HA was localised in the cytoplasm and at the surface of coinfected cells (Figure 3-16A). Pleiomorphic HA-positive particles were stuck to the coverslip around infected cells, and these are likely to be released IAV virions (Figure 3-16A). In RSV single infection, RSV was primarily localised to sites of budding virus at the cell surface, and filamentous structures positive for F were seen extending from infected cells (Figure 3-16B).

In coinfected cells, both glycoproteins localised to the cell surface and colocalisation of both HA and F was observed. Further, both glycoproteins appeared to colocalise in regions of filamentous structures (Figure 3-16C). These filaments were positive for RSV F and similar in morphology to RSV filaments in single infection, suggesting that these structures were budding RSV. The detection of HA within these regions implies that HA is not actively excluded from regions of RSV budding, therefore mixing of viral components may occur within these regions.

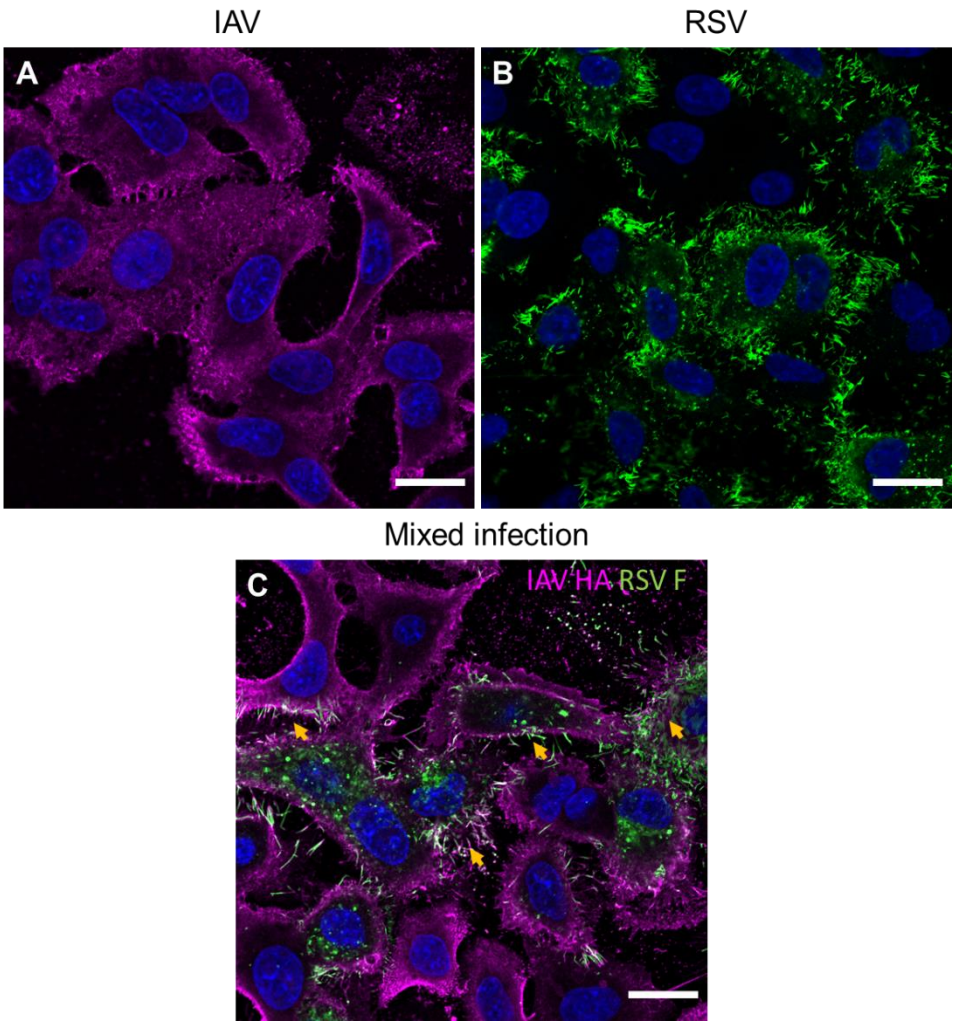

Figure 3-16: Localisation of IAV HA and RSV F in single and mixed infections. A549 cells were infected with IAV (MOI=1) and RSV (MOI=4) for 24 hours, before

fixation and staining for IAV HA and RSV F. Cells were imaged by confocal microscopy on Zeiss LSM880. (**A**) IAV single infection displays diffuse HA staining (magenta) in the cytoplasm of infected cells. (**B**) RSV F staining (green) in RSV single infection is primarily localised to the cell surface, at sites of filament budding. (**C**) In mixed infection, coinfected cells are positive for both HA and F and glycoproteins mix in regions of budding filaments (indicated by yellow arrows). White signal indicates colocalisation of HA and F. Scale bars represent 20 µm.

3.4 Discussion

This chapter describes the development of an *in vitro* model of coinfection between IAV and RSV, in which key phenotypes of infection were characterised for both IAV and RSV single virus infections and coinfections.

To selectively measure IAV and RSV replication in coinfection, MDCK and HEp-2 cells were validated to allow the identification of plaques by IAV or RSV respectively. Plaque assays allow the quantification of infectious virions, i.e., those containing a complete genome, capable of establishing infection. This provides important information on the overall fitness of each virus in mixed infection. However, the limitation of this measure is that it does not capture the true yield of progeny virions - infectious, semi-infectious and defective – that are produced. IAVs have a high particle to infection ratio, with only 1-10% of particles produced capable of independently establishing infection (Donald and Isaacs, 1954; Enami et al., 1991; Tremaglio et al., 2013). Similarly, RSV has also been demonstrated to produce defective interfering particles and they are required for establishing persistent infection in human epithelial cell lines (Valdovinos and Gómez, 2003). Due to time constraints, genome replication was not measured by qPCR, however this would be an important experiment to carry out, to quantify infectious and non-infectious genomes and determine if particle to pfu ratios are altered in mixed infection. This could indicate whether interactions occurring during viral assembly or genome packaging may be influencing the observed growth kinetics.

Viral replication experiments showed that IAV replication was uninhibited by the presence of RSV and in fact, IAV replicated to marginally higher infectious titres in mixed infection. Conversely, RSV replication was significantly reduced in coinfection with IAV. This observation is consistent with in vitro coinfection experiments (Shinjoh

et al., 2000; Drori et al., 2020), and animal challenge studies which all report a reduction in RSV gene expression or infectivity in coinfection with IAV (Shinjoh et al., 2000; Chan et al., 2018; Ayegbusi et al., 2019; Drori et al., 2020). Goto *et al.* demonstrated that IAV replication was increased in coinfection with parainfluenza 2 (PIV2) due to cell fusion induced by PIV2, which facilitated IAV spread. RSV induces syncytium formation in A549 cells, therefore this interaction may have contributed towards the observed increase in IAV titre. However, this interaction may not be of physiological relevance. Whilst formation of syncytium has been reported in histopathological analysis of human RSV infections (Johnson et al., 2007), it is unlikely to be a widespread cytopathology that would contribute to substantial increases in IAV spread within the respiratory tract.

To provide a competitive advantage to RSV, IAV input was reduced 10-fold and 100-fold relative to the input of RSV. However, this did not impact viral replication phenotypes and RSV replication was still significantly reduced in mixed infection, despite the relative reduction in IAV input virus. IAV was still able to replicate to the same or higher titres in the presence of a greater inoculum of RSV. This implies that the negative interactions that result in a reduction in RSV titre occur despite IAV being at an initial competitive disadvantage, and that RSV does not appear to exert negative interactions that impact IAV replication.

Further, staggered infections were carried out, where cells were first infected with RSV, followed by IAV infection up to 24 hours after the primary infection with RSV. IAV replicated to significantly higher titres at 6 and 16 hours and the same titre at 24 hours staggered infections compared to mock primary infections, despite infecting cells that were already actively infected by RSV. This shows that cells do not become refractory after infection by RSV, which allows IAV to superinfect, resulting in coinfection. This experiment was not carried out in the reverse order with IAV as the primary infecting virus, however it would be interesting to determine if cells infected by IAV are permissive to infection by a secondary unrelated virus, as superinfection exclusion is known to occur between related IAV strains (Sun and Brooke, 2018). Timing of infection may be an important regulator of superinfection and perhaps leaving a longer delay between primary and secondary infection would result in different infection outcomes. Interestingly, Czerkies *et al.* reported in a recent pre-print that after a delay of 30 hours between primary RSV infection and secondary IAV infection, IAV preferentially superinfected RSV infected cells, rather

than uninfected bystander cells, as the bystander cells were refractory to infection due to RSV-induced antiviral signalling (Czerkies et al., 2021). Other coinfection studies have showed that rhinovirus (RV), a strong inducer of the interferon (IFN) response, blocks the replication of SARS-CoV-2 and IAV, by rendering all cells refractory to secondary infection (Wu et al., 2020; Dee et al., 2021; Cheemarla et al., 2021). Further experiments investigating the role of the cellular innate immune response are important in establishing how viral interference interactions contribute to IAV and RSV dynamics in coinfection. Both viruses possess potent anti-viral proteins non-structural protein 1 (NS1) for IAV and NS1 and NS2 for RSV (Reviewed by [Hao, Wang and Li, 2020; Thornhill and Verhoeven, 2020]). A549 cells are IFN competent (Xiao et al., 2013; Hillyer et al., 2015), but no reduction to IAV titre was observed during staggered infection or when IAV input titre was low. Down regulation of innate immune signalling in a cell primarily infected by RSV may facilitate superinfection. In staggered infections, experiments were carried out with RSV at high MOI, so all IAV in the secondary infection may have occurred by superinfection. Reducing RSV MOI in the primary infection would be an important experimental variation, to confirm if IAV preferentially infects RSV infected cells due to RSV immune antagonism mechanisms, while being unable to infect refractory bystander cells. This could have important implications in understanding the likelihood of opportunities for IAV and RSV to directly interact at the cellular level within the coinfected respiratory tract.

To understand viral dynamics at the cellular level, the proportion of cells infected with IAV, RSV or coinfected were determined for single and mixed infections, at matched MOIs to replication kinetics experiments. Replication kinetic data showed that IAV titre was the same or increased in coinfection at 24 hpi and this was matched by the proportion of IAV positive cells (IAV infected and coinfected), where there was no significant difference between single and mixed infection. However, at the earlier timepoint of 8 hpi, the proportion of IAV+ cells was significantly lower in mixed infection at IAV MOIs 4 and 0.4, compared to corresponding single infections. Conversely, a higher proportion of cells were positive for RSV in mixed infections, at both 8 and 24 hpi, despite observing a reduction in RSV titre at 24 hpi in growth kinetics experiments. Differences in cell survival post infection by IAV and RSV may explain the trends observed. If cell survival is promoted in cells positive for RSV infection (RSV-only or coinfected), they may be over-represented in mixed infection by 24 hpi, by surviving longer than cells infected only with IAV. Therefore, the

observed proportion of RSV infected cells may be inflated, due to removal of IAV infected cells from the observed population. However, at 8 hpi, there was no evidence of cell death, therefore other interactions that promote the expression of RSV N in coinfection must be occurring. It is possible that IAV-induced signalling pathways allow the acceleration of the RSV replication cycle and translation of N, which in turn creates competition interactions that slow the replication of IAV and expression of HA. IAV induces host shutoff to repress translation of cellular mRNA, allowing preferential translation of viral mRNA. This is achieved by reducing the level of cellular mRNA, rather than the preferential promotion of viral mRNA translation (Bercovich-Kinori et al., 2016). One plausible explanation for the trends in antigen positivity observed is that IAV-induced host shutoff may favour translation of RSV mRNA, by reducing competition from host transcripts. In turn, this may negatively impact IAV, as the RSV provides a further source of competition for translational machinery, without expending resource to promote host shutoff.

This data also highlights the importance of analysing both released infectious virus and viral protein expression at the cellular level, as the seemingly contradictory findings shed light on potential sources of interaction and the kinetics of such interactions. Interactions at early timepoints during the first round of replication may later be overshadowed by more dominant interactions during later infection that drive observed viral growth kinetics. These infections were carried out at high MOI, such that the majority of cells were infected during the first round of infection. Further experiments using low MOIs are important to understand how foci of infection spread into one another and if inhibitory interactions that prevent coinfection may arise.

Single cell RNAseq may provide the means to explore these interactions in more detail. Comparison of the transcriptomes of cells infected with IAV, RSV or both viruses would inform on which viral induced pathways are activated in coinfected cells. Analysis of the transcriptome of coinfected cells at multiple time points would shed light on the temporal nature of viral interactions, that may be occurring at different stages of the replication cycle. Collecting individual cell data would also provide information about the of viral dynamics within a coinfected cell and the variability of viral replication on an individual cell level, which was demonstrated to be extremely variable in IAV infection (Russell et al., 2018). Further, analysis of the transcriptomes of the uninfected cells in single infections or mixed infections would

illuminate differences in cytokine signaling initiated from coinfected or single infected cells.

To further understand the dynamics of infection, live cell imaging was employed to observe infection over a continuous timescale. Live cell imaging highlighted differences in virus induced cytopathic effect and revealed the kinetics of cell survival following single infections or mixed infections. Cell survival was high following infection by RSV but was substantially lower following infection by IAV in single or mixed infection. Analysis of cell survival times showed that coinfected cells (positive for IAV-mCherry and RSV-GFP) survived on average 8 hours longer than cells infected only with IAV in the mixed infection. This suggests that the presence of RSV in coinfected cells may prolong cell survival and delay IAV induced cell death. Promotion of cell survival may allow coinfected cells to have a longer productive period to produce viral particles and may contribute to the increase in IAV titre observed in mixed infections. This could be investigated by examining expression of cellular mediators of cell survival and apoptosis. Comparison of cleaved caspase 3 (CC3) expression in single or coinfected cells over a time course would confirm if induction of apoptosis is delayed in coinfected cells. Further, analysis of expression of markers of cell survival and proliferation, such as Ki-67, and activation of the phosphatidylinositol 3-kinase (PI-3K)/AKT pathway, may illuminate how RSV can promote survival of coinfected cells (Thomas et al., 2002). However overall, cell survival in mixed infection was drastically reduced compared to RSV single infection. Therefore, it is likely that cell death induced by IAV infection plays an important role in the observed reduction of RSV titre in mixed infections. RSV infection may spread into an equivalent proportion of cells in single and mixed infection, however, if coinfected cells undergo cell death earlier, then the yield of infectious RSV released into the supernatant of mixed infections will be lower.

When comparing results from experiments quantifying the number of RSV-infected cells in coinfection (Figure 3-9) to the relative GFP fluorescence associated with RSV (Figure 3-10), there appeared to be a discrepancy between datasets. Quantification of RSV-infected cells revealed that there was an increase, rather than reduction, in the proportion of cells infected with RSV in mixed infection at 24 hpi, compared to single RSV infection (Figure 3-9). In contrast, in live cell experiments, GFP signal associated with RSV infection was substantially lower in mixed infection compared to single infection, and almost entirely eliminated by 36 hpi (Figure 3-10).

This difference could be due to differences in sensitivity in detecting RSV infection between live cell imaging and confocal microscopy experiments, where measuring relative fluorescence may not capturing cells with low expression of GFP.

Replication kinetics, viral spread and live cell experiments provide a global overview of how IAV and RSV interact within a population of coinfected cells and the impact of viral interactions in this system. To attempt to identify potential sources of interactions at the single cell level, cells were immunostained for viral proteins. Staining for IAV NP and RSV N showed that features of both virus's replication cycles can be observed in coinfected cells, and the localisation of nucleoproteins looks similar to single IAV or RSV infected cells. This indicates that many process involved in each virus's replication cycle, including transcription and translation of viral gene products and trafficking of proteins can occur in the presence of the coinfecting virus. Whilst there may be sources of interaction or competition occurring within these processes, the interactions are not sufficient to block either IAV or RSV from progressing replication. The fact that each virus replicates in a different cellular compartment may explain why IAV and RSV are tolerant to the presence of the other within the same cell. Upon infection, IAV RNPs are trafficked directly into the nucleus for genome replication and transcription (O'Neill et al., 1995). RSV replicates within the cytoplasm and initiates the formation of cytoplasmic inclusion bodies, to which the proteins of the polymerase complex localise (Galloux et al., 2020) to carry out genome replication and transcription (Lahaye et al., 2009). This spatial segregation of viral replication centres may be sufficient to prevent interactions, for example competition for cellular resources, from occurring.

Late in infection, newly formed viral genomes are trafficked to the plasma membrane of the cell for assembly of new virions (Bruce et al., 2010; Amorim et al., 2011; Ke et al., 2018). IAV and RSV target lipid raft regions of the plasma membrane to concentrate viral proteins and assemble new virions (Carrasco et al., 2004; Fleming et al., 2006). Super-resolution confocal microscopy imaging of IAV NP and RSV N localisation at the plasma membrane indicated that both viral genomes are trafficked to the same regions in coinfected cells. In addition, staining for IAV HA and RSV F showed that these glycoproteins can also be found within the same regions of the plasma membrane, where filamentous structures likely representing budding RSV filaments are formed. This indicates that IAV and RSV may assemble and bud within close proximity, therefore providing the opportunity for viral interactions within these

pathways. Interactions within these steps could have important implications for viral progeny and may affect infectivity or virion stability. Interactions at this stage therefore may impact observed viral growth kinetics and may contribute towards the reduction in RSV titre observed in mixed infections. Interactions during viral assembly and budding are explored in more detail in Chapter 4.

Overall, the work described in this chapter characterises IAV and RSV infection in a model of coinfection in A549 cells. By comparing overall phenotypes in viral replication and cell spread to analysis of the localisation of key viral proteins, potential sources of viral interaction can be identified. The findings in this chapter support previously published studies (Shinjoh et al., 2000; Chan et al., 2018; Ayegbusi et al., 2019; Drori et al., 2020) and also provide novel insights to IAV and RSV coinfection at the single cell level. Finally, an important potential source of interaction was identified during virion assembly and budding, which warranted further study in the following chapter.

Chapter 4

Coinfection by IAV and RSV results in the formation of hybrid viral particles with altered tropism

4.1 Introduction

The experiments described in Chapter 3 show that Influenza A virus (IAV) and respiratory syncytial virus (RSV) readily coinfect lung epithelial cells (A549), with no evidence of the occurrence of superinfection exclusion interactions. Additionally, IAV and RSV viral proteins are both expressed in coinfected cells and their localisation does not appear markedly different to localisation in single infected cells. IAV and RSV glycoproteins both localised to the plasma membrane of coinfected cells and appear to be expressed in close proximity. This leads to the question: do components of IAV and RSV mix during viral assembly and budding in coinfected cells?

IAV and RSV share tropism for cell types within the respiratory tract. Studies using differentiated airway cultures report that both IAV and RSV target ciliated airway epithelial cells (Thompson et al., 2006; Zhang et al., 2011; Hui et al., 2018). Further, both viruses bud from the apical surface of polarised cells. Using thin section transmission electron microscopy (TEM) of differentiated normal human bronchial epithelial cells, Ke *et al.* demonstrated that RSV virions exhibit filamentous morphology and bud from the apical surface, within ciliated regions (Ke et al., 2018). Additionally, multiple studies have shown that RSV budding occurs at the apical surface in immortalised polarised cell lines including Madin Darby Canine Kidney (MDCK) cells and Vero C1008 cells, by culturing the cells on transwell inserts (Roberts et al., 1995; Brock et al., 2003; Batonick et al., 2008). IAV budding also occurs strictly at the apical surface of polarised cells and multiple studies report that even an introduction of a basolateral localisation signal to haemagglutinin (HA) or neuraminidase (NA) did not alter the polarity of IAV budding (Mora et al., 2002; Barman et al., 2003). The apical surface of ciliated cells therefore provides an environment in which IAV and RSV may come into direct contact within coinfected cells.

IAV and RSV, like many other enveloped viruses, share a preference for assembly and budding in lipid raft regions on the apical membrane of cells. Lipid rafts are structured membrane domains, rich in cholesterol and sphingolipids. By concentrating proteins within these regions, lipid raft microdomains play an important role in many cellular processes, including endocytosis, signal transduction and regulation of cell adhesion and migration (reviewed by [Munro, 2003]). IAV

targets these regions for concentration of structural proteins prior to viral assembly. Coordinated trafficking of HA and NA has been shown to accelerate apical targeting of viral proteins, compared to the kinetics of trafficking HA alone (Ohkura et al., 2014), and IAV ribonucleoprotein (RNP) has been shown to independently traffic to lipid rafts on the apical surface of cells, therefore directing polarity of IAV budding (Carrasco et al., 2004). RSV fusion glycoprotein (F) also localises to lipid raft regions, via targeting signals in the extracellular domain of the glycoprotein (Fleming et al., 2006). Disruption of lipid rafts by depletion of cholesterol was shown to reduce RSV infectivity (Chang et al., 2012). Incorporation of lipid rafts into budding viral filaments has been shown to be important for the stability of both IAV and RSV. Bajimaya *et al.* showed that, whilst depletion of cholesterol did not reduce the production of IAV or RSV virions, it did reduce the stability, and therefore infectivity, of the progeny of both viruses (Bajimaya et al., 2017). With lipid raft microdomains playing an important role in the concentration of structural proteins and initiation of viral budding, it is possible that IAV and RSV proteins may be concentrated to the same regions of the cellular membrane. If so, it is plausible that proteins derived from IAV and RSV will directly interact within these regions.

Enveloped viruses can incorporate selected host-derived membrane proteins into viral particles. This is driven by selective, rather than passive mechanisms, indicating that viruses have capacity to take up non-self proteins for functional gain. This process is well described for many retroviruses, and human immunodeficiency virus 1 (HIV-1) has been demonstrated to incorporate Intracellular adhesion molecule 1 (ICAM-1), which retains functionality and in fact enhances HIV-1 infectivity (Fortin et al., 1997). Calveolin, a lipid raft associated protein, is specifically recruited and incorporated into mature RSV filaments and is thought to contribute towards the properties of the RSV envelope (Brown et al., 2002; Ludwig et al., 2017). Transmembrane proteins tetraspanins are incorporated into the envelope of IAV virions (Shaw et al., 2008; Hutchinson et al., 2014). The incorporation of host proteins to viral membranes indicates that there may be capacity within IAV and RSV envelopes to incorporate components from other sources. Therefore, there may be potential for incorporation of viral proteins from a coinfecting virus.

Assembly and budding of IAV and RSV particles in close proximity could result in mixing and incorporation of components of both viruses into newly forming viral particles. Interactions during viral assembly have been described previously.

Pseudotyping or phenotypic mixing is a direct virus-virus interaction, which results in the incorporation of glycoproteins from one virus to the envelope of a coinfecting virus. This interaction has been demonstrated to occur for multiple, taxonomically diverse viruses (Granoff and Hirst, 1954; Choppin Atn and Compans, 1970; Huang et al., 1974; Heng et al., 1994; Tang et al., 2014). Pseudotyping results in changes to biological properties, including evasion of expansion of viral tropism (Heng et al., 1994; Tang et al., 2014) and evasion of neutralising sera (Granoff and Hirst, 1954; Choppin Atn and Compans, 1970; Tang et al., 2014). These studies provide important evidence that direct viral interactions can alter viral progeny, and this in turn impacts viral function.

Advancements in the understanding of IAV and RSV structure and viral assembly have been made possible by cryo-electron tomography (cryo-ET) studies. In contrast to single particle electron microscopy methods, where proteins or viral particles are first isolated and purified, cryo-ET allows *in situ* imaging within the wider context of the cell or infection (Turk and Baumeister, 2020). Biological samples are preserved by rapid freezing in vitrified ice, which captures structures within their native state. Three-dimensional data is collected by collecting incremental images of a specimen across a tilt axis, usually +/- 60˚ (Hagen et al., 2017), which are then reconstructed in a process of image alignment. Alignment using gold fiducials allows motion correction across the tilt series (Mastronarde and Held, 2017). Samples must be less than 500 nm in thickness to allow electron penetration and for virion preparations, samples should be thin enough for imaging for cryo-ET without additional processing. For thicker samples, for example regions within a cell, sample thinning methodologies can be carried out. Sectioning of frozen samples using a cryo-microtome allows thin slices to be cut from frozen cells, while focused ion beam (FIB) milling of a frozen sample to generate a thin lamella through a sample which is suitable for imaging (Marko et al., 2007). Cryo-EM imaging can be directed by using a correlative light and electron microscopy (CLEM) approach, where regions of interest are highlighted by fluorescence, predominantly via the incorporation of a fluorescent tag to a target protein (Tuijtel et al., 2019). Regions of interest can then be identified by light microscopy, prior to imaging by cryo-ET (Hampton et al., 2016). Whilst cryo-ET methodologies cannot attain the resolution of single particle methods, high resolution structures can be determined by sub-tomogram averaging to sub nanometer resolution (Chen et al., 2019). This process involves extracting repeated structures of interest from within tomograms and

aligning and averaging them with or without a common reference structure. The benefit of this method is it allows elucidation of the structure of macromolecules within context of larger assemblies, accounting for their geometry and spatial arrangement. Cryo-ET workflows have been used to gain high resolution structural information about the structure of IAV and RSV virions, as well as processes involved in virion assembly. Liljeroos *et al.* first characterised the structure of RSV filaments by cryo-ET and further studies by Kiss *et al.* and Ke *et al*. provide important information on interactions with M2-1 within the virion and mechanisms involved in RSV assembly and budding (Liljeroos et al., 2013; Kiss et al., 2014; Ke et al., 2018). Recently, Conley *et al.* used cryo-ET and sub-tomogram averaging to demonstrate the helical arrangement of RSV matrix and glycoprotein incorporation (Conley et al., 2021). The structure of IAV virions have been extensively studied by cryo-ET (Harris et al., 2006; Calder et al., 2010; Vijayakrishnan et al., 2013). Peukes *et al.* recently determined the structure of helical assemblies of M1 within IAV filaments using sub-tomogram averaging (Peukes et al., 2020). Cryo-ET workflows have not previously been applied to study virus-virus interactions within coinfected cells.

This chapter builds on the observation that IAV and RSV components colocalise to the plasma membrane of coinfected cells and I explored the hypothesis that viral interactions occur during viral assembly and budding, which could impact viral progeny from coinfected cells. The first objective was to determine at higher resolution the extent to which IAV and RSV glycoproteins mix at the plasma membrane, and if there were qualitative differences in filamentous viruses budding from coinfected cells. Following this, I applied cryo-ET to characterise the ultra-structure of viruses produced in coinfection, with the aim to identify structural differences between viral progeny from coinfection and single virus infections. Finally, I carried out functional experiments to determine if coinfection has the capacity to alter the function of IAV and RSV, by carrying out experiments assessing viral tropism and antigenicity.

4.2 Acknowledgements

I would like to thank the following individuals for their contributions to the research described in this chapter. Margaret Mullin processed and imaged samples by scanning electron microscopy. Daniel Goldfarb provided laminin coated grids for

TEM experiments. Marie Clarke screened grids on JEOL JEM-F200 microscope. James Streetley imaged grids on the JEOL CRYOARM 300. Swetha Vijayakrishnan for training in all aspects of sample preparation for cryo-EM and cryo-ET data analysis. All tomography data was generated and analysed with help from Swetha. Kieran Dee carried out infections for the neuraminidase experiment positive control.

4.3 Results

4.3.1 Confocal microscopy reveals viral filaments that incorporate the glycoproteins of both IAV and RSV budding from coinfected cells

To investigate mixing of viral proteins during assembly and budding, expression of IAV and RSV glycoproteins at the plasma membrane of coinfected cells was assessed. A549 cells were coinfected with IAV (MOI=1) and RSV (MOI=4), a combination that was previously validated for imaging coinfected cells (Chapter 3) and fixed at 24 hpi. Cells stained for the major glycoproteins of IAV and RSV: IAV haemagglutinin (HA) and RSV fusion glycoprotein (F).

IAV HA coated the plasma membrane of infected cells, while RSV F staining was localised to cytoplasmic bodies and regions near to budding viral filaments at the plasma membrane (Figure 4-1A). In coinfected cells IAV HA did not appear to be excluded from RSV budding sites and glycoproteins from both viruses were observed in close proximity in these regions (Figure 4-1B). The fluorescence intensity profile of HA and F staining confirmed that both glycoproteins colocalized in regions of budding filaments (Figure 4-1C). Peaks of HA and F staining intensity appeared to correspond to filamentous structures, suggesting that they may be incorporated into the same viral particles.

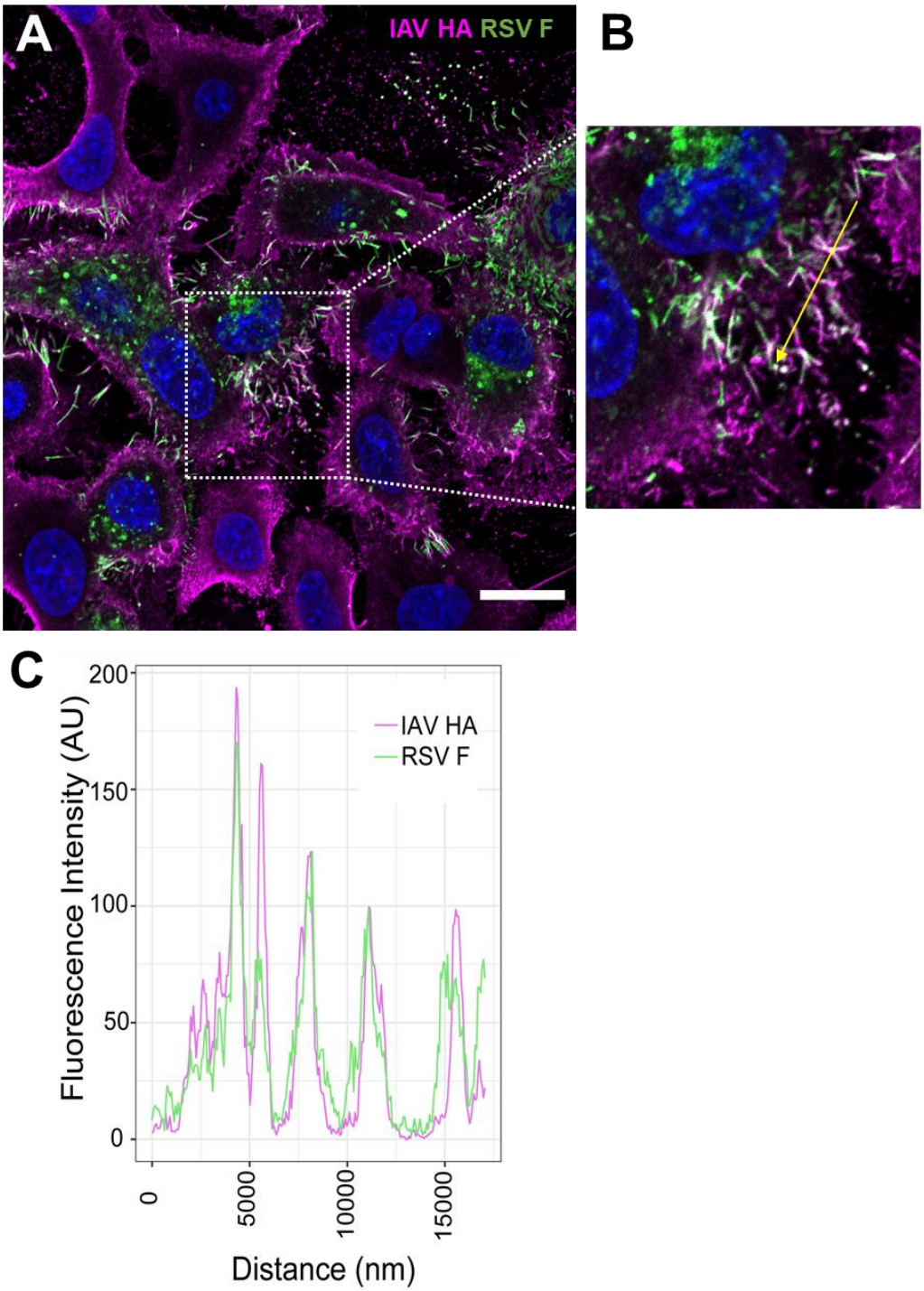

Figure 4-1: IAV HA and RSV F colocalize in regions where RSV filaments are budding. (**A**) A549 cells were infected IAV MOI 1 and RSV MOI 4 and incubated for 24 hpi, before fixation and immunostaining for IAV HA (magenta) and RSV F (green). Cells were imaged by confocal microscopy on Zeiss LSM880. Scale bar indicates 20µm. (**B**) Magnified view of boxed region in A shows that both HA and F are found in regions where viral filaments are budding. White signal indicates areas of colocalisation. Yellow arrow indicates region where fluorescence intensity was

measured. (**C**) Relative fluorescence intensity profile shows colocalisation of HA and F in regions with budding filaments.

To further assess if HA and F were colocalizing within individual viral particles, super resolution confocal microscopy was used to examine virus budding from coinfected cells. Filaments that incorporated HA and F were identified (Figure 4-2). While most of these viruses appeared to be cell associated (Figure 4-2A), dual positive filament structures distant from coinfected cells were also observed (Figure 4-2B). These released particles resembled the cell associated particles in staining profile, and retained their filamentous morphology, suggesting that the dual-positive filaments can be effectively released from coinfected cells.

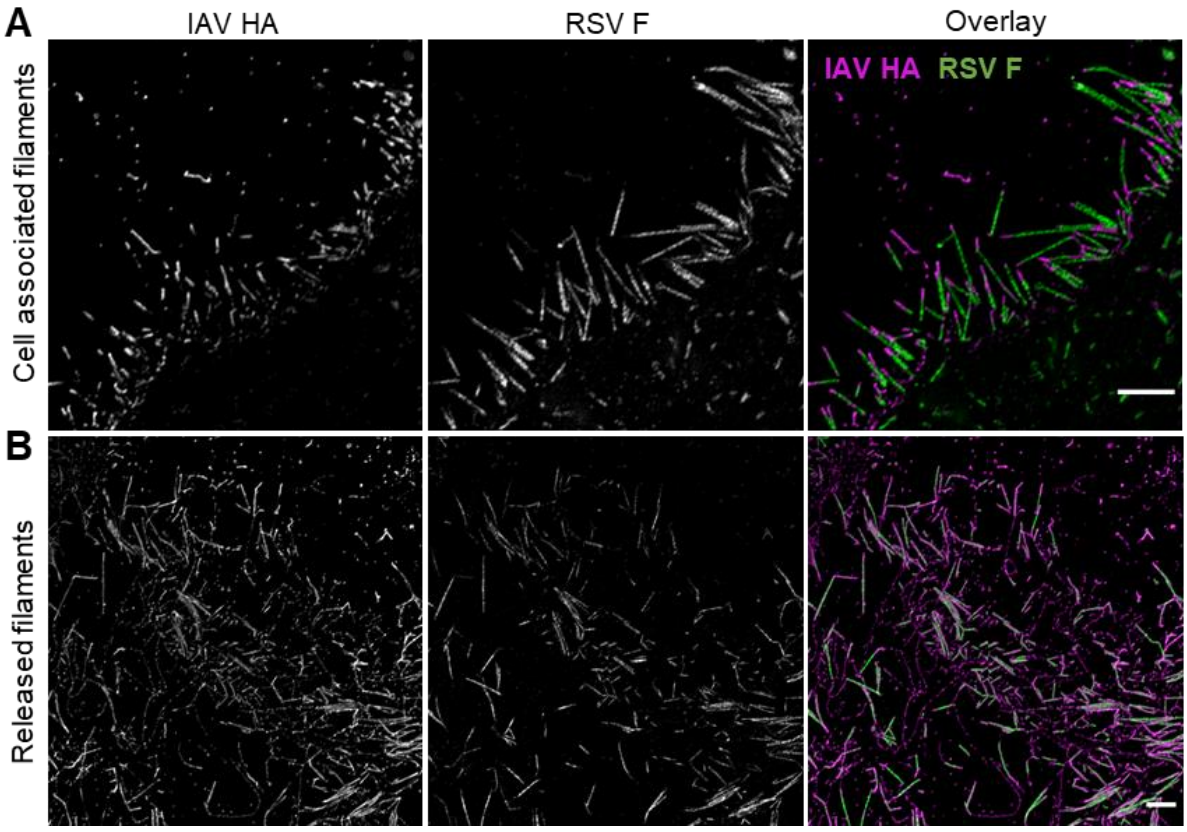

Figure 4-2: Super-resolution confocal microscopy revealed filaments that incorporate both HA and F. A549 cells were infected IAV MOI 1 and RSV MOI 4 and incubated for 24 hpi, before fixation and immunostaining for IAV HA (magenta) and RSV F (green). Cells were imaged by super-resolution confocal microscopy on Zeiss LSM880 with Airyscan detector. Filaments positive for both IAV HA (magenta)

and RSV F (green) were identified both (**A**) attached and (**B**) released from cells. Scale bars indicate 500 nm.

The two glycoproteins were expressed in distinct patches along the length of the filament (Figure 4-3A). Analysis of fluorescence intensity along the length of dual-positive filaments (filaments measured shown in Figure 4-3B) showed that there was little colocalisation between HA and F, as peaks of fluorescence intensity rarely overlapped between proteins (Figure 4-3C). Additionally, IAV HA was incorporated at the distal end of the majority of filaments. IAV and RSV virions could also be identified amongst the dual positive filaments (Figure 4-3C), suggesting that regions in which these filaments form could contain both IAV and RSV budding sites.

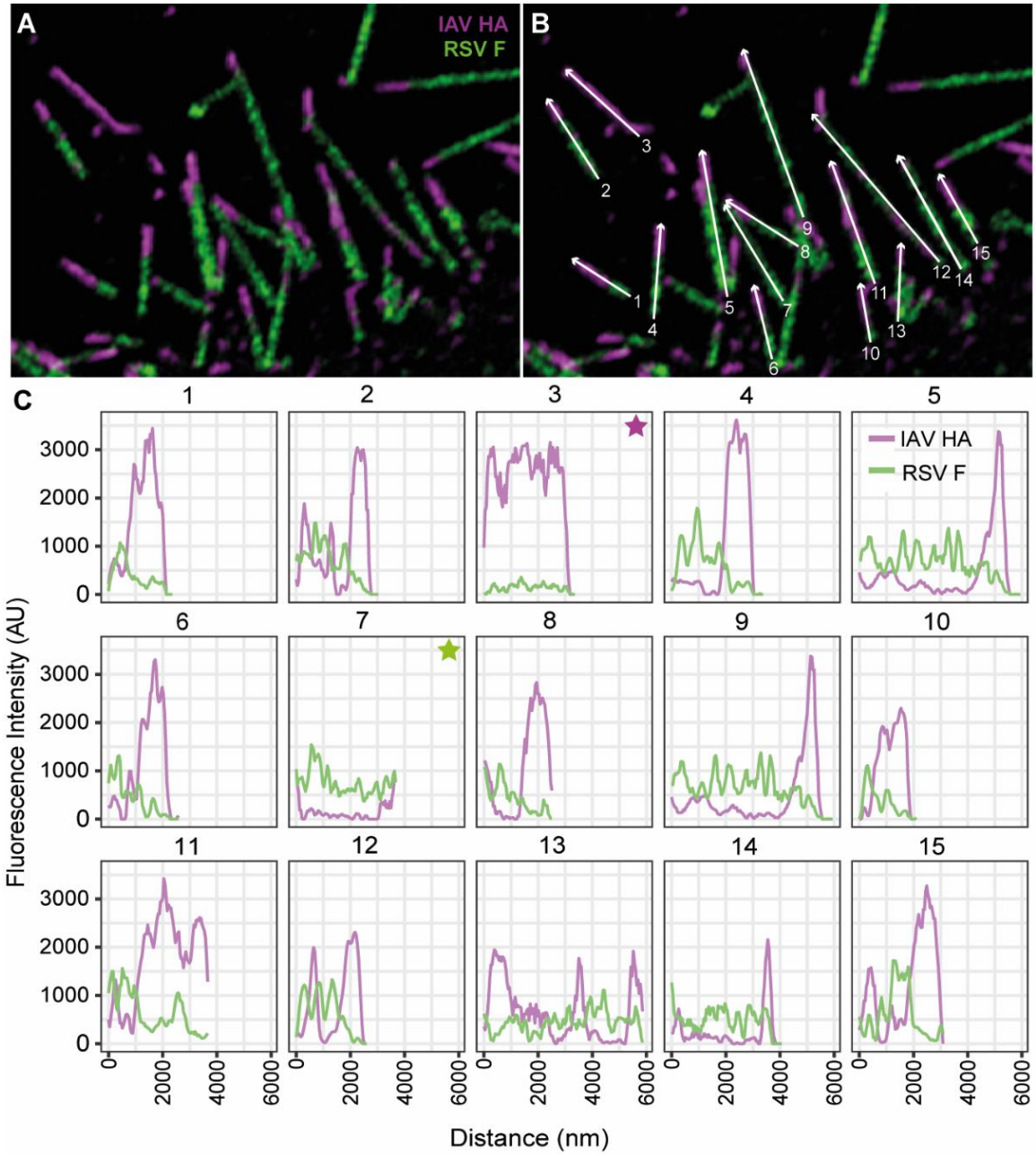

Figure 4-3: HA and F do not colocalise on filaments, but appear as distinct patches with HA predominantly at distal end. (**A**) Magnified view of cell associated filaments (full image shown in figure 2) show filaments with distinct patches of IAV HA (magenta) and RSV F (green) glycoproteins along the length of the filaments. (**B**) White arrows and filament numbering correspond to fluorescence intensity profiles displayed in (C). Minimal colocalisation was observed in the fluorescence intensity profiles (**C**) for IAV HA (magenta line) and RSV F (green line) signal along filaments numbered 1-15. IAV (filament 3, magenta star) and RSV (filament 7, green star) filaments were also identified among dual positive filaments.

To determine the overall proportion of cells that produced these dual-positive filamentous structures, cells were infected with IAV (MOI=1) and RSV (MOI=4) for 24 hours and stained for HA and F. Cells were imaged by tile scanning, to collect a wide field of view. Three fields were collected per coverslip, from three independent experiments, and cells producing dual-positive filaments were manually counted. More than half of coinfected cells (56±9.1%, mean ± SD) produced dual-positive filaments to varying extents. Many cells displayed extensive production of dual-positive filaments, which could be observed to be extending from the cell membrane surrounding the whole cell (Figure 4-4A-B). There did not appear to be obvious morphological changes, for example rounding of the cell or fragmentation of the nucleus, that would indicate cell damage on these cells, suggesting coinfected cells have a high capacity for producing viral progeny (Figure 4-4B and C).

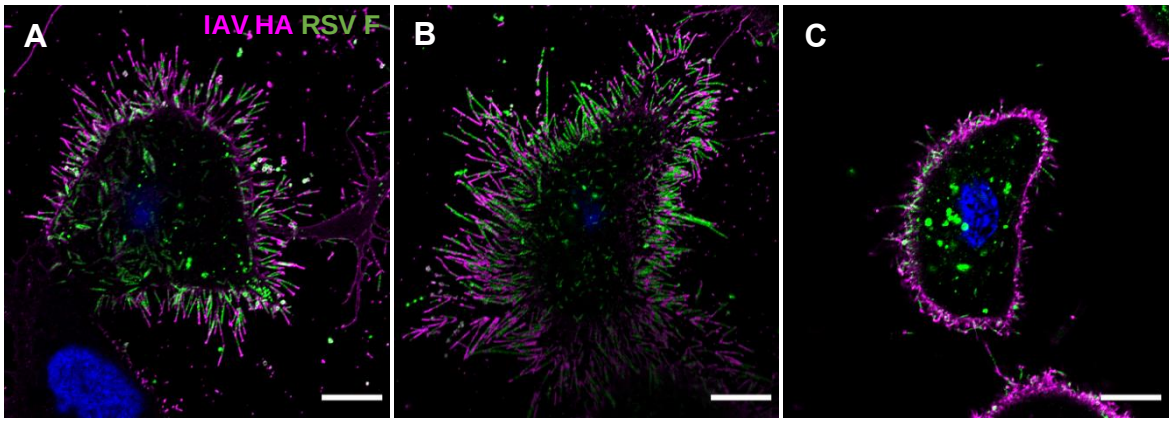

Figure 4-4: Cells produce dual positive filaments to a large extent, without obvious morphological changes that would indicate virus-induced damage. A549 cells were infected IAV MOI 1 and RSV MOI 4 and incubated for 24 hpi, before fixation and immunostaining for IAV HA (magenta) and RSV F (green). Cells were imaged by super-resolution confocal microscopy on Zeiss LSM880 with Airyscan detector. (**A**) and (**B**) Cells immunostained for HA (magenta) and F (green) showing extensive production of dual-positive filaments across whole cell edges. (**C**) Image taken through centre of same cell as (B), showing no obvious virus-induced changes to morphology. Scale bars indicate 10µm.

Imaging data shown in Figures 4-1 to 4-4 was carried out on fixed and permeablised samples and these procedures may impact the morphology of cells or viral filaments. To determine the native organisation of filaments budding from coinfected cells, live cells were coinfected and immunostained for HA and F without fixation or

permeablisation at 24 hpi. Cells were then imaged using super-resolution confocal microscopy and Z-stacks were collected through the entirety of coinfected cells. Live staining revealed the formation of bundles of dual positive filaments extending from the apical surface of coinfected cells (Figure 4-5A). To better observe filament organisation, two-dimensional images through the Z-plane of the cell were created from Z-stacks. Like in fixed cells, filaments were predominantly positive for F along the length of the filament, and HA at the distal end (Figure 4-5B).

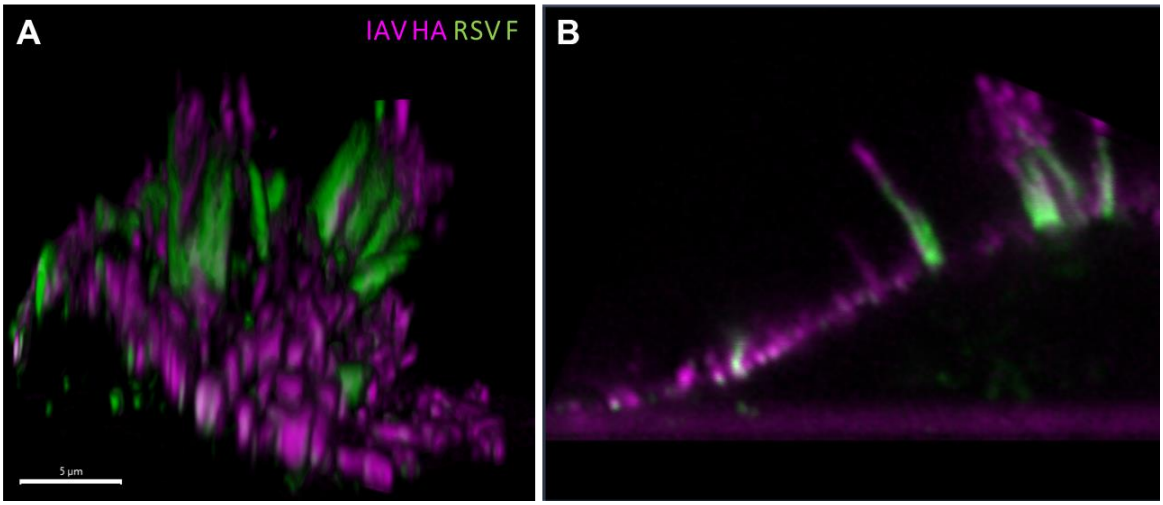

Figure 4-5: Live cell imaging shows dual-positive filaments extend in bundles from apical cell surface. Live coinfected A549 cells were immunostained for HA (magenta) and F (green) and imaged by super-resolution confocal microscopy using Zeiss LSM880 with Airyscan detector. Z-stack were collected at 100 nm intervals through entire coinfected cell. (**A**) A three-dimensional rendering of the whole cell reconstructed from Z-stack and (**B**) a two dimensional image through the Z-plane of the cell. Both images show the native organisation of dual-positive filaments extending from apical cell surface in bundles. Scale bar indicates 5 µm.

Super-resolution confocal microscopy confirmed that IAV and RSV glycoproteins interact in regions of budding virus on coinfected cells and provide compelling evidence to suggest that HA and F interact and may be incorporated into the same viral filaments. However, due to the resolution limits of light microscopy, it was not possible to determine with certainty that IAV and RSV co-assemble into the same filamentous structures. To address this, a higher resolution imaging technique was required to gain structural information about the filaments.

4.3.2 Coinfection generates viral filaments with morphological differences compared to typical IAV and RSV filaments

To gain increased resolution, scanning electron microscopy (SEM) was carried out on single infected, coinfected or mock infected cells (Figure 4-6). Mock infected cells displayed a relatedly smooth cell surface with small, unevenly shaped filopodia extending from the cell surface. Cells were spread out and elongated. In contrast, all infected samples showed clear evidence of production of viral particles (Figure 4-6A).

IAV single infection showed cells are heavily infected, with extensive viral budding on cell surfaces. IAV infection produced a pleomorphic population of spherical, bacilliform and filamentous virions (Figure 4-6B). IAV strain A/Puerto Rico/8/34 is considered to have predominantly spherical morphology (Seladi-Schulman et al., 2014b), however cell-specific differences have been shown to impact IAV morphology (Roberts and Compans, 1998; Al-Mubarak et al., 2015), so may account for the abundance of filament formation in A549 cells. RSV single infection resulted in cells with dense patches of budding filaments that were more uniform in morphology (Figure 4-6B).

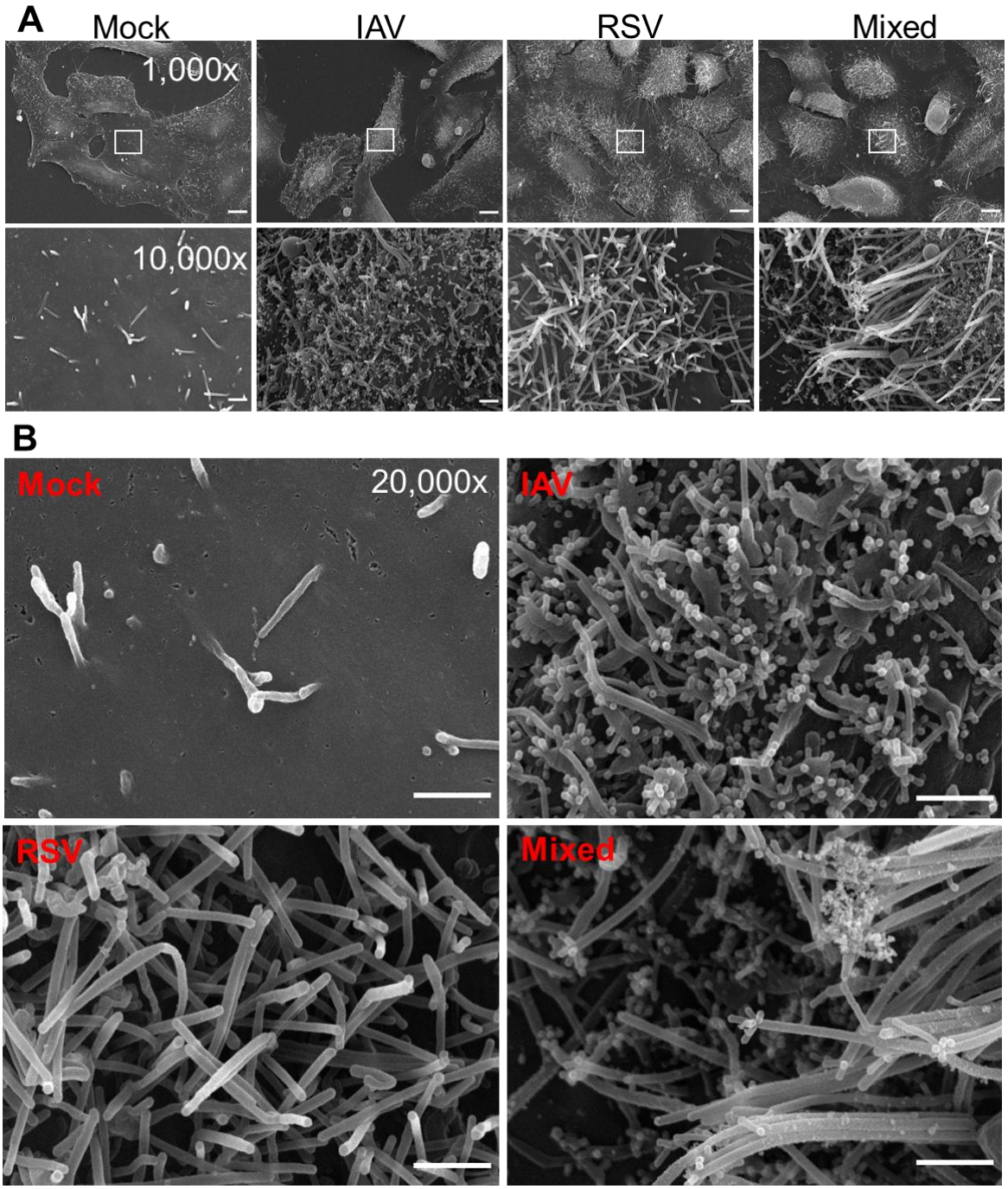

Figure 4-6: Scanning electron microscopy shows the morphology of budding viruses in IAV and RSV single infection and mixed infections. Scanning electron micrographs of IAV, RSV, coinfected or mock infected cells imaged at (**A**) 1000x, 10,000x and (**B**) 20,000x magnification, region of magnification is denoted by the white box shown in 1000x images. Scale bars represent 10 µm at 1000x and 1 µm at 10,000x and 20,000x magnification.

The distribution of budding virions on the cell surface was markedly different to single infection by either virus. In coinfected cells, organisation of budding virus closely reflected the glycoprotein staining profile on live infected cells: coinfected cells were decorated with budding pleiomorphic IAV particles, while filaments extended from the cell in tight bundles, rather than larger dense patches seen in RSV single infection (Figure 4-6 and 4-8).

Comparative measurement of filament width between infection conditions revealed a substantial difference between IAV and RSV particle size, with average widths of 84±6.6 nm (mean±SD) for IAV and 134±17.3 nm for RSV, consistent with published measurements of IAV and RSV particle size (Vijayakrishnan et al., 2013; Liljeroos et al., 2013; Ke et al., 2018). The width measurements in coinfection reflected a mixed population of both IAV and RSV filaments, a distribution of peaks matching both IAV and RSV filament measurements from single infections (Figure 4-7).

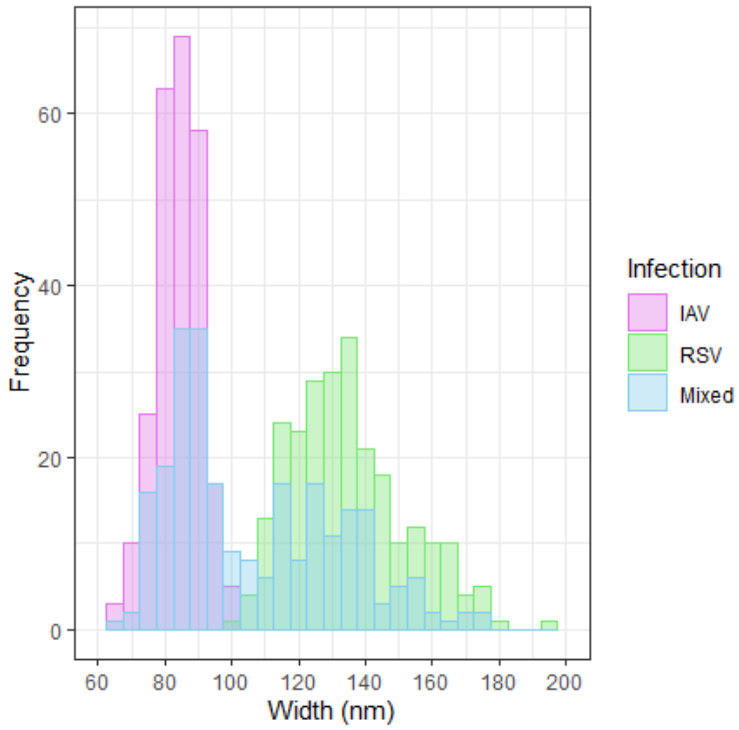

Figure 4-7: Filament width measurements show differences in IAV and RSV filament structure. Viral filaments from each infection condition (n=250 per infection) were measured. Histogram shows frequency of measurements binned in 5nm intervals and shows distribution filament widths from IAV infection (magenta bars), RSV infection (green bars) and mixed infection (blue bars).

Importantly, from coinfected cells, a population of virus particles that was structurally different to filaments observed in either IAV or RSV single infection was also identified. These long filamentous virions had smaller structures branching from the distal ends (Figure 4-8). The branching structures showed a strong resemblance in morphology and size with small pleomorphic IAV virions. This observation was consistent with confocal microscopy data, which showed that dual-positive filament structures were predominantly positive for RSV F along the body of the filament, with IAV HA positivity primarily at the distal end.

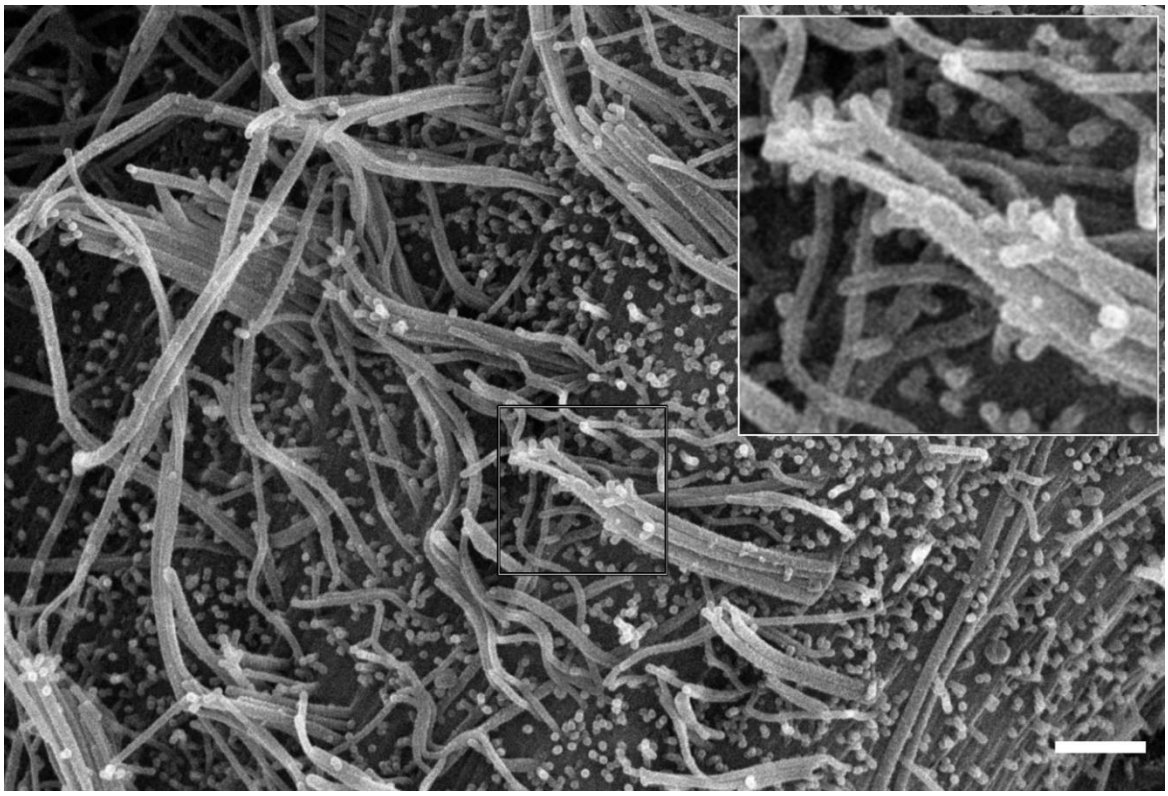

Figure 4-8: Filaments with branching ends were identified budding from coinfected cells. SEM micrograph show filaments with branched ends consistent in size and shape with small bacilliform IAV particles, shown in magnified inset image. Image collected at 10000x magnification and scale bar indicates 1 µm.

Taken together with the light microscopy data showing HA incorporation at filament ends, these findings provide strong indication that IAV and RSV glycoproteins are incorporated into the same filamentous structures, with consequences on morphology.

4.3.3 Screening grids for cryo-electron tomography experiments

To understand precisely how these dual positive filaments were forming, a higher resolution imaging technique was required. To achieve this, cryo-electron tomography (cryo-ET) was used to study virus budding from coinfected cells. Cryo-ET allows visualization of viral particles in three-dimensions near native state, therefore would allow elucidation of the nature of the interaction occurring between IAV and RSV during viral assembly and budding.

A549 cells were cultured directly on laminin-coated carbon support grids. Cells were then infected with IAV (MOI=1) and RSV (MOI=4) for 24 hpi. Following this, gold fiducials, used for tomogram alignment, were added to grids, before plunge freezing in liquid ethane. Once frozen, samples underwent the workflow described in Figure 4-9.

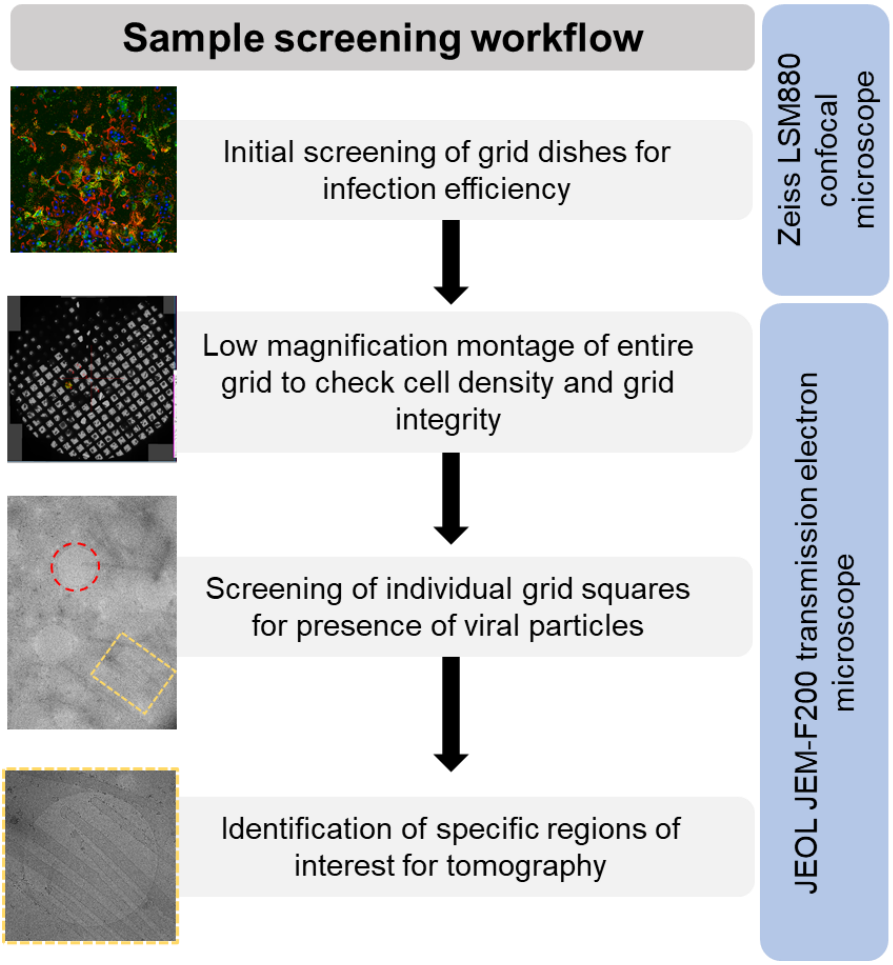

Figure 4-9: Workflow for sample screening prior to selection of grids for imaging by cryo-ET. Samples were assessed by confocal microscopy and cryo-TEM for the efficiency of infection, quality of grids and regions of interest.

To confirm that the infections had achieved a high proportion of coinfection and there was evidence of viral filament formation, the remaining cells in the glass bottom dishes in which the grids were infected were stained for IAV HA and RSV F (Figure 4-10). Images were collected at 40x objective using tile-scanning, to allow imaging of a large area of the grid whilst maintaining sufficient resolution to identify filament formation. Whilst not a direct indicator of infection on the frozen grids, this screening step provided a guide for the level of infection expected on the grids without the risk of potential contamination or damage of the grids themselves.

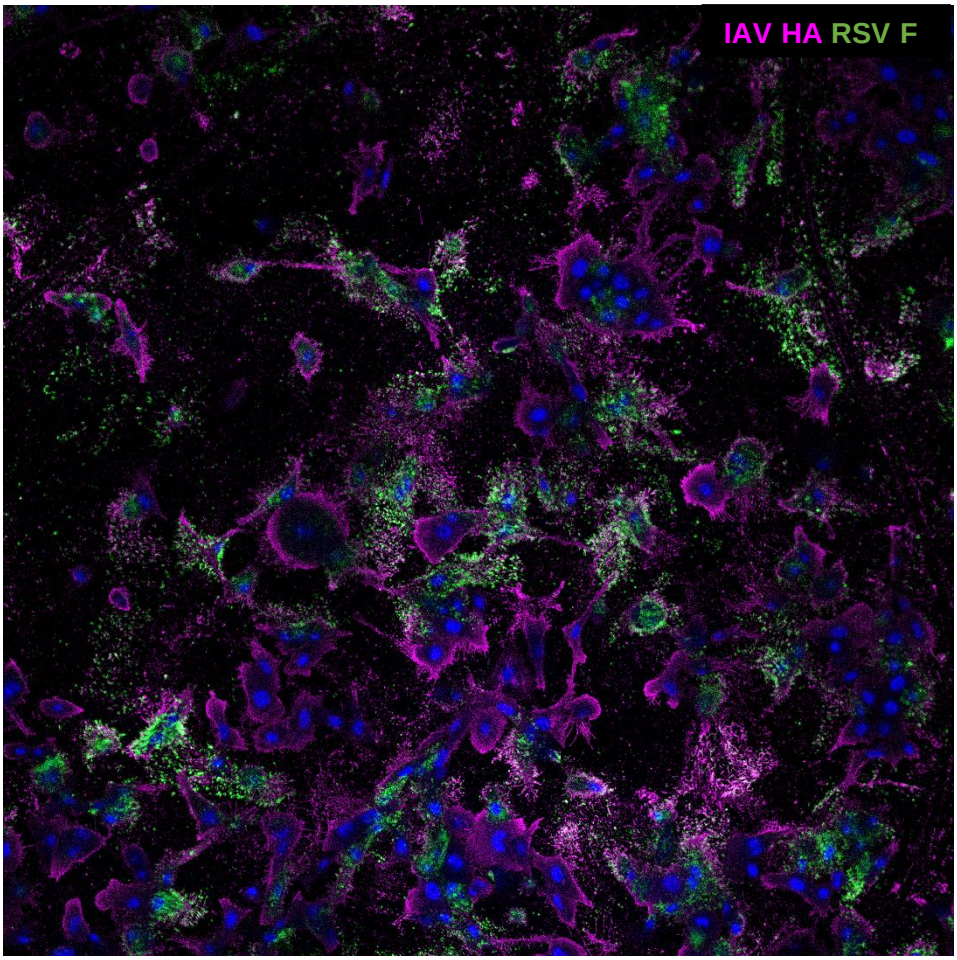

Figure 4-10: Immunofluorescence staining of grid dishes provides confirmation of coinfection and formation of filaments. Dishes were stained for IAV HA (magenta) and RSV F (green), nuclei stained with DAPI (blue). The grid from this dish was plunge frozen for cryo-EM imaging.

Frozen infected grids were initially screened using the 200 kV JEOL FEM-200 cryo transmission electron microscope (TEM). This screening served two purposes: first to ensure the quality of the grids, including seeding density, gold concentration and

grid integrity, was suitable for cryo-ET, and second to identify potential areas of interest for tomography. Grids were mapped at low magnification (Figure 4-11A) before individual grid squares were screened for virus (Figure 4-11B-C).

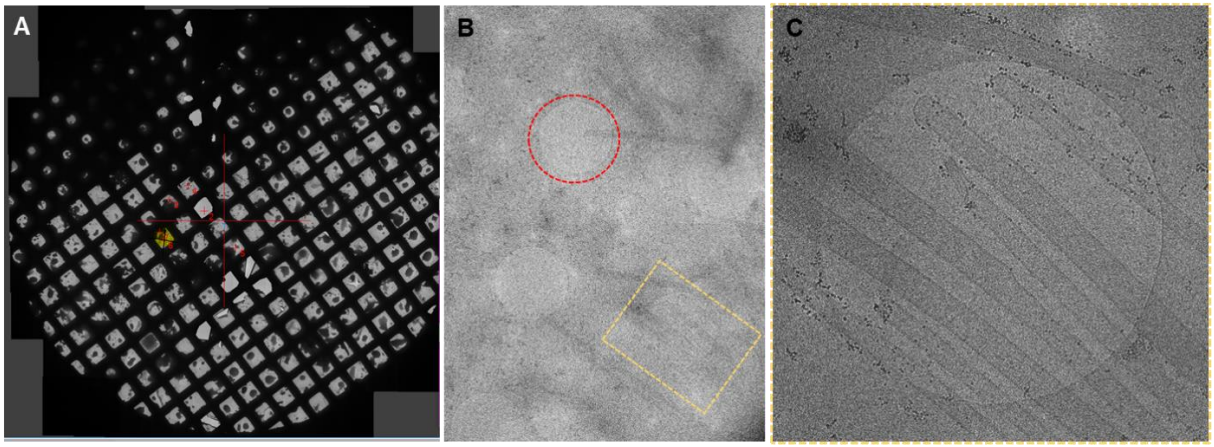

Figure 4-11: Screening of TEM grids prior to selection for tomography. (**A**) Whole grids were first mapped at low magnification. (**B**) Individual grid squares were screened at 2500x magnification for regions of interest. Red dashed circle and yellow box indicate holes in carbon support that contain virus. (**C**) Region of interest (yellow box in [B]) imaged at 8000x magnification showing bundle of budding RSV filaments.

After screening, suitable grids were selected for imaging on the JEOL CRYOARM 300, to collect high resolution tomograms of viral particles. Images were collected in a dose-symmetric tilt series in 3˚ increments along a 60˚ axis, with defocus of -6 µm and dose of 2.26 e/Å/tilt. Tilt series were screened for quality and features of interest and then processed for tomography. Tomogram processing and alignment was carried out using IMOD, using gold fiducials to align tilt series (Kremer et al., 1996).

4.3.4 IAV and RSV virions can be identified on coinfected grids

Virions that were consistent with IAV (Calder et al., 2010; Vijayakrishnan et al., 2013) and RSV published structures (Liljeroos et al., 2013; Ke et al., 2018) were identified on coinfected grids (Figures 4-12 and 4-13). This indicates that there is capacity for assembly of both IAV and RSV virions with the expected ultrastructural composition and morphology to be produced from coinfection. IAV and RSV single

infected grids were prepared and frozen, but due to time and resource constraints, these grids were not imaged.

Virions consistent with pleiomorphic IAV particles (Figure 4-12A) and IAV filaments (Figure 4-12B) were identified. IAV filaments varied in length, with an average diameter of 84.8±6.97 nm (mean ± SD), measured from glycoprotein ends. On both filaments and bacilliform particles, dense decoration of glycoproteins could be identified coating the virions. IAV RNPs could be observed within virions, with polarised packaging of genomes at the distal end of filaments, consistent with published reports (Figure 4-12B and C) (Calder et al., 2010; Vijayakrishnan et al., 2013; Vahey and Fletcher, 2019). Complete sets of eight genome segments could be identified in many virions, in a '7+1' arrangement (Figure 4-12D). Glycoproteins were densely packed with no regular arrangement on the surface of the virion and the triangular heads of HA trimers could be identified (Figure 4-12E).

Whilst maintaining IAV-like morphology, some virions were joined by fusion of viral envelopes, with a thin layer of density potentially attributed to M1 matrix layer, remaining in place (Figure 4-12B). Glycoproteins did not appear to be associated with the regions of membrane that join the filaments. 'Beads on a string' assemblies of IAV particles, where virions assemble in end-to-end arrangements due to incomplete scission events, have been reported, but these are predominantly associated with viruses with impaired M2 activity (Rossman et al., 2010). Fusion between IAV particles has been proposed before, after acid treatment of virions (Calder et al., 2010), but in these experiments it is unclear if the formation of IAV multi-virion bodies was mediated by a IAV-dependent process, or was a result of coinfection with RSV. Analysis of IAV single infected grids is required to understand this.

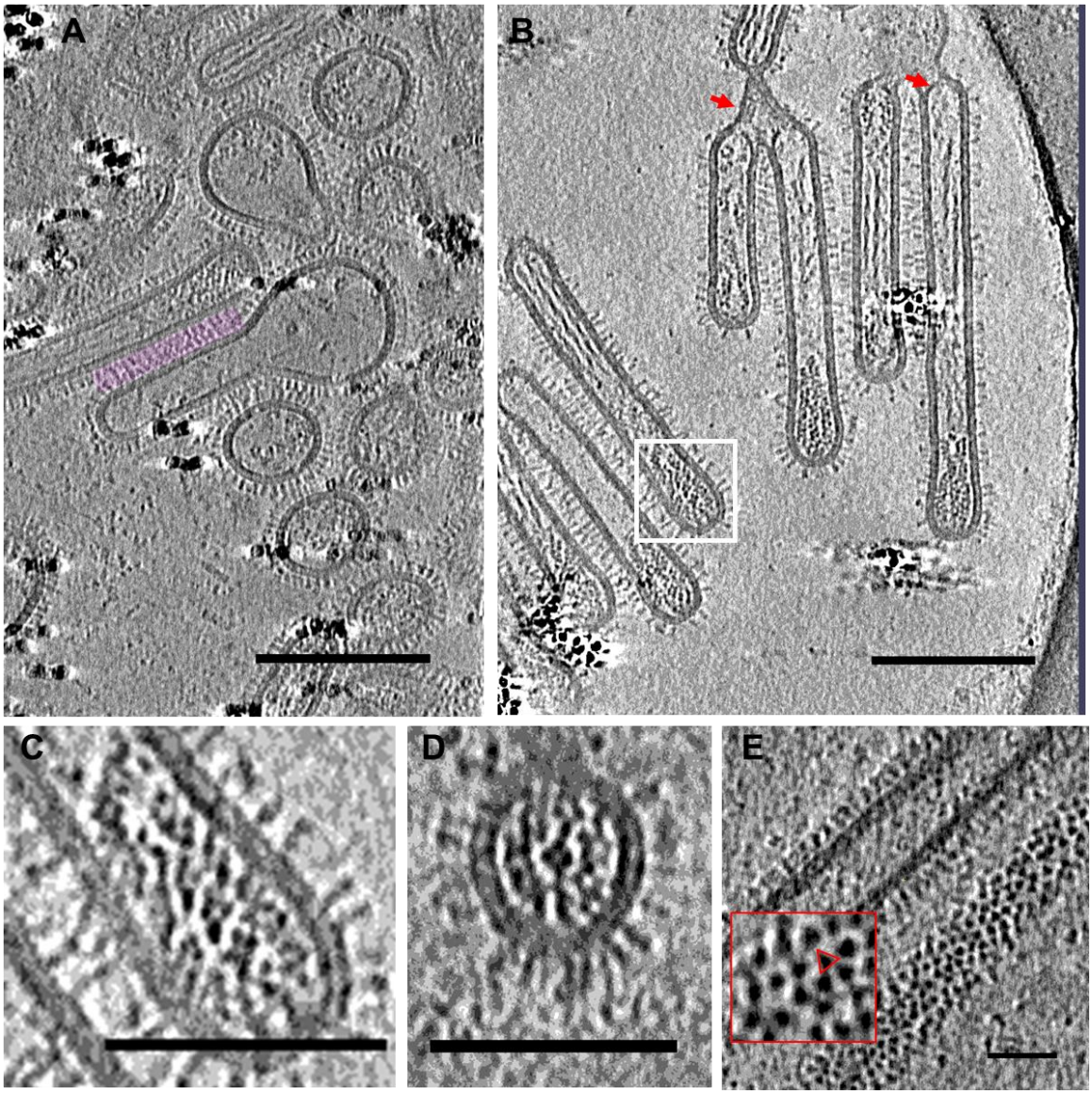

Figure 4-12: Structure of IAV virions on cryo-EM grids. (**A**) Pleiomorphic population of IAV virions, showing filamentous, spherical and bacilliform virions. Magenta shaded region highlights dense glycoproteins. Scale bar represents 200nm. (**B**) Filamentous IAV virions with packaged genome segments clearly visible (white box, magnified in [C]). Red arrows indicate regions of membrane fusion and remaining structure which may correspond to matrix protein. Scale bar represents 200nm. (**C**) Magnified region highlighted in white box in (B) showing packed RNPs. Scale bar represents 100 nm. (**D**) Cross-section through a filament showing 7+1 arrangement of RNPs. Scale bar represents 100nm. (**E**) Two IAV filaments, one with cross section through the filament showing side on view of IAV glycoproteins and the second showing a top-down view of the filament showing organisation of HA, with HA heads showing triangular shape of HA trimer (inset image, red triangle). Scale bar represents 50nm.

RSV filaments were also identified on grids (Figure 4-13A and B). Filaments had an average width of 158 (+/-14.6) nm measured from glycoprotein ends, but many irregular shaped virions were also observed. Filaments contained RNPs packed throughout the length of the virion, with multiple genome copies packaged per filament, consistent with reports that RSV is polyploid (Loney et al., 2009). The flexible herringbone arrangement of the nucleocapsid-RNA structures could be clearly visualized within filaments (Figure 4-13B), along with ring-like structures of N (Figure 4-13A) (Bhella et al., 2002a; Bakker et al., 2013; Conley et al., 2021). RSV glycoproteins form a helical arrangement on the surface of the virions and pairing between glycoproteins can be identified (Figure 13C) (Conley et al., 2021).

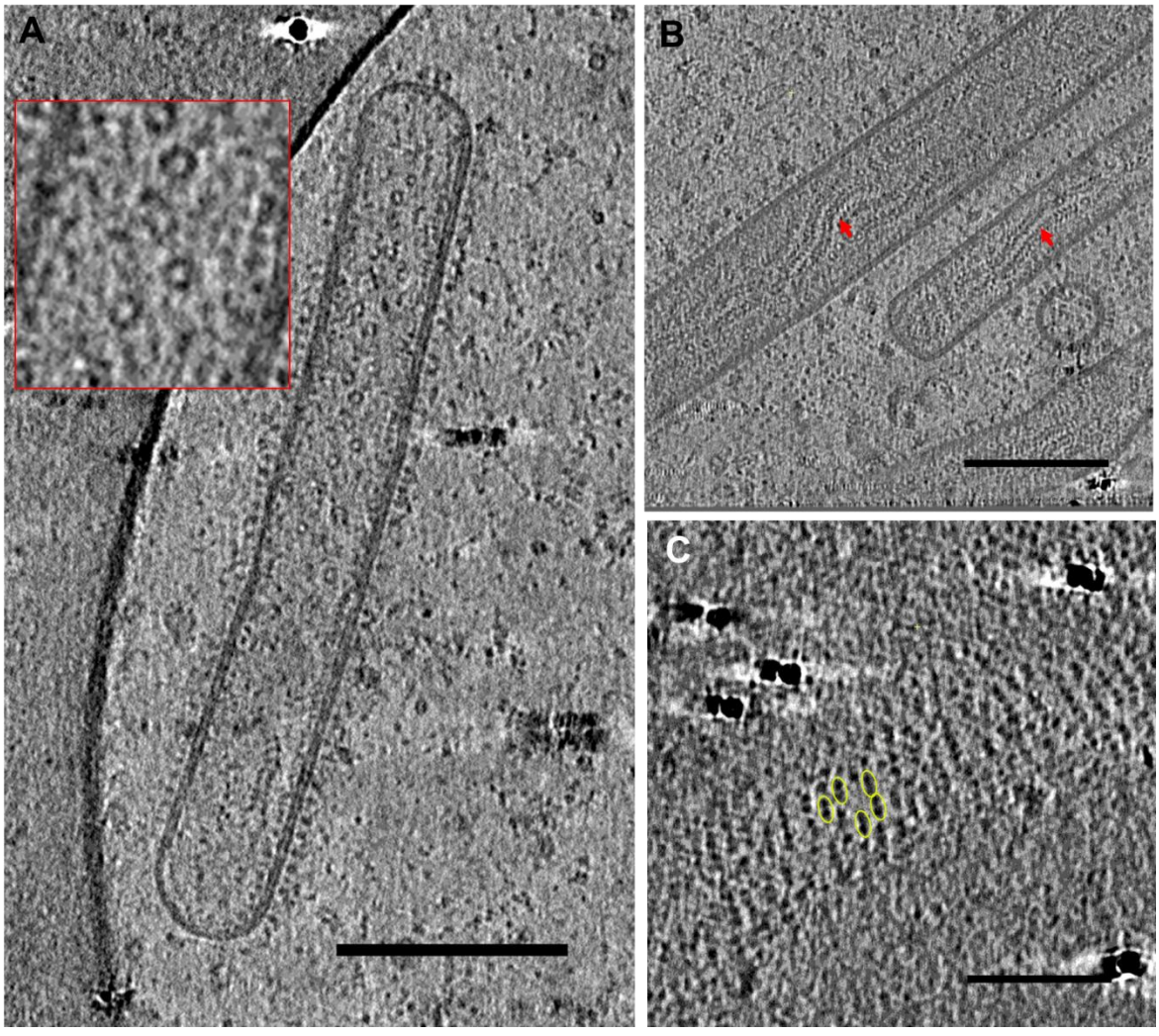

Figure 4-13: Structure of RSV filaments detected on cryo-EM grids. (**A**) Short RSV filament containing RNP rings, indicated by red arrows and magnified in inset image. Scale bar represents 200nm. (**B**) RSV filaments containing multiple RNPs in herringbone structure, indicated by red arrows. Scale bar represents 200 nm. (**C**)

Top-down view of viral glycoproteins shows helical arrangement. Glycoproteins are arranged into pairs, indicated by yellow ellipses. Scale bar represents 100 nm.

4.3.5 IAV and RSV virions budding sites are in close proximity on coinfected cell membranes

By immunofluorescence and SEM, IAV and RSV were identified budding in close proximity on the plasma membrane of coinfected cells. Figure 4-14 shows different Z-slices within the same tomogram, showing IAV and RSV particles budding from the same region of the plasma membrane. At the site of budding, RNPs can be seen packaging into the budding RSV filament extending from the cellular membrane (Figure 4-13-4A, yellow box). In the same region, a small bacilliform IAV particle (Figure 4-14B, magenta box) can be seen budding less than 500 nm from the RSV budding site (yellow arrow). Multiple genome segments appear to be packaged within the IAV particle. In the cytoplasm surrounding the budding sites, vesicle structures are present and cortical actin bundles run beneath the membrane.

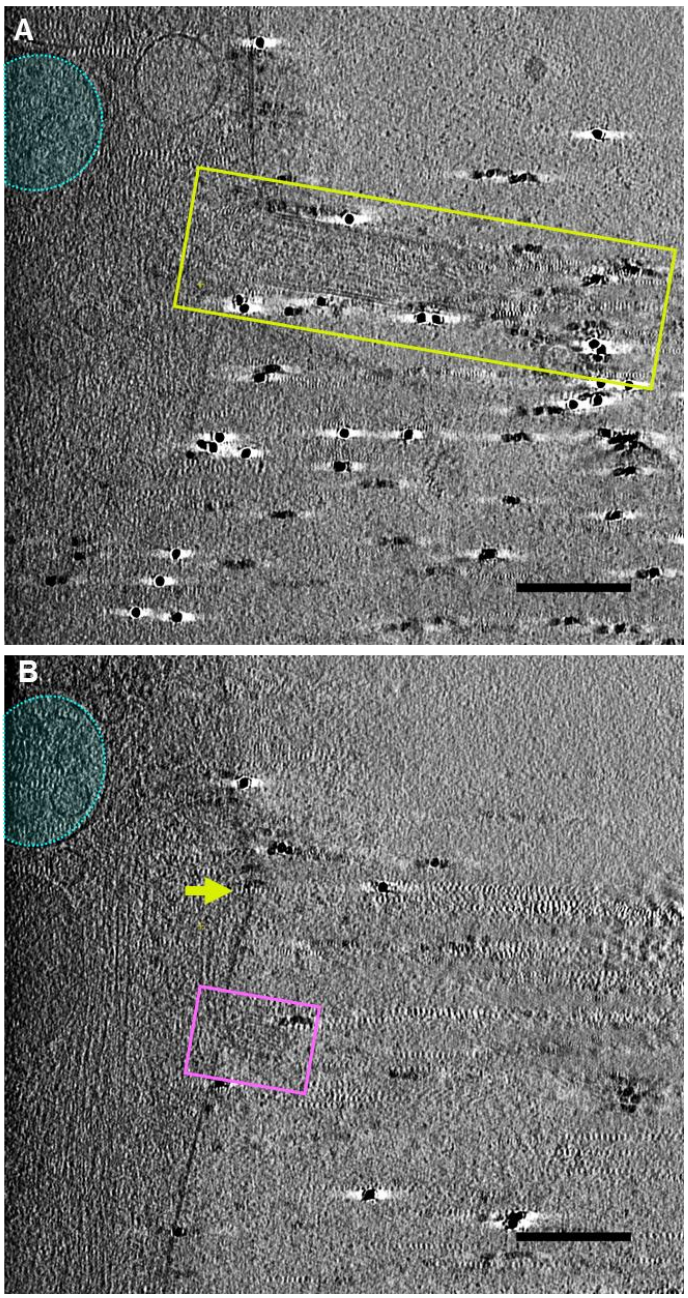

Figure 4-14: IAV and RSV budding sites are in close proximity to one another on coinfected cells. Two images of the same membrane region show (**A**) RSV, highlighted by yellow box, and (**B**) IAV, highlighted by magenta box, budding less than 1µm apart on the cell surface. RSV budding site is visible next to the budding IAV particle in (B), indicated by yellow arrow. Vesicle highlighted in cyan provides reference to demonstrate that the same region of the membrane was imaged. Scale bar represents 200 nm.

Once released IAV and RSV particles were found in heterogenous populations on the TEM grid (Figure 4-15). Pleiomorphic IAV particles could be seen close to both

newly assembling RSV particles (Figure 4-15B and C) and assembled RSV particles (Figure 4-15D).

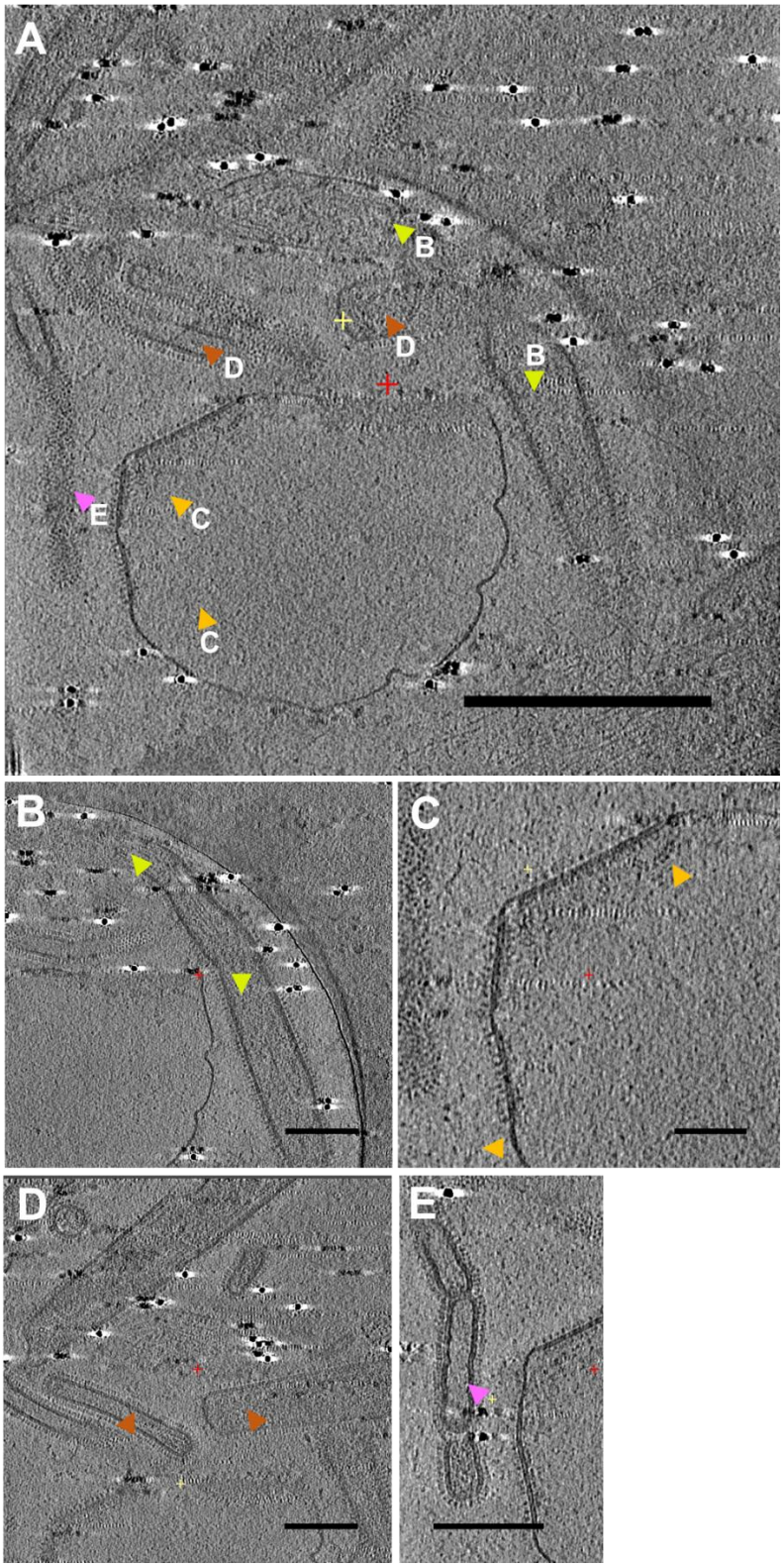

Figure 4-15: Released IAV and RSV particles form heterogenous virus populations. (**A**) Example area showing released IAV and RSV in close proximity, alongside RSV assembly events. Scale bar indicates 500 nm. Areas labelled with

coloured arrows correspond to structures shown in panels B-E. (**B**) RSV filament budding from cellular filopodia. Filopodia, indicated by top yellow arrow, becomes decorated with RSV components and then extends into a structured RSV filament. Actin filaments extend from the filopodia into the filament. Scale bar indicates 200 nm. (**C**) RSV glycoproteins and matrix proteins concentrating and assembling on a membrane, resulting in formation of straight structured regions. RSV RNP is associated with one edge, indicated by gold arrow. Scale bar indicates 100 nm. (**D**) Released IAV filaments in close proximity to RSV filament. (**E**) Bacilliform IAV particles and small filaments forming a 'beads on a string' assembly. Only the leading IAV particle appears to contain RNPs. Scale bars in (D) and (E) indicate 200 nm.

4.3.6 Coinfection results in the formation of chimeric viral particles that contain the structural features and genomes of both IAV and RSV

Confocal and SEM imaging data indicated the potential for formation of viral particles that contained components from both IAV and RSV to form on coinfected cells. To understand the nature of the interactions, grids were assessed for evidence of particles that may contain elements from both viruses. Using cryo-ET, the ultrastructure of these particles was determined, and two classes of hybrid viral particles were identified.

The first class of viral particles, described as chimeric viral particles (CVPs), contained regions that were structurally analogous to both RSV and IAV and were joined by a continuous membrane (Figure 4-16A and B). The RSV-like region was widest in diameter and contained glycoproteins corresponding to RSV (Figure 4-16F). Extending from this was a narrower IAV-like region (Figure 4-16A and B), containing glycoprotein arrangement consistent with IAV glycoproteins (Figure 4-16D). Viral genomes could be identified confined within each structural region (Figure 4-16D and G). In the RSV region, herringbone shaped RNP structures could be identified (Figures 4-16D and 4-17B). In the IAV region, density at the distal end of the filament corresponded to a packaged RNPs (Figure 4-16A, B and D).

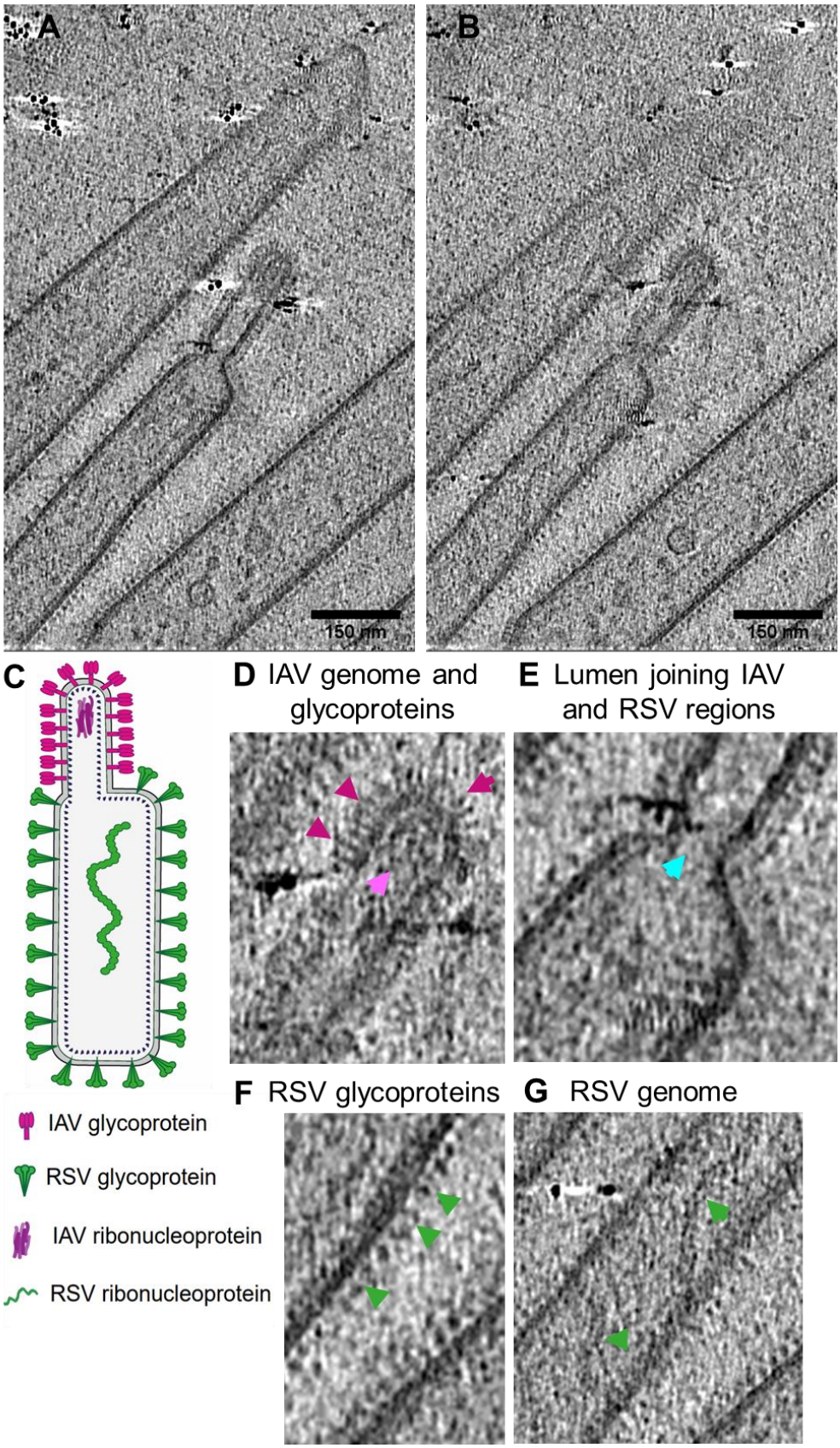

Figure 4-16: Coinfected cells produce chimeric virus particles containing IAV-like and RSV-like structural components and genomes from both viruses. Chimeric virus particle (CVP) imaged by cryo-ET. (**A**-**B**) Two z-positions through the same particle. CVPs contain two structurally distinct regions that reflect IAV and

RSV structure and contain IAV and RSV genomes. Scale bar indicates 150 nm. (**C**) Schematic representation of CVPs with IAV and RSV -like regions. (**D**) Magnified view of distal end of CVP, showing IAV region containing IAV glycoproteins and RNPs (magenta and pink arrows respectively). (**E**) IAV and RSV regions joined by a continuous membrane with a clear lumen (cyan arrow). (**F**) Magnified envelope CVP showing an RSV-like glycoprotein arrangement (green arrows). (**G**) RSV region of CVP containing herringbone structured RNPs (green arrows).

CVPs displayed fusion between the two IAV-like and RSV-like regions to differing extents. The majority had a continuous membrane join with a clear lumen between IAV and RSV sections (Figure 4-16A, B and E). Other CVPs had narrow join between IAV and RSV regions, with membranes of IAV and RSV regions fused, but with no clear lumen. Additionally, some CVPs contained multiple IAV regions fused to a single RSV region (Figure 4-17). This was consistent with SEM images, in which some filaments contained multiple small branching structures extending from the filament end.

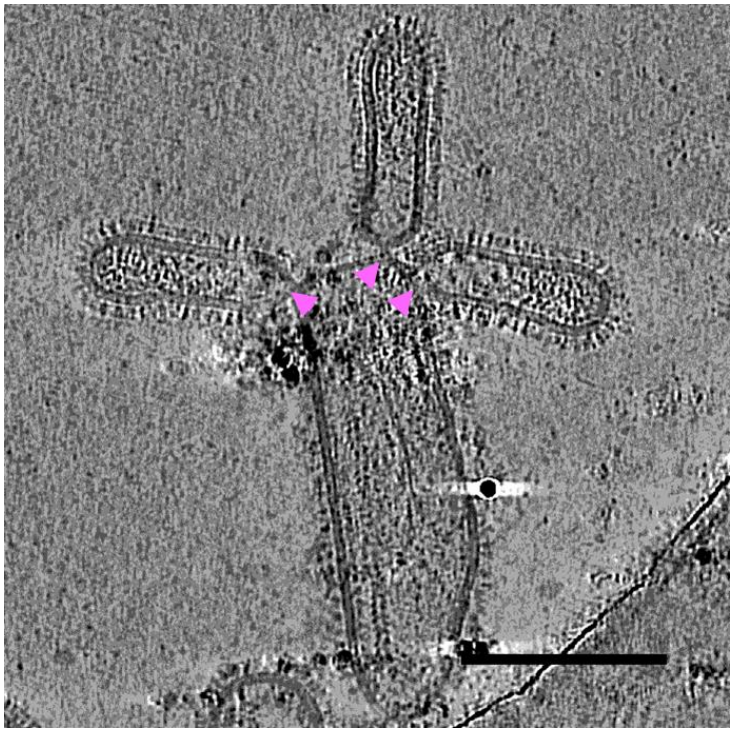

Figure 4-17: Chimeric particle composed of multiple IAV regions. Other CVPs had narrow membrane joins between IAV and RSV regions and contained multiple IAV-like regions. Adjoining regions indicated by pink arrows, scale bar indicates 200 nm.

In some particles, curved density could be identified at the bottom of the IAV region, near the membrane join (Figure 4-18). This structure was similar to that seen in the fused IAV particles (Figure 4-12) and may correspond to a matrix protein.

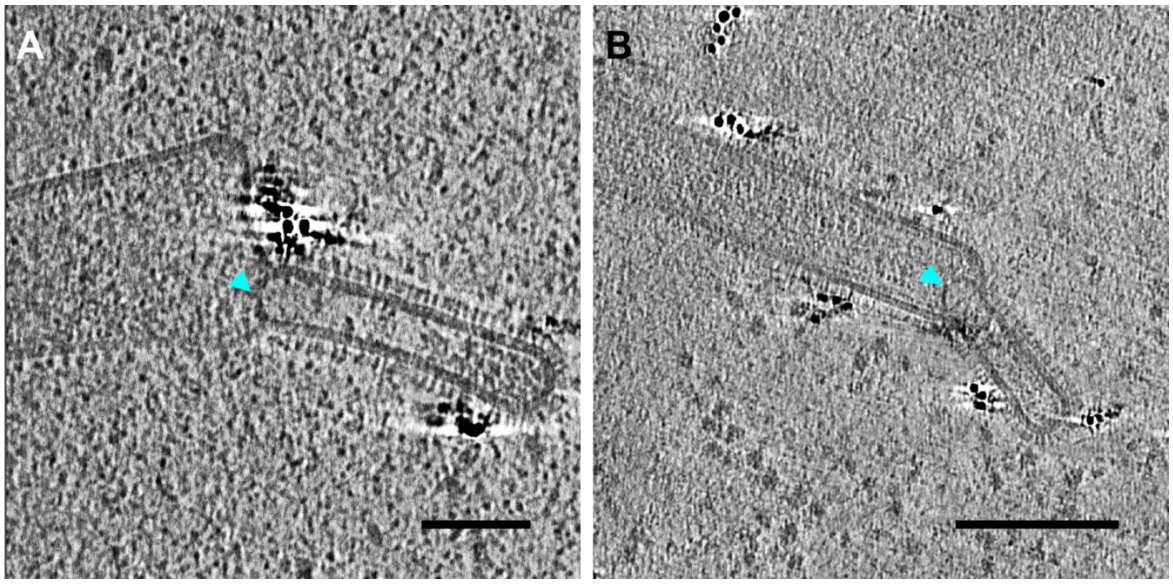

Figure 4-18: Some CVPs contained a curved density at join region. (**A**) and (**B**) show examples of CVPs with curved density, indicated by cyan arrows. Scale bars indicate 100 nm (A) and 200 nm (B).

Importantly, CVPs structure were only identified in one order: the IAV region extended from the tip of the RSV region. No evidence of CVPs forming the other way round was found, which may provide important insights into how these CVPs may be assembling.

The formation of viral particles that contain structural components and genomes from unrelated, taxonomically different respiratory viruses has never previously been described in the literature and represents a previously uncharacterised mode of virus-virus interaction.

4.3.7 Coinfection also generates naturally pseudotyped RSV filaments that contain RSV genome but are coated in IAV glycoproteins

Coinfection by IAV and RSV also resulted in the formation of a second class of hybrid viral particles: RSV filaments pseudotyped with IAV glycoproteins. These

filaments appeared structurally consistent with RSV filaments and contained genomes, but the envelope of these particles incorporated glycoproteins that had consistent shape and arrangement with IAV glycoproteins. Some filaments were entirely coated in IAV glycoproteins (Figure 4-19A and B), while others contained patches of both IAV and RSV glycoproteins (Fig 4-19C and D). In these filaments, the IAV patches appeared predominantly at the distal end of the filament (Figure 4-19D).

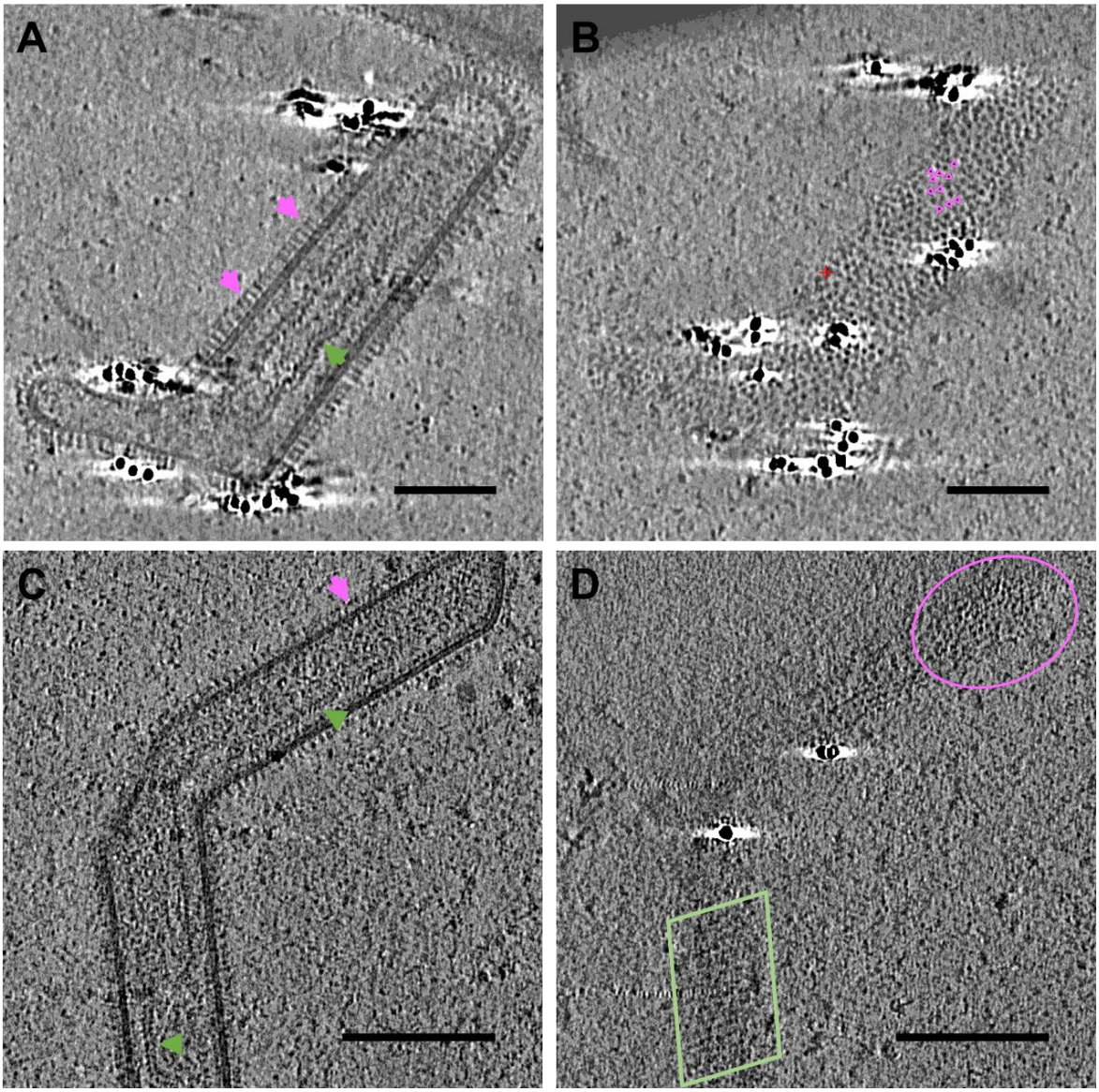

Figure 4-19: Coinfection generates pseudotyped RSV filaments, which incorporate IAV glycoproteins. (**A**) Example of a pseudotyped RSV virion containing RSV RNP, indicated by green arrow, which is coated in IAV glycoproteins, indicated by magenta arrows. (**B**) The filament is entirely coated in IAV glycoproteins (indicated by magenta triangles), characterised by the triangular shaping of HA head domain and irregular, tightly packed ordering. Scale bars in (A)

and (B) represent 100 nm. (**C**) Example of pseudotyped filament containing IAV (magenta arrow) and RSV glycoproteins, with RSV RNPs identifiable in both regions (indicated by green arrows). (**D**) Top-down view of glycoproteins on pseudotyped filament shown in (C), shows distinct differences in glycoprotein ordering in different regions of filament. Near the base of the filament, helical ordering of RSV glycoproteins is observed (indicated by green box), whilst IAV glycoproteins are incorporated near the filament tip (indicated by magenta oval). Scale bars in (C) and (D) represent 200 nm.

IAV and RSV have different glycoprotein arrangements on IAV and RSV particles (Harris et al., 2006; Calder et al., 2010; Conley et al., 2021). To quantify differences between glycoproteins on pseudotyped RSV particles, compared to ordinary RSV particles, the distance between glycoproteins was measured. Glycoproteins were visualized from the top down and measurements were taken from the centre of one protein to the centre of an adjacent glycoprotein (Figure 4-20A-C). First, inter-glycoprotein distances were collected on a larger set of control IAV or RSV tomograms (11 tomograms per condition, total measurements n=326 for IAV, n=236 for RSV), before measurements of glycoproteins on suspected pseudotyped particles (n=50 measurements per pseudotyped particle) were compared for statistical differences to controls (Figure 4-20D). RSV exhibited a mean (± SD) inter-glycoprotein spacing of 12.9±2.3 nm, while IAV had a smaller spacing of 8.71±1.18 nm. Pseudotyped particles had an average spacing ranging from 8.31-9.56 nm. This measurement was within a similar range to IAV inter-glycoprotein spacing, but significantly different to RSV spacing ($p<0.0001$ by unpaired t-test). This provides additional evidence that RSV filaments incorporate IAV glycoproteins, resulting in the formation of pseudotyped particles. Interestingly, pseudotyped IAV particles (IAV virions containing RSV glycoproteins) were not identified, potentially suggesting that IAV glycoproteins are structurally compatible with RSV virions, but not vice versa. However, this observation is based on a relatively small sample of tomograms, without comparison to IAV single infected grids. Further analysis of a large data set of IAV particles formed both from coinfection and single infection is required to rule out the formation of pseudotyped IAV particles.

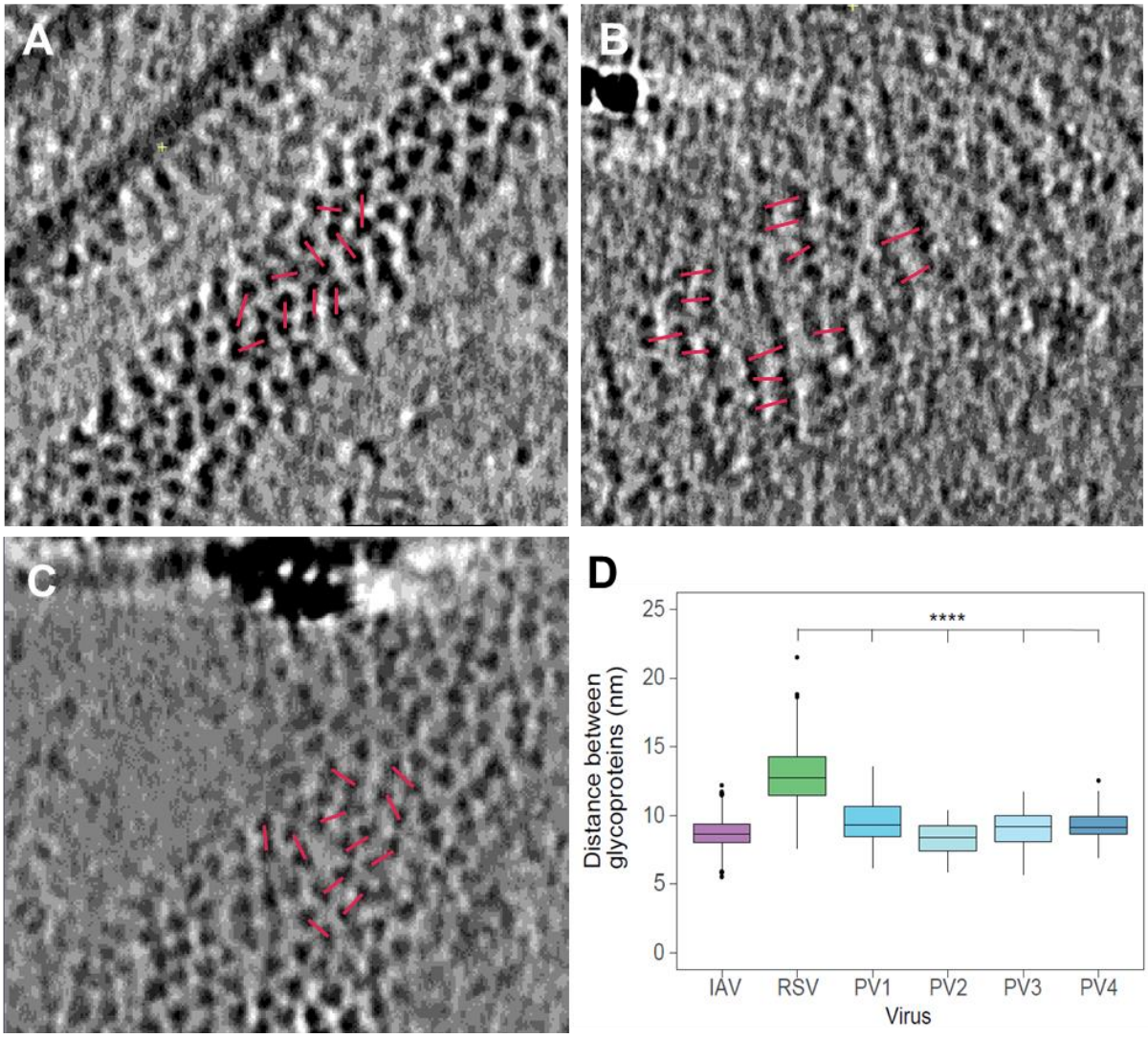

Figure 4-20: Inter-spike distance measurements reveal that pseudotyped viruses are decorated with IAV glycoproteins. To determine the glycoprotein arrangement on pseudotype viruses, inter-spike distances (red lines) were measured between glycoprotein pairs. Representative examples are shown for IAV (**A**), RSV (**B**) and pseudotyped virions (**C**), with red lines demonstrating inter-glycoprotein measurements. (**D**) Unpaired t-test analysis (**** $p<0.0001$) confirmed glycoproteins distance measurements were significant different between RSV controls and pseudotyped virions (PV1-PV4), with average inter-spike distances of 8.71 nm for IAV, 12.9 nm for RSV and a range of 8.31-9.56 nm for pseudotypes.

4.3.8 CVPs display expanded tropism and facilitate IAV entry into sialic acid deficient cells

Cryo-ET imaging demonstrated that CVPs contain the glycoproteins from both IAV and RSV. IAV and RSV utilise different attachment and entry receptors. Influenza

viruses target host cell receptors via binding to terminal sialic acids joined to glycans by α-2,3-gal, α-2,6-gal linkages (Matrosovich et al., 2004). RSV interacts with a range of attachment receptors, including nucleolin (Tayyari et al., 2011; Mastrangelo et al., 2021) and entry is mediated via interaction with insulin-like growth factor receptor 1 (IGFR1) (Griffiths et al., 2020). Through incorporation of both IAV and RSV envelope glycoproteins, CVPs may possess the receptor specificity of both viruses, therefore expanding the tropism properties of IAV and RSV.

To test this hypothesis, A549 cells were stripped of sialic acid using an exogenous neuraminidase (NA) from *Clostridium perfringens* which has sialidase activity against both α2,3- and α2,6- linked sialic acids. The removal of sialic acids was confirmed by staining with Maackia Amurensis Lectin II (MAL II), which selectively binds α2,3- sialic acids, and lectin from Erythrina Cristagalli (ECL), which binds the terminal galactose residues that become exposed after sialic acid cleavage (Figure 4-21A).

Experimental set up is described in Figure 4-21B. A549 cells were infected with IAV (MOI=1) and RSV (MOI=4) or a mixed inoculum of both viruses for 24 hours. Following this, the supernatant (containing released virus) and virus associated with the cell pellet (cell associated virus) were harvested from single virus infections and mixed infection. These virus samples were then transferred immediately without freeze thawing to infect sialic acid deficient cells (NA-treated) or untreated control cells. Inoculum was also titrated, to determine the input titre of the virus to the treated and control wells. At 12 hpi, infections were fixed and immunostained for IAV NP or RSV N and infected cells were counted (Figure 4-21B). Entry was measured as a ratio of virus positive cells in the NA-treated wells over the untreated control wells.

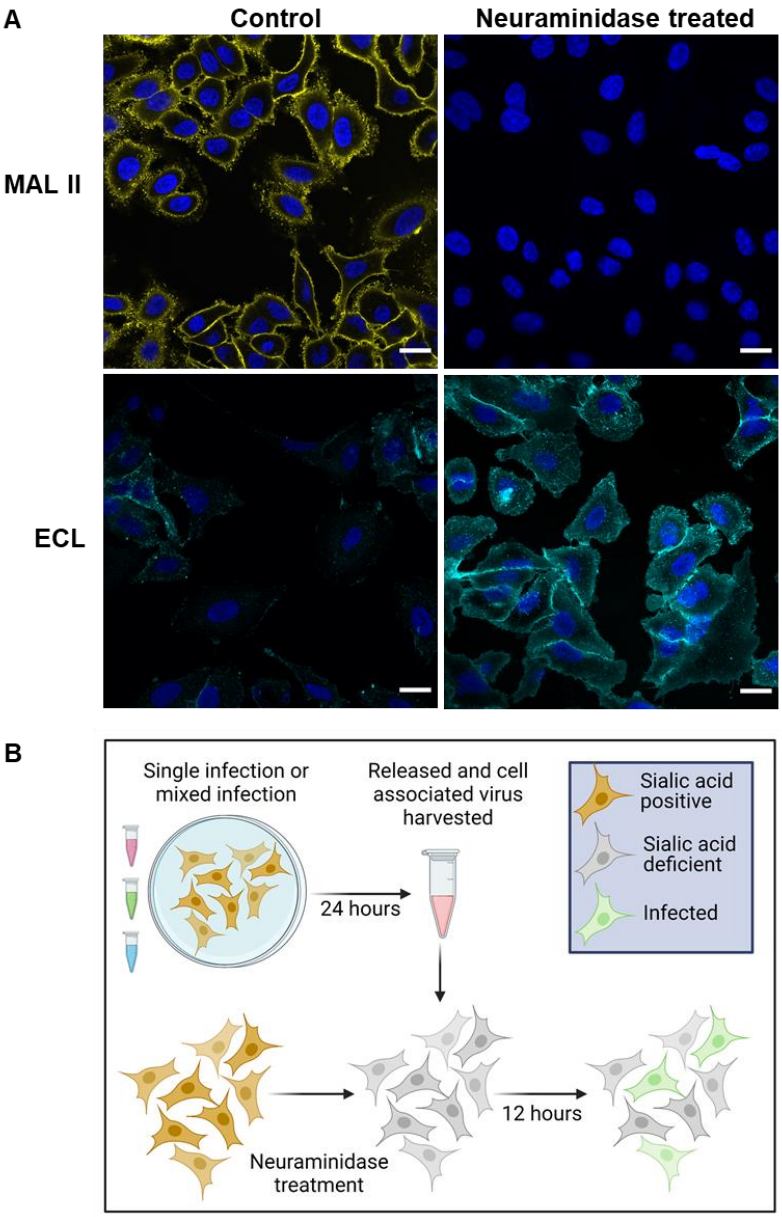

Figure 4-21: Experimental set up for neuraminidase experiment. (A) 1mU/ml neuraminidase treatment removes sialic acids. Control (untreated) and neuraminidase (NA) treated cells were stained with MAL II (yellow) and ECL (cyan) to confirm cleavage of sialic acids. Scale bars indicated 20 µm. (**B**) Schematic detailing the experimental set up for the neuraminidase experiment.

IAV entry in NA-treated cells was completely blocked compared to untreated control cells when inoculated with the supernatant of single IAV- infected cells, whereas entry of cell pellet IAV collected from single IAV infections was reduced by 85%, compared to the entry in the untreated control (Figure 4-22A).

In mixed infection, IAV entry to NA-treated cells was significantly increased, for both supernatant (p=0.045) and cell pellet virus (p=0.0091) samples, compared to single IAV infection. Entry of IAV from the supernatant of a single infection was completely blocked in NA-treated cells, however, when harvested from the supernatant of a mixed infection, IAV entry increased to 20% of the level of entry to untreated cells. The increase in IAV entry was more marked in the cell pellet fraction and IAV entry in NA-treated cells was restored to 77% of the level of control cells (Figure 4-22A). RSV entry was unaffected by the removal of sialic acids and there were no significant differences between RSV entry in NA-treated or control cells, in single RSV infection or mixed infection (Figure 4-22B). This result was as expected, as RSV uses alternative attachment and entry receptors, therefore removal of sialic acids should not interfere with RSV entry mechanisms.

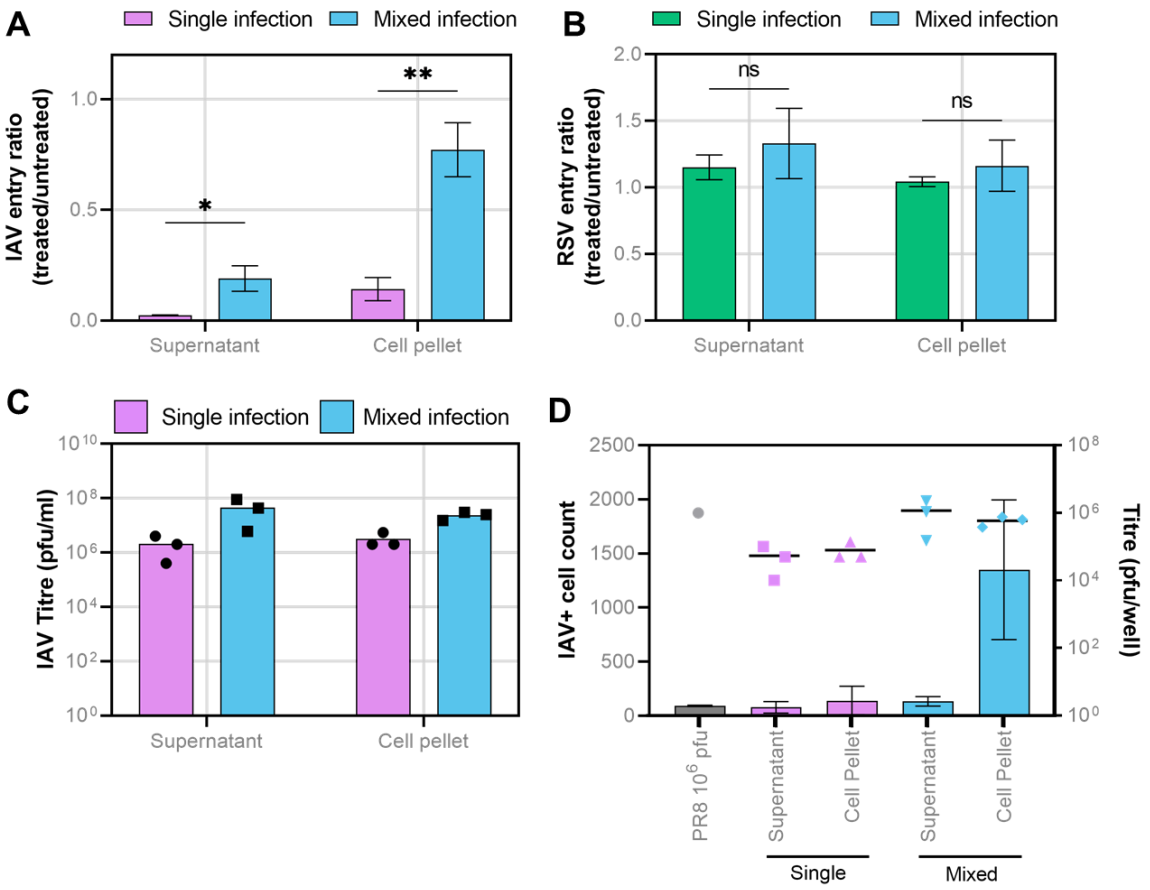

Figure 4-22: Neuraminidase experiments show CVPs facilitate expansion of IAV receptor tropism. (**A**) Ratio of IAV entry into NA-treated cells versus control cells when harvested from single infection (magenta bars) or mixed infection (blue bars). (**B**) Ratio of RSV entry into NA-treated cells over control cells when harvested from single infection (green bars) or mixed infection (blue bars). Error bars represent

standard error and significance was determined by unpaired t-test with, ns $p \geq 0.05$, * $p < 0.05$, ** $p < 0.01$. (**C**) Back titration of IAV input from supernatant and cell pellet samples from three independent single (magenta bars) or mixed (blue bars) infections. (**D**) Bars show raw IAV positive cell counts (left axis) in NA-treated wells and points show IAV titre (right axis) for an IAV positive control (grey), compared to IAV in single infection (magenta) and mixed infection (blue).

Supernatant and cell pellet stocks were back titrated by IAV plaque assay, to determine IAV input to the neuraminidase experiment (Figure 4-22C and D). As observed in growth kinetics experiments described in Chapter 3, IAV titre was slightly increased in coinfections. As virus stocks were transferred directly from initial infections to the neuraminidase experiment, it was not possible to control for the viral input, therefore viral input varied between samples. Therefore, to confirm that the increase in IAV entry in the samples harvested from coinfection was not the result of a higher viral input, a positive control of 10^6 pfu/well of IAV stock virus was added to NA-treated or untreated wells. Analysis of IAV positive cell counts showed that entry of the stock virus was low in NA-treated cells (Figure 4-22D). Further, input titres of supernatant samples from coinfection were calculated to be greater than 10^6 pfu/well by back titration, and IAV positive cell counts were low in NA-treated wells for these samples (Figure 4-22D). This provided confidence that NA-treatment was sufficient to block the entry of this amount of IAV input. Therefore, the increased viral entry in the cell pellet sample from mixed infection was unlikely to be due to increased viral titre compared to single infection and rather due to the action of CVPs.

To determine if aggregation of viral particles may have contributed to this phenotype, IAV and RSV viral stocks were pre-mixed to allow opportunity for aggregation between viral particles, before infecting NA-treated or control cells. There were no significant differences in entry to receptor-deficient cells for IAV that had been pre-incubated with RSV (Figure 4-23), compared to IAV alone. This indicates that IAV and RSV do not readily aggregate upon mixing, however, more complex interactions may occur that result in aggregation *in vivo* (Cuevas et al., 2017).

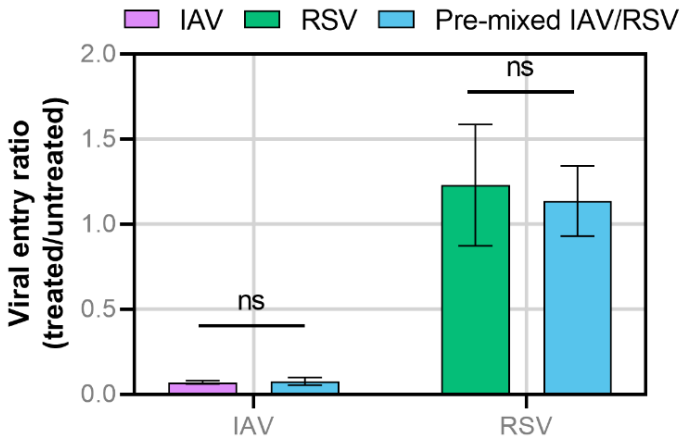

Figure 4-23: Increased IAV entry is not caused by viral aggregation. Ratio of virus entry of IAV only (magenta bar) or RSV only (green bar) into NA-treated over control cells, compared to entry of IAV pre-mixed with RSV or RSV pre-mixed with IAV into NA-treated over control cells (blue bars). Error bars represent standard error and significance was determined by unpaired t-test with, ns $p \geq 0.05$.

To determine whether CVPs were facilitating entry of both viral genomes, or just IAV genomes, NA-treated cells on coverslips were infected with cell associated virus harvested from coinfection for 12 hours, followed by fixation and immunostaining for IAV HA and RSV F (Figure 4-24). Imaging by confocal microscopy revealed the presence RSV single infected cells and more importantly, coinfected cells (Figure 4-24A). It is likely that the coinfected cells were coinfected by IAV and RSV simultaneously due to two factors. First, the timing of fixation (12 hours) was too early to enable secondary rounds of viral replication that may allow foci of infection to overlap, resulting in coinfection. Secondly, the viral MOI was low, estimated between 0.01-0.1 based on the cell density used for seeding cells to coverslips and the back titration of the cell associated fraction from coinfection. This means that the probability of IAV and RSV particles infecting the same cell at random would be low, therefore it is more likely that viral genomes were delivered together. These two factors, in addition with the fact that the cells had been NA-treated and therefore rendered more resistant to IAV infection, makes it highly likely that coinfected cells are a result of infection by CVPs. This implies that some CVPs are dual infectious units, carrying infectious genomes for both IAV and RSV.

Super-resolution confocal microscopy was used to examine coinfected cells. Filamentous structures that were dual positive for both IAV HA and RSV F were observed extending from coinfected cells (Figure 4-24B). This suggests that both IAV and RSV can establish their replication cycle in a cell that has been coinfected by a CVP. Further to this, the CVP forming phenotype is maintained upon transmission between cells, and infection by a CVP results in formation of more CVPs in the viral progeny.

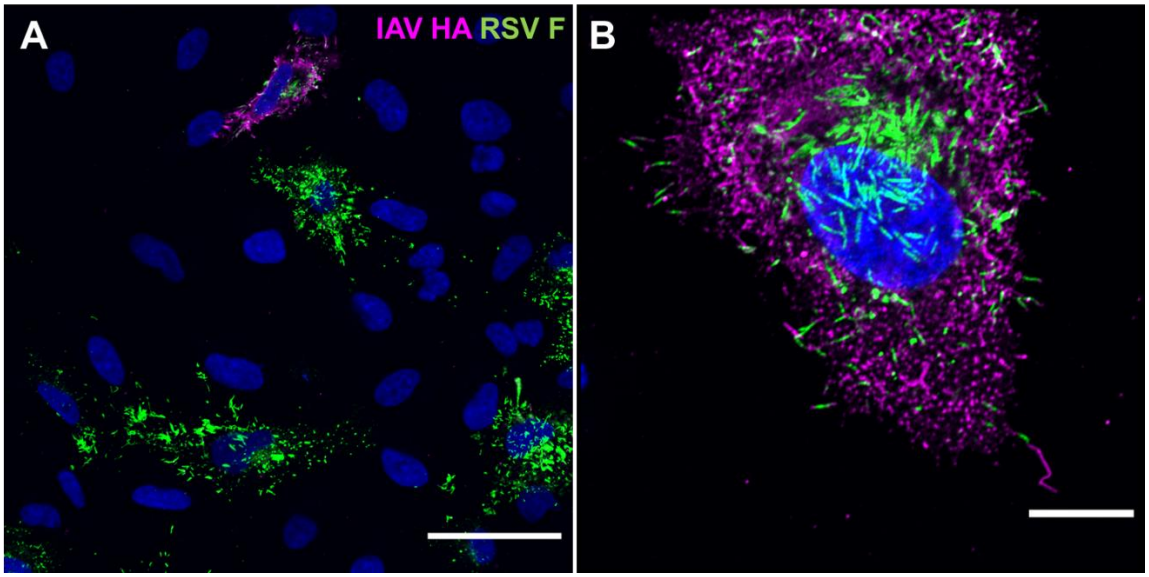

Figure 4-24: Chimeric viral particles facilitate coinfection of neuraminidase treated cells. A549 cells were treated with neuraminidase, then infected with cell associated virus harvested from mixed infection. Cells were fixed at 12 hpi stained for HA (magenta) and F (green) and imaged by standard and super-resolution confocal microscopy. (**A**) Neuraminidase treated cells infected by RSV or coinfected, imaged a low magnification (40x objective) by confocal microscopy. Scale bar indicates 50 µm. (**B**) Super-resolution confocal image of a cell that has likely been coinfected by a CVP, producing HA and F positive filaments. Scale bar indicates 10 µm.

Overall, these findings indicate that CVPs represent a subpopulation of infectious virus particles with expanded tropism. This property facilitates IAV entry by an alternative mechanism mediated by the RSV glycoproteins.

4.3.9 Investigating neutralising antibody escape by chimeric viral particles

As well as essential roles in viral entry and budding, viral envelope proteins are important antigens which elicit an adaptive immune response. Binding of antibodies to IAV and RSV glycoproteins can result in viral neutralisation, by preventing interaction between glycoproteins and cellular entry receptors. By incorporating glycoproteins from both IAV and RSV, CVPs may have means of evading neutralising antibodies targeted towards IAV or RSV, by ultilising the glycoproteins of the other virus.

To test whether IAV can use this mechanism to evade neutralising antibodies, virus harvested from single and mixed infections was incubated with a polyclonal antibody targeting IAV HA. Serum was checked for cross-reactivity with RSV by titrating serum against 1000 pfu/well IAV and RSV viral stocks. Figure 4-25A and B shows that HA anti-serum used was completely neutralising up to 1/1600 dilution against IAV and showed no cross-neutralisation activity with RSV. Anti-serum targeting RSV was also tested, however, complete neutralisation of RSV was only observed at low antibody dilutions and cross-neutralising reactivity with IAV also occurred at these dilutions (Figure 4-25C). Therefore, this anti-serum was not used for further experiments. Due to time constraints, further RSV anti-serums were not tested, therefore RSV neutralisation was not investigated.

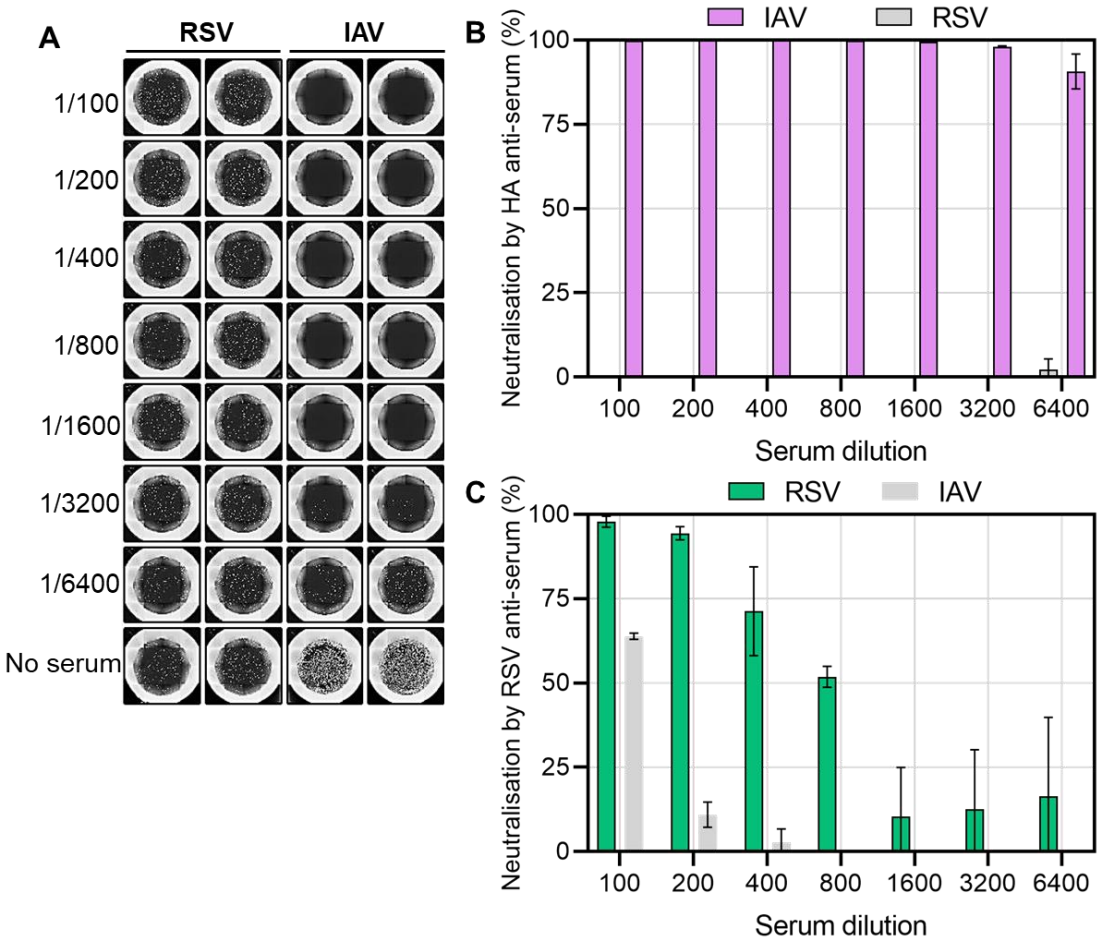

Figure 4-25: Cross-reactivity testing of IAV and RSV anti-sera. Anti-serum was titrated starting at 1/100 dilution, to 1/6400 dilution, against 10^4 pfu/well of IAV or RSV stock. Serum and virus were incubated together, prior to transfer to A549 cells. Infections were incubated for 24 hours, followed by fixation. Cells were immunostained for IAV NP or RSV N and infection was measured using Celigo automated cytometer. (**A**) Well images of viruses incubated with HA anti-serum show no difference in RSV infection in the presence of serum or serum-free control (bottom row), whilst showing inhibition of IAV infection in all wells containing compared to the serum-free control. (**B**) Neutralisation by HA anti-serum was calculated as a percentage of the serum-free control for each dilution. Complete neutralisation of IAV infection was observed up to 1/1600 dilution (magenta bars), while no neutralisation was observed against RSV, indicating that the serum does not cross-react. (**C**) Neutralisation by RSV anti-serum was calculated as a percentage of the serum-free control for each dilution. Complete neutralisation of RSV infection was only observed at 1/100 dilution (green bars) and cross-reactive neutralisation of IAV was observed at 1/100 to 1/400 dilutions (grey bars).

To determine if CVPs could mediate evasion of IAV targeting antibodies, A549 cells were infected with IAV (MOI=1) and RSV (MOI=4), or a mixed inoculum of both viruses, and released and cell associated virus was collected at 24 hpi. These virus samples were immediately incubated with neutralising sera targeting HA for two hours, before transfer to A549 cells. A saturating antibody dilution of 1/200 was selected for neutralisation experiments to ensure that any IAV infection observed was due to antibody evasion. Positive control wells containing 10^5 pfu of IAV stock virus were used to confirm that the concentration of antibodies used was completely neutralising at this viral titre, and samples were back titrated to determine pfu/well. Infections were incubated for 24 hours, without TPCK in the infection media to limit IAV spread, before fixation, immunostaining for IAV NP and counting of infected cells.

Released IAV from single infection was completely neutralised by the serum, while the entry of cell associated virus from single infection was reduced by 90%, compared to the matched serum-free wells (Figure 4-26A and B). In mixed infection, for cell associated virus there was a noticeable reduction in neutralisation in mixed infection compared to single infection (figure 4-26B). However, the extent of neutralisation (both from single and mixed infection) was highly variable and no statistically significant difference in neutralisation between cell associated samples was observed. However, immunofluorescence imaging of cells stained for IAV NP showed a clear trend toward increased evasion of neutralising serum for cell associated virus from mixed infection, compared to single infection samples (Figure 4-26D).

Samples were back titrated by plaque assay to determine pfu/well (Figure 4-26C). In the mixed infection, cell associated virus titres were greater than other sample types, approaching 10^5 pfu/well. Whilst the positive control shows that 10^5 pfu of IAV was completely neutralised by the concentration of serum applied, defective particles or other HA-coated artifacts were not controlled for. These may have varied in abundance between single and mixed infections, which could have affected the extent of neutralisation, by providing alternative HA-coated targets for neutralising antibodies. Therefore, it is not clear if the reduction in neutralisation observed may be due to a higher input of virus, rather than true antibody evasion by CVPs. Overall, these experiments suggest that CVP formation may play a role in antibody evasion. However, further optimisation of experimental design is required to determine if the

trends observed are truly a reflection of the action of CVPs, rather than issues with experimental design.

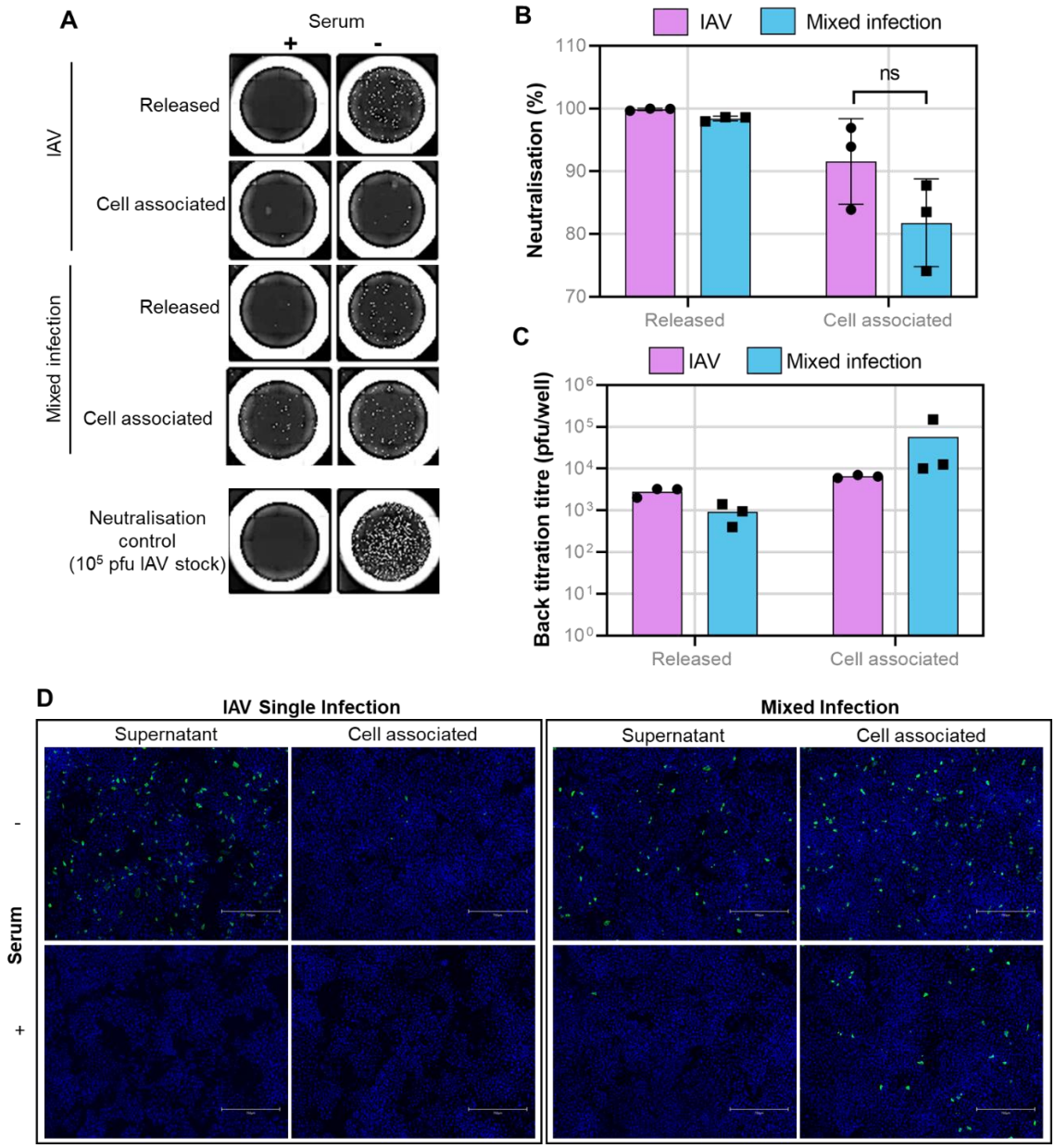

Figure 4-26: Neutralisation assays show a trend towards antibody evasion in the mixed infection. (A) IAV infection was measured on the Celigo automated cytometer. Well images show levels of IAV infection when incubated with sera or without sera for single and mixed infection samples and positive control. (**B**) Neutralisation was calculated from the mean count of IAV infected wells from the wells containing serum, as a percentage of the mean infection from the serum-free wells (mean from 3 technical replicates). Data points show data from three independent experiments and error bars show standard deviation. Statistical significance was determined by unpaired t-test, ns $p \geq 0.05$. (**C**) Back titration of

samples to determine pfu/well for released and cell associated virus in single (magenta) and mixed (blue) infection. (**D**) Immunofluorescence images of levels of IAV infection after A549 cells infected with released or cell associated virus in single and mixed infection at 24 hpi. Samples were incubated without (top row) or with (bottom row) serum prior to infection of A549s. Scale bars indicate 50 µm.

4.4 Discussion

Our understanding of virus-virus interactions within coinfected cells is limited and few studies have characterised these interactions. A shared tropism for ciliated airway cells, along with shared routes of egress, assembly and budding provide the potential for virus interactions to occur between IAV and RSV within a coinfected cell. Experiments described in Chapter 3 demonstrate that IAV and RSV readily coinfect A549 cells and coinfected cells exhibit features of the replication cycles of both viruses. IAV and RSV nucleoproteins and glycoproteins appeared to colocalise to the same regions on the plasma membrane, therefore, this chapter set out to explore the hypothesis that IAV and RSV components interact during viral assembly and budding. A combination of high-resolution imaging methodologies, along with functional experiments, were used to characterise a novel interaction that occurs during viral assembly and budding.

Concordance between imaging methodologies provided strong evidence of the formation of chimeric viral particles. Super-resolution confocal microscopy showed that viral filaments incorporate glycoproteins from both IAV and RSV, with IAV HA predominantly incorporated at this distal end of the filaments. Next, SEM imaging of coinfected cells showed that some viral filaments contained branching structures that were analogous in morphology to bacilliform IAV particles. Finally, cryo-ET provided evidence of formation of two classes of hybrid viral particles, formed from components of both IAV and RSV. The formation of CVPs represents a previously undescribed interaction between unrelated viruses, with important implications for coinfection pathogenesis and for our understanding of viral assembly and interaction.

The formation of CVPs challenges our understanding of virus assembly. Assembly and budding are considered to be tightly regulated processes, in which virus particles form through coordinated interactions between viral components and the

host cytoskeleton. The experiments described in this chapter show that CVPs can form within coinfected cells, and that they maintain structural integrity and infectivity. This is at odds with the concept of tightly regulated assembly pathways, and indicates that, at least for some viruses, there is flexibility within these processes. By studying viruses in isolation in tightly controlled experimental environments, this flexibility may be overlooked. Viral coinfection studies can provide important information about viral interactions, but also shed light on important properties of the individual viruses themselves.

The CVPs identified in by cryo-ET only formed in one order: RSV with IAV extending from the filament tip, not vice versa. Additionally, pseudotyped RSV particles were identified, but not pseudotyped IAV particles. This suggests RSV may possess important structural properties that allow it a greater capacity to incorporate non-self components, while IAV may be less compatible. RSV is a highly pleomorphic virus, with filamentous RSV morphology widely considered to be the infectious form (Liljeroos et al., 2013). Structural studies show tight association of the matrix layer to straight edges on RSV filaments, but the matrix did not extend to the top of the filament, and becomes dissociated in pleiomorphic RSV virions (Kiss et al., 2014; Kuppan et al., 2021). Incorporation of IAV particles was observed only at the tip of RSV filaments and it's possible that this occurs within these regions due to the lack of highly regulated structure, driven by the association of matrix protein with the viral envelope and F glycoproteins.

It is unclear however how the IAV is incorporated in the first instance. CVPs may be forming during the viral budding process. SEM data showed extensive formation of small IAV particles budding at the surface of coinfected cells, while RSV filament formation appears restricted to form tight bundles. This contrasts with RSV single infection, where filaments are produced across more extensive areas. Cryo-ET showed IAV and RSV particles can bud in very close proximity (>500nm) on the surface of the cell. RSV filaments are considerably larger than bacilliform IAV particles and can extend up to 12µm in length (Ke et al., 2018), therefore, incorporation of IAV particles could occur during RSV budding, where small IAV particles that are budding next to an RSV particle are simply incorporated in the process of forming a larger RSV filament. Imaging of IAV and RSV budding sites in coinfected cells may provide more insight into the formation of CVPs. Only two viral budding sites on thin sections of filopodia were imaged by cryo-ET and it was not

possible to visualize further budding sites due to sample thickness. Samples must be less than ~500nm thick to allow cryo-EM imaging. Methodologies could be applied to allow access to the cell membrane and cytoplasm. Grids were coated with laminin to aid cell adhesion to the carbon support surface, however different extracellular matrix substrates, for example fibronectin (Carter et al., 2020), can be applied to encourage cells to spread, therefore increasing the surface area of thin cytoplasmic regions that are accessible for imaging. Alternatively, focused ion beam (FIB) milling could be used to generate thin lamellae sections in the cytoplasm, which could then be accessed for cryo-ET. To increase the probability of finding CVPs, a correlated light and electron microscopy (CLEM) approach could be taken, where targets are fluorescently labelled and imaged using light microscopy, prior to electron microscopy imaging. In this chapter, live immunolabelling of coinfected cells for HA and F was optimised (Figure 4-5). This could be used to identify the coinfected cells within grids that appear to be producing viral filaments, which would enable a more targeted approach for identifying regions of interest to image by tomography.

An alternative potential mechanism for the formation of CVPs is that they form after virion assembly. The RSV fusion glycoprotein induces the fusion between adjacent lipid membranes, by the triggering of a dramatic conformational change in the protein, that enables its insertion into the adjacent membrane (Zhao et al., 2000; McLellan et al., 2011), bringing the membranes close enough to enable membrane fusion. If newly formed RSV and IAV particles become associated due to the close proximity of their budding sites, the RSV F may interact with the lipid envelope of IAV virions, which could potentially trigger fusion of viral envelopes. This hypothesis is supported by the curved density in some tomograms, at the site of membrane joining. This structure is potentially the M1 matrix layer of IAV or matrix associated with membrane. It is not possible to conclude with certainty what these structures are within this cryo-ET dataset, however it's possible to speculate as to how these structures may be forming. If a fully formed IAV virion interacts with the F glycoproteins on a neighboring RSV filament, this may be sufficient to fuse viral membranes, causing the membrane to dissociate from the matrix and leaving behind an intact IAV matrix layer at the site of membrane fusion.

Another interesting research question is related to the assembly of pseudotyped RSV particles. In our cryo-ET dataset, incorporation of HA to RSV filaments often

occurred at the distal end of the filament. As proposed for formation of CVPs, lack of matrix association to viral envelope at the distal end of the filament may enable pseudotyping here. However, multiple examples of pseudotyped RSV virions that incorporated HA down the full length of the filament were also identified. This raises a number of questions about the assembly and structural compatibility of pseudotyped particles. First, how are these IAV glycoproteins being incorporated? Kiss *et al.* showed that ~85% of the surface area of filaments membranes were associated with matrix (Kiss *et al.*, 2014). The matrix has been shown to interact with the C-terminus of RSV F glycoprotein, therefore mediating the assembly of RSV filaments (Shaikh et al., 2012). Conley *et al.* showed that helical arrangement of RSV glycoproteins is directed by the helical lattice that matrix proteins form within an RSV filament (Conley et al., 2021). From our tomograms, it was not possible to discern differences between IAV and RSV matrix, to allow identification of the matrix layer in RSV pseudotypes. If pseudotypes contain RSV matrix, then an interesting question arises as to how IAV glycoproteins are incorporated in an arrangement that is similar to that seen in IAV virions, while in non-pseudotyped RSV filaments, the matrix directs the helical arrangement of RSV glycoproteins (Conley et al., 2021). Further studies are essential to characterise the nature of the interaction between structural proteins within pseudotyped particles. Sub-tomogram averaging may provide an indication of the interaction, however, generating and imaging a sufficient number pseudotyped RSV particles to gather sufficient structures for averaging may be technically challenging.

CVPs incorporate the glycoproteins of both IAV and RSV. This generated the hypothesis that this property could allow CVPs to possess the receptor specificity for both IAV and RSV cellular entry receptors, thereby expanding tropism of IAV and RSV. To determine if this was the case, IAV's receptor, sialic acid, was removed from cells using exogenous NA treatment. Analysis of IAV entry in NA-treated cells compared to untreated control cells showed that entry of IAV harvested from a single infection was blocked by the degradation of IAV receptors. In the cell associated fraction, there was an increased level of IAV entry compared to released virus. It is unclear why this occurred, but the phenotype was also observed in cell associated fractions in the neutralisation assay, in that a proportion of cell associated virus escaped neutralisation by HA anti-serum, while the released virus fraction was completely neutralised. Potentially, virus associated with fragments of cell debris

are internalised by different mechanisms, via receptors or endocytosis signals on the cell debris.

While entry of IAV from a single infection was blocked in NA-treated cells, entry of IAV from a mixed infection was significantly increased and this phenotype was particularly prominent for cell associated virus. This demonstrates that IAV has expanded tropism when generated in a coinfection and this phenotype is likely to be mediated by CVPs, via use of RSV glycoproteins for cellular entry. Furthermore, confocal imaging of NA-treated cells infected with virus from a mixed infection and stained for IAV HA and RSV F showed that infection by a CVP results in coinfection by IAV and RSV. This demonstrates that some CVPs possess dual infectivity for both IAV and RSV. Additionally, cells infected by CVPs showed evidence of production of more CVPs, indicating that CVP formation is a phenotype that is maintained upon transmission between cells. The next step is to understand whether CVPs mediate viral spread within a population of cells. This experiment could be achieved by measuring the spread of CVPs using a focus forming assay, in cells deficient of sialic acid, or in the presence of a neutralising antibodies targeting IAV or RSV. This would determine if the viruses eventually segregate, resulting in distinct IAV and RSV foci of infection, or is coinfection maintained, by consistent co-transmission of IAV and RSV genomes between cells via formation of CVPs.

In natural infection, CVP formation, and the resulting alteration to viral tropism, may have implications for within host dissemination of viruses, by allowing entry to cells that may be refractory to infection by one of the parental viruses. Two thirds of RSV infections progress to the cells in the lower respiratory tract, which results in more severe disease, including bronchiolitis. The majority of uncomplicated seasonal IAV infections by H1N1 and H3N2 viruses do not progress to the lower respiratory tract (LRT), however if infection does progress to the LRT it can result in severe disease, including viral pneumonia and acute respiratory distress syndrome (Kalil and Thomas, 2019). RSV has specific cellular tropism for ciliated epithelial cells and type I alveolar pneumocytes (Johnson et al., 2006). IAVs can also infect type I and II alveolar pneumocytes, but progression of infection to the LRT is less frequent with seasonal human IAVs, due to the distribution of sialic acids within the respiratory tract. The clinical outcome of IAV and RSV coinfections are unclear, but some studies do report coinfections with increased incidence of viral pneumonia

(Echenique et al., 2013; Asner et al., 2014). If CVPs form within the respiratory tract, this may facilitate IAV spread cell types within the lung, potentially resulting in more severe disease.

RSV tropism in the context of CVPs was not investigated, due to time constraints and technical challenges with experimental design due to RSV interactions with multiple cellular receptors. Multiple host cell proteins, including heparin sulphate (Krusat and Streckert, 1997), CX3C-chemokine receptor 1 (CX_3CR1) (Johnson et al., 2015), ICAM-1 (Behera et al., 2001) and epidermal growth factor receptor (EGFR) (Currier et al., 2016), have been implicated in RSV attachment in cell culture. Recently IGFR1 was identified as an important entry receptor that interacts directly with F (Griffiths et al., 2020), alongside co-receptor nucleolin which may be a primary mediator of RSV attachment (Tayyari et al., 2011; Mastrangelo et al., 2021). Due to the potential involvement of multiple attachment and entry receptors, it could prove technically challenging to entirely block RSV entry in our cell system. Incubation of RSV with neutralising serum would be a cleaner method for blocking RSV entry. This experiment was explored, however, due to time constraints, only IAV neutralisation experiments were carried out.

The ability of CVPs to evade neutralising antibodies was also investigated. Entry of IAV from single infection completely neutralised by serum targeting HA. Some IAV harvested from a coinfection was able to enter cells after incubation with sera, suggesting some evasion of neutralisation may be occurring, however the difference between entry in single infection and coinfection was not statistically significant. In the cell associated fractions, there was high variability in neutralisation across biological replicates. This was likely to be a result of high variation in raw count data, therefore experimental protocol used for this experiment must be further optimised, to reduce inter-experiment variability. An important factor that may have increased variability was the timing of fixation. Virus was incubated with neutralising serum, followed by infection for 24 hours. IAV can undergo multiple rounds of replication within 24 hours, therefore, IAV that has escaped neutralisation would have been able to replicate and spread, confounding subsequent cell counts collected at 24 hpi. Trypsin TPCK was omitted from infection media in neutralisation experiments to limit IAV spread, but this may not have reduced IAV spread entirely in A549 cells.

The ability of CVPs to alter the antigenicity of IAV and RSV and facilitate evasion of neutralising antibodies is an important biological property. If sustained coinfection

driven by cell-cell transmission of CVPs can be achieved within a host, then a virus may be able to evade neutralisation and establish infection within the respiratory tract of a host that would otherwise be protected from infection. Neutralisation experiments carried out for this project indicated a potential phenotype, but experimental protocols must be refined to investigate this properly. Further, the role of CVPs in mediating neutralising antibodies targeting RSV must be investigated. This was explored, by testing the RSV anti-serum, but surprisingly, cross-reactive neutralisation was identified with IAV. Therefore, this serum could not be used to determine if IAV glycoproteins mediate RSV antibody escape. Palivizumab is a humanized IgG monoclonal antibody targeting an antigenic epitope of RSV F, which is a licensed therapeutic for use as a prophylactic against severe RSV disease (Luna et al., 2020). It has potent RSV neutralisation properties, therefore would be a suitable reagent for neutralisation experiments to determine the functional impact of CVPs on RSV antibody evasion.

The identification of CVPs represents a previously uncharacterised, direct interaction between two clinically important respiratory viruses, which results in the form of a structural hybrid particle, containing genomes from both viruses. From a public engagement perspective, the nature of these particles raises questions about potential for recombination between IAV and RSV genomes. Therefore, it is important to discuss the potential for biosafety risks associated with this finding. First, the virus stains used in these experiments were prototypic, laboratory adapted viruses. Both viruses could be safely handled in a biosafety level two laboratory, therefore the pathogenic risks of combining these viruses in coinfection experiments is low. However, even if CVPs formed between clinically relevant and currently circulating strains of IAV and RSV, the risk of recombination between these viruses would be negligible in these experiments. Unlike dsRNA viruses, retroviruses and some (+)ssRNA viruses, such as coronaviruses (Su et al., 2016) and enteroviruses (Savolainen-Kopra and Blomqvist, 2010), (-)ssRNA viruses have extremely low rates of homologous recombination (Chare et al., 2003; Boni et al., 2010). Whilst there is huge genetic diversity between IAVs due to segment reassortment, there is little evidence of homologous recombination within IAV genomes (Boni et al., 2010). There is a reported example of homologous recombination between RSV genomes *in vitro*, however no evidence of recombination has been found in evolutionary RSV sequences (Spann et al., 2003). Low levels of (-)ssRNA genome recombination is attributed to tight control of genome expression, which results in fast sequestering

of newly formed genomes with nucleocapsid proteins to form RNP complexes. This vastly reduces the opportunity for RNA hybridization, so prevents template switching, that could enable recombination to occur. Additionally, RNA-dependent RNA Polymerases (RdRPs) specifically use RNA in the context of RNP as a substrate (te Velthuis et al., 2021), which reduces the size of the pool of substrates available to the RdRP, further reducing the potential for template switching. In a cell coinfected with IAV and RSV, not only will opportunity for recombination be low due to the factors described above, but also due to the physical separation of replication centres into specific sub-compartments of the cell. Once inside the cell, IAV vRNPs are quickly trafficked into the nucleus for replication (Dou et al., 2017), while RSV replication occurs within cytoplasmic inclusion bodies (Rincheval et al., 2017). The formation of CVPs results in the formation of a structural hybrid, rather than a genetic hybrid and once the CVP infects the cell, the consequence is the same as if IAV and RSV independently infected the same cell.

An important limitation of this work is the use of an *in vitro* cell system. Whilst derived from the human lung, A549 cells lack the heterogeneity, spatial arrangement, and multi-layered polarity of the airway epithelium in the upper respiratory tract. IAV and RSV share tropism to infect ciliated epithelial cells (Johnson et al., 2006; Wu et al., 2016), therefore, if coinfection were to occur during natural infection, is likely to occur predominantly in these cells. Both viruses also assemble and bud from the apical surface of ciliated cells (Rossman and Lamb, 2011; Ke et al., 2018), so there is potential for interactions that could result in the formation of CVPs. However, it is likely that the fundamental processes involved in viral assembly and budding would be conserved between continuous cell culture systems and primary differentiated cells. Therefore, there is potential for IAV and RSV CVPs to form by similar mechanisms as in A549 cells, provided ciliated cells become coinfected by IAV and RSV. To identify individual CVPs budding from differentiated airway cells proves technically very challenging, due to the morphology of the airway cells and the diffraction limits of light microscopy when imaging in three-dimensions. However, whilst imaging of budding viral filaments was no achieved, the following results chapter discusses IAV and RSV coinfection in a model of the differentiated airway epithelium and explores localisation of IAV and RSV proteins within coinfected airway epithelial cells.

Overall, the formation of hybrid viral particles represents a previously uncharacterised virus-virus interaction, between co-circulating and clinically important respiratory viruses. This interaction has important functional implications in viral transmission within host and also provides novel insights into viral assembly and interaction between viral components.

Chapter 5

Influenza A virus and respiratory syncytial virus coinfection in a differentiated model of the airway epithelium

5.1 Introduction

Coinfection studies described in Chapters 3 and 4 were carried out using A549 cells: a transformed cell line, derived from the human lung. This system has many benefits, including uniformity allowing for tightly regulated experimental conditions; being highly permissible to infection by both IAV and RSV; and being easy to image at high resolution. However, this system lacks the heterogeneity, spatial and structural organisation, and physiological conditions of the airway epithelium.

A549 cells are derived from alveolar adenocarcinoma (Giard et al., 1973). Transformed cell lines, including tumour derived cell lines, are known to have dysregulated signaling pathways, that may impact cellular response to infection (Hillyer et al., 2015; Charman et al., 2021). Hillyer *et al.* compared RSV infection in A549 cells and BEAS-2B cells, a non-tumour cell line, derived from the bronchial epithelium. They showed that while RSV infection was widespread in A549 cells, infection was restricted to small puncta in BEAS-2B cells. Additionally, they showed that virus induced host response was altered: A549 cells expressed more pro-inflammatory cytokines regulated by nuclear factor κB (NF-κB), while infection of BEAS-2B resulted in increased expression of anti-viral signaling proteins and pathogen recognition receptors (Hillyer et al., 2015). Charman *et al.* demonstrated that intrinsic immune protein, tripartite motif 22 (TRIM22), is constitutively expressed in primary and differentiated airway cells, however it was absent in a number of transformed cell lines, including A549 cells (Charman et al., 2021). Differences in intrinsic immunity and virus-induced signaling pathways will likely affect permissiveness to infection by IAV and RSV infection and viral spread throughout the system, therefore impacting likelihood of coinfection.

Additionally, cell type can impact virus-induced cytopathic effect. In monolayer cell culture, RSV induces fusion of cells, to form multi-nucleated syncytia after which the virus was named (Shigeta, 1968). In coinfection with IAV, parainfluenza virus 2 induced cell fusion has been demonstrated to enhance IAV replication, as IAV infects syncytia, resulting in rapid viral spread (Goto et al., 2016). In differentiated cultures of the airway epithelium syncytia also forms, albeit at lower frequency (Neilson and Yunis, 1990; Tristam et al., 1998; Zhang et al., 2011; Broadbent et al., 2016). This may impact routes of viral spread during coinfection, therefore the

interaction phenotypes observed in coinfection may not reflect viral interactions in systems that are more representative of the human respiratory tract.

Animal models have provided a good experimental system to investigate IAV and RSV interactions during coinfection. Ayegbusi *et al.* found that RSV replication was reduced in a mouse model of coinfection with IAV, compared to RSV infection alone. They also found that coinfection resulted in reduced disease pathology, particularly when mice were inoculated with IAV and RSV simultaneously, compared to either IAV or RSV single infection (Ayegbusi et al., 2019). Further, Chan *et al.* used a ferret model of coinfection and observed that RSV replication was delayed in the presence of IAV, and that signs of morbidity due to infection were reduced during coinfection, compared to IAV single infection (Chan et al., 2018). However, neither study examined localisation of infectious foci within the respiratory tract, therefore the extent of coinfection at the cellular level in these animals could not be determined. Whilst animal models provide a good model for the systemic response to infection, it is difficult to study direct interactions between IAV and RSV due to technical challenges in identifying and isolating samples from coinfected regions of the respiratory tract. Therefore, application of a more simplified model that still recapitulates many of the important physiological features of the airway is important.

Air-liquid interface (ALI) models of the differentiated epithelium provide an experimental system derived from human tissue, that is easily obtainable and reflects the physiology of the human airway. Derived from primary cells obtained through nasal, tracheal or bronchial brushing, this culture system provides the biological conditions to enable differentiation of cells to form a pseudostratified epithelium. Cells are seeded onto transwell inserts, such that the apical surface of the culture is exposed to the air and the basal surface is submerged in media, containing the necessary growth factors for differentiation (Broadbent et al., 2016). This initial cell population then proliferates and differentiates to form a multi-layered, polarised epithelium, consisting of multiple airway cell types (Figure 5-1). Primary differentiated airway cultures reflect functional features of the upper respiratory tract, including coordinated cilia beating and mucus production. Additionally, as they are derived from primary cells, these cultures more closely reflect signaling pathways of in vivo tissues (Charman et al., 2021). Ex vivo respiratory explant cultures can also provide excellent systems for studying virus-induced cytopathology in the respiratory tract, however, accessibility for obtaining human tissue represents a

barrier to widespread use of this system for studying human pathogens. Primary differentiated culture systems, on the other hand, are increasingly available and are now widely used for respiratory pathogen research for animal and human viruses.

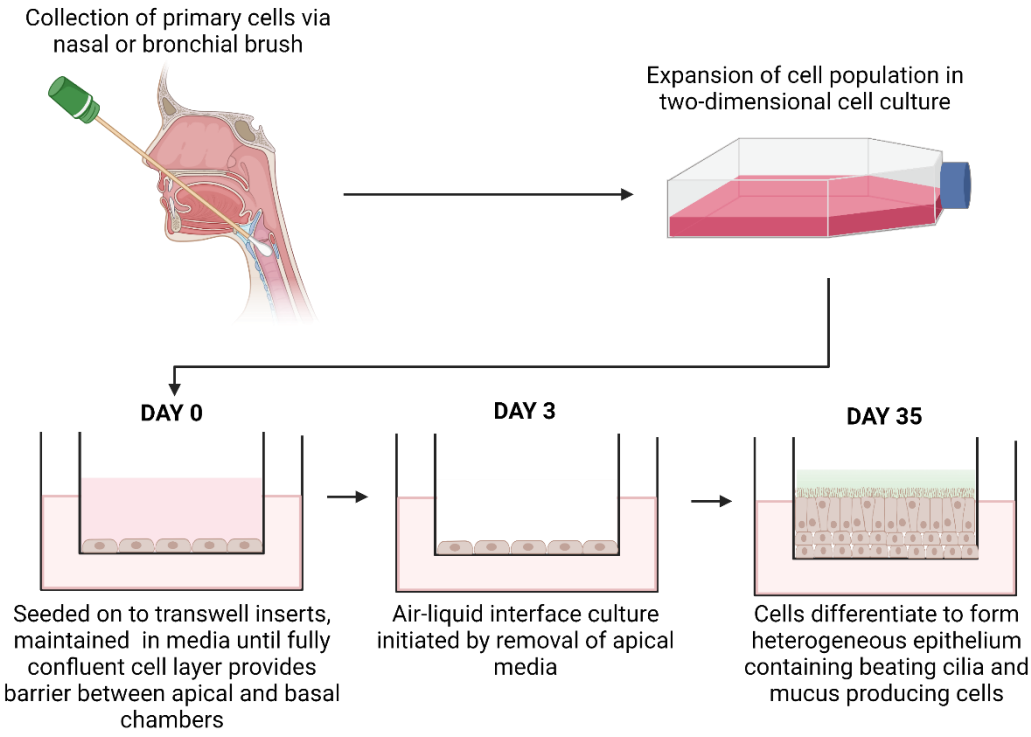

Figure 5-1: Schematic of primary differentiated airway culture system. Primary cells are collected from donor via nasal or bronchial brushing and expanded via standard two-dimensional tissue culture. Cells are then seeded into transwell inserts and undergo a process of expansion, followed by differentiation. This results in the formation of a multilayered, polarised and heterogeneous culture containing multiple cell types and functional features of the upper respiratory epithelium.

In primary differentiated and explant models of the airway epithelium, IAV infection results in substantial damage to the airway epithelium. In differentiated models of the porcine respiratory tract infected with swine, equine or canine influenza virus, widespread cilia loss was observed, but epithelial barrier function was maintained (Nunes et al., 2010; Patrono et al., 2015; Wu et al., 2016). Similarly, infection by human IAV H1N1 virus A/WSN has been shown to reduce cilia motility on ciliated epithelial cell cultures as early as 18 hpi (Smith et al., 2019).

Histopathological analyses of fatal RSV cases showed loss of cilia, cell sloughing and excess mucus production. However, this pathology is thought to be associated

with the inflammatory response to infection rather than the virus itself, as immunostaining for RSV antigen in sections from paediatric cases of RSV showed large areas of infected tissue with no obvious signs of pathology (Welliver et al., 2007). This is supported by published reports of RSV infection in differentiated airway cultures, where RSV has been shown to persist in cultures for over one month, without destruction of the epithelium (Zhang et al., 2002). Other studies report increased incidence of cell sloughing and formation of mucus plugs, containing apoptotic sloughed cells (Villenave et al., 2012). RSV infection occurs via the apical surface, targeting ciliated airway cells (Zhang et al., 2002; Broadbent et al., 2016). Disruption to cilia beating has been reported (Tristam et al., 1998) and a study by Mata *et al.*, demonstrated that RSV infection results in down regulation of β-tubulin and a reduction in the number of cells with beating cilia (Mata et al., 2012). RSV has also been demonstrated to infect non-ciliated cells, however there is no evidence that infection occurs in mucus producing cells (Villenave et al., 2012; Broadbent et al., 2016). There are, however, multiple reports of hyperplasia of goblet cells in RSV infected cultures (Villenave et al., 2012; Mata et al., 2012).

Primary differentiated culture systems have been used as a model to study coinfection between respiratory viruses, particularly in studying the role of viral interference, where infection by one virus blocks infection by a secondary virus. Wu *et al.* showed that cultures infected with RV, followed by IAV after a three-day interval, showed significant inhibition of IAV replication, compared to IAV infection alone. Using BX795, a drug that blocks innate immune signaling, they demonstrated that IAV inhibition was dependent on RV-induced interferon signaling, as IAV replication was restored in the absence of induction of interferon stimulated genes (Wu et al., 2020). Similarly, SARS-CoV-2 replication was completely inhibited in simultaneous coinfection with RV in differentiated bronchial cell cultures and was even inhibited when cultures were inoculated with RV 24 hours after initial infection with SARS-CoV-2. Experiments with BX795 also demonstrated that this viral interference was mediated by the interferon response to RV (Dee et al., 2021). Conversely, another study showed that both IAV and RSV mediated interference resulted in inhibition of RV replication during sequential challenge with RV as the secondary virus, but RV did not exert interference on either coinfecting virus (Essaidi-Laziosi et al., 2020). Interference induced by swine IAV in a model of the porcine respiratory epithelium was demonstrated to block coronavirus replication in a time dependent manner (Peng et al., 2021).

Whilst viral interference has been extensively studied in primary differentiated cultures, few studies described co-detection of both viruses replicating within the same culture system and there are no published examples of viral coinfection at the cellular level in primary differentiated airway cultures. This represents an important gap in our understanding of how viruses interact within the respiratory airway. Respiratory viral coinfections occur quite frequently (Nickbakhsh et al., 2016), however the extent to which coinfecting viruses interact within the respiratory epithelium is unclear. Many respiratory viruses share tropism for specific regions and cell types within the respiratory tract. IAV and RSV are known to infect the same regions of the upper airway with specificity for ciliated cells (Johnson et al., 2007; Wu et al., 2016). This shared tropism provides the opportunity for coinfection and subsequent viral interactions to arise. Experiments described in Chapter 3 show that IAV can superinfect cells prior infected with RSV. If this property is conserved in natural infection, IAV may readily spread into regions containing RSV infectious foci, resulting in coinfection. High viral burst sizes (Möhler et al., 2005) and a shared tropism for regions of the respiratory tract mean there is strong potential for interactions at the cellular level between IAV and RSV in a coinfected host.

Results described in the previous two chapters were identified in A549 cells, which do not reflect the biological complexity of the respiratory tract. Therefore, the overall aim of this chapter was to characterise features of coinfection by IAV and RSV in a primary differentiated model of the human bronchial epithelium, to determine if previously identified findings hold true in a more complex, physiologically relevant system. To this end, I had the following aims. First, to assess viral replication and spread of IAV and RSV during single virus infection and mixed in hBEC cultures. Next, to determine the extent of coinfection in hBEC cultures and understand the potential for interactions during viral assembly in coinfected cells. Finally, to compare the expression of key mediators of cellular signaling pathways in single and mixed infections.

5.2 Acknowledgements

I would like to thank the following individuals for their contribution to the work described in this chapter. Kieran Dee optimised hBEC culture and differentiation protocols and provided the first and second batches of differentiated transwells for

coinfection experiments. Frazer Bell, Lynn Stevenson and Lynn Oxford processed tissue samples for paraffin embedding and sectioning; stained sections with hematoxylin and eosin; and performed immunohistochemistry staining for cleaved caspase 3. Verena Schultz optimised protocols for dewaxing and antigen retrieval for immunofluorescence staining.

5.3 Results

5.3.1 Differentiation of primary human bronchial epithelial cells at air-liquid interface generates cultures that recapitulate features of the upper respiratory tract

Primary human bronchial epithelial cells (hBECs) were seeded onto transwell inserts and cultured at air-liquid interface (ALI). The apical side of the epithelium was exposed to air, while the basal side was submerged in growth media, which replicates the physiology of the epithelium in the respiratory tract. At ALI, hBECs differentiate to form a multi-layered, heterogeneous culture, consisting of multiple airway cell types (Figure 5-2).

Hematoxylin and eosin (H&E) staining of sections of uninfected hBEC cultres showed the presence of multiple cell types, that reflect cell morphologies observed in human airway tissues (Figure 5-2A). Basal cells adhere to the transwell membrane and above this, multiple layers of cells can be identified. Columnar ciliated cells extend out to the apical surface of the culture and cilia decorates the apical surface. Coordinated beating of cilia can be observed in cultures from approximately >15 days post ALI initiation. Goblet cells, which do not incorporate H&E staining, can be identified in the apical layer, interspersed between ciliated cells (Figure 5-2A). This multilayered culture provides a tight barrier separating apical and basal surfaces. Staining of actin filaments using a fluorescently labelled phalloidin stain shows tight packing of epithelial cells when imaged from the apical surface (Figure 5-2B). While epithelial barrier function was not measured, the cultures displayed the hallmarks of a healthy, differentiated epithelium and therefore provided a suitable model for coinfection experiments

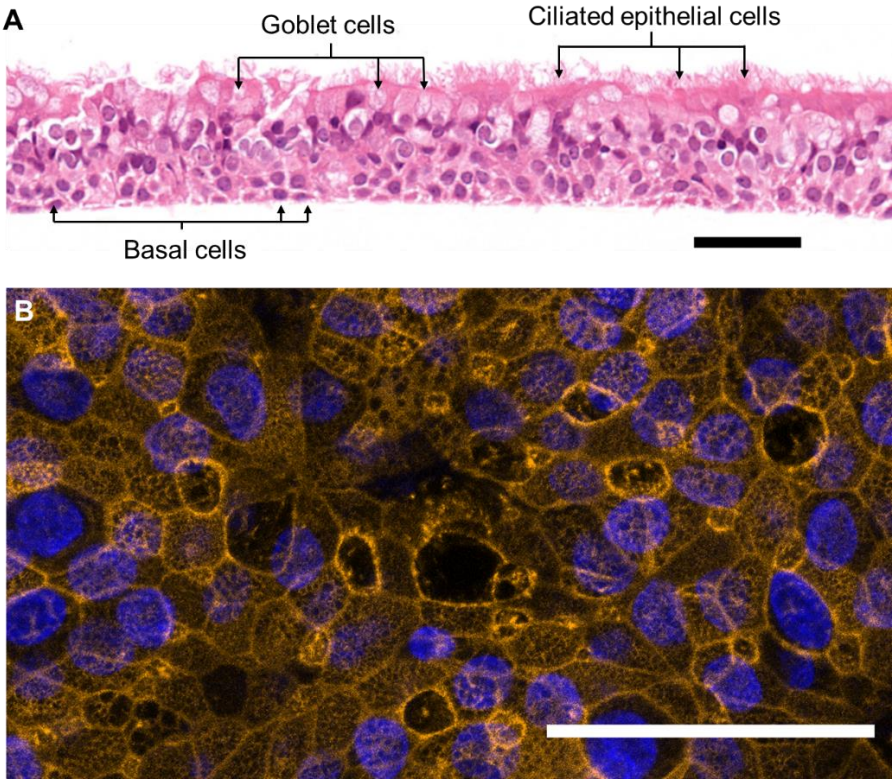

Figure 5-2: hBECs differentiate to form heterogeneous cultures with multiple airway cell types. (**A**) The apical surface of differentiated hBEC cultures is decorated with cilia and mucus is produced and released from goblet cells. Basal cells can be identified along the basal surface of the culture. Section from paraffin embedded transwell, fixed >35 days post ALI initiation. Section was stained with hematoxylin and eosin. Scale bar represents 50µm. (**B**) Apical staining of transwell for filamentous actin shows tight organisation of cells in differentiated cultures. Image shows maximum intensity projection of apical surface of hBEC culture, stained with phalloidin for filamentous actin (orange) and DAPI for nuclei (blue). Scale bar represents 50µm.

5.3.2 IAV and RSV coinfection results in similar replication phenotypes to those observed in A549 cells

In order to characterise replication of IAV and RSV in hBEC cultures, hBEC cultures were infected with 10^5 pfu of IAV, RSV, a mixed inoculum of both viruses, or mock infected. This inoculum concentration was greater than that used in previous coinfection studies in the same hBEC culture system (Dee et al., 2021) and was selected to try to establish a high level of coinfection. Samples were collected at 24, 48 and 72 hpi by washing of the apical surface and titrated by plaque assay.

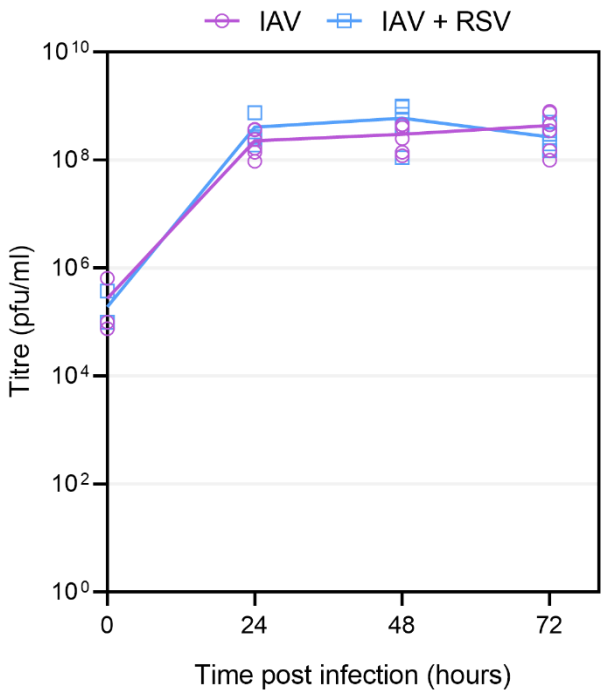

Figure 5-3: IAV replication kinetics are unchanged in coinfection with RSV. IAV replication kinetics in single infection (magenta line, circular points) and mixed infection (blue line, square points). Lines indicate the mean of six data points. The experiment was carried out in technical duplicate, from three independent experiments in different hBEC culture batches. The zero-hour timepoint was calculated from back titration of virus inoculum. Statistical significance was determined by Mann Witney test at each timepoint, no statistical differences were identified, $p \geq 0.05$ not indicated.

In single IAV infection, IAV replication peaked at 24 hpi, reaching titres above 10^8 pfu/ml and remained constant at 47 and 72 hpi. In mixed infection with RSV, IAV replication kinetics were unchanged compared to single IAV infection, with IAV reaching its replication plateau at 24 hpi and maintaining a consistent titre above 10^8 pfu/ml until 72 hpi (Figure 5-3). This indicates that IAV is replication unaffected by the presence of RSV in coinfected cultures.

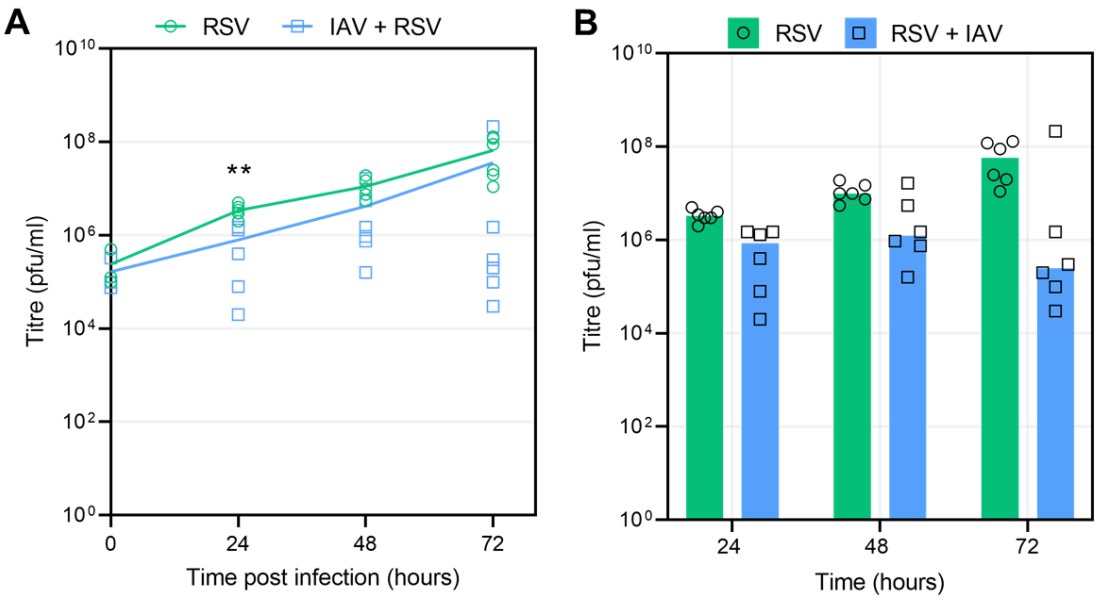

Figure 5-4: RSV replication is variable, but generally reduced in coinfection with IAV. (A) RSV replication kinetics in single infection (green line, circular points) and mixed infection (blue line, square points). Lines indicate the mean of six data points. The zero hours timepoint was calculated from back titration of virus inoculum. Statistical significance was determined by Mann Witney test at each timepoint, ** $p<0.01$, $p \geq 0.05$ is not indicated. (**B**) Median of each time point for single RSV infection (green bars) and mixed infection (blue bars), with individual data points shown in black. The experiment was carried out in technical duplicate, from three independent experiments in different hBEC culture batches.

In single RSV infection, titres rose steadily over the 72-hour time course, reaching over 10^7 pfu/ml at 72 hpi (Figure 5-4A). The peak of RSV replication was not captured by 72 hpi, so an extended timescale would be required in future experiments to achieve this. In single RSV infections, titres from replicate samples across three independent experiments were quite consistent, with approximately 1 log pfu/ml variation observed. In contrast, in mixed infections, RSV titres were highly variable, with titres from replicate samples ranging greater than 2 log pfu/ml per timepoint. At 24 hpi, RSV was significantly lower in mixed infection compared to single infection ($p=0.0065$ by Mann Witney test), but statistical differences were not identified at later timepoints, likely due to high variation between replicates. However, comparison of medians shows that there was a clear trend towards a

reduction in RSV titre in mixed infection with IAV, compared to single infection (Figure 5-4B).

Overall, the replication phenotypes observed in hBEC culture infections were consistent with infections in A549 cells, suggesting conserved interactions may be occurring in both systems.

5.3.3 IAV and RSV exhibit different cytopathic effects, and IAV-induced pathology dominates in mixed infection

To compare the cytopathic effects induced in each infection, formalin fixed paraffin embedded (FFPE) cultures were sectioned and H&E stained, (Figure 3-5). Mock infected cultures show healthy morphology at all experimental timepoints. Mock infected cultures had even epithelial thickness across the culture and decoration with cilia across the apical surface, with no evidence of cell sloughing. There were differences in epithelial thickness between individual cultures, which was likely to be due to within batch variation in differentiation between cultures, rather than as a result of the experimental protocol.

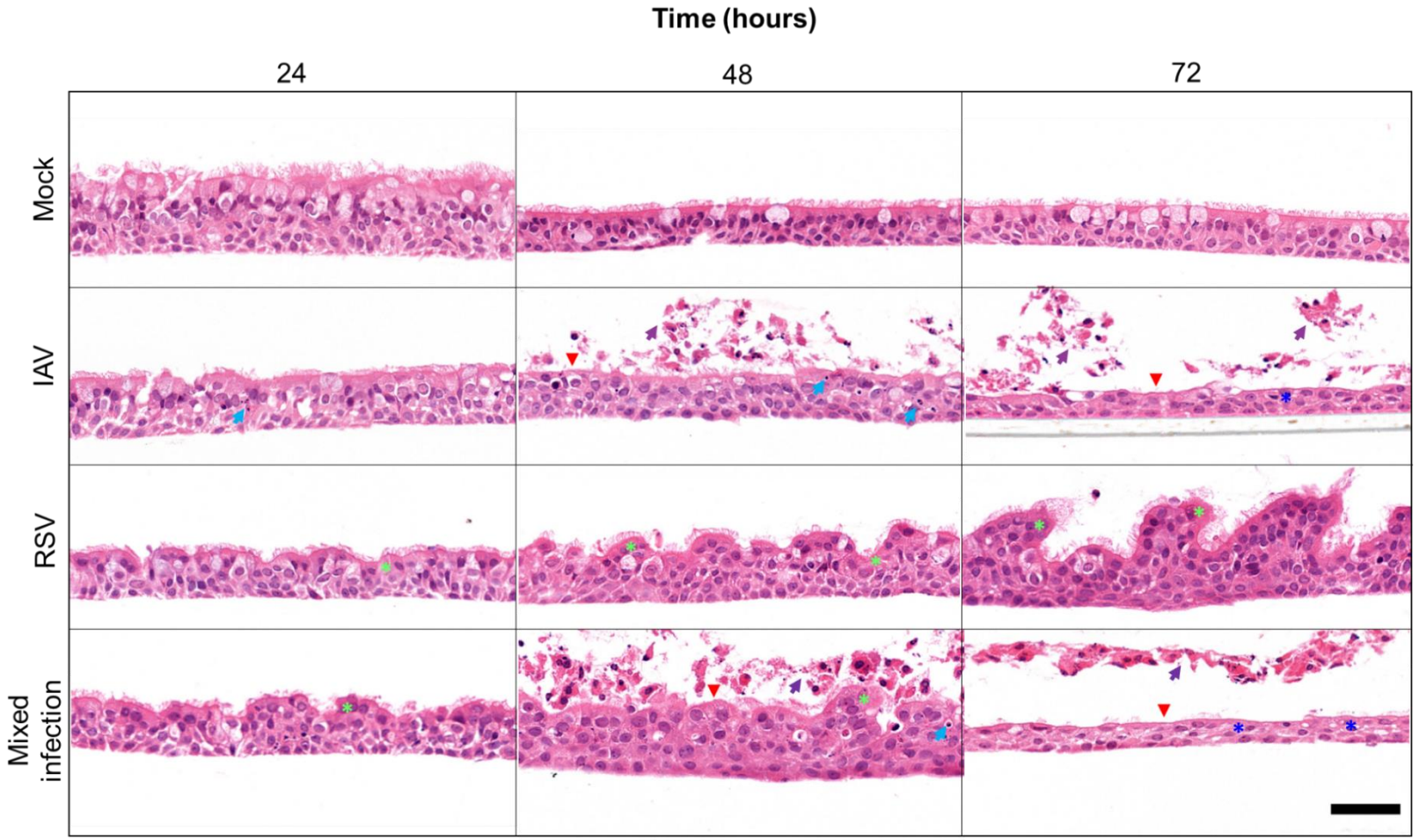

Figure 5-5: IAV and RSV induce markedly different cytopathic effects. H&E stained sections across the time course of infection show pathology induced by virus infection. Scale bar represents 50µm. Annotations indicate cytopathic effects: pyknotic nuclei (blue arrows), sloughed cells (purple arrows), loss of cilia (red arrows), metaplasia (dark blue asterisk), RSV-induced remodeling (green asterisk).

IAV infection induced clear cytopathic effect and substantial damage to the epithelium by 48 hpi. Sloughed cells were detached from the epithelium, which suggests cell death in response to IAV infection (Figure 5-5, purple arrows). Pyknotic nuclei were also identified at 24 hpi and were more frequent at 48 hpi (Figure 5-5, blue arrows). Loss of nuclear integrity is an indicator of apoptosis. Epithelial thinning occurred over the time course and by 72 hpi, the epithelium consisted of only 1-2 layers of cells. Loss of cilia was also observed by 48 hpi (Figure 5-5, red arrows) and virtually all columnar ciliated cells were depleted by 72 hpi. A few remaining cells did possess cilia structures, however these cells may have undergone metaplasia, as they no longer exhibited columnar morphology (Figure 5-5, blue asterisk).

RSV infection induced a markedly different CPE to IAV and resulted in remodeling of the epithelium. By 24 hpi, small depressions were observed on the surface of the epithelium, which increased by 48 and 72 hpi to form large indents across the epithelium (Figure 5-5, green asterisk). There was no evidence of cell death (indicated by cell sloughing or epithelial thinning) and no loss of cilia across the infection time course. RSV induces cell fusion to form multi-nucleated syncytia readily in monolayer cell culture. This CPE has also been observed in histopathological sections from the lungs of patients with fatal RSV cases (Johnson et al., 2007). However, there was no evidence of syncytium formation in the RSV infections described.

In mixed infections, evidence of CPE induced by both RSV and IAV was present on sections. At 24 hpi, small indentations formed at the apical surface of the epithelium and some evidence of onset of cell death (Figure 5-5). There was batch to batch variation in the timing of the onset of CPE. In some infections the epithelium retained integrity at 24 hpi (Figure 5-5), while in other infections cell sloughing was observed at 24 hpi (data not shown by H&E, immunofluorescence Figure 5-6). However, by 48 hpi, CPE was consistent between batches and substantial cell death was observed. By 72 hpi, coinfected cultures displayed the same pathological features as IAV-only infection: the epithelium had thinned to 1-2 cell layers and sloughed cells had detached from the epithelium. Wide-spread loss of ciliated cells had also occurred.

5.3.4 Immunofluorescence staining shows robust infection by both viruses and absence of exclusion interactions in coinfected sections

Next, to understand viral spread within the tissue, sections were stained for viral proteins (Figure 5-6). IAV was detected using a mouse monoclonal antibody targeting IAV HA and RSV was detected using a polyclonal antibody, that was raised against the whole virus. These antibodies were selected due to their compatibility in staining protocols in FFPE sections. Primary antibodies used previously in Chapter 4 were tested to stain FFPE sections for IAV HA and RSV F but did not produce any signal after optimisation attempts, potentially due to destruction of epitopes in paraffin embedded sections.

IAV infection resulted in diffuse infection across the apical surface of the airway epithelium by 24 hpi. Some signal was also detected in the lower layers of the epithelium, suggesting IAV spread from the apical surface down into the epithelium (Figure 5-6). At 48 hpi, sloughed cells were highly positive for HA and some HA positive cells remained on the epithelium. At 72 hpi, little IAV HA staining was observed, and signal was predominantly associated with sloughed cells. The remaining epithelium was only 1-2 cell layers thick and very few remaining cells were positive for IAV (Figure 5-6), suggesting that, whilst the infection was widespread across the rest of the epithelial culture, it was not able to spread to the basal cell layer. The pattern of HA staining implies that cells infected with IAV undergo cell death and detachment, resulting in a clearance of IAV infection from the remaining cell layer. It also suggests that the remaining basal cells may confer a level of resistance to IAV infection.

Infection by RSV also resulted in robust viral spread by 24 hpi (Figure 5-6). Antigen positivity was primarily detected at the apical surface of infected cultures. RSV infection remained limited to the apical layer of cells over the 72-hour time course, despite extensive remodeling of the epithelial structure. This was expected, as RSV demonstrates specific tropism for ciliated cells in the upper respiratory epithelium (Johnson et al., 2007; Zhang et al., 2011).

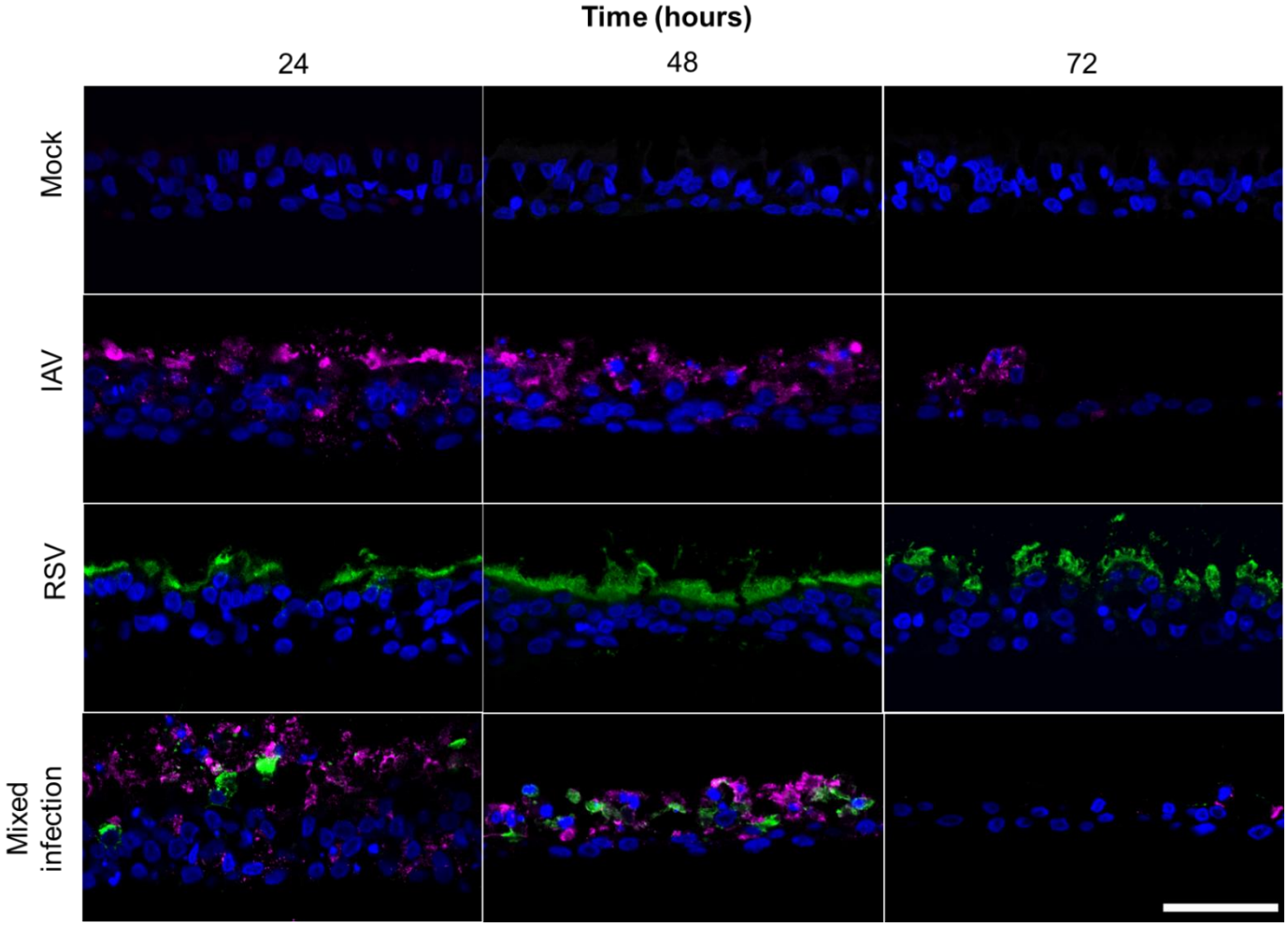

Figure 5-6: Immunostaining for viral proteins shows IAV and RSV spread throughout the epithelium. Sections of FFPE hBEC cultures were stained for IAV HA (magenta) and RSV (green). Diffuse staining was observed for both viruses in single infection. Mixed infected cultures contained cells positive for IAV and RSV, with some evidence of coinfection. Scale bar indicates 50 µm.

In mixed infected cultures, IAV and RSV positive cells could be identified at 24 and 48 hpi. As described for figure 5-4, there was batch to batch variation in the onset of CPE seen at 24 hpi. In the cultures shown in Figure 5-6, cell sloughing could be observed by 24 hpi. All sloughed cells appeared positive for HA but some also contained positivity for RSV. In other batches, the epithelium remained intact at 24 hpi and both IAV and RSV positive cells could be identified in the epithelium (Figure 5-7). The majority of cells were infected by IAV or RSV (Figure 5-7). Some cells were coinfected, however, the proportion of coinfected cells was low at 24 hpi. This suggests that primary differentiated hBEC cells are less susceptible to coinfection than A549 cells, where a high level of coinfection was identified at 24 hpi. At 48 hpi, sloughed cells positive for IAV and RSV were identified, and the remaining epithelium was markedly thinner. Similar to IAV only infection, at 72 hpi, little viral antigen remained in the epithelium, with 1-2 layers of cells remaining (Figure 5-6).

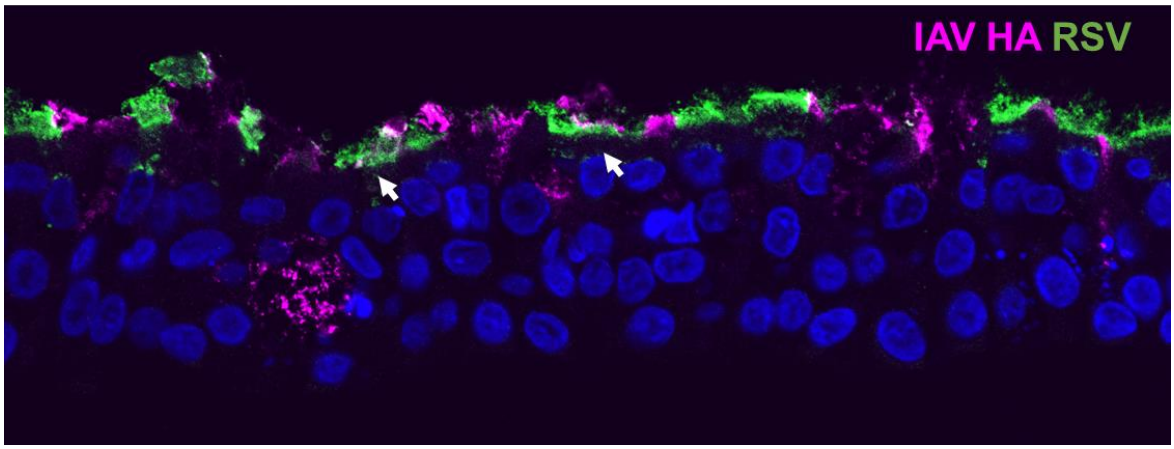

Figure 5-7: IAV and RSV infection occurs within the same epithelium and coinfection occurs. Coinfected culture at 24 hpi, with intact epithelium coinfected with IAV (magenta) and RSV (green). White arrows indicate examples of coinfected cells.

5.3.5 Apical localisation of IAV and RSV proteins in coinfected cells provides opportunity for viral interactions

The experiments described in Chapter 4 show that IAV and RSV readily coinfect A549 cells and viral glycoproteins mix in regions of budding viral filaments. Further, cryo-electron tomography (cryo-ET) revealed that hybrid viral progeny were formed from coinfected cells. IAV and RSV share tropism for ciliated cell types and viral assembly and budding occurs at the apical surface of the epithelium (Oomens et al., 2006; Johnson et al., 2007; Wu et al., 2016). In a coinfected cell, formation of chimeric viruses requires opportunity for assembling IAV and RSV particles to interact at the apical surface of the cell. Therefore, to determine the potential for chimeric virus formation in hBEC cultures, we examined virus interaction at the apical surface of coinfected cells by looking at localisation of viral proteins using super resolution microscopy. Sections stained for IAV HA and RSV were regions containing coinfected cells were specifically targeted for imaging.

There did not appear to be substantial colocalisation between viral proteins, however, both appeared in close proximity within apical regions (Figure 5-8). At this resolution, it was not possible to distinguish between budding filamentous virions and cilia, however the presence of both viruses' proteins at the apical surface of coinfected cells is promising indication that IAV and RSV may come into contact during viral assembly and budding from coinfected primary differentiated airway cells.

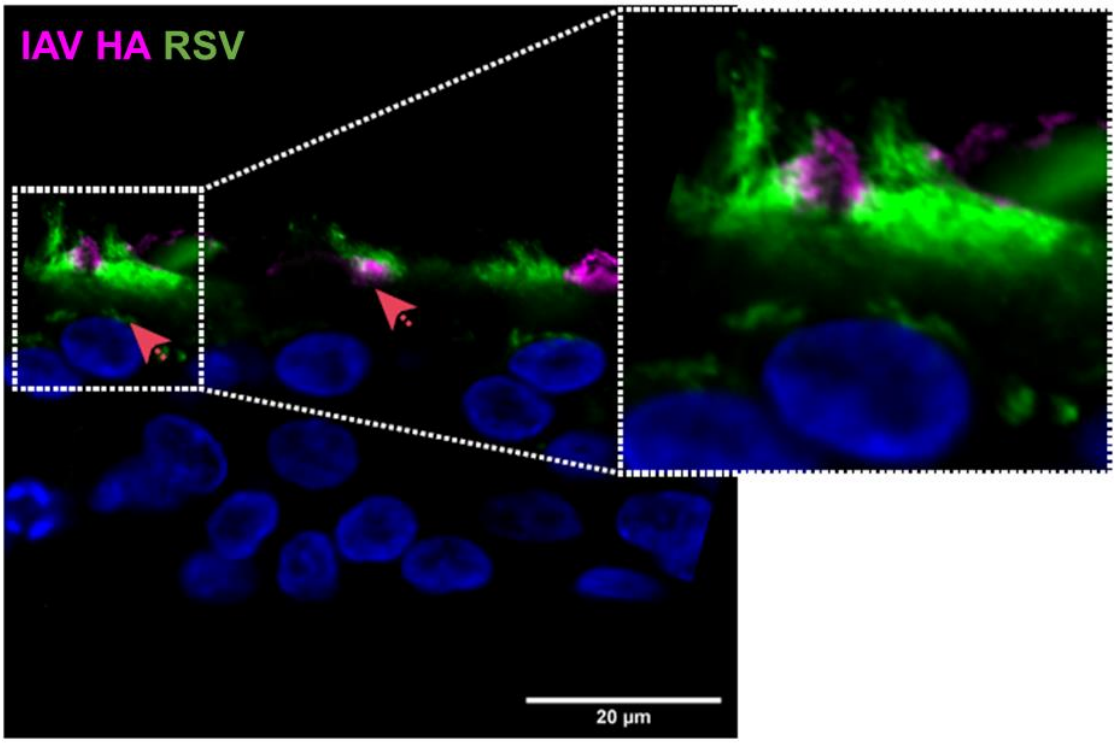

Figure 5-8: IAV and RSV proteins localise to the apical surface of coinfected cells. FFPE section from a coinfected culture, fixed at 24 hpi and stained for HA (magenta) and RSV antigen (green). Image shows coinfected cells, indicated by red arrows. Inset image of magnified coinfected cell shows localisation of HA and RSV proteins to the apical surface of cells. Scale bar represents 20 µm.

FFPE sections were analysed from transwells fixed at 24 hpi. At this timepoint, coinfection was observed, but it was not widespread throughout the culture. By 48 hpi, substantial viral induced damage to the epithelium prevented the detection of coinfected cells with intact morphology. To capture coinfection before the onset of CPE, cultures were fixed at 30 hpi and were imaged from the apical surface (Figure 5-9). This allowed for imaging of a wider area of the epithelium, so gave a better indication of the extent of coinfection. Cultures were stained for IAV HA and RSV F, using antibodies optimised for immunofluorescence of formalin fixed cells (described in Chapters 3 and 4). Z-stacks were collected through the top layer of cells in the culture. Apical staining showed widespread infection across the culture by both IAV and RSV (Figure 5-9). Foci of coinfection could be observed from the apical surface of cultures and in some cells, HA and F were colocalized in filamentous structures extending from the cell surface (Figure 5-9 B-E). Further

analysis by co-staining for β-tubulin is required to determine if these structures are cilia or budding viral filaments.

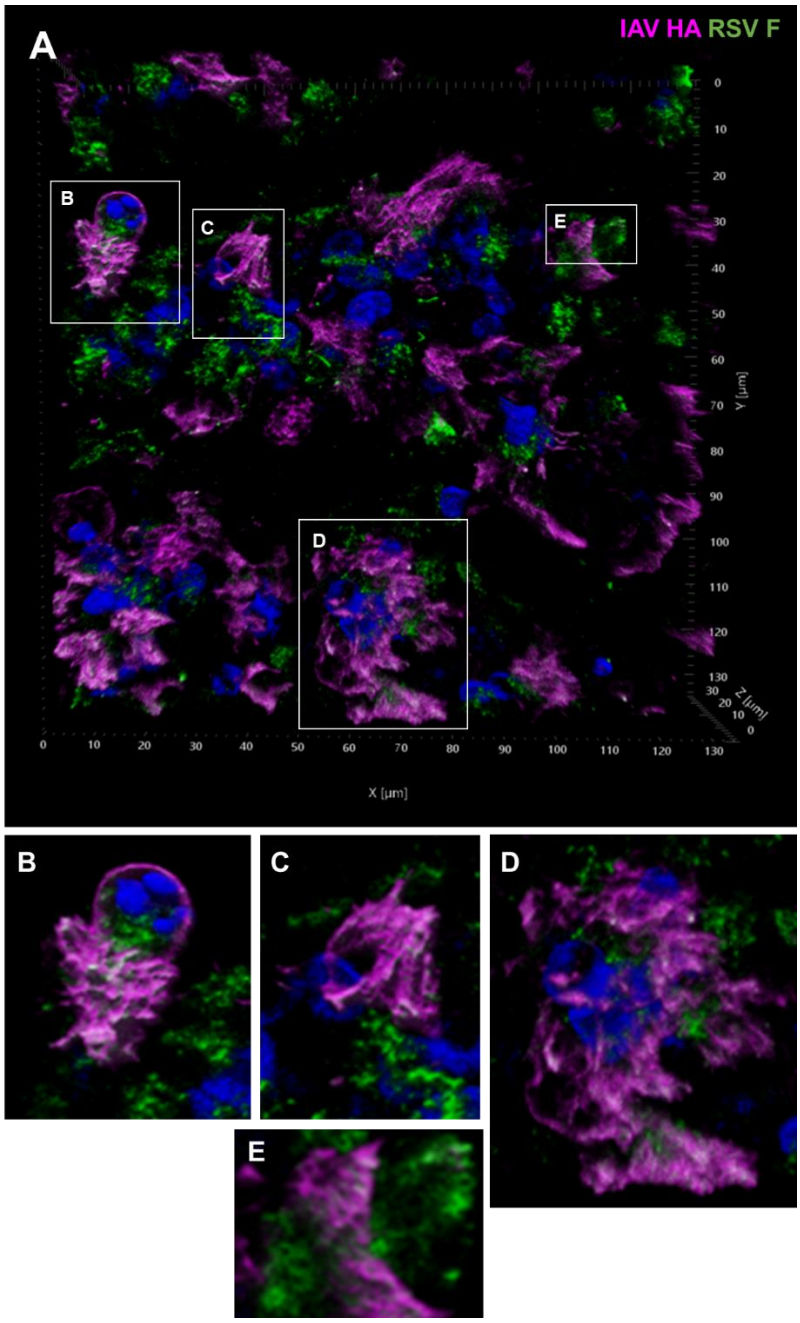

Figure 5-9: Three-dimensional reconstruction of apical surface of coinfected cultures showing coinfected foci. Cultures stained from apical surface for IAV HA (magenta) and RSV F (green). White regions show areas of colocalisation between viral proteins. (**A**-**D**) show magnified regions of coinfection highlighted in main image by white boxes. Scale in from 0 to 130 µm X and Y dimensions, and 0 to 30 µm in Z dimension, markings in 10 µm increments.

5.3.6 Antiviral signaling pathways are induced by both IAV and RSV infection

To understand how infection by IAV and RSV impacted host cell signaling, sections were stained for host proteins that are important mediators of virus-induced signaling pathways

First, sections were stained against myxovirus resistance protein A (MxA). MxA is an interferon-induced protein, whose expression is upregulated in response to type I (α and β) and type III (λ) interferon (IFN) signaling. Mx proteins possess conserved antiviral activity over multiple host species, active against a diverse range of viruses, in particular RNA viruses (reviewed by [Verhelst, Hulpiau and Saelens, 2013]). IAV has been demonstrated across different experimental systems to be sensitive to Mx protein activity (Pavlovic et al., 1995; Grimm et al., 2007). RSV has also been shown to confer some resistance to the antiviral activity of MxA (Atreya and Kulkarni, 1999).

To understand the activation of the IFN response in coinfection, sections were stained by immunofluorescence for MxA (Figure 5-10). In mock infected cultures, no signal was detected. This reflects the fact that MxA is not constitutively expressed and is upregulated in response to infection.

In IAV infection, MxA expression was detected from 24 hpi. MxA signal was greater in basal cells and reduced towards the apical surface. This may reflect the infection status of the cells at the apical surface: as IAV suppresses induction of antiviral signaling via NS1, MxA expression in IAV infected cells may be lower. At later timepoints, MxA signal was more pronounced across the cultures, but the strongest signal was still observed in basal cells (Figure 5-10). Interestingly, in sloughed cells, no MxA signal was detected (Figure 5-11).

RSV infection also resulted in upregulation of MxA expression, detected from 24 hpi (Figure 5-10). Signal increased over the infection time course and was widespread at 48 and 72 hpi. Like IAV infected cultures, MxA was expressed as a gradient across the epithelium, with more MxA detected in basal cells (Figure 5-10). RSV encodes antiviral proteins NS1 and NS2, which may suppress MxA expression in ciliated cells at the apical surface of the cultures, which were infected with RSV. There did not appear to be a qualitative difference in the level of MxA expression between IAV and RSV infections, however quantification of MxA expression, via image analysis or western blot, would be required to determine these differences.

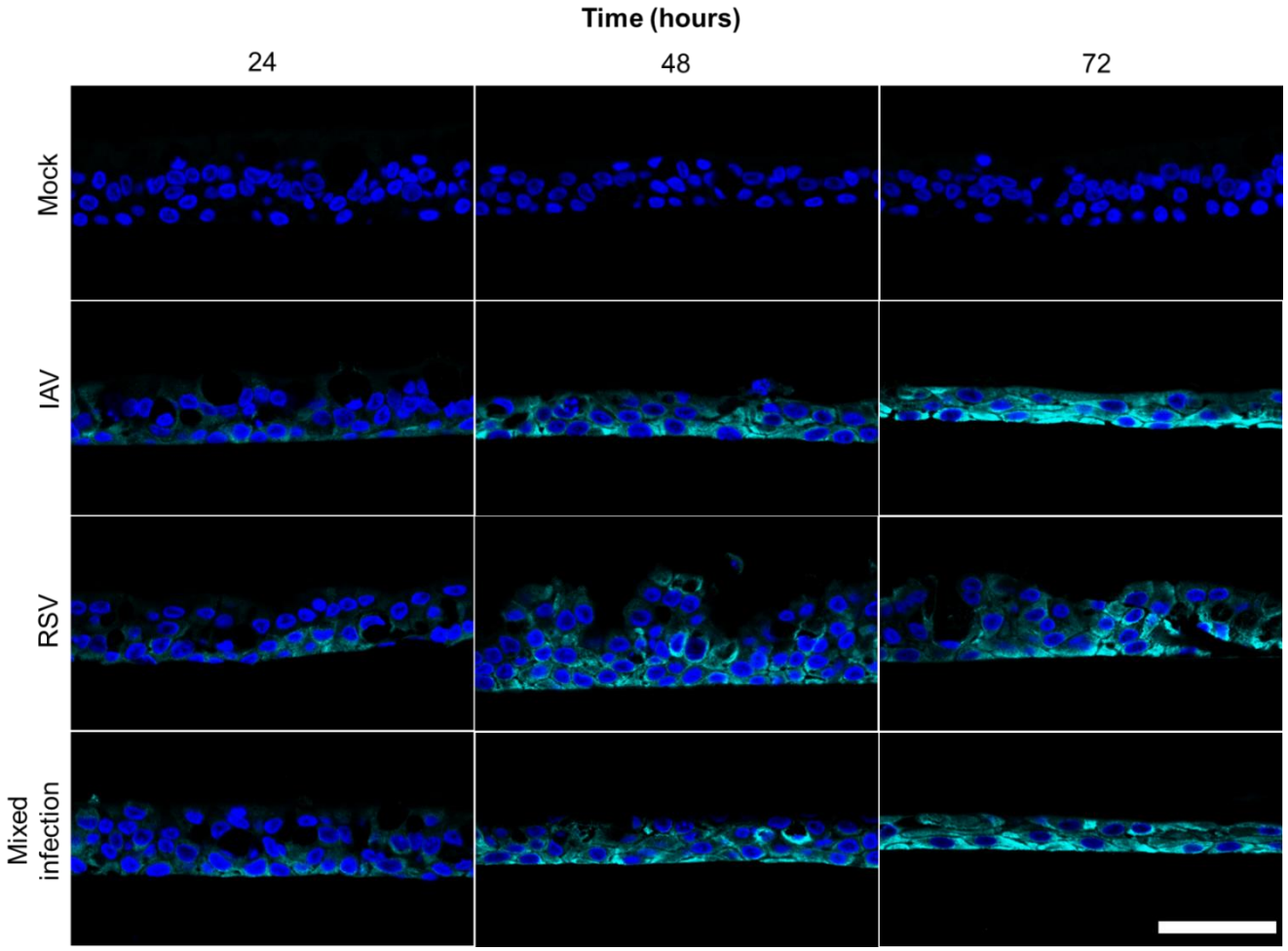

Figure 5-10: MxA expression is induced by both IAV and RSV infection. FFPE sections stained for interferon-induced signaling protein MxA (cyan). MxA expression was detected in all infected cultures, but not mock infected cultures. Scale bar represents 50 µm.

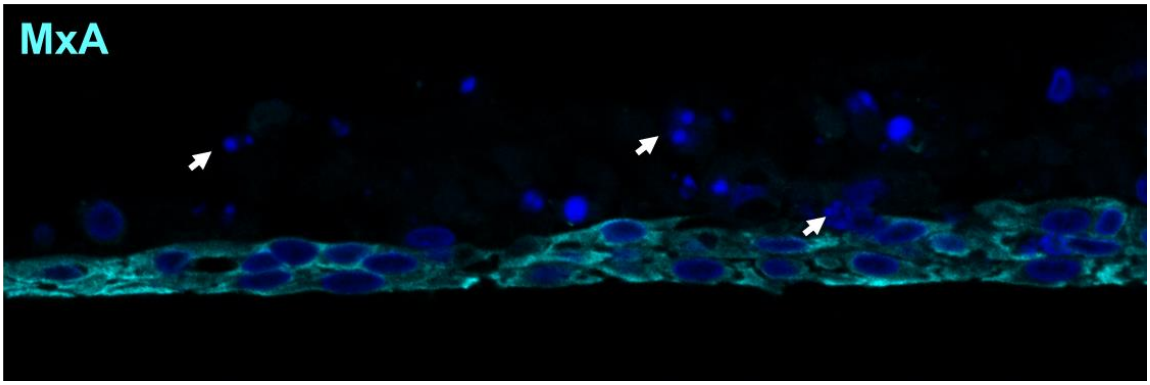

Figure 5-11: MxA expression was not detected in sloughed cells from IAV infected cultures. FFPE section at 48 hours post infection with IAV, stained MxA (cyan). Signal corresponding to MxA expression was not observed in sloughed cells, indicated by white arrows.

In coinfected cultures, MxA was detected at all time points and levels of expression appeared consistent with that observed in IAV and RSV infection (Figure 5-10). This again implies that both IAV and RSV are able to replicate despite the induction of antiviral signaling within the cultures. Additionally, it suggests that the reduction to RSV titre seen in mixed infections is independent of the innate immune response, as comparable levels of Mx induction were observed between RSV single infection and mixed infections.

5.3.7 Apoptosis is induced in response to IAV infection, but not RSV infection

H&E staining of infected sections showed that IAV infection induced cell death as early as 24 hpi and this phenotype is also observed in mixed infection. In contrast, RSV did not appear to induce cell death, despite widespread infection and induction of morphological changes in the epithelium. To understand if cell death was caused by apoptosis, cells were stained for cleaved caspase 3 (CC-3). Caspase 3 is an executioner caspase which is activated in response to pro-apoptotic signals by cleavage by an initiator caspase. CC-3 then utilises its activity as a cysteine protease to degrade structural proteins within the cell, as well as mediating DNA degradation and nuclear collapse (Slee et al., 2001).

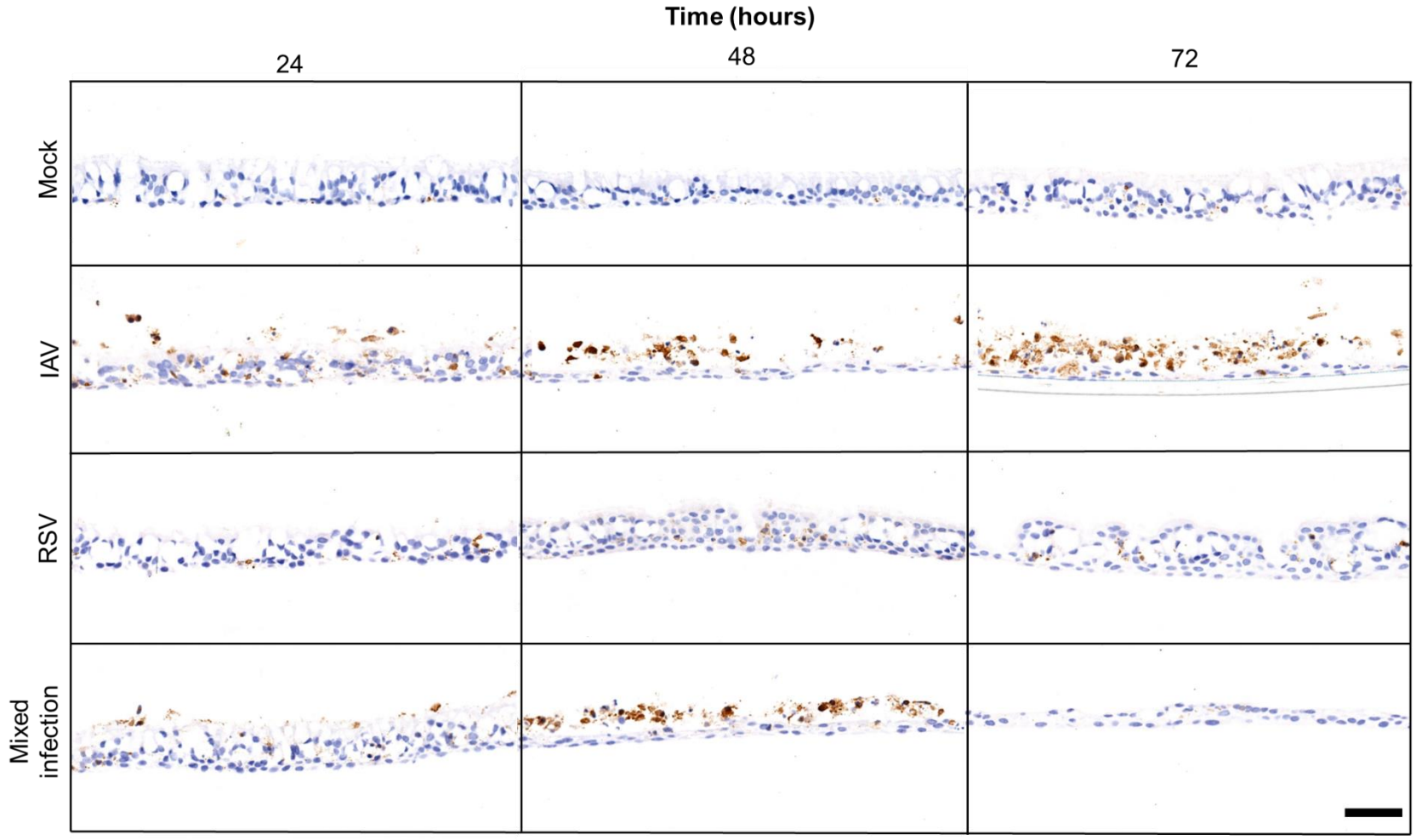

Figure 5-12: Apoptosis is induced by IAV infection, but not by RSV infection. FFPE sections stained by immunohistochemistry for cleaved caspase 3 (brown staining). Scale bar represents 50 µm.

Sections were stained CC-3 by immunohistochemistry. Minimal CC-3 staining was detected in mock infected sections, which may represent a baseline level of apoptosis in these cultures (Figure 5-12). In IAV infection, CC-3 positive cells were readily detected throughout from 24 hpi. Signal was identified in both sloughed cells and cells in the epithelium (Figure 5-12), suggesting that IAV infection induces apoptosis within the epithelium, which results in cell death and detachment from the epithelial layer.

In RSV infection, there was little CC-3 staining detected (Figure 5-12). This was consistent with previous observations that RSV infection did not appear to induce cell death. Even by 72 hpi, CC-3 expression appeared comparable to the level in mock infected tissues (Figure 5-12), despite there being a high level of RSV infection at this timepoint detected by immunofluorescence staining (Figure 5-6).

At 24 hpi, CC-3 expression in mixed infection appeared marginally lower than IAV infection (Figure 5-12). However further experimental replicates would be required to confirm if this difference is significant or a result of batch variation. Additional analysis, for example western blot for CC-3 expression, could also be carried out to quantify this difference. CC-3 signal was comparable to IAV infection at 48 hpi, with signal predominantly observed in sloughed cells. At 72 hpi, little CC-3 was detected, but this is likely due to the fact that sloughed cells were not captured in the section of embedded tissue.

CC-3 staining confirms that cell death caused by apoptosis is induced following infection by IAV. In mixed infections, this phenotype may contribute towards the reduction in RSV titre observed, as higher rates of cell death due to IAV would prevent prolonged replication of RSV and release of infectious RSV virions at the apical surface of cultures. This finding is consistent with infections in A549 cells described in Chapter 3, where live cell imaging revealed that cell death is induced much sooner following IAV infection, compared to RSV infection.

5.4 Discussion

Primary differentiated airway cultures provide a representative experimental system that recapitulates many features of the upper airway. Studies using hBEC cultures have provided substantial insight in respiratory viral pathogenesis in the epithelium and virus-induced host cell responses to infection. In this chapter, IAV and RSV single and mixed infections were characterised in hBEC cultures and potential sources of viral interaction were identified.

In single virus infection, viral replication kinetics indicated that IAV can establish robust infection in the hBEC system, peaking between 24-48 hpi. RSV infectious titre increased slowly over the 72-hour timescale but did not reach the replication peak. This may have been due to the method for collecting samples for titration, via apical washing. RSV is known to remain predominantly cell associated in cell culture, therefore, if this phenotype is consistent in differentiated airway cultures, apical washing may not be sufficient to collect the full RSV yield if a large proportion of viral particles remain bound to the epithelial cell surface. Due to limitations in the number of hBEC cultures available, a comparison of apical virus to cell associated virus was not carried out, however this is an important experiment to get a more comprehensive understanding of RSV replication in hBEC cultures.

In coinfection, IAV replication was unchanged compared to single IAV infection. This was consistent with replication trends observed in coinfections in A549 cells. RSV titres were generally reduced in coinfection with IAV. There was high variability in RSV titre in mixed infection, such that a statistically significant difference between RSV titres in single infection or mixed infection was only detected at 24 hpi. This level of variability was not observed in RSV single infection, suggesting that coinfection with IAV could be the source of the variation in titre. Overall, the replication kinetics in hBEC cultures were consistent with the trends observed in A549 cells. The conservation of interactions between these two cell systems provides assurance that A549 cells do reflect the biology observed in more physiologically relevant systems.

IAV and RSV showed markedly different patterns of cytopathic effect. IAV infection resulted in apoptosis induced cell death, depletion of ciliated cells and thinning of the epithelial layer. CPE was clearly evident between 24-48 hpi, and variation in CPE onset may have been caused by slight variations in input titre of IAV. RSV did

not induce cell death or cell sloughing, with no loss of ciliated cells. Instead, RSV infection induced a marked remodeling of the epithelium, resulting in formation of clefts along the length of the epithelial surface. RSV infection has been previously associated with tissue remodeling pathways. Xu *et al.*, demonstrated that RSV induces chromatin remodeling that results in exposure of new open chromatin regions that are enriched with genes involved in extracellular matrix formation, tissue remodeling and growth factor signaling (Xu et al., 2020). If RSV infection modifies both extracellular matrix composition and cell motility, then it could induce the changes observed in the tissue morphology. Further, RSV has been reported to induce hyperplasia of mucus producing cells (Broadbent et al., 2016), which may result in increased epithelial area in some regions. In coinfection, CPE initially reflected a combination of the effects of both IAV and RSV, however by 48 hpi, IAV-induced CPE became dominant, as demonstrated by increased cell death, sloughing and depletion of ciliated cells. RSV preferentially infects ciliated cells (Johnson et al., 2007; Zhang et al., 2011), so if IAV-induce cell death occurs rapidly in coinfected ciliated cells, this may explain the reduction in RSV infectious titre observed in mixed infections. In support of this hypothesis, CC-3 staining showed that apoptosis was strongly induced by IAV infection and was present in sloughed cells, however, was not induced in response to RSV infection. The timing of IAV-induced cell death may determine the yield of infectious RSV that can be produced and released from the coinfected tissue. There was between batch variation in CPE onset, therefore this may explain the variability observed in RSV titre in the coinfected cultures.

To determine the localisation and spread of infection, cultures were stained for viral proteins and imaged by confocal microscopy. In single infections by both viruses, viral antigen staining was diffuse across the apical surface of the cultures and could be observed extending into filamentous structures that are likely to be cilia on some cells. Co-staining for β-tubulin is required to confirm this, but unfortunately due to time constraints this was not carried out. In mixed infection at 24 hpi, the majority of cells were infected with either IAV or RSV, with some cells showing signs of coinfection. This finding highlights the virus-specific nature of viral interactions: while some virus interactions render tissues refractory to coinfection by a second virus (Dee et al., 2021), other viruses can co-exist and establish replication in close proximity, within the same regions of the epithelium.

Cultures were infected simultaneously with IAV and RSV, at relatively high viral input, which likely does not reflect the conditions of natural infection. Staggering the timing of infection allows infection by the primary virus to spread throughout the tissue and elicit a virus-specific host immune response, which may impact the ability of the secondary virus to establish replication. Experiments described in Chapter 3 show that IAV infection can establish in A549 cells previously infected with RSV, therefore it would in interesting to determine if this happens in hBEC cultures, with physiological and immunological features that more closely replicate the human airway.

At later timepoints, increased incidence of coinfection was observed. Apical staining at 30 hpi for IAV HA and RSV F showed coinfected foci, with localisation of the glycoproteins from both viruses to the apical surface of coinfected cells. This suggests there may be potential for interaction between IAV and RSV at the apical surface, potentially resulting in the formation of chimeric viral particles. High resolution imaging of sections of coinfected cells, showed that IAV HA and RSV antigen come into close proximity at the apical surface, and incorporation of both viral proteins can be observed in cilia. In ciliated cells, IAV haemagglutinin (HA) localises at the apical surface the cell, as well as being incorporated into the cilia, demonstrated via colocalisation with β-tubulin, and can be found at cilia tips (Smith et al., 2019). Co-staining against β-tubulin and viral antigen may provide the means to distinguish between cilia and budding viral filaments. Alternatively, a higher resolution imaging technique could be used. Transmission electron microscopy (TEM) of resin embedded tissue sections may shed light on the organisation of budding filaments on the apical surface of ciliated cells and should provide sufficient resolution to distinguish between IAV and RSV filaments, and cilia structures (Ke et al., 2018). Further optimisation of super-resolution imaging of apically stained cultures, combined with TEM approaches or targeted cryo-electron tomography, are essential to fully characterise organisation and structure of virus budding from coinfected differentiated airway cells.

Previous coinfection studies highlight the importance of interferon (IFN) mediated responses to viral infection in determining outcome of coinfection (Wu et al., 2020; Dee et al., 2021). To investigate this in hBEC cultures infected with IAV and RSV, sections from single and mixed infections were stained for anti-viral protein MxA. IAV and RSV induced MxA expression to similar extents, with a gradient of

expression of MxA observed and greatest level of expression observed in basal cells. In coinfection, the profile of MxA expression was comparable to that observed in single virus infections and at later timepoints MxA expression in coinfected cultures resembled IAV single infected cultures, due to IAV induced cytopathic effects. This suggests that viral interference interactions are unlikely account for the reduction in RSV titre observed in coinfection. Both IAV and RSV encode potent IFN antagonist proteins, NS1 for IAV, and NS1 and NS2 for RSV. These proteins interact with a multitude of different host proteins involved in the induction and response to IFN (reviewed by [Nogalez *et al.*, 2018; Thornhill and Verhoeven, 2020]). The fact that both IAV and RSV are able to modulate the induction of innate immune responses may be one reasons why their co-replication is compatible within the same tissue, by allowing viral spread within cells at the apical surface, where immune signaling has been downregulated by viral immune antagonists. Neither IAV or RSV infection spread to basal cells in our experiments and these cells expressed the highest level of MxA expression. Single cell transcriptomics or proteomics to determine host signaling pathways induced or downregulated in cells of different infection status would be an informative experiment to aid understanding why some cells may be refractory to infection by either virus, while others are permissive to coinfection.

Overall, this chapter characterised coinfection in between IAV and RSV in a representative model of the human airway. Observed phenotypes in viral replication and CPE were consistent between this complex, physiologically relevant model and A549 cells, a simplified cell model. Confocal imaging showed IAV and RSV establish infection in the same regions of the culture and that coinfection of primary differentiated cells does occur. Within coinfected cells, IAV and RSV proteins colocalise at the apical surface, therefore there is potential for interactions to occur during viral assembly.

Chapter 6

Final discussion and future research questions

Virus-virus interactions underpin respiratory viral dynamics at the cellular, host and population level. Despite this, our fundamental understanding of biology of these interactions is limited. Whilst immune-mediated, indirect viral interactions are increasingly well characterised, little is known about the mechanisms of direct interaction between coinfecting viruses. Therefore, the overarching aim of this research project was to develop an experimental model of coinfection, to identify sources of interactions between two unrelated respiratory viruses at the cellular level.

Influenza A virus (IAV) and respiratory syncytial virus (RSV) are of high clinical importance, share epidemiological features and possess similar tropism within the respiratory tract. For these reasons, these viruses were selected as a model for viral interactions occurring within the same coinfected cell and tissue. Chapter 3 describes the development of an *in vitro* coinfection system, using a cell line derived from the human lung (A549 cells). RSV replication was significantly reduced in coinfection with IAV, while IAV replication was unchanged or in some cases marginally increased. This finding supported published data from experimental IAV and RSV coinfections, showing that coinfection results in inhibition of RSV replication, but not of IAV (Shinjoh et al., 2000; Chan et al., 2018). Further, reducing IAV MOI or delaying IAV infection relative to RSV did not reduce IAV replication compared to single infection, indicating that IAV can establish replication within a system that contains a high level of RSV infection. At the cellular level, infection was assessed by immunofluorescence staining for viral proteins, IAV haemagglutinin (HA) and RSV nucleoprotein (N). At 8 hours post infection (hpi), fewer cells were positive for IAV in mixed infection, compared to single infection, while more cells were positive for RSV in mixed, compared to single, infection. At 24 hpi, this trend was still observed for RSV, which is counter-intuitive compared to the observed replication kinetics in coinfection. This implies that multiple interactions may be occurring at different stages of IAV and RSV replication cycles, that impact both expression of viral proteins and release of infectious virus.

Analysis of nucleoprotein localisation in coinfected cells revealed important features of the replication cycles of both viruses, including the presence of RSV inclusion bodies and nuclear localisation of IAV NP. This shows that both viruses are able to establish their replication cycles within different compartments of the same cell and implies that superinfection exclusion does not occur between IAV and RSV in our

A549 cell system. The nucleoproteins of both viruses also localised to the same regions of plasma membrane, indicating trafficking of genomes prior to viral assembly occurs, which may present a source of competition as both viruses engage with Rab11 positive endosomes for transport of RNPs (Bruce et al., 2012). Further to the finding that IAV NP and RSV N localise to the same regions of the plasma membrane, colocalisation between IAV HA and RSV fusion glycoprotein (F) was observed in regions of budding viral filaments. This led to the question whether interactions between IAV and RSV occurred during viral assembly and budding steps, which was explored in more detail in Chapter 4. Super-resolution confocal microscopy and scanning electron microscopy (SEM) revealed filamentous structures budding from coinfected cells that incorporated the glycoproteins from both viruses and exhibited structural features of both viruses. To determine if these filamentous structures were virions composed of both IAV and RSV, cryo-electron tomography was used. Two classes of structural hybrid particles were identified: 1) chimeric viral particles (CVPs), containing genomes from both IAV and RSV, and 2) pseudotyped RSV filaments, coated in IAV glycoproteins.

The identification of CVPs represents a novel virus-virus interaction, with implications on our understanding of viral assembly and structure. There are a number of unanswered questions relating to the formation of CVPs. Firstly, the mechanism of formation is yet to be elucidated. IAV and RSV share preference to assemble and bud from lipid raft regions of the membrane (Lin et al., 1998; Fleming et al., 2006), and cryo-ET data described in Chapter 4 shows that both IAV and RSV budding sites occur in close proximity (less than 500 nm apart) on the plasma membrane of coinfected cells. As the larger virus, RSV may acquire budding IAV particles as during the course of its own assembly. On the other hand, density was observed at the point of fusion between IAV and RSV, which potentially corresponded to IAV matrix. This points to a mechanism that occurs after the IAV virion is fully assembled, potentially mediated by RSV F. Experiments using a sialidase to remove IAVs receptor showed that CVPs facilitate an expansion of IAV tropism and further, CVPs facilitate coinfection by IAV and RSV, demonstrating that they are dual-infectious units.

Coinfection by IAV and RSV also resulted in the formation of pseudotyped RSV filaments. Pseudotyping is a well described interaction, that can occur between genetically and structurally heterogenous viruses (Granoff and Hirst, 1954; Choppin

Atn and Compans, 1970). Cryo-ET confirmed that IAV and RSV do interact by the process of pseudotyping, but that the interaction only appeared compatible one way, as no pseudotyped IAV particles were identified. An important question regarding the compatibility of viral components is yet to be answered (Zavada, 1982). RSV glycoprotein incorporation is directed by the matrix structure, resulting in a helical arrangement of glycoproteins (Conley et al., 2021). Therefore, how IAV glycoproteins are incorporated in an arrangement consistent with that of IAV virions remains to be determined. Immunofluorescence staining or fluorescent tagging to allow combined imaging of IAV HA with RSV matrix (M) or IAV matrix (M1) and RSV N or labelled RNA genomes, would provide important insight into the composition of the matrix layer of pseudotyped virions, which is an essential mediator for both IAV and RSV filament formation (Kiss et al., 2014; Peukes et al., 2020; Conley et al., 2021).

The nature of hybrid particle formation (both CVP and pseudotype) gives rise to interesting questions about the compatibility of different viruses to engage in these interactions. CVPs consist of IAV extending from RSV and pseudotyping was only observed on RSV filaments, not IAV virions. This suggests that RSV may have a degree of structural flexibility which enables them to engage in these interactions, while IAV structure may be more restricted. This is the first reported example of pseudotyping of RSV, however, early pseudotyping experiments involved closely related paramyxoviruses, including Newcastle disease virus and parainfluenza virus SV5 (Granoff and Hirst, 1954; Choppin and Compans, 1970). Therefore, this structural compatibility may be a more general trait, which is shared between the closely related Pneumoviridae and Paramyxoviridae families, rather than an RSV-specific trait. The Paramyxovidae family contains a wide range of human and animal pathogens, including emerging viruses Hendra virus and Nipah virus (Plemper and Lamb, 2021). Further investigation in what drives this structural flexibility is essential to understand the likelihood of these events occurring during natural coinfection, and the viruses that could potentially be involved. Coinfection experiments using HMPV and PIVs may provide important insight into conservation of this trait between viral families. If the potential for hybrid virion formation, either by CVP or pseudotype formation, can be extended to included viruses closely related to RSV, then the pool of compatible respiratory viruses that cocirculate within human populations substantially increases.

Heng *et al.* described the formation of structurally different virions with altered tropism, found in skin biopsies from patients coinfected with HIV-1 and HSV-1 (Heng et al., 1994). The finding that CVPs containing structural features from both viruses supports the observation from Heng *et al.*, who described structurally distinct hybrid infectious progeny as a result of HIV-1/HSV-1 coinfection. These particles were observed in clinical samples, which demonstrates the biological feasibility of the formation of hybrid viral particles during natural infection, as a result of coinfection. Whilst it was not possible to examine human respiratory tissue from a coinfected individual, the closest experimental model was employed. Primary differentiated airway cultures recapitulate important physiological features of the respiratory, as well as more closely resembling the homeostatic profile of the human airway, compared to transformed cell lines (Charman et al., 2021). Staining coinfected cultures for IAV and RSV proteins, demonstrated that both viruses can establish robust infection within the same tissue and that coinfection occurs at the cellular level. Further to this, in coinfected cells, IAV and RSV components colocalise at the apical surface. These observations in hBEC cultures provide promising indication that there is opportunity for interactions between IAV and RSV to occur in the coinfected respiratory tract.

A key unanswered question is regarding how likely it is for infectious foci from multiple viruses to come into contact within a coinfected respiratory tract. While IAV and RSV are reported to have shared tropism within the respiratory tract (Johnson et al., 2006; Wu et al., 2016), further characterisation of the dissemination of each virus within respiratory tissues is required to understand how likely it is for foci to establish within the same region. Infections described in Chapter 5, show that in simultaneous IAV and RSV infection in hBEC culture, both viruses can replicate, resulting in coinfection at the individual cell level. However, timing may play an important role in initiating interference interactions, that may prevent widespread coinfection of respiratory tissue (Drori et al., 2020).

Another important question is what population groups are more likely to host respiratory viral interactions. Coinfections more frequently occur in children, compared to adult populations (Nickbakhsh et al., 2016; Mandelia et al., 2021). Therefore, interactions between respiratory viruses may be most likely to occur in children. Prevalence of RSV in young children is high and almost all children are seropositive against RSV by the age of two (Andeweg et al., 2021). Our data

suggest that unknown structural properties of RSV may render it more likely to form CVPs than IAV (and potentially other respiratory viruses), therefore coinfection in young children may result in a higher likelihood of CVP formation, compared to other population groups. Further, Heng *et al.* described hybrid virion formation in immunocompromised patients (Heng et al., 1994). Impaired immune function may enable enhanced replication and spread of coinfecting viruses within the respiratory tract, therefore increasing the likelihood of direct contact between viruses and coinfection at the cellular level. Further, establishment of persistent infections in immunocompromised patients may provide a prolonged opportunity for viral coinfection or viral interactions to occur. Within host evolution in immunocompromised patients can result in emergence of diverse viral variants (Choi et al., 2020) and this process may be impacted by viral interactions. Identifying population groups that are potentially more susceptible to the occurrence of direct viral interactions as a consequence of coinfection, is essential to understand how they can influence the progression of infection and potentially the pathogenesis of disease.

The research questions explored in this project have been in the context of infections by human respiratory viruses, within human populations. However, these principles are equally applicable to animal populations. The understanding of role of coinfection in shaping viral dynamics in wild and domestic animal populations is limited compared to human populations and warrants further study. The formation of CVPs in coinfected animals is just as feasible as in coinfected humans and demonstration that CVPs can expand viral tropism has important potential implications for zoonotic infections. CVP-mediated coinfection by virus that is adapted to a specific host species, along with a less adapted virus may sufficiently reduce host barriers to enable the less adapted virus to initiate productive infection within the new host species. This hypothesis warrants further study to understand cross-species transmission by CVPs is possible and to determine whether this is sufficient to enable a virus to establish in a new host.

Overall, this project set out to develop a model of coinfection in which potential sources of interaction could be identified. The primary motivation was to address a current gap in our understanding of respiratory viral infections: to understand the mechanisms by which co-circulating respiratory viruses may be able to directly interact with one another, within a coinfected tissue or cell. This project resulted in

characterisation of a novel interaction between two unrelated, clinically important respiratory viruses and also confirmed previously published data regarding IAV and RSV replication dynamics in coinfection and the occurrence of natural pseudotyping between taxonomically distinct viruses. The research described in this project adds to a growing body of information surrounding viral interactions, which informs our understanding of viral pathogenesis and dynamics during coinfection. Understanding the drivers of respiratory viral dynamics ultimately will allow better prediction of population level viral dynamics and identification of mechanisms of disease, or potentially correlates of protection associated with coinfection. Further, studying viruses in a community dynamic allows for a more comprehensive understanding of the context of respiratory viral infections, and the fundamental biology that underpins them.

List of references

Achdout, H., Vitner, E.B., Politi, B., Melamed, S., Yahalom-Ronen, Y., Tamir, H., Erez, N., Avraham, R., Weiss, S., Cherry, L., Bar-Haim, E., Makdasi, E., Gur, D., Aftalion, M., Chitlaru, T., Vagima, Y., Paran, N. and Israely, T. 2021. Increased lethality in influenza and SARS-CoV-2 coinfection is prevented by influenza immunity but not SARS-CoV-2 immunity. *Nature Communications*. **12**(1), pp.1–10.

Adams, O., Bonzel, L., Kovacevic, A., Mayatepek, E., Hoehn, T. and Voge, M. 2010. Palivizumab-resistant human respiratory syncytial virus infection in infancy. *Clinical Infectious Diseases*. **51**(2), pp.185–188.

Al-Mubarak, F., Daly, J., Christie, D., Fountain, D. and Dunham, S.P. 2015. Identification of morphological differences between avian influenza A viruses grown in chicken and duck cells. *Virus Research*. **199**, pp.9–19.

Ali, A., Avalos, R.T., Ponimaskin, E. and Nayak, D.P. 2000. Influenza virus assembly: effect of influenza virus glycoproteins on the membrane association of M1 protein. *Journal of Virology*. **74**(18), pp.8709–8719.

Ali, S.T., Kadi, A.S. and Ferguson, N.M. 2013. Transmission dynamics of the 2009 influenza A (H1N1) pandemic in India: the impact of holiday-related school closure. *Epidemics*. **5**(4), pp.157–163.

Aliprantis, A.O., Shaw, C.A., Griffin, P., Farinola, N., Railkar, R.A., Cao, X., Liu, W., Sachs, J.R., Swenson, C.J., Lee, H., Cox, K.S., Spellman, D.S., Winstead, C.J., Smolenov, I., Lai, E., Zaks, T., Espeseth, A.S. and Panther, L. 2021. A phase 1, randomized, placebo-controlled study to evaluate the safety and immunogenicity of an mRNA-based RSV prefusion F protein vaccine in healthy younger and older adults. *Human Vaccines & Immunotherapeutics*. **17**(5), pp.1248–1261.

Amorim, M.J., Bruce, E.A., Read, E.K.C., Foeglein, Á., Mahen, R., Stuart, A.D. and Digard, P. 2011. A Rab11- and Microtubule-Dependent Mechanism for Cytoplasmic Transport of Influenza A Virus Viral RNA. *Journal of Virology*. **85**(9), pp.4143–4156.

Andeweg, S.P., Schepp, R.M., van de Kassteele, J., Mollema, L., Berbers, G.A.M. and van Boven, M. 2021. Population-based serology reveals risk factors for RSV infection in children younger than 5 years. *Scientific Reports*. **11**(1), pp.1–8.

Andreu-Moreno, I. and Sanjuán, R. 2020. Collective Viral Spread Mediated by Virion Aggregates Promotes the Evolution of Defective Interfering Particles. *mBio*. **11**(1).

Andreu, Z. and Yáñez-Mó, M. 2014. Tetraspanins in extracellular vesicle formation and function. *Frontiers in Immunology*. **5**(SEP), p.442.

Ånestad, Gabriel, Nordbø, S.A. 2011. Virus interference. Did rhinoviruses activity hamper the progress of the 2009 influenza A (H1N1) pandemic in Norway? *Medical Hypotheses*. **77**(6), pp.1132–1134.

Anestad, G. and Nordbo, S.A. 2009. Interference between outbreaks of respiratory viruses. *Euro surveillance : bulletin europ??en sur les maladies transmissibles = European communicable disease bulletin*. **14**(41), p.19359.

Arranz, R., Coloma, R., Chichón, F.J., Conesa, J.J., Carrascosa, J.L., Valpuesta, J.M., Ortín, J. and Martín-Benito, J. 2012. The structure of native influenza virion ribonucleoproteins. *Science*. **338**(6114), pp.1634–1637.

Asner, S. a, Rose, W., Petrich, a, Richardson, S. and Tran, D.J. 2015. Is virus coinfection a predictor of severity in children with viral respiratory infections? *Clinical microbiology and infection : the official publication of the European Society of Clinical Microbiology and Infectious Diseases*. **21**(3), 264.e1–6.

Asner, S.A., Science, M.E., Tran, D., Smieja, M., Merglen, A. and Mertz, D. 2014. Clinical Disease Severity of Respiratory Viral Co-Infection versus Single Viral Infection: A Systematic Review and Meta-Analysis O. Schildgen, ed. *PLoS ONE*. **9**(6), p.e99392.

van Asten, L., Bijkerk, P., Fanoy, E., van Ginkel, A., Suijkerbuijk, A., van der Hoek, W., Meijer, A. and Vennema, H. 2016. Early occurrence of influenza A epidemics coincided with changes in occurrence of other respiratory virus infections. *Influenza and Other Respiratory Viruses*. **10**(1), pp.14–26.

Atreya, P.L. and Kulkarni, S. 1999. Respiratory Syncytial Virus Strain A2 Is Resistant to the Antiviral Effects of Type I Interferons and Human MxA. *Virology*. **261**(2), pp.227–241.

Avalos, R.T., Yu, Z. and Nayak, D.P. 1997. Association of influenza virus NP and M1 proteins with cellular cytoskeletal elements in influenza virus-infected cells. *Journal of Virology*. **71**(4), pp.2947–2958.

Ayegbusi, O.T., Ajagbe, O.A., Afowowe, T.O., Aransi, A.T., Olusola, B.A., Awogbindin, I.O., Ogunsemowo, O.O., Faneye, A.O., Odaibo, G.N. and Olaleye, D.O. 2019. Virus genes and host correlates of pathology are markedly reduced during respiratory syncytial and influenza virus co-infection in BALB/c mice. *Heliyon*. **5**(1), p.e01094.

Bai, L., Zhao, Y., Dong, J., Liang, S., Guo, M., Liu, X., Wang, X., Huang, Z., Sun, X., Zhang, Z., Dong, L., Liu, Q., Zheng, Y., Niu, D., Xiang, M., Song, K., Ye, J., Zheng, W., Tang, Z., Tang, M., Zhou, Y., Shen, C., Dai, M., Zhou, L., Chen, Y., Yan, H., Lan, K. and Xu, K. 2021. Coinfection with influenza A virus enhances SARS-CoV-2 infectivity. *Cell Research*. **31**(4), pp.395–403.

Baidaliuk, A., Miot, E.F., Lequime, S., Moltini-Conclois, I., Delaigue, F., Dabo, S., Dickson, L.B., Aubry, F., Merkling, S.H., Cao-Lormeau, V.-M. and Lambrechts, L. 2019. Cell-Fusing Agent Virus Reduces Arbovirus Dissemination in Aedes aegypti Mosquitoes In Vivo . *Journal of Virology*. **93**(18).

Bajimaya, S., Frankl, T., Hayashi, T. and Takimoto, T. 2017. Cholesterol is required for stability and infectivity of influenza A and respiratory syncytial viruses. *Virology*. **510**, pp.234–241.

Bakker, S.E., Duquerroy, S., Galloux, M., Loney, C., Conner, E., Eléouet, J.F., Rey, F.A. and Bhella, D. 2013. The respiratory syncytial virus nucleoprotein–RNA complex forms a left-handed helical nucleocapsid. *Journal of General Virology*. **94**(Pt 8), p.1734.

Balis, J.U., Bumgarner, S.D., Paciga, J.E., Paterson, J.F. and Shelley, S.A. 1984. Synthesis of lung surfactant-associated glycoproteins by a549 cells: Description of an in vitro model for human type II cell dysfunction. *Experimental Lung Research*. **6**(3–4), pp.197–213.

Ban, J., Lee, N.R., Lee, N.J., Lee, J.K., Quan, F.S. and Inn, K.S. 2018. Human Respiratory Syncytial Virus NS 1 Targets TRIM25 to Suppress RIG-I Ubiquitination and Subsequent RIG-I-Mediated Antiviral Signaling. *Viruses*. **10**(12).

Banerjee, I., Miyake, Y., Philip Nobs, S., Schneider, C., Horvath, P., Kopf, M., Matthias, P., Helenius, A. and Yamauchi, Y. 2014. Influenza A virus uses the aggresome processing machinery for host cell entry. *Science*. **346**(6208), pp.473–477.

Baral, R., Li, X., Willem, L., Antillon, M., Vilajeliu, A., Jit, M., Beutels, P. and Pecenka, C. 2020. The impact of maternal RSV vaccine to protect infants in Gavi-supported countries: Estimates from two models. *Vaccine*. **38**(33), pp.5139–5147.

Barman, S., Adhikary, L., Kawaoka, Y. and Nayak, D.P. 2003. Influenza A Virus Hemagglutinin Containing Basolateral Localization Signal Does Not Alter the Apical Budding of a Recombinant Influenza A Virus in Polarized MDCK Cells. *Virology*. **305**(1), pp.138–152.

Barman, S. and Nayak, D.P. 2000. Analysis of the transmembrane domain of influenza virus neuraminidase, a type II transmembrane glycoprotein, for apical sorting and raft association. *Journal of Virology*. **74**(14), pp.6538–6545.

Barnard, R.J.O., Elleder, D. and Young, J.A.T. 2006. Avian sarcoma and leukosis virus-receptor interactions: from classical genetics to novel insights into virus-cell membrane fusion. *Virology*. **344**(1), pp.25–29.

Batonick, M., Oomens, A. and Wertz, G. 2008. Human respiratory syncytial virus glycoproteins are not required for apical targeting and release from polarized epithelial cells. *Journal of Virology*. **82**(17), pp.8664–8672.

Baudin, F., Bach, C., Cusack, S. and Ruigrok, R.W.H. 1994. Structure of influenza virus RNP. I.

Influenza virus nucleoprotein melts secondary structure in panhandle RNA and exposes the bases to the solvent. *The EMBO Journal*. **13**(13), p.3158.

Behera, A., Matsuse, H., Kumar, M., Kong, R., Lockey, R. and Mohapatra, S. 2001. Blocking intercellular adhesion molecule-1 on human epithelial cells decreases respiratory syncytial virus infection. *Biochemical and biophysical research communications*. **280**(1), pp.188–195.

Benhaim, M.A., Mangala Prasad, V., Garcia, N.K., Guttman, M. and Lee, K.K. 2020. Structural monitoring of a transient intermediate in the hemagglutinin fusion machinery on influenza virions. *Science Advances*. **6**(18).

Bepler, T., Kelley, K., Noble, A.J. and Berger, B. 2020. Topaz-Denoise: general deep denoising models for cryoEM and cryoET. *Nature Communications 2020 11:1*. **11**(1), pp.1–12.

Bercovich-Kinori, A., Tai, J., Gelbart, I.A., Shitrit, A., Ben-Moshe, S., Drori, Y., Itzkovitz, S., Mandelboim, M. and Stern-Ginossar, N. 2016. A systematic view on influenza induced host shutoff. *eLife*. **5**(AUGUST).

Beretta, A., Cranage, M. and Zipeto, D. 2020. Is Cross-Reactive Immunity Triggering COVID-19 Immunopathogenesis? *Frontiers in Immunology*. **11**, p.2695.

Bermingham, A. and Collins, P.L. 1999. The M2–2 protein of human respiratory syncytial virus is a regulatory factor involved in the balance between RNA replication and transcription. *Proceedings of the National Academy of Sciences*. **96**(20), pp.11259–11264.

Bhagwat, A.R., Le Sage, V., Nturibi, E., Kulej, K., Jones, J., Guo, M., Tae Kim, E., Garcia, B.A., Weitzman, M.D., Shroff, H. and Lakdawala, S.S. 2020. Quantitative live cell imaging reveals influenza virus manipulation of Rab11A transport through reduced dynein association. *Nature Communications*. **11**(1), pp.1–14.

Bhattacharyya, S., Gesteland, P.H., Korgenski, K., Bjørnstad, O.N. and Adler, F.R. 2015. Cross-immunity between strains explains the dynamical pattern of paramyxoviruses. *Proceedings of the National Academy of Sciences of the United States of America*. **112**(43), pp.13396–13400.

Bhella, D., Ralph, A., Murphy, L.B. and Yeo, R.P. 2002a. Significant differences in nucleocapsid morphology within the Paramyxoviridae. *Journal of General Virology*. **83**(8), pp.1831–1839.

Birger, R., Morita, H., Comito, D., Filip, I., Galanti, M., Lane, B., Ligon, C., Rosenbloom, D., Shittu, A., Ud-Dean, M., Desalle, R., Planet, P. and Shaman, J. 2018. Asymptomatic Shedding of Respiratory Virus among an Ambulatory Population across Seasons. *mSphere*. **3**(4).

Bitko, V., Shulyayeva, O., Mazumder, B., Musiyenko, A., Ramaswamy, M., Look, D.C. and Barik, S. 2007. Nonstructural Proteins of Respiratory Syncytial Virus Suppress Premature Apoptosis by an NF-κB-Dependent, Interferon-Independent Mechanism and Facilitate Virus Growth. *Journal of Virology*. **81**(4), pp.1786–1795.

Blitvich, B.J. and Firth, A.E. 2015. Insect-Specific Flaviviruses: A Systematic Review of Their Discovery, Host Range, Mode of Transmission, Superinfection Exclusion Potential and Genomic Organization. *Viruses*. **7**(4), pp.1927–1959.

Bloom-Feshbach, K., Alonso, W.J., Charu, V., Tamerius, J., Simonsen, L., Miller, M.A. and Viboud, C. 2013. Latitudinal Variations in Seasonal Activity of Influenza and Respiratory Syncytial Virus (RSV): A Global Comparative Review. *PLOS ONE*. **8**(2), p.e54445.

Boni, M.F., Jong, M.D. de, Doorn, H.R. van and Holmes, E.C. 2010. Guidelines for Identifying Homologous Recombination Events in Influenza A Virus. *PLOS ONE*. **5**(5), p.e10434.

Böttcher, E., Matrosovich, T., Beyerle, M., Klenk, H.-D., Garten, W. and Matrosovich, M. 2006. Proteolytic Activation of Influenza Viruses by Serine Proteases TMPRSS2 and HAT from Human Airway Epithelium. *Journal of Virology*. **80**(19), pp.9896–9898.

Boyapalle, S., Wong, T., Garay, J., Teng, M., San Juan-Vergara, H., Mohapatra, Subhra and Mohapatra, Shyam 2012. Respiratory Syncytial Virus NS1 Protein Colocalizes with Mitochondrial Antiviral Signaling Protein MAVS following Infection. *PLOS ONE*. **7**(2), p.e29386.

Breiman, R.F., Cosmas, L., Njenga, M.K., Williamson, J., Mott, J.A., Katz, M.A., Erdman, D.D.,

Schneider, E., Oberste, M.S., Neatherlin, J.C., Njuguna, H., Ondari, D.M., Odero, K., Okoth, G.O., Olack, B., Wamola, N., Montgomery, J.M., Fields, B.S. and Feikin, D.R. 2015. Severe acute respiratory infection in children in a densely populated urban slum in Kenya, 2007-2011. *BMC infectious diseases*. **15**(1).

Brittain-Long, R., Andersson, L.M., Olofsson, S., Lindh, M. and Westin, J. 2012. Seasonal variations of 15 respiratory agents illustrated by the application of a multiplex polymerase chain reaction assay. *Scandinavian journal of infectious diseases*. **44**(1), pp.9–17.

Broadbent, L., Villenave, R., Guo-Parke, H., Douglas, I., Shields, M.D. and Power, U.F. 2016. In Vitro Modeling of RSV Infection and Cytopathogenesis in Well-Differentiated Human Primary Airway Epithelial Cells (WD-PAECs). *Methods in Molecular Biology*. **1442**, pp.119–139.

Broberg, E.K., Waris, M., Johansen, K., Snacken, R., Penttinen, P., Trebbien, R., Emborg, H.D., Krause, T.G., Fischer, T.K., Kuznetsova, N., Dotsenko, L., Sadikova, O., Behillil, S., Blanchon, T., Capai, L., Cohen, J.M., Enouf, V., Falchi, A., Guerrisi, C., Lina, B., Hanslik, T., Masse, S., Mosnier, A., Turbelin, C., Valette, M., Van Der Werf, S., Schweiger, B., Reiche, J., Biere, B., Buda, S., Baldvinsdottir, G.E., Domegan, L., Donnell, J.O., Byrne, C., O'Reilly, P., Moran, J., Waters, A., Gascun, C. De, Zamjatina, N., Pakarna, G., Nikiforova, R., Melillo, J.M., Melillo, T., Meijer, A., Teirlinck, A., Brydak, L.B., Cieślak, K., Guiomar, R., Cristóvão, P., Pechirra, P., Rodrigues, A.P., Prosenc, K., Socan, M., Larrauri, A., Delgado-Sanz, C., Oliva, J., Jiménez-Jorge, S., Pozo, F., Casas, I., Navarro, J.M., Gallardo, V., Omeñaca, M., Miguel, H.U., Marco, E., Melón, S., Huerta, I., Reina, J., González, C.P., González, L., Rivera, M.V.G., Lejarazu, R.O. De, Vega, T., Marcos, M.Á., Torner, N., Castro, S.P., Costa, J.G., Purriños, M.J., Docón, A.M., Fernández, M., Ezpeleta, C., Castilla, J., Blasco, M., Quiñones, C., Barba, J.L., Rivas, A., Carnahan, A., Axelsson, S., Englund, H., Rapp, M., Brytting, M., Pebody, R., Ellis, J., Zambo, M., de Lusignan, S., Gallagher, N., Nugent, C., Kearns, C., Cottrell, S., Moore, C. and McMenamin, J. 2018. Seasonality and geographical spread of respiratory syncytial virus epidemics in 15 european countries, 2010 to 2016. *Eurosurveillance*. **23**(5), pp.17–00284.

Brock, S.C., Goldenring, J.R. and Crowe, J.E. 2003. Apical recycling systems regulate directional budding of respiratory syncytial virus from polarized epithelial cells. *Proceedings of the National Academy of Sciences*. **100**(25), pp.15143–15148.

Brooke, C.B., Ince, W.L., Wrammert, J., Ahmed, R., Wilson, P.C., Bennink, J.R. and Yewdell, J.W. 2013. Most Influenza A Virions Fail To Express at Least One Essential Viral Protein. *Journal of Virology*. **87**(6), pp.3155–3162.

Brown, G., Aitkein, J., Rixon, H.W.M.L. and Sugrue, R.J. 2002. Caveolin-1 is incorporated into mature respiratory syncytial virus particles during virus assembly on the surface of virus-infected cells. *Journal of General Virology*. **83**(3), pp.611–621.

Bruce, E.A., Digard, P. and Stuart, A.D. 2010. The Rab11 pathway is required for influenza A virus budding and filament formation. *Journal of Virology*. **84**(12), pp.5848–5859.

Bruce, E.A., Stuart, A., McCaffrey, M.W. and Digard, P. 2012. Role of the Rab11 pathway in negative-strand virus assembly. *Biochemical Society transactions*. **40**(6), pp.1409–1415.

Budischak, S.A., Wiria, A.E., Hamid, F., Wammes, L.J., Kaisar, M.M.M., van Lieshout, L., Sartono, E., Supali, T., Yazdanbakhsh, M. and Graham, A.L. 2018. Competing for blood: the ecology of parasite resource competition in human malaria-helminth co-infections. *Ecology letters*. **21**(4), pp.536–545.

Bui, M., Whittaker, G. and Helenius, A. 1996. Effect of M1 protein and low pH on nuclear transport of influenza virus ribonucleoproteins. *Journal of Virology*. **70**(12), pp.8391–8401.

Bukreyev, A., Yang, L., Fricke, J., Cheng, L., Ward, J.M., Murphy, B.R. and Collins, P.L. 2008. The secreted form of respiratory syncytial virus G glycoprotein helps the virus evade antibody-mediated restriction of replication by acting as an antigen decoy and through effects on Fc receptor-bearing leukocytes. *Journal of virology*. **82**(24), pp.12191–12204.

Bullido, R., Gómez-Puertas, P., Albo, C. and Portela, A. 2000. Several protein regions contribute to determine the nuclear and cytoplasmic localization of the influenza A virus nucleoprotein. *Journal of General Virology*. **81**(Pt 1), pp.135–142.

Calder, L.J., Wasilewski, S., Berriman, J.A. and Rosenthal, P.B. 2010. Structural organization of a

filamentous influenza A virus. *Proceedings of the National Academy of Sciences of the United States of America*. **107**(23), pp.10685–10690.

Calvo, C., Garcia-Garcia, M.L., Pozo, F., Paula, G., Molinero, M., Calderon, A., Gonzalez-Esguevillas, M. and Casas, I. 2015. Respiratory Syncytial Virus Coinfections With Rhinovirus and Human Bocavirus in Hospitalized Children. *Medicine*. **94**(42), p.e1788.

Cannell, J.J., Vieth, R., Umhau, J.C., Holick, M.F., Grant, W.B., Madronich, S., Garland, C.F. and Giovannucci, E. 2006. Epidemic influenza and vitamin D. *Epidemiology and Infection*. **134**(6), p.1129.

Cao, D., Gao, Y., Roesler, C., Rice, S., D'Cunha, P., Zhuang, L., Slack, J., Domke, M., Antonova, A., Romanelli, S., Keating, S., Forero, G., Juneja, P. and Liang, B. 2020. Cryo-EM structure of the respiratory syncytial virus RNA polymerase. *Nature Communications*. **11**(1), pp.1–9.

Carr, C.M., Chaudhry, C. and Kim, P.S. 1997. Influenza hemagglutinin is spring-loaded by a metastable native conformation. *Proceedings of the National Academy of Sciences*. **94**(26), pp.14306–14313.

Carrasco, M., Amorim, M.J. and Digard, P. 2004. Lipid raft-dependent targeting of the influenza A virus nucleoprotein to the apical plasma membrane. *Traffic*. **5**(12), pp.979–992.

Carrat, F., Vergu, E., Ferguson, N.M., Lemaitre, M., Cauchemez, S., Leach, S. and Valleron, A.J. 2008. Time Lines of Infection and Disease in Human Influenza: A Review of Volunteer Challenge Studies. *American Journal of Epidemiology*. **167**(7), pp.775–785.

Carrique, L., Fan, H., Walker, A.P., Keown, J.R., Sharps, J., Staller, E., Barclay, W.S., Fodor, E. and Grimes, J.M. 2020. Host ANP32A mediates the assembly of the influenza virus replicase. *Nature 2020 587:7835*. **587**(7835), pp.638–643.

Carter, S.D., Hampton, C.M., Langlois, R., Melero, R., Farino, Z.J., Calderon, M.J., Li, W., Wallace, C.T., Tran, N.H., Grassucci, R.A., Siegmund, S.E., Pemberton, J., Morgenstern, T.J., Eisenman, L., Aguilar, J.I., Greenberg, N.L., Levy, E.S., Yi, E., Mitchell, W.G., Rice, W.J., Wigge, C., Pilli, J., George, E.W., Aslanoglou, D., Courel, M., Freyberg, R.J., Javitch, J.A., Wills, Z.P., Area-Gomez, E., Shiva, S., Bartolini, F., Volchuk, A., Murray, S.A., Aridor, M., Fish, K.N., Walter, P., Balla, T., Fass, D., Wolf, S.G., Watkins, S.C., Carazo, J.M., Jensen, G.J., Frank, J. and Freyberg, Z. 2020. Ribosome-associated vesicles: A dynamic subcompartment of the endoplasmic reticulum in secretory cells. *Science Advances*. **6**(14), p.17.

Casalegno, J S, Ottmann, M., Bouscambert-Duchamp, M., Valette, M., Morfin, F. and Lina, B. 2010. Impact of the 2009 influenza A(H1N1) pandemic wave on the pattern of hibernal respiratory virus epidemics, France, 2009. *Eurosurveillance*. **15**(6), p.19485.

Casalegno, J.S., Ottmann, M., Bouscambert Duchamp, M., Escuret, V., Billaud, G., Frobert, E., Morfin, F. and Lina, B. 2010. Rhinoviruses delayed the circulation of the pandemic influenza A (H1N1) 2009 virus in France. *Clinical Microbiology and Infection*. **16**(4), pp.326–329.

De Castro Martin, I.F., Fournier, G., Sachse, M., Pizarro-Cerda, J., Risco, C. and Naffakh, N. 2017. Influenza virus genome reaches the plasma membrane via a modified endoplasmic reticulum and Rab11-dependent vesicles. *Nature Communications*. **8**(1), pp.1–12.

Cauchemez, S., Valleron, A.J., Boëlle, P.Y., Flahault, A. and Ferguson, N.M. 2008. Estimating the impact of school closure on influenza transmission from Sentinel data. *Nature*. **452**(7188), pp.750–754.

Cervantes-Ortiz, S.L., Cuervo, N.Z. and Grandvaux, N. 2016. Respiratory Syncytial Virus and Cellular Stress Responses: Impact on Replication and Physiopathology. *Viruses*. **8**(5), p.124.

Chaipan, C., Kobasa, D., Bertram, S., Glowacka, I., Steffen, I., Solomon Tsegaye, T., Takeda, M., Bugge, T.H., Kim, S., Park, Y., Marzi, A. and Pöhlmann, S. 2009. Proteolytic Activation of the 1918 Influenza Virus Hemagglutinin. *Journal of Virology*. **83**(7), pp.3200–3211.

Chan, K.F., Carolan, L.A., Korenkov, D., Druce, J., Mccaw, J., Reading, P.C., Barr, I.G. and Laurie, K.L. 2018. Investigating viral interference between influenza a virus and human respiratory syncytial virus in a ferret model of infection. *Journal of Infectious Diseases*. **218**(3), pp.406–417.

Chang, T.H., Segovia, J., Sabbah, A., Mgbemena, V. and Bose, S. 2012. Cholesterol-rich lipid rafts are required for release of infectious human respiratory syncytial virus particles. *Virology*. **422**(2), pp.205–213.

Chare, E.R., Gould, E.A. and Holmes, E.C. 2003. Phylogenetic analysis reveals a low rate of homologous recombination in negative-sense RNA viruses. *Journal of General Virology*. **84**(10), pp.2691–2703.

Charman, M., McFarlane, S., Wojtus, J.K., Sloan, E., Dewar, R., Leeming, G., Al-Saadi, M., Hunter, L., Carroll, M.W., Stewart, J.P., Digard, P., Hutchinson, E. and Boutell, C. 2021. Constitutive TRIM22 Expression in the Respiratory Tract Confers a Pre-Existing Defence Against Influenza A Virus Infection. *Frontiers in Cellular and Infection Microbiology*. **11**, p.689707.

Chatterjee, S., Luthra, P., Esaulova, E., Agapov, E., Yen, B.C., Borek, D.M., Edwards, M.R., Mittal, A., Jordan, D.S., Ramanan, P., Moore, M.L., Pappu, R. V., Holtzman, M.J., Artyomov, M.N., Basler, C.F., Amarasinghe, G.K. and Leung, D.W. 2017. Structural basis for human respiratory syncytial virus NS1-mediated modulation of host responses. *Nature Microbiology 2017 2:9*. **2**(9), pp.1–8.

Cheemarla, N.R., Watkins, T.A., Mihaylova, V.T., Wang, B., Zhao, D., Wang, G., Landry, M.L. and Foxman, E.F. 2021. Dynamic innate immune response determines susceptibility to SARS-CoV-2 infection and early replication kinetics. *Journal of Experimental Medicine*. **218**(8).

Chen, B.J., Leser, G.P., Morita, E. and Lamb, R.A. 2007. Influenza Virus Hemagglutinin and Neuraminidase, but Not the Matrix Protein, Are Required for Assembly and Budding of Plasmid-Derived Virus-Like Particles. *Journal of Virology*. **81**(13), pp.7111–7123.

Chen, C. and Zhuang, X. 2008. Epsin 1 is a cargo-specific adaptor for the clathrin-mediated endocytosis of the influenza virus. *Proceedings of the National Academy of Sciences*. **105**(33), pp.11790–11795.

Chen, M., Bell, J.M., Shi, X., Sun, S.Y., Wang, Z. and Ludtke, S.J. 2019. A complete data processing workflow for cryo-ET and subtomogram averaging. *Nature Methods*. **16**(11), pp.1161–1168.

Chen, W., Calvo, P.A., Malide, D., Gibbs, J., Schubert, U., Bacik, I., Basta, S., O'Neill, R., Schickli, J., Palese, P., Henklein, P., Bennink, J.R. and Yewdell, J.W. 2001. A novel influenza A virus mitochondrial protein that induces cell death. *Nature Medicine*. **7**(12), pp.1306–1312.

Chertow, D.S. and Memoli, M.J. 2013. Bacterial Coinfection in Influenza: A Grand Rounds Review. *JAMA*. **309**(3), pp.275–282.

Chlanda, P., Schraidt, O., Kummer, S., Riches, J., Oberwinkler, H., Prinz, S., Kräusslich, H.-G. and Briggs, J.A.G. 2015. Structural Analysis of the Roles of Influenza A Virus Membrane-Associated Proteins in Assembly and Morphology. *Journal of Virology*. **89**(17), pp.8957–8966.

Choi, B., Choudhary, M.C., Regan, J., Sparks, J.A., Padera, R.F., Qiu, X., Solomon, I.H., Kuo, H.-H., Boucau, J., Bowman, K., Adhikari, U. Das, Winkler, M.L., Mueller, A.A., Hsu, T.Y.-T., Desjardins, M., Baden, L.R., Chan, B.T., Walker, B.D., Lichterfeld, M., Brigl, M., Kwon, D.S., Kanjilal, S., Richardson, E.T., Jonsson, A.H., Alter, G., Barczak, A.K., Hanage, W.P., Yu, X.G., Gaiha, G.D., Seaman, M.S., Cernadas, M. and Li, J.Z. 2020. Persistence and Evolution of SARS-CoV-2 in an Immunocompromised Host. *The New England Journal of Medicine*. **383**(23), pp.2291–2293.

Choppin, P.W. and Compans, R.W. 1970. Phenotypic Mixing of Envelope Proteins of the Parainfluenza Virus SV5 and Vesicular Stomatitis Virus. *Journal of virology*. **5**(5), pp.609–616.

Coates, M., Brookes, D., Kim, Y.I., Allen, H., Fordyce, E.A.F., Meals, E.A., Colley, T., Ciana, C.L., Parra, G.F., Sherbukhin, V., Stockwell, J.A., Thomas, J.C., Hunt, S.F., Anderson-Dring, L., Onions, S.T., Cass, L., Murray, P.J., Ito, K., Strong, P., DeVincenzo, J.P. and Rapeport, G. 2017. Preclinical characterization of PC786, an inhaled small-molecule respiratory syncytial virus L protein polymerase inhibitor. *Antimicrobial Agents and Chemotherapy*. **61**(9).

Collins, P.L., Dickens, L.E., Buckler-White, A., Olmsted, R.A., Spriggs, M.K., Camargo, E. and Coelingh, K. V. 1986. Nucleotide sequences for the gene junctions of human respiratory syncytial virus reveal distinctive features of intergenic structure and gene order. *Proceedings of the National Academy of Sciences of the United States of America*. **83**(13), p.4594.

Collins, P.L. and Karron, R.A. 2013. Respiratory Syncytial Virus and Metapneumovirus *In*: *Fields Virology*. Philadelphia: Lippincott Williams & Wilkins, pp.1086–1123.

Collins, P.L. and Mottet, G. 1992. Oligomerization and post-translational processing of glycoprotein G of human respiratory syncytial virus: altered O-glycosylation in the presence of brefeldin A. *The Journal of general virology*. **73 (Pt 4)**(4), pp.849–863.

Conley, M.J., Short, J.M., Hutchings, J., Burns, A.M., Streetley, J., Bakker, S.E., Jaffery, H., Stewart, M., Power, B.J., Zanetti, G., Fearns, R., Vijayakrishnan, S. and Bhella, D. 2021. Helical Ordering of Envelope Associated Proteins and Glycoproteins in Respiratory Syncytial Virus Filamentous Virions. *bioRxiv*., 2021.08.04.455049.

Cros, J.F., García-Sastre, A. and Palese, P. 2005. An unconventional NLS is critical for the nuclear import of the influenza A virus nucleoprotein and ribonucleoprotein. *Traffic*. **6**(3), pp.205–213.

Cuesta, I., Geng, X., Asenjo, A. and Villanueva, N. 2000. Structural Phosphoprotein M2-1 of the Human Respiratory Syncytial Virus Is an RNA Binding Protein. *Journal of Virology*. **74**(21), pp.9858–9867.

Cuevas, J.M., Durán-Moreno, M. and Sanjuán, R. 2017. Multi-virion infectious units arise from free viral particles in an enveloped virus. *Nature Microbiology*. **2**.

Currier, M.G., Lee, S., Stobart, C.C., Hotard, A.L., Villenave, R., Meng, J., Pretto, C.D., Shields, M.D., Nguyen, M.T., Todd, S.O., Chi, M.H., Hammonds, J., Krumm, S.A., Spearman, P., Plemper, R.K., Sakamoto, K., Peebles, R.S., Jr., Power, U.F. and Moore, M.L. 2016. EGFR Interacts with the Fusion Protein of Respiratory Syncytial Virus Strain 2-20 and Mediates Infection and Mucin Expression. *PLoS Pathogens*. **12**(5).

Czerkies, M., Kochańczyk, M., Korwek, Z., Prus, W. and Lipniacki, T. 2021. RSV immunizes bystander cells to IAV infection using interferons β and λ. *bioRxiv*., 2021.10.11.463877.

Dadonaite, B., Gilbertson, B., Knight, M.L., Trifkovic, S., Rockman, S., Laederach, A., Brown, L.E., Fodor, E. and Bauer, D.L.V. 2019. The Structure of the Influenza A Virus Genome. *Nature Microbiology*. **4**(11), p.1781.

Dadonaite, B., Vijayakrishnan, S., Fodor, E., Bhella, D. and Hutchinson, E.C. 2016. Filamentous influenza viruses. *Journal of General Virology*. **97**(8), pp.1755–1764.

Daniel Harari, Matthew Keep and Philip Brien 2020. Coronavirus: Economic impact - House of Commons Library. *House of commons library*. [Online]. [Accessed 8 November 2021]. Available from: https://commonslibrary.parliament.uk/research-briefings/cbp-8866/.

Daniels, R., Svedine, S. and Hebert, D.N. 2004. N-linked carbohydrates act as lumenal maturation and quality control protein tags. *Cell Biochemistry and Biophysics*. **41**(1), pp.113–137.

Danis, K., Epaulard, O., Bénet, T., Gaymard, A., Campoy, S., Botelho-Nevers, E., Bouscambert-Duchamp, M., Spaccaferri, G., Ader, F., Mailles, A., Boudalaa, Z., Tolsma, V., Berra, J., Vaux, S., Forestier, E., Landelle, C., Fougere, E., Thabuis, A., Berthelot, P., Veil, R., Levy-Bruhl, D., Chidiac, C., Lina, B., Coignard, B. and Saura, C. 2020. Cluster of Coronavirus Disease 2019 (COVID-19) in the French Alps, February 2020. *Journal of Clinical infectious diseases*. **71**(15), pp.825–832.

DaPalma, T., Doonan, B.P., Trager, N.M. and Kasman, L.M. 2010. A systematic approach to virus-virus interactions. *Virus Research*. **149**(1), pp.1–9.

Das, D.K., Govindan, R., Nikić-Spiegel, I., Krammer, F., Lemke, E.A. and Munro, J.B. 2018. Direct Visualization of the Conformational Dynamics of Single Influenza Hemagglutinin Trimers. *Cell*. **174**(4), pp.926-937.e12.

Datta, S., Walsh, E.E., Peterson, D.R. and Falsey, A.R. 2017. Can Analysis of Routine Viral Testing Provide Accurate Estimates of Respiratory Syncytial Virus Disease Burden in Adults? *The Journal of Infectious Diseases*. **215**(11), pp.1706–1710.

Dee, K., Goldfarb, D.M., Haney, J., Amat, J.A.R., Herder, V., Stewart, M., Szemiel, A.M., Baguelin, M. and Murcia, P.R. 2021. Human Rhinovirus Infection Blocks Severe Acute Respiratory Syndrome Coronavirus 2 Replication Within the Respiratory Epithelium: Implications for COVID-19 Epidemiology. *The Journal of Infectious Diseases*. **224**(1), pp.31–38.

Deng, T., Engelhardt, O.G., Thomas, B., Akoulitchev, A. V., Brownlee, G.G. and Fodor, E. 2006. Role of ran binding protein 5 in nuclear import and assembly of the influenza virus RNA polymerase complex. *Journal of virology*. **80**(24), pp.11911–11919.

Deshpande, S.A. and Northern, V. 2003. The clinical and health economic burden of respiratory syncytial virus disease among children under 2 years of age in a defined geographical area. *Archives of disease in childhood*. **88**(12), pp.1065–1069.

Dias, A., Bouvier, D., Crépin, T., McCarthy, A.A., Hart, D.J., Baudin, F., Cusack, S. and Ruigrok, R.W.H. 2009. The cap-snatching endonuclease of influenza virus polymerase resides in the PA subunit. *Nature*. **458**(7240), pp.914–918.

Díaz-Muñoz, S.L., Sanjuán, R. and West, S. 2017. Sociovirology: Conflict, Cooperation, and Communication among Viruses. *Cell Host and Microbe*. **22**(4), pp.437–441.

Docherty, A.B., Harrison, E.M., Green, C.A., Hardwick, H.E., Pius, R., Norman, L., Holden, K.A., Read, J.M., Dondelinger, F., Carson, G., Merson, L., Lee, J., Plotkin, D., Sigfrid, L., Halpin, S., Jackson, C., Gamble, C., Horby, P.W., Nguyen-Van-Tam, J.S., Ho, A., Russell, C.D., Dunning, J., Openshaw, P.J.M., Baillie, J.K. and Semple, M.G. 2020. Features of 20 133 UK patients in hospital with covid-19 using the ISARIC WHO Clinical Characterisation Protocol: prospective observational cohort study. *BMJ (Clinical research ed.)*. **369**.

Domingo-Calap, P., Segredo-Otero, E., Durán-Moreno, M. and Sanjuán, R. 2019. Social evolution of innate immunity evasion in a virus. *Nature Microbiology*. **4**(6), pp.1006–1013.

Donald, H. and Isaacs, A. 1954. Counts of Influenza Virus Particles. *Journal of General Microbiology*. **10**, pp.457–464.

Dou, D., Hernández-Neuta, I., Wang, H., Östbye, H., Qian, X., Thiele, S., Resa-Infante, P., Kouassi, N.M., Sender, V., Hentrich, K., Mellroth, P., Henriques-Normark, B., Gabriel, G., Nilsson, M. and Daniels, R. 2017. Analysis of IAV Replication and Co-infection Dynamics by a Versatile RNA Viral Genome Labeling Method. *Cell Reports*. **20**(1), pp.251–263.

Dou, D., Da Silva, D. V., Nordholm, J., Wang, H. and Daniels, R. 2014. Type II transmembrane domain hydrophobicity dictates the cotranslational dependence for inversion. *Molecular Biology of the Cell*. **25**(21), pp.3363–3374.

Drori, Y., Jacob-Hirsch, J., Pando, R., Glatman-Freedman, A., Friedman, N., Mendelson, E. and Mandelboim, M. 2020. Influenza A Virus Inhibits RSV Infection via a Two-Wave Expression of IFIT Proteins. *Viruses*. **12**(10).

Dubois, J., Terrier, O. and Rosa-Calatrava, M. 2014. Influenza viruses and mRNA splicing: Doing more with less. *mBio*. **5**(3).

Ducatez, M.F., Pelletier, C. and Meyer, G. 2015. Influenza D virus in cattle, France, 2011-2014. *Emerging Infectious Diseases*. **21**(2), pp.368–371.

Echenique, I.A., Chan, P.A., Chapin, K.C., Andrea, S.B., Fava, J.L. and Mermel, L.A. 2013. Clinical Characteristics and Outcomes in Hospitalized Patients with Respiratory Viral Co-Infection during the 2009 H1N1 Influenza Pandemic. *PLoS ONE*. **8**(4).

Eckard, L.E. 2016. Assessment of the Zoonotic Potential of a Novel Bovine Influenza Virus.

Ehrhardt, C., Wolff, T., Pleschka, S., Planz, O., Beermann, W., Bode, J.G., Schmolke, M. and Ludwig, S. 2007. Influenza A Virus NS1 Protein Activates the PI3K/Akt Pathway To Mediate Antiapoptotic Signaling Responses. *Journal of Virology*. **81**(7), p.3058.

Eisfeld, A.J., Kawakami, E., Watanabe, T., Neumann, G. and Kawaoka, Y. 2011. RAB11A is essential for transport of the influenza virus genome to the plasma membrane. *Journal of Virology*. **85**(13), pp.6117–6126.

Elleman, C.J. and Barclay, W.S. 2004. The M1 matrix protein controls the filamentous phenotype of influenza A virus. *Virology*. **321**(1), pp.144–153.

Elliott, J., Lynch, O.T., Suessmuth, Y., Qian, P., Boyd, C.R., Burrows, J.F., Buick, R., Stevenson, N.J., Touzelet, O., Gadina, M., Power, U.F. and Johnston, J.A. 2007. Respiratory syncytial virus NS1 protein degrades STAT2 by using the Elongin-Cullin E3 ligase. *Journal of virology*. **81**(7), pp.3428–3436.

Elton, D., Medcalf, L., Bishop, K., Harrison, D. and Digard, P. 1999. Identification of Amino Acid Residues of Influenza Virus Nucleoprotein Essential for RNA Binding. *Journal of Virology*. **73**(9), pp.7357–7367.

Enami, K., Sato, T.A., Nakada, S. and Enami1, M. 1994. Influenza virus NS1 protein stimulates translation of the M1 protein. *Journal of Virology*. **68**(3), pp.1432–1437.

Enami, M., Sharma, G., Benham, C. and Palese, P. 1991. An influenza virus containing nine different RNA segments. *Virology*. **185**(1), pp.291–298.

Esper, F.P., Spahlinger, T. and Zhou, L. 2011. Rate and influence of respiratory virus co-infection on pandemic (H1N1) influenza disease. *Journal of Infection*. **63**(4), pp.260–266.

Essaidi-Laziosi, M., Geiser, J., Huang, S., Constant, S., Kaiser, L. and Tapparel, C. 2020. Interferon-Dependent and Respiratory Virus-Specific Interference in Dual Infections of Airway Epithelia. *Scientific Reports*. **10**(1), pp.1–9.

Fan, H., Walker, A.P., Carrique, L., Keown, J.R., Serna Martin, I., Karia, D., Sharps, J., Hengrung, N., Pardon, E., Steyaert, J., Grimes, J.M. and Fodor, E. 2019. Structures of influenza A virus RNA polymerase offer insight into viral genome replication. *Nature*. **573**(7773), pp.287–290.

Faria, P.A., Chakraborty, P., Levay, A., Barber, G.N., Ezelle, H.J., Enninga, J., Arana, C., Van Deursen, J. and Fontoura, B.M.A. 2005. VSV disrupts the Rae1/mrnp41 mRNA nuclear export pathway. *Molecular Cell*. **17**(1), pp.93–102.

Fearns, R. and Collins, P.L. 1999. Role of the M2-1 transcription antitermination protein of respiratory syncytial virus in sequential transcription. *Journal of virology*. **73**(7), pp.5852–5864.

Feldman, S.A., Hendry, R.M. and Beeler, J.A. 1999. Identification of a linear heparin binding domain for human respiratory syncytial virus attachment glycoprotein G. *Journal of virology*. **73**(8), pp.6610–6617.

Flamaing, J., Engelmann, I., Joosten, E., Van Ranst, M., Verhaegen, J. and Peetermans, W.E. 2003. Viral Lower Respiratory Tract Infection in the Elderly: A Prospective In-Hospital Study. *European Journal of Clinical Microbiology & Infectious Diseases*. **22**(12), p.720.

Flannery, B., Kondor, R.J.G., Chung, J.R., Gaglani, M., Reis, M., Zimmerman, R.K., Nowalk, M.P., Jackson, M.L., Jackson, L.A., Monto, A.S., Martin, E.T., Belongia, E.A., McLean, H.Q., Kim, S.S., Blanton, L., Kniss, K., Budd, A.P., Brammer, L., Stark, T.J., Barnes, J.R., Wentworth, D.E., Fry, A.M. and Patel, M. 2020. Spread of Antigenically Drifted Influenza A(H3N2) Viruses and Vaccine Effectiveness in the United States During the 2018–2019 Season. *The Journal of Infectious Diseases*. **221**(1), pp.8–15.

Fleming, D.M., Taylor, R.J., Lustig, R.L., Schuck-Paim, C., Haguinet, F., Webb, D.J., Logie, J., Matias, G. and Taylor, S. 2015. Modelling estimates of the burden of Respiratory Syncytial virus infection in adults and the elderly in the United Kingdom. *BMC Infectious Diseases*. **15**(1), p.443.

Fleming, E.H., Kolokoltsov, A.A., Davey, R.A., Nichols, J.E., Roberts, N.J. and Jr. 2006. Respiratory Syncytial Virus F Envelope Protein Associates with Lipid Rafts without a Requirement for Other Virus Proteins. *Journal of Virology*. **80**(24), p.12160.

Fodha, I., Vabret, A., Ghedira, L., Seboui, H., Chouchane, S., Dewar, J., Gueddiche, N., Trabelsi, A., Boujaafar, N. and Freymuth, F. 2007. Respiratory syncytial virus infections in hospitalized infants: association between viral load, virus subgroup, and disease severity. *Journal of medical virology*. **79**(12), pp.1951–1958.

Fodor, E. and Velthuis, A.J.W.T. 2020. Structure and Function of the Influenza Virus Transcription and Replication Machinery. *Cold Spring Harbor Perspectives in Medicine*. **10**(9), p.a038398.

Folimonova, S.Y. 2012. Superinfection Exclusion Is an Active Virus-Controlled Function That Requires a Specific Viral Protein. *Journal of Virology*. **86**(10), pp.5554–5561.

Förster, A., Maertens, G.N., Farrell, P.J. and Bajorek, M. 2015. Dimerization of Matrix Protein Is Required for Budding of Respiratory Syncytial Virus. *Journal of Virology*. **89**(8), p.4624.

Fortin, J.F., Cantin, R., Lamontagne, G. and Tremblay, M. 1997. Host-derived ICAM-1

glycoproteins incorporated on human immunodeficiency virus type 1 are biologically active and enhance viral infectivity. *Journal of Virology*. **71**(5), p.3588.

Fukuyama, S., Katsura, H., Zhao, D., Ozawa, M., Ando, T., Shoemaker, J.E., Ishikawa, I., Yamada, S., Neumann, G., Watanabe, S., Kitano, H. and Kawaoka, Y. 2015. Multi-spectral fluorescent reporter influenza viruses (Color-flu) as powerful tools for in vivo studies. *Nature Communications*. **6**(1), pp.1–8.

Galanti, M., Birger, R., Ud-Dean, M., Filip, I., Morita, H., Comito, D., Anthony, S., Freyer, G.A., Ibrahim, S., Lane, B., Matienzo, N., Ligon, C., Rabadan, R., Shittu, A., Tagne, E. and Shaman, J. 2019. Rates of asymptomatic respiratory virus infection across age groups. *Epidemiology & Infection*. **147**.

Galloux, M., Risso-Ballester, J., Richard, C.A., Fix, J., Rameix-Welti, M.A. and Eléouët, J.F. 2020. Minimal Elements Required for the Formation of Respiratory Syncytial Virus Cytoplasmic Inclusion Bodies In Vivo and In Vitro. *mBio*. **11**(5), pp.1–16.

Gambaryan, A.S., Tuzikov, A.B., Piskarev, V.E., Yamnikova, S.S., Lvov, D.K., Robertson, J.S., Bovin, N. V. and Matrosovich, M.N. 1997. Specification of Receptor-Binding Phenotypes of Influenza Virus Isolates from Different Hosts Using Synthetic Sialylgly copolymers: Non-Egg-Adapted Human H1 and H3 Influenza A and Influenza B Viruses Share a Common High Binding Affinity for 6′-Sialyl(N-acetyllactosamine). *Virology*. **232**(2), pp.345–350.

Gan, S.W., Tan, E., Lin, X., Yu, D., Wang, J., Tan, G.M.Y., Vararattanavech, A., Yeo, C.Y., Soon, C.H., Soong, T.W., Pervushin, K. and Torres, J. 2012. The small hydrophobic protein of the human respiratory syncytial virus forms pentameric ion channels. *The Journal of biological chemistry*. **287**(29), pp.24671–24689.

García-Sastre, A., Egorov, A., Matassov, D., Brandt, S., Levy, D.E., Durbin, J.E., Palese, P. and Muster, T. 1998. Influenza A Virus Lacking the NS1 Gene Replicates in Interferon-Deficient Systems. *Virology*. **252**(2), pp.324–330.

Garcia, N.K., Guttman, M., Ebner, J.L. and Lee, K.K. 2015. Dynamic changes during acid-induced activation of influenza hemagglutinin. *Structure*. **23**(4), pp.665–676.

Gaush, C.R. and Smith, T.F. 1968. Replication and Plaque Assay of Influenza Virus in an Established Line of Canine Kidney Cells. *Applied Microbiology*. **16**(4), p.588.

GBD 2016 Causes of Death Collaborators. 2017. Global, regional, and national age-sex specific mortality for 264 causes of death, 1980-2016: a systematic analysis for the Global Burden of Disease Study 2016. *Lancet (London, England)*. **390**(10100), pp.1151–1210.

Geiser, J., Boivin, G., Huang, S., Constant, S., Kaiser, L., Tapparel, C. and Essaidi-Laziosi, M. 2021. RSV and HMPV Infections in 3D Tissue Cultures: Mechanisms Involved in Virus-Host and Virus-Virus Interactions. *Viruses*. **13**(1), p.139.

Geleziunas, R., Bour, S. and Wainberg, M.A. 1994. Cell surface down-modulation of CD4 after infection by HIV-1. *FASEB journal*. **8**(9), pp.593–600.

Geoghegan, S., Erviti, A., Caballero, M.T., Vallone, F., Zanone, S.M., Losada, J.V., Bianchi, A., Acosta, P.L., Talarico, L.B., Ferretti, A., Grimaldi, L.A., Sancilio, A., Dueñas, K., Sastre, G., Rodriguez, A., Ferrero, F., Barboza, E., Gago, G.F., Nocito, C., Flamenco, E., RodriguezPerez, A., Rebec, B., Martin Ferolla, F., Libster, R., Karron, R.A., Bergel, E. and Polack, F.P. 2017. Mortality due to respiratory syncytial virus burden and risk factors. *American Journal of Respiratory and Critical Care Medicine*. **195**(1), pp.96–103.

George, J.A., Alshamsi, S.H., Alhammadi, M.H. and Alsuwaidi, A.R. 2021. Exacerbation of Influenza A Virus Disease Severity by Respiratory Syncytial Virus Co-Infection in a Mouse Model. *Viruses*. **13**(8), p.1630.

Gerl, M.J., Sampaio, J.L., Urban, S., Kalvodova, L., Verbavatz, J.M., Binnington, B., Lindemann, D., Lingwood, C.A., Shevchenko, A., Schroeder, C. and Simons, K. 2012. Quantitative analysis of the lipidomes of the influenza virus envelope and MDCK cell apical membrane. *Journal of Cell Biology*. **196**(2), pp.213–221.

Ghedin, E., Sengamalay, N.A., Shumway, M., Zaborsky, J., Feldblyum, T., Subbu, V., Spiro, D.J., Sitz, J., Koo, H., Bolotov, P., Dernovoy, D., Tatusova, T., Bao, Y., St George, K., Taylor, J.,

Lipman, D.J., Fraser, C.M., Taubenberger, J.K. and Salzberg, S.L. 2005. Large-scale sequencing of human influenza reveals the dynamic nature of viral genome evolution. *Nature 2005 437:7062*. **437**(7062), pp.1162–1166.

Ghildyal, R., Baulch-Brown, C., Mills, J. and Meanger, J. 2003. The matrix protein of Human respiratory syncytial virus localises to the nucleus of infected cells and inhibits transcription. *Archives of virology*. **148**(7), pp.1419–1429.

Ghildyal, R., Mills, J., Murray, M., Vardaxis, N. and Meanger, J. 2002. Respiratory syncytial virus matrix protein associates with nucleocapsids in infected cells. *Journal of General Virology*. **83**(4), pp.753–757.

Giard, D., Aaronson, S., Todaro, G., Arnstein, P., Kersey, J., Dosik, H. and Parks, W. 1973. In vitro cultivation of human tumors: establishment of cell lines derived from a series of solid tumors. *Journal of the National Cancer Institute*. **51**(5), pp.1417–1423.

Glezen, W.P., Taber, L.H., Frank, A.L. and Kasel, J.A. 1986. Risk of primary infection and reinfection with respiratory syncytial virus. *American Journal of Diseases of Children*. **140**(6), pp.543–546.

Góes, L.G.B., Zerbinati, R.M., Tateno, A.F., de Souza, A.V., Ebach, F., Corman, V.M., Moreira-Filho, C.A., Durigon, E.L., da Silva Filho, L.V.R.F. and Drexler, J.F. 2020. Typical epidemiology of respiratory virus infections in a Brazilian slum. *Journal of Medical Virology*. **92**(8), pp.1316–1321.

Goka, E.A., Vallely, P.J., Mutton, K.J. and Klapper, P.E. 2015. Single, dual and multiple respiratory virus infections and risk of hospitalization and mortality. *Epidemiology & Infection*. **143**(1), pp.37–47.

Gonzalez, A.J., Ijezie, E.C., Balemba, O.B. and Miura, T.A. 2018. Attenuation of Influenza A Virus Disease Severity by Viral Coinfection in a Mouse Model. *Journal of Virology*. **92**(23).

Görlich, D., Prehn, S., Hartmann, E., Kalies, K.U. and Rapoport, T.A. 1992. A mammalian homolog of SEC61p and SECYp is associated with ribosomes and nascent polypeptides during translocation. *Cell*. **71**(3), pp.489–503.

Goto, H., Ihira, H., Morishita, K., Tsuchiya, M., Ohta, K., Yumine, N., Tsurudome, M. and Nishio, M. 2016. Enhanced growth of influenza A virus by coinfection with human parainfluenza virus type 2. *Medical Microbiology and Immunology*. **205**(3), pp.209–218.

Gould, P.S. and Easton, A.J. 2007. Coupled Translation of the Second Open Reading Frame of M2 mRNA Is Sequence Dependent and Differs Significantly within the Subfamily Pneumovirinae. *Journal of Virology*. **81**(16), p.8488.

Granoff, A. and Hirst, G.K. 1954. Experimental Production of Combination Forms of Virus." IV. Mixed Influenza A-Newcastle Disease Virus Infections. *Proceedings of the Society for Experimental Biology and Medicine*. **86**(1), pp.84–88.

Griffin, M.P., Yuan, Y., Takas, T., Domachowske, J.B., Madhi, S.A., Manzoni, P., Simões, E.A.F., Esser, M.T., Khan, A.A., Dubovsky, F., Villafana, T. and DeVincenzo, J.P. 2020. Single-Dose Nirsevimab for Prevention of RSV in Preterm Infants. *New England Journal of Medicine*. **383**(5), pp.415–425.

Griffiths, C.D., Bilawchuk, L.M., McDonough, J.E., Jamieson, K.C., Elawar, F., Cen, Y., Duan, W., Lin, C., Song, H., Casanova, J.-L., Ogg, S., Jensen, L.D., Thienpont, B., Kumar, A., Hobman, T.C., Proud, D., Moraes, T.J. and Marchant, D.J. 2020. IGF1R is an entry receptor for respiratory syncytial virus. *Nature*. **583**(7817), pp.615–619.

Grimm, D., Staeheli, P., Hufbauer, M., Koerner, I., Martínez-Sobrido, L., Solórzano, A., García-Sastre, S., Haller, O. and Kochs, G. 2007. Replication fitness determines high virulence of influenza A virus in mice carrying functional Mx1 resistance gene. *Proceedings of the National Academy of Sciences of the United States of America*. **104**(16), pp.6806–6811.

Groskreutz, D.J., Monick, M.M., Yarovinsky, T.O., Powers, L.S., Quelle, D.E., Varga, S.M., Look, D.C. and Hunninghake, G.W. 2007. Respiratory syncytial virus decreases p53 protein to prolong survival of airway epithelial cells. *Journal of immunology (Baltimore, Md. : 1950)*. **179**(5), pp.2741–7.

Guilligay, D., Tarendeau, F., Resa-Infante, P., Coloma, R., Crepin, T., Sehr, P., Lewis, J., Ruigrok, R.W.H., Ortin, J., Hart, D.J. and Cusack, S. 2008. The structural basis for cap binding by influenza virus polymerase subunit PB2. *Nature Structural & Molecular Biology*. **15**(5), pp.500–506.

Hagen, W.J.H., Wan, W. and Briggs, J.A.G. 2017. Implementation of a cryo-electron tomography tilt-scheme optimized for high resolution subtomogram averaging. *Journal of Structural Biology*. **197**(2), pp.191–198.

Hall, C.B., Walsh, E.E., Long, C.E. and Schnabel, K.C. 1991. Immunity to and frequency of reinfection with respiratory syncytial virus. *The Journal of Infectious Diseases*. **163**(4), pp.693–698.

Hall, C.B., Weinberg, G.A., Iwane, M.K., Blumkin, A.K., Edwards, K.M., Staat, M.A., Auinger, P., Griffin, M.R., Poehling, K.A., Erdman, D., Grijalva, C.G., Zhu, Y. and Szilagyi, P. 2009. The Burden of Respiratory Syncytial Virus Infection in Young Children. *New England Journal of Medicine*. **360**(6), pp.588–598.

Halldorsson, S., Sader, K., Turner, J., Calder, L.J. and Rosenthal, P.B. 2021. In situ structure and organization of the influenza C virus surface glycoprotein. *Nature Communications 2021 12:1*. **12**(1), pp.1–9.

Hampton, C.M., Strauss, J.D., Ke, Z., Dillard, R.S., Hammonds, J.E., Alonas, E., Desai, T.M., Marin, M., Storms, R.E., Leon, F., Melikyan, G.B., Santangelo, P.J., Spearman, P.W. and Wright, E.R. 2016. Correlated fluorescence microscopy and cryo-electron tomography of virus-infected or transfected mammalian cells. *Nature Protocols*. **12**(1), pp.150–167.

Hao, W., Wang, L. and Li, S. 2020. Roles of the Non-Structural Proteins of Influenza A Virus. *Pathogens*. **9**(10), pp.1–19.

Harcourt, J., Alvarez, R., Jones, L.P., Henderson, C., Anderson, L.J. and Tripp, R.A. 2006. Respiratory syncytial virus G protein and G protein CX3C motif adversely affect CX3CR1+ T cell responses. *Journal of immunology (Baltimore, Md. : 1950)*. **176**(3), pp.1600–1608.

Harris, A., Cardone, G., Winkler, D.C., Heymann, J.B., Brecher, M., White, J.M. and Steven, A.C. 2006. Influenza virus pleiomorphy characterized by cryoelectron tomography. *Proceedings of the National Academy of Sciences of the United States of America*. **103**(50), pp.19123–19127.

Hashimoto, K. and Hosoya, M. 2017. Neutralizing epitopes of RSV and palivizumab resistance in Japan. *Fukushima journal of medical science*. **63**(3), pp.127–134.

Hatada, E. and Fukuda, R. 1992. Binding of influenza a virus NS1 protein to dsRNA in vitro. *Journal of General Virology*. **73**(12), pp.3325–3329.

Hause, B.M., Collin, E.A., Liu, R., Huang, B., Sheng, Z., Lu, W., Wang, D., Nelson, E.A. and Li, F. 2014. Characterization of a novel influenza virus in cattle and swine: Proposal for a new genus in the Orthomyxoviridae family. *mBio*. **5**(2).

Hause, B.M., Ducatez, M., Collin, E.A., Ran, Z., Liu, R., Sheng, Z., Armien, A., Kaplan, B., Chakravarty, S., Hoppe, A.D., Webby, R.J., Simonson, R.R. and Li, F. 2013. Isolation of a novel swine influenza virus from Oklahoma in 2011 which is distantly related to human influenza C viruses. *PLoS Pathogens*. **9**(2).

Haynes, A.K., Manangan, A.P., Iwane, M.K., Sturm-Ramirez, K., Homaira, N., Brooks, W.A., Luby, S., Rahman, M., Klena, J.D., Zhang, Y., Yu, H., Zhan, F., Dueger, E., Mansour, A.M., Azazzy, N., McCracken, J.P., Bryan, J.P., Lopez, M.R., Burton, D.C., Bigogo, G., Breiman, R.F., Feikin, D.R., Njenga, K., Montgomery, J., Cohen, A.L., Moyes, J., Pretorius, M., Cohen, C., Venter, M., Chittaganpitch, M., Thamthitiwat, S., Sawatwong, P., Baggett, H.C., Luber, G. and Gerber, S.I. 2013. Respiratory Syncytial Virus Circulation in Seven Countries With Global Disease Detection Regional Centers. *The Journal of Infectious Diseases*. **208**(suppl_3), pp.S246–S254.

Hebert, D.N., Zhang, J.X., Chen, W., Foellmer, B. and Helenius, A. 1997. The Number and Location of Glycans on Influenza Hemagglutinin Determine Folding and Association with Calnexin and Calreticulin. *Journal of Cell Biology*. **139**(3), pp.613–623.

Hemmings, B.A. and Restuccia, D.F. 2012. PI3K-PKB/Akt Pathway. *Cold Spring Harbor Perspectives in Biology*. **4**(9).

Henderson, G., Murray, J. and Yeo, R.P. 2002. Sorting of the respiratory syncytial virus matrix protein into detergent-resistant structures is dependent on cell-surface expression of the glycoproteins. *Virology*. **300**(2), pp.244–254.

Heng, M.C.Y., Heng, S.Y. and Allen, S.G. 1994. Co-infection and synergy of human immunodeficiency virus-1 and herpes simplex virus-1. *The Lancet*. **343**(8892), pp.255–258.

Hens, N., Ayele, G.M., Goeyvaerts, N., Aerts, M., Mossong, J., Edmunds, J.W. and Beutels, P. 2009. Estimating the impact of school closure on social mixing behaviour and the transmission of close contact infections in eight European countries. *BMC infectious diseases*. **9**.

Herrler, G., Rott, R., Klenk, Hans-Dieter, Mullerl, H.-P., Shukla2, A.K., Schauer2, R. and Klenk, H.-D 1985. The receptor-destroying enzyme of influenza C virus is neuraminate-O-acetylesterase. *The EMBO Journal*. **4**(6), pp.1503–1506.

Hessa, T., Meindl-Beinker, N.M., Bernsel, A., Kim, H., Sato, Y., Lerch-Bader, M., Nilsson, I., White, S.H. and Von Heijne, G. 2007. Molecular code for transmembrane-helix recognition by the Sec61 translocon. *Nature*. **450**(7172), pp.1026–1030.

Hillyer, P., Shepard, R.E., Uehling, M., Sheik, F., Luongo, C., Buchholz, U.J., Collins, P.L., Donnelly, R.P. and Rabin, R.L. 2015. Respiratory Syncytial Virus-Induced Host IFN Signaling Differs Between A549 and BEAS-2B Epithelial Cell Lines. *Journal of Allergy and Clinical Immunology*. **135**(2), p.AB9.

Hirst, G.K. and Pons, M.W. 1973. Mechanism of influenza recombination. II. Virus aggregation and its effect on plaque formation by so-called noninfective virus. *Virology*. **56**(2), pp.620–631.

Homma, M., Ohyama, S. and Katagiri, S. 1982. Age Distribution of the Antibody to Type C Influenza Virus. *Microbiology and Immunology*. **26**(7), pp.639–642.

Horga, M.-A., Gusella, G.L., Greengard, O., Poltoratskaia, N., Porotto, M. and Moscona, A. 2000. Mechanism of Interference Mediated by Human Parainfluenza Virus Type 3 Infection. *Journal of Virology*. **74**(24), p.11792.

Huang, A.S., Palma, E.L., Hewlett, N. and Roizman, B. 1974. Pseudotype formation between enveloped RNA and DNA viruses. *Nature*. **252**(5485), pp.743–745.

Huang, I.-C., Li, W., Sui, J., Marasco, W., Choe, H. and Farzan, M. 2008. Influenza A Virus Neuraminidase Limits Viral Superinfection. *Journal of Virology*. **82**(10), pp.4834–4843.

Huang, Y.T., Collins, P.L. and Wertz, G.W. 1985. Characterization of the 10 proteins of human respiratory syncytial virus: Identification of a fourth envelope-associated protein. *Virus Research*. **2**(2), pp.157–173.

Hui, K.P.Y., Ching, R.H.H., Chan, S.K.H., Nicholls, J.M., Sachs, N., Clevers, H., Peiris, J.S.M. and Chan, M.C.W. 2018. Tropism, replication competence, and innate immune responses of influenza virus: an analysis of human airway organoids and ex-vivo bronchus cultures. *The Lancet Respiratory Medicine*. **6**(11), pp.846–854.

Hutchinson, E.C., Charles, P.D., Hester, S.S., Thomas, B., Trudgian, D., Martínez-Alonso, M. and Fodor, E. 2014. Conserved and host-specific features of influenza virion architecture. *Nature Communications 2014 5:1*. **5**(1), pp.1–11.

Inglis, S.C. and Brown, C.M. 1981. Spliced and unspliced RNAs encoded by virion RNA segment 7 of influenza virus. *Nucleic Acids Research*. **9**(12), pp.2727–2740.

Ito, T., Couceiro, J.N.S.S., Kelm, S., Baum, L.G., Krauss, S., Castrucci, M.R., Donatelli, I., Kida, H., Paulson, J.C., Webster, R.G. and Kawaoka, Y. 1998. Molecular Basis for the Generation in Pigs of Influenza A Viruses with Pandemic Potential. *Journal of Virology*. **72**(9), pp.7367–7373.

Ivanova, P.T., Myers, D.S., Milne, S.B., McClaren, J.L., Thomas, P.G. and Brown, H.A. 2015. Lipid composition of viral envelope of three strains of influenza virus – not all viruses are created equal. *ACS infectious diseases*. **1**(9), p.399.

Jané, M., Vidal, M.J., Soldevila, N., Romero, A., Martínez, A., Torner, N., Godoy, P., Launes, C., Rius, C., Marcos, M.A. and Dominguez, A. 2019. Epidemiological and clinical characteristics of children hospitalized due to influenza A and B in the south of Europe, 2010–2016. *Scientific Reports*. **9**(1), pp.1–7.

Jarsch, I.K., Daste, F. and Gallop, J.L. 2016. Membrane curvature in cell biology: An integration of molecular mechanisms. *Journal of Cell Biology*. **214**(4), pp.375–387.

Jeffree, C.E., Brown, G., Aitken, J., Su-Yin, D.Y., Tan, B.H. and Sugrue, R.J. 2007. Ultrastructural analysis of the interaction between F-actin and respiratory syncytial virus during virus assembly. *Virology*. **369**(2), pp.309–323.

Jeong, K. Il, Piepenhagen, P.A., Kishko, M., DiNapoli, J.M., Groppo, R.P., Zhang, L., Almond, J., Kleanthous, H., Delagrave, S. and Parrington, M. 2015. CX3CR1 Is Expressed in Differentiated Human Ciliated Airway Cells and Co-Localizes with Respiratory Syncytial Virus on Cilia in a G Protein-Dependent Manner. *PLoS ONE*. **10**(6).

Johnson, J., Gonzales, R., Olson, S., Wright, P. and Graham, B. 2007. The histopathology of fatal untreated human respiratory syncytial virus infection. *Modern Pathology*. **20**(1), pp.108–119.

Johnson, S.M., McNally, B.A., Ioannidis, I., Flano, E., Teng, M.N., Oomens, A.G., Walsh, E.E. and Peeples, M.E. 2015. Respiratory Syncytial Virus Uses CX3CR1 as a Receptor on Primary Human Airway Epithelial Cultures. *PLOS Pathogens*. **11**(12), p.e1005318.

Jureka, A.S., Kleinpeter, A.B., Cornilescu, G., Cornilescu, C.C. and Petit, C.M. 2015. Structural Basis for a Novel Interaction between the NS1 Protein Derived from the 1918 Influenza Virus and RIG-I. *Structure*. **23**(11), pp.2001–2010.

Jureka, A.S., Kleinpeter, A.B., Tipper, J.L., Harrod, K.S. and Petit, C.M. 2020. The influenza NS1 protein modulates RIG-I activation via a strain-specific direct interaction with the second CARD of RIG-I. *Journal of Biological Chemistry*. **295**(4), pp.1153–1164.

Kalil, A.C. and Thomas, P.G. 2019. Influenza virus-related critical illness: Pathophysiology and epidemiology. *Critical Care*. **23**(1), pp.1–7.

Karpf, A.R., Lenches, E., Strauss, E.G., Strauss, J.H. and Brown, D.T. 1997. Superinfection exclusion of alphaviruses in three mosquito cell lines persistently infected with Sindbis virus. *Journal of virology*.

Karron, R.A., Atwell, J.E., McFarland, E.J., Cunningham, C.K., Muresan, P., Perlowski, C., Libous, J., Spector, S.A., Yogev, R., Aziz, M., Woods, S., Wanionek, K., Collins, P.L. and Buchholz, U.J. 2021. Live-attenuated Vaccines Prevent Respiratory Syncytial Virus-associated Illness in Young Children. *American journal of respiratory and critical care medicine*. **203**(5), pp.594–603.

Ke, Z., Dillard, R.S., Chirkova, T., Leon, F., Stobart, C.C., Hampton, C.M., Strauss, J.D., Rajan, D., Rostad, C.A., Taylor, J. V., Yi, H., Shah, R., Jin, M., Hartert, T. V., Peebles, R.S., Graham, B.S., Moore, M.L., Anderson, L.J. and Wright, E.R. 2018. The morphology and assembly of respiratory syncytial virus revealed by cryo-electron tomography. *Viruses*. **10**(8), p.446.

Khaperskyy, D.A. and McCormick, C. 2015. Timing Is Everything: Coordinated Control of Host Shutoff by Influenza A Virus NS1 and PA-X Proteins. *Journal of Virology*. **89**(13), pp.6528–6531.

Killikelly, A.M., Kanekiyo, M. and Graham, B.S. 2016. Pre-fusion F is absent on the surface of formalin-inactivated respiratory syncytial virus. *Scientific Reports*. **6**(1), pp.1–7.

Killingley, B. and Nguyen-Van-Tam, J. 2013. Routes of influenza transmission. *Influenza and Other Respiratory Viruses*. **7**(SUPPL.2), pp.42–51.

Kim, D., Quinn, J., Pinsky, B., Shah, N.H. and Brown, I. 2020. Rates of Co-infection Between SARS-CoV-2 and Other Respiratory Pathogens. *JAMA*. **323**(20), pp.2085–2086.

Kim, Hyun Wha, Canchola', J.G., Brandt, Carl D, Pyles, Gloria, Chanock, Robert M, Jensen, Keith, Parrott, Robert H, Kim, H W, Canchola, J.G., Brandt, C D, Pyles, G, Chanock, R M, Jensen, K and Parrott, R H 1969. Respiratory syncytial virus disease in infants despite prior administration of antigenic inactivated vaccine. *American Journal of Epidemiology*. **89**(4), pp.422–434.

Kinnula, H., Mappes, J. and Sundberg, L.R. 2017. Coinfection outcome in an opportunistic pathogen depends on the inter-strain interactions. *BMC Evolutionary Biology*. **17**(1).

Kiss, G., Holl, J.M., Williams, G.M., Alonas, E., Vanover, D., Lifland, A.W., Gudheti, M., Guerrero-Ferreira, R.C., Nair, V., Yi, H., Graham, B.S., Santangelo, P.J. and Wright, E.R. 2014. Structural Analysis of Respiratory Syncytial Virus Reveals the Position of M2-1 between the Matrix Protein and the Ribonucleoprotein Complex. *Journal of Virology*. **88**(13), p.7602.

Kleinnijenhuis, J., Quintin, J., Preijers, F., Joosten, L.A.B., Ifrim, D.C., Saeed, S., Jacobs, C., Van Loenhout, J., De Jong, D., Hendrik, S., Xavier, R.J., Van Der Meer, J.W.M., Van Crevel, R. and Netea, M.G. 2012. Bacille Calmette-Guérin induces NOD2-dependent nonspecific protection from reinfection via epigenetic reprogramming of monocytes. *Proceedings of the National Academy of Sciences of the United States of America*. **109**(43), pp.17537–17542.

Klenk, H.D., Rott, R., Orlich, M. and Blödorn, J. 1975. Activation of influenza A viruses by trypsin treatment. *Virology*. **68**(2), pp.426–439.

Kneyber, M.C.J., Brandenburg, A.H., Rothbarth, P.H., De Groot, R., Ott, A. and Van Steensel-Moll, H.A. 1996. Relationship between clinical severity of respiratory syncytial virus infection and subtype. *Archives of disease in childhood*. **75**(2), pp.137–140.

Koliopoulos, M.G., Lethier, M., Van Der Veen, A.G., Haubrich, K., Hennig, J., Kowalinski, E., Stevens, R. V., Martin, S.R., Reis E Sousa, C., Cusack, S. and Rittinger, K. 2018. Molecular mechanism of influenza A NS1-mediated TRIM25 recognition and inhibition. *Nature Communications*. **9**(1), pp.1–13.

Kremer, J.R., Mastronarde, D.N. and McIntosh, J.R. 1996. Computer visualization of three-dimensional image data using IMOD. *Journal of Structural Biology*. **116**(1), pp.71–76.

Krusat, T. and Streckert, H.J. 1997. Heparin-dependent attachment of respiratory syncytial virus (RSV) to host cells. *Archives of virology*. **142**(6), pp.1247–1254.

Krzyzaniak, M.A., Zumstein, M.T., Gerez, J.A., Picotti, P. and Helenius, A. 2013. Host Cell Entry of Respiratory Syncytial Virus Involves Macropinocytosis Followed by Proteolytic Activation of the F Protein. *PLOS Pathogens*. **9**(4), p.e1003309.

Kumar, P., Sweeney, T.R., Skabkin, M.A., Skabkina, O. V., Hellen, C.U.T. and Pestova, T. V. 2014. Inhibition of translation by IFIT family members is determined by their ability to interact selectively with the 5′-terminal regions of cap0-, cap1- and 5′ppp- mRNAs. *Nucleic Acids Research*. **42**(5), pp.3228–3245.

Kuo, L., Fearns, R. and Collins, P.L. 1997. Analysis of the gene start and gene end signals of human respiratory syncytial virus: quasi-templated initiation at position 1 of the encoded mRNA. *Journal of Virology*. **71**(7), p.4944.

Kuppan, J.P., Mitrovich, M.D. and Vahey, M.D. 2021. A morphological transformation in respiratory syncytial virus leads to enhanced complement deposition. *eLife*. **10**.

Lackenby, A., Gilad, J.M., Pebody, R., Miah, S., Calatayud, L., Bolotin, S., Vipond, I., Muir, P., Guiver, M., Mcmenamin, J., Reynolds, A., Moore, C., Gunson, R., Thompson, C., Galiano, M., Bermingham, A., Ellis, J. and Zambon, M. 2011. Continued emergence and changing epidemiology of oseltamivir-resistant influenza A(H1N1)2009 virus, United Kingdom, winter 2010/11. *Eurosurveillance*. **16**(5), p.19784.

Lahaye, X., Vidy, A., Pomier, C., Obiang, L., Harper, F., Gaudin, Y. and Blondel, D. 2009. Functional Characterization of Negri Bodies (NBs) in Rabies Virus-Infected Cells: Evidence that NBs Are Sites of Viral Transcription and Replication. *Journal of Virology*. **83**(16), pp.7948–7958.

Laliberte, J.P. and Moss, B. 2014. A Novel Mode of Poxvirus Superinfection Exclusion That Prevents Fusion of the Lipid Bilayers of Viral and Cellular Membranes. *Journal of Virology*. **88**(17), pp.9751–9768.

Lamb, R.A. and Choppin, P.W. 1979. Segment 8 of the influenza virus genome is unique in coding for two polypeptides. *Proceedings of the National Academy of Sciences*. **76**(10), pp.4908–4912.

Lang, J.M. and Benbow, M.E. 2013. Species Interactions and Competition. *Nature Education*

Knowledge. **4**(4), p.8.

Lapeña, S., Robles, M.B., Castañón, L., Martínez, J.P., Reguero, S., Alonso, M.P. and Fernández, I. 2005. Climatic factors and lower respiratory tract infection due to respiratory syncytial virus in hospitalised infants in northern Spain. *European journal of epidemiology*. **20**(3), pp.271–276.

Lee, Y.-M., Tscherne, D.M., Yun, S.-I., Frolov, I. and Rice, C.M. 2005. Dual Mechanisms of Pestiviral Superinfection Exclusion at Entry and RNA Replication. *Journal of Virology*. **79**(6), pp.3231–3242.

Leser, G.P. and Lamb, R.A. 2017. Lateral Organization of Influenza Virus Proteins in the Budozone Region of the Plasma Membrane. *Journal of Virology*. **91**(9).

Leung, N.H.L. 2021. Transmissibility and transmission of respiratory viruses. *Nature Reviews Microbiology*. **19**(8), pp.528–545.

Levine, S., Kaliaber-Franco, R. and Paradiso, P.R. 1987. Demonstration that glycoprotein G is the attachment protein of respiratory syncytial virus. *Journal of general virology*. **68 (Pt 9)**(9), pp.2521–2524.

Li, D., Jans, D.A., Bardin, P.G., Meanger, J., Mills, J. and Ghildyal, R. 2008. Association of respiratory syncytial virus M protein with viral nucleocapsids is mediated by the M2-1 protein. *Journal of Virology*. **82**(17), pp.8863–8870.

Li, H., Zhao, X., Zhao, Y., Li, J., Zheng, H., Xue, M., Guo, L., Zhou, J., Yang, J., Zuo, Y., Chen, Y., Yang, Z., Fan, Q., Qin, L., Shi, H. and Liu, L. 2021. H1N1 exposure during the convalescent stage of SARS-CoV-2 infection results in enhanced lung pathologic damage in hACE2 transgenic mice. *Emerging Microbes and Infections*. **10**(1), pp.1156–1168.

Li, S., Sieben, C., Ludwig, K., Höfer, C.T., Chiantia, S., Herrmann, A., Eghiaian, F. and Schaap, I.A.T. 2014. pH-Controlled Two-Step Uncoating of Influenza Virus. *Biophysical Journal*. **106**(7), pp.1447–1456.

Li, T., Li, Z., Deans, E.E., Mittler, E., Liu, M., Chandran, K. and Ivanovic, T. 2021. The shape of pleomorphic virions determines resistance to cell-entry pressure. *Nature Microbiology*., pp.1–13.

Lieber, M., Smith, B., Szakal, A., Nelson-Rees, W. and Todaro, G. 1976. A continuous tumor-cell line from a human lung carcinoma with properties of type II alveolar epithelial cells. *International journal of cancer*. **17**(1), pp.62–70.

Lifland, A.W., Jung, J., Alonas, E., Zurla, C., Crowe, J.E. and Santangelo, P.J. 2012. Human Respiratory Syncytial Virus Nucleoprotein and Inclusion Bodies Antagonize the Innate Immune Response Mediated by MDA5 and MAVS. *Journal of Virology*. **86**(15), pp.8245–8258.

Liljeroos, L., Krzyzaniak, M.A., Helenius, A. and Butcher, S.J. 2013. Architecture of respiratory syncytial virus revealed by electron cryotomography. *Proceedings of the National Academy of Sciences of the United States of America*. **110**(27), pp.11133–11138.

Lin, S., Naim, H.Y., Rodriguez, A.C. and Roth, M.G. 1998. Mutations in the middle of the transmembrane domain reverse the polarity of transport of the influenza virus hemagglutinin in MDCK epithelial cells. *Journal of Cell Biology*. **142**(1), pp.51–57.

Lin, Y.P., Gregory, V., Bennett, M. and Hay, A. 2004. Recent changes among human influenza viruses. *Virus Research*. **103**(1–2), pp.47–52.

Linde, A., Rotzén-Ostlund, M., Zweygberg-Wirgart, B., Rubinova, S. and Brytting, M. 2009. Does viral interference affect spread of influenza? *Euro surveillance : bulletin européen sur les maladies transmissibles = European communicable disease bulletin*. **14**(40).

Ling, Z., Tran, K.C. and Teng, M.N. 2009. Human respiratory syncytial virus nonstructural protein NS2 antagonizes the activation of beta interferon transcription by interacting with RIG-I. *Journal of virology*. **83**(8), pp.3734–3742.

Liuzzi, M., Mason, S.W., Cartier, M., Lawetz, C., McCollum, R.S., Dansereau, N., Bolger, G., Lapeyre, N., Gaudette, Y., Lagacé, L., Massariol, M.-J., Dô, F., Whitehead, P., Lamarre, L.,

Scouten, E., Bordeleau, J., Landry, S., Rancourt, J., Fazal, G. and Simoneau, B. 2005. Inhibitors of Respiratory Syncytial Virus Replication Target Cotranscriptional mRNA Guanylylation by Viral RNA-Dependent RNA Polymerase. *Journal of Virology*. **79**(20), pp.13105–13115.

Lo, M.S., Brazas, R.M. and Holtzman, M.J. 2005. Respiratory syncytial virus nonstructural proteins NS1 and NS2 mediate inhibition of Stat2 expression and alpha/beta interferon responsiveness. *Journal of virology*. **79**(14), pp.9315–9319.

Loney, C., Mottet-Osman, G., Roux, L. and Bhella, D. 2009. Paramyxovirus Ultrastructure and Genome Packaging: Cryo-Electron Tomography of Sendai Virus. *Journal of Virology*. **83**(16), pp.8191–8197.

Lowen, A.C., Mubareka, S., Steel, J. and Palese, P. 2007. Influenza Virus Transmission Is Dependent on Relative Humidity and Temperature. *PLOS Pathogens*. **3**(10), p.e151.

Lozano, R., Naghavi, M., Foreman, K., Lim, S., Shibuya, K., Aboyans, V., Abraham, J., Adair, T., Aggarwal, R., Ahn, S.Y., AlMazroa, M.A., Alvarado, M., Anderson, H.R., Anderson, L.M., Andrews, K.G., Atkinson, C., Baddour, L.M., Barker-Collo, S., Bartels, D.H., Bell, M.L., Benjamin, E.J., Bennett, D., Bhalla, K., Bikbov, B., Bin Abdulhak, A., Birbeck, G., Blyth, F., Bolliger, I., Boufous, S., Bucello, C., Burch, M., Burney, P., Carapetis, J., Chen, H., Chou, D., Chugh, S.S., Coffeng, L.E., Colan, S.D., Colquhoun, S., Colson, K.E., Condon, J., Connor, M.D., Cooper, L.T., Corriere, M., Cortinovis, M., Courville De Vaccaro, K., Couser, W., Cowie, B.C., Criqui, M.H., Cross, M., Dabhadkar, K.C., Dahodwala, N., De Leo, D., Degenhardt, L., Delossantos, A., Denenberg, J., Des Jarlais, D.C., Dharmaratne, S.D., Dorsey, E.R., Driscoll, T., Duber, H., Ebel, B., Erwin, P.J., Espindola, P., Ezzati, M., Feigin, V., Flaxman, A.D., Forouzanfar, M.H., Fowkes, F.G.R., Franklin, R., Fransen, M., Freeman, M.K., Gabriel, S.E., Gakidou, E., Gaspari, F., Gillum, R.F., Gonzalez-Medina, D., Halasa, Y.A., Haring, D., Harrison, J.E., Havmoeller, R., Hay, R.J., Hoen, B., Hotez, P.J., Hoy, D., Jacobsen, K.H., James, S.L., Jasrasaria, R., Jayaraman, S., Johns, N., Karthikeyan, G., Kassebaum, N., Keren, A., Khoo, J.P., Knowlton, L.M., Kobusingye, O., Koranteng, A., Krishnamurthi, R., Lipnick, M., Lipshultz, S.E., Lockett Ohno, S., Mabweijano, J., MacIntyre, M.F., Mallinger, L., March, L., Marks, G.B., Marks, R., Matsumori, A., Matzopoulos, R., Mayosi, B.M., McAnulty, J.H., McDermott, M.M., McGrath, J., Memish, Z.A., Mensah, G.A., Merriman, T.R., Michaud, C., Miller, M., Miller, T.R., Mock, C., Mocumbi, A.O., Mokdad, A.A., Moran, A., Mulholland, K., Nair, M.N., Naldi, L., Narayan, K.M.V., Nasseri, K., Norman, P., O'Donnell, M., Omer, S.B., Ortblad, K., Osborne, R., Ozgediz, D., Pahari, B., Pandian, J.D., Panozo Rivero, A., Perez Padilla, R., Perez-Ruiz, F., Perico, N., Phillips, D., Pierce, K., Pope, C.A., Porrini, E., Pourmalek, F., Raju, M., Ranganathan, D., Rehm, J.T., Rein, D.B., Remuzzi, G., Rivara, F.P., Roberts, T., Rodriguez De León, F., Rosenfeld, L.C., Rushton, L., Sacco, R.L., Salomon, J.A., Sampson, U., Sanman, E., Schwebel, D.C., Segui-Gomez, M., Shepard, D.S., Singh, D., Singleton, J., Sliwa, K., Smith, E., Steer, A., Taylor, J.A., Thomas, B., Tleyjeh, I.M., Towbin, J.A., Truelsen, T., Undurraga, E.A., Venketasubramanian, N., Vijayakumar, L., Vos, T., Wagner, G.R., Wang, M., Wang, W., Watt, K., Weinstock, M.A., Weintraub, R., Wilkinson, J.D., Woolf, A.D., Wulf, S., Yeh, P.H., Yip, P., Zabetian, A., Zheng, Z.J., Lopez, A.D. and Murray, C.J.L. 2012. Global and regional mortality from 235 causes of death for 20 age groups in 1990 and 2010: a systematic analysis for the Global Burden of Disease Study 2010. *The Lancet*. **380**(9859), pp.2095–2128.

Lu, Y., Wambach, M., Katze, M.G. and Krug, R.M. 1995. Binding of the Influenza Virus NS1 Protein to Double-Stranded RNA Inhibits the Activation of the Protein Kinase That Phosphorylates the eIF-2 Translation Initiation Factor. *Virology*. **214**(1), pp.222–228.

Ludwig, A., Nguyen, T., Leong, D., Ravi, L., Tan, B., Sandin, S. and Sugrue, R. 2017. Caveolae provide a specialized membrane environment for respiratory syncytial virus assembly. *Journal of Cell Science*. **130**(6), pp.1037–1050.

Luna, M.S., Manzoni, P., Paes, B., Baraldi, E., Cossey, V., Kugelman, A., Chawla, R., Dotta, A., Rodríguez Fernández, R., Resch, B. and Carbonell-Estrany, X. 2020. Expert consensus on palivizumab use for respiratory syncytial virus in developed countries. *Paediatric Respiratory Reviews*. **33**, pp.35–44.

MacIntyre, C.R., Chughtai, A.A., Barnes, M., Ridda, I., Seale, H., Toms, R. and Heywood, A. 2018. The role of pneumonia and secondary bacterial infection in fatal and serious outcomes of pandemic influenza a(H1N1)pdm09 11 Medical and Health Sciences 1103 Clinical Sciences

11 Medical and Health Sciences 1117 Public Health and Health Services. *BMC Infectious Diseases*. **18**(1), pp.1–20.

Madhi, S.A., Polack, F.P., Piedra, P.A., Munoz, F.M., Trenholme, A.A., Simões, E.A.F., Swamy, G.K., Agrawal, S., Ahmed, K., August, A., Baqui, A.H., Calvert, A., Chen, J., Cho, I., Cotton, M.F., Cutland, C.L., Englund, J.A., Fix, A., Gonik, B., Hammitt, L., Heath, P.T., de Jesus, J.N., Jones, C.E., Khalil, A., Kimberlin, D.W., Libster, R., Llapur, C.J., Lucero, M., Pérez Marc, G., Marshall, H.S., Masenya, M.S., Martinón-Torres, F., Meece, J.K., Nolan, T.M., Osman, A., Perrett, K.P., Plested, J.S., Richmond, P.C., Snape, M.D., Shakib, J.H., Shinde, V., Stoney, T., Thomas, D.N., Tita, A.T., Varner, M.W., Vatish, M., Vrbicky, K., Wen, J., Zaman, K., Zar, H.J., Glenn, G.M. and Fries, L.F. 2020. Respiratory Syncytial Virus Vaccination during Pregnancy and Effects in Infants. *The New England Journal of Medicine*. **383**(5), pp.426–439.

Mahmoudabadi, G., Milo, R. and Phillips, R. 2017. Energetic cost of building a virus. *Proceedings of the National Academy of Sciences of the United States of America*. **114**(22), pp.E4324–E4333.

Mak, G.C., Wong, A.H., Ho, W.Y.Y. and Lim, W. 2012. The impact of pandemic influenza A (H1N1) 2009 on the circulation of respiratory viruses 2009-2011. *Influenza and Other Respiratory Viruses*. **6**(3), pp.e6–e10.

Mandelia, Y., Procop, G.W., Richter, S.S., Worley, S., Liu, W. and Esper, F. 2021. Dynamics and predisposition of respiratory viral co-infections in children and adults. *Clinical Microbiology and Infection*. **27**(4), 631.e1-631.e6.

Marcos, M.A., Ramón, S., Antón, A., Martinez, E., Vilella, A., Olivé, V., Cillóniz, C., Moreno, A., Torrese, A. and Pumarola, T. 2011. Clinical relevance of mixed respiratory viral infections in adults with influenza A H1N1. *European Respiratory Journal*. **38**(3), pp.739–742.

Marko, M., Hsieh, C., Schalek, R., Frank, J. and Mannella, C. 2007. Focused-ion-beam thinning of frozen-hydrated biological specimens for cryo-electron microscopy. *Nature Methods*. **4**(3), pp.215–217.

Martin, E.T., Kuypers, J., Wald, A. and Englund, J.A. 2012. Multiple versus single virus respiratory infections: Viral load and clinical disease severity in hospitalized children. *Influenza and other Respiratory Viruses*. **6**(1), pp.71–77.

Marty, A., Meanger, J., Mills, J., Shields, B. and Ghildyal, R. 2004. Association of matrix protein of respiratory syncytial virus with the host cell membrane of infected cells Brief Report. *Archives of Virology*. **149**, pp.199–210.

Mastrangelo, P., Chin, A.A., Tan, S., Jeon, A.H., Ackerley, C.A., Siu, K.K., Lee, J.E. and Hegele, R.G. 2021. Identification of RSV Fusion Protein Interaction Domains on the Virus Receptor, Nucleolin. *Viruses*. **13**(2), p.261.

Mastronarde, D.N. and Held, S.R. 2017. Automated Tilt Series Alignment and Tomographic Reconstruction in IMOD. *Journal of Structural Biology*. **197**(2), p.102.

Mata, M., Sarrion, I., Armengot, M., Carda, C., Martinez, I., Melero, J.A. and Cortijo, J. 2012. Respiratory Syncytial Virus Inhibits Ciliagenesis in Differentiated Normal Human Bronchial Epithelial Cells: Effectiveness of N-Acetylcysteine. *PLOS ONE*. **7**(10), p.e48037.

Matrosovich, M.N., Matrosovich, T.Y., Gray, T., Roberts, N.A. and Klenk, H.-D. 2004. Human and avian influenza viruses target different cell types in cultures of human airway epithelium. *Proceedings of the National Academy of Sciences of the United States of America*. **101**(13), pp.4620–4624.

Matsuzaki, Y., Katsushima, N., Nagai, Y., Shoji, M., Itagaki, T., Sakamoto, M., Kitaoka, S., Mizuta, K. and Nishimura, H. 2006. Clinical features of influenza C virus infection in children. *Journal of Infectious Diseases*. **193**(9), pp.1229–1235.

McConnochie, K.M., Hall, C.B., Walsh, E.E. and Roghmann, K.J. 1990. Variation in severity of respiratory syncytial virus infections with subtype. *The Journal of pediatrics*. **117**(1 Pt 1), pp.52–62.

McCurdy, L.H. and Graham, B.S. 2003. Role of Plasma Membrane Lipid Microdomains in Respiratory Syncytial Virus Filament Formation. *Journal of Virology*. **77**(3), pp.1747–1756.

McKinney, H.H. 1929. Mosaic diseases in the Canary Islands, West Africa and Gibraltar. *Journal of Agricultural Research.* **39**, pp.577–578.

McLellan, J., Yang, Y., Graham, B. and Kwong, P. 2011. Structure of respiratory syncytial virus fusion glycoprotein in the postfusion conformation reveals preservation of neutralizing epitopes. *Journal of Virology*. **85**(15), pp.7788–7796.

Meskill, S.D., Revell, P.A., Chandramohan, L. and Cruz, A.T. 2017. Prevalence of co-infection between respiratory syncytial virus and influenza in children. *The American journal of emergency medicine*. **35**(3), pp.495–498.

Min, J. and Krug, R. 2006. The primary function of RNA binding by the influenza A virus NS1 protein in infected cells: Inhibiting the 2'-5' oligo (A) synthetase/RNase L pathway. *Proceedings of the National Academy of Sciences*. **103**(18), pp.7100–7105.

Mitra, R., Baviskar, P., Duncan-Decocq, R.R., Patel, D. and Oomens, A.G.P. 2012. The Human Respiratory Syncytial Virus Matrix Protein Is Required for Maturation of Viral Filaments. *Journal of Virology*. **86**(8), pp.4432–4443.

Miyake, Y., Keusch, J.J., Decamps, L., Ho-Xuan, H., Iketani, S., Gut, H., Kutay, U., Helenius, A. and Yamauchi, Y. 2019. Influenza virus uses transportin 1 for vRNP debundling during cell entry. *Nature Microbiology* . **4**(4), pp.578–586.

Moeller, A., Kirchdoerfer, R.N., Potter, C.S., Carragher, B. and Wilson, I.A. 2012. Organization of the influenza virus replication machinery. *Science*. **338**(6114), pp.1631–1634.

Möhler, L., Flockerzi, D., Sann, H. and Reichl, U. 2005. Mathematical model of influenza A virus production in large-scale microcarrier culture. *Biotechnology and bioengineering*. **90**(1), pp.46–58.

Momose, F., Sekimoto, T., Ohkura, T., Jo, S., Kawaguchi, A., Nagata, K. and Morikawa, Y. 2011. Apical transport of influenza A virus ribonucleoprotein requires Rab11-positive recycling endosome. *PloS one*. **6**(6).

Mora, R., Rodriguez-Boulan, E., Palese, P. and García-Sastre, A. 2002. Apical Budding of a Recombinant Influenza A Virus Expressing a Hemagglutinin Protein with a Basolateral Localization Signal. *Journal of Virology*. **76**(7), pp.3544–3553.

Morens, D.M. and Fauci, A.S. 2007. The 1918 Influenza Pandemic: Insights for the 21st Century. *The Journal of Infectious Diseases*. **195**(7), pp.1018–1028.

Morrison, T.G. and McGinnes, L.W. 1989. Avian cells expressing the Newcastle disease virus hemagglutinin-neuraminidase protein are resistant to Newcastle disease virus infection. *Virology*. **171**(1), pp.10–17.

Mufson, M.A., Orvell, C., Rafnar, B. and Norrby, E. 1985. Two distinct subtypes of human respiratory syncytial virus. *Journal of General Virology*. **66**(10), pp.2111–2124.

Munro, S. 2003. Lipid Rafts: Elusive or Illusive? *Cell*. **115**(4), pp.377–388.

Nair, H., Nokes, D.J., Gessner, B.D., Dherani, M., Madhi, S.A., Singleton, R.J., O'Brien, K.L., Roca, A., Wright, P.F., Bruce, N., Chandran, A., Theodoratou, E., Sutanto, A., Sedyaningsih, E.R., Ngama, M., Munywoki, P.K., Kartasasmita, C., Simões, E.A., Rudan, I., Weber, M.W. and Campbell, H. 2010. Global burden of acute lower respiratory infections due to respiratory syncytial virus in young children: a systematic review and meta-analysis. *The Lancet*. **375**(9725), pp.1545–1555.

Neilson, K. and Yunis, E. 1990. Demonstration of respiratory syncytial virus in an autopsy series. *Pediatric pathology*. **10**(4), pp.491–502.

Nemeroff, M.E., Barabino, S.M.L., Li, Y., Keller, W. and Krug, R.M. 1998. Influenza Virus NS1 Protein Interacts with the Cellular 30 kDa Subunit of CPSF and Inhibits 3′ End Formation of Cellular Pre-mRNAs. *Molecular Cell*. **1**(7), pp.991–1000.

Netea, M.G., Domínguez-Andrés, J., Barreiro, L.B., Chavakis, T., Divangahi, M., Fuchs, E., Joosten, L.A.B., van der Meer, J.W.M., Mhlanga, M.M., Mulder, W.J.M., Riksen, N.P., Schlitzer, A., Schultze, J.L., Stabell Benn, C., Sun, J.C., Xavier, R.J. and Latz, E. 2020. Defining trained immunity and its role in health and disease. *Nature Reviews Immunology*.

20(6), p.375.

Nickbakhsh, S., Mair, C., Matthews, L., Reeve, R., Johnson, P.C.D., Thorburn, F., von Wissmann, B., Reynolds, A., McMenamin, J., Gunson, R.N. and Murcia, P.R. 2019. Virus–virus interactions impact the population dynamics of influenza and the common cold. *Proceedings of the National Academy of Sciences*., p.201911083.

Nickbakhsh, S., Nickbakhsh, S., Ho, A., Marques, D.F.P., McMenamin, J., Gunson, R.N. and Murcia, P.R. 2020. Epidemiology of Seasonal Coronaviruses: Establishing the Context for the Emergence of Coronavirus Disease 2019. *The Journal of Infectious Diseases*. **222**(1), pp.17–25.

Nickbakhsh, S., Thorburn, F., Von Wissmann, B., McMenamin, J., Gunson, R.N. and Murcia, P.R. 2016. Extensive multiplex PCR diagnostics reveal new insights into the epidemiology of viral respiratory infections. *Epidemiology and Infection*. **144**(10), pp.2064–2076.

Noda, T., Murakami, S., Nakatsu, S., Imai, H., Muramoto, Y., Shindo, K., Sagara, H. and Kawaoka, Y. 2018. Importance of the 1+7 configuration of ribonucleoprotein complexes for influenza A virus genome packaging. *Nature Communications*. **9**(1), pp.1–10.

Noda, T., Sagara, H., Yen, A., Takada, A., Kida, H., Cheng, R.H. and Kawaoka, Y. 2006. Architecture of ribonucleoprotein complexes in influenza A virus particles. *Nature*. **439**(7075), pp.490–492.

Nogalez, A., Martinez-Sobrido, L., Topham, D. and DeDeiego, M. 2018. Modulation of Innate Immune Responses by the Influenza A NS1 and PA-X Proteins. *Viruses*. **10**(12).

Noton, S.L., Medcalf, E., Fisher, D., Mullin, A.E., Elton, D. and Digard, P. 2007. Identification of the domains of the influenza A virus M1 matrix protein required for NP binding, oligomerization and incorporation into virions. *Journal of General Virology*. **88**(Pt 8), p.2280.

Noton, S.L., Nagendra, K., Dunn, E.F., Mawhorter, M.E., Yu, Q. and Fearns, R. 2015. Respiratory Syncytial Virus Inhibitor AZ-27 Differentially Inhibits Different Polymerase Activities at the Promoter. *Journal of Virology*. **89**(15), pp.7786–7798.

Nunes, S.F., Murcia, P.R., Tiley, L.S., Brown, I.H., Tucker, A.W., Maskell, D.J. and Wood, J.L.N. 2010. An ex vivo swine tracheal organ culture for the study of influenza infection. *Influenza and Other Respiratory Viruses*. **4**(1), p.7.

O'Neill, R.E., Jaskunas, R., Blobel, G., Palese, P. and Moroianu, J. 1995. Nuclear import of influenza virus RNA can be mediated by viral nucleoprotein and transport factors required for protein import. *The Journal of Biological Chemistry*. **270**(39), pp.22701–22704.

Ohkura, T., Momose, F., Ichikawa, R., Takeuchi, K. and Morikawa, Y. 2014. Influenza A Virus Hemagglutinin and Neuraminidase Mutually Accelerate Their Apical Targeting through Clustering of Lipid Rafts. *Journal of Virology*. **88**(17), pp.10039–10055.

Ohuchi, M., Ohuchi, R. and Mifune, K. 1982. Demonstration of hemolytic and fusion activities of influenza C virus. *Journal of Virology*. **42**(3), pp.1076–1079.

Okamoto, S., Kawabata, S., Nakagawa, I., Okuno, Y., Goto, T., Sano, K. and Hamada, S. 2003. Influenza A Virus-Infected Hosts Boost an Invasive Type of Streptococcus pyogenes Infection in Mice. *Journal of Virology*. **77**(7), pp.4104–4112.

Oomens, A.G.P., Bevis, K.P. and Wertz, G.W. 2006. The Cytoplasmic Tail of the Human Respiratory Syncytial Virus F Protein Plays Critical Roles in Cellular Localization of the F Protein and Infectious Progeny Production. *Journal of Virology*. **80**(21), pp.10465–10477.

Oomens, A.G.P., Megaw, A.G. and Wertz, G.W. 2003. Infectivity of a Human Respiratory Syncytial Virus Lacking the SH, G, and F Proteins Is Efficiently Mediated by the Vesicular Stomatitis Virus G Protein. *Journal of Virology*. **77**(6), pp.3785–3798.

Ozawa, M., Fujii, K., Muramoto, Y., Yamada, S., Yamayoshi, S., Takada, A., Goto, H., Horimoto, T. and Kawaoka, Y. 2007. Contributions of two nuclear localization signals of influenza A virus nucleoprotein to viral replication. *Journal of Virology*. **81**(1), pp.30–41.

Palese, P. and Shaw, M. 2013. Orthomyxoviridae: The viruses and their replication *In*: P. M. Knipe, D. M. & Howley, ed. *Fields Virology*. Philadelphia: Lippincott Williams & Wilkins., pp.1647–

1689.

Papadopoulos, N.G., Gourgiotis, D., Javadyan, A., Bossios, A., Kallergi, K., Psarras, S., Tsolia, M.N. and Kafetzis, D. 2004. Does respiratory syncytial virus subtype influences the severity of acute bronchiolitis in hospitalized infants? *Respiratory medicine*. **98**(9), pp.879–882.

Paterson, D. and Fodor, E. 2012. Emerging Roles for the Influenza A Virus Nuclear Export Protein (NEP). *PLOS Pathogens*. **8**(12), p.e1003019.

Patrono, L. V., Bonfante, F., Zanardello, C., Terregino, C., Capua, I. and Murcia, P.R. 2015. Phylogenetically distinct equine influenza viruses show different tropism for the swine respiratory tract. *The Journal of General Virology*. **96**(Pt 5), p.969.

Pavlovic, J., Arzet, H.A., Hefti, H.P., Frese, M., Rost, D., Ernst, B., Kolb, E., Staeheli, P. and Haller, O. 1995. Enhanced virus resistance of transgenic mice expressing the human MxA protein. *Journal of Virology*. **69**(7), p.4506.

Pei, J., Beri, N.R., Zou, A.J., Hubel, P., Dorando, H.K., Bergant, V., Andrews, R.D., Pan, J., Andrews, J.M., Sheehan, K.C.F., Pichlmair, A., Amarasinghe, G.K., Brody, S.L., Payton, J.E. and Leung, D.W. 2021. Nuclear-localized human respiratory syncytial virus NS1 protein modulates host gene transcription. *Cell Reports*. **37**(2), p.109803.

Peng, D., Zhao, D., Liu, J., Wang, X., Yang, K., Xicheng, H., Li, Y. and Wang, F. 2009. Multipathogen infections in hospitalized children with acute respiratory infections. *Virology*. **6**(1), pp.1–7.

Peng, J., Shin, J., Li, G., Wu, N. and Herrler, G. 2021. Time-dependent viral interference between influenza virus and coronavirus in the infection of differentiated porcine airway epithelial cells. *Virulence*. **12**(1), pp.1111–1121.

Peukes, J., Xiong, X., Erlendsson, S., Qu, K., Wan, W., Calder, L.J., Schraidt, O., Kummer, S., V Freund, S.M., Kräusslich, H.-G. and G Briggs, J.A. 2020. The native structure of the assembled matrix protein 1 of influenza A virus. *Nature*., pp.1–4.

Pinilla, J., Barber, P., Vallejo-torres, L., Rodríguez-mireles, S., López-valcárcel, B.G. and Serra-majem, L. 2021. The Economic Impact of the SARS-COV-2 (COVID-19) Pandemic in Spain. *International journal of environmental research and public health*. **18**(9).

Pinky, L. and Dobrovolny, H.M. 2016. Coinfections of the respiratory tract: Viral competition for resources. *PLoS ONE*. **11**(5).

Pinky, L., González-Parra, G. and Dobrovolny, H. 2019. Superinfection and cell regeneration can lead to chronic viral coinfections. *Journal of Theoretical Biology*. **466**, pp.24–38.

Pinto, A.K., Williams, G.D., Szretter, K.J., White, J.P., Proença-Módena, J.L., Liu, G., Olejnik, J., Brien, J.D., Ebihara, H., Mühlberger, E., Amarasinghe, G., Diamond, M.S. and Boon, A.C.M. 2015. Human and Murine IFIT1 Proteins Do Not Restrict Infection of Negative-Sense RNA Viruses of the Orthomyxoviridae, Bunyaviridae, and Filoviridae Families. *Journal of Virology*. **89**(18), pp.9465–9476.

Pinto, R.M., Lycett, S., Gaunt, E. and Digard, P. 2020. Accessory Gene Products of Influenza A Virus. *Cold Spring Harbor Perspectives in Medicine*., p.a038380.

Plemper, R.K. and Lamb, R.A. 2021. Paramyxoviridae: The Viruses and Their Replication *In*: *Fields Virology: Emerging Viruses*. Philadelphia: Lippincott Williams & Wilkins, pp.504–595.

Plotkowski, M.C., Puchelle, E., Beck, G., Jacquot, J. and Hannoun, C. 2015. Adherence of Type I Streptococcus pneumoniae to Tracheal Epithelium of Mice Infected with Influenza A/PR8 Virus1–3. *The American Review of Respiratory Disease*. **134**(5), pp.1040–1044.

Price, R.H.M., Graham, C. and Ramalingam, S. 2019. Association between viral seasonality and meteorological factors. *Scientific Reports*. **9**(1).

Pritlove, D.C., Poon, L.L.M., Devenish, L.J., Leahy, M.B. and Brownlee, G.G. 1999. A Hairpin Loop at the 5′ End of Influenza A Virus Virion RNA Is Required for Synthesis of Poly(A)+ mRNA In Vitro. *Journal of Virology*. **73**(3), p.2109.

Public Heath England 2020. Surveillance of influenza and other respiratory viruses in the UK.

Qin, C., Li, W., Li, Q., Yin, W., Zhang, X., Zhang, Z., Zhang, X.E. and Cui, Z. 2019. Real-time dissection of dynamic uncoating of individual influenza viruses. *Proceedings of the National Academy of Sciences of the United States of America*. **116**(7), pp.2577–2582.

Ramaekers, K., Keyaerts, E., Rector, A., Borremans, A., Beuselinck, K., Lagrou, K. and Van Ranst, M. 2017. Prevalence and seasonality of six respiratory viruses during five consecutive epidemic seasons in Belgium. *Journal of Clinical Virology*. **94**, pp.72–78.

Ramaswamy, M., Shi, L., Varga, S.M., Barik, S., Behlke, M.A. and Look, D.C. 2006. Respiratory syncytial virus nonstructural protein 2 specifically inhibits type I interferon signal transduction. *Virology*. **344**(2), pp.328–339.

Regamey, N., Kaiser, L., Roiha, H.L., Deffernez, C., Kuehni, C.E., Latzin, P., Aebi, C. and Frey, U. 2008. Viral etiology of acute respiratory infections with cough in infancy: A community-based birth cohort study. *Pediatric Infectious Disease Journal*. **27**(2), pp.100–105.

Reich, S., Guilligay, D., Pflug, A., Malet, H., Berger, I., Crepin, T., Hart, D., Lunardi, T., Nanao, M., Ruigrok, R.W.H. and Cusack, S. 2014. Structural insight into cap-snatching and RNA synthesis by influenza polymerase. *Nature*. **516**(7531), pp.361–366.

Rim, A., Nacira, L., Jihene, N., Said, S., Khaled, M., Ahmed, R. and Abdeljelil, G. 2019. Viral interference between H9N2-low pathogenic avian influenza virus and avian infectious bronchitis virus vaccine strain H120 in vivo. *Comparative Immunology, Microbiology and Infectious Diseases*. **65**, pp.219–225.

Rincheval, V., Lelek, M., Gault, E., Bouillier, C., Sitterlin, D., Blouquit-Laye, S., Galloux, M., Zimmer, C., Eleouet, J.-F. and Rameix-Welti, M.-A. 2017. Functional organization of cytoplasmic inclusion bodies in cells infected by respiratory syncytial virus. *Nature Communications*. **8**(1), pp.1–11.

Roberts, P.C. and Compans, R.W. 1998. *Host cell dependence of viral morphology* [Online]. [Accessed 6 May 2021]. Available from: www.pnas.org.

Roberts, S., Compans, R. and Wertz, G. 1995. Respiratory syncytial virus matures at the apical surfaces of polarized epithelial cells. *Journal of Virology*. **69**(4), pp.2667–2673.

Rogers, G.N., Herrlerb, G., Paulson, J.C. and Klenkg, H.-D. 1986. Influenza C Virus Uses 9-0-Acetyl-N-acetylneuraminic Acid as a High Affinity Receptor Determinant for Attachment to Cells*. *The Journal of Biological Chemistry*. **261**(13), pp.5947–5951.

Rogers, G.N., Paulson, J.C., Daniels, R.S., Skehel, J.J., Wilson, I.A. and Wiley, D.C. 1983. Single amino acid substitutions in influenza haemagglutinin change receptor binding specificity. *Nature*. **304**(5921), pp.76–78.

Rohou, A. and Grigorieff, N. 2015. CTFFIND4: Fast and accurate defocus estimation from electron micrographs. *Journal of structural biology*. **192**(2), pp.216–221.

Rossman, J. and Lamb, R. 2011. Influenza virus assembly and budding. *Virology*. **411**(2), pp.229–236.

Rossman, J.S., Jing, X., Leser, G.P. and Lamb, R.A. 2010. Influenza Virus M2 Protein Mediates ESCRT-Independent Membrane Scission. *Cell*. **142**(6), pp.902–913.

Rossman, J.S., Leser, G.P. and Lamb, R.A. 2012. Filamentous influenza virus enters cells via macropinocytosis. *Journal of Virology*. **86**(20), pp.10950–10960.

Rota, P.A., Wallis, T.R., Harmon, M.W., Rota, J.S., Kendal, A.P. and Nerome, K. 1990. Cocirculation of two distinct evolutionary lineages of influenza type B virus since 1983. *Virology*. **175**(1), pp.59–68.

Rovenolt, F.H. and Tate, A.T. 2021. The Impact of Coinfection Dynamics on Host Competition and Coexistence*. *https://doi.org/10.1086/717180*.

Rowe, H.M., Meliopoulos, V.A., Iverson, A., Bomme, P., Schultz-Cherry, S. and Rosch, J.W. 2019. Direct interactions with influenza promote bacterial adherence during respiratory infections. *Nature Microbiology*. **4**(8), pp.1328–1336.

Roymans, D., Alnajjar, S.S., Battles, M.B., Sitthicharoenchai, P., Furmanova-Hollenstein, P.,

Rigaux, P., Van Den Berg, J., Kwanten, L., Van Ginderen, M., Verheyen, N., Vranckx, L., Jaensch, S., Arnoult, E., Voorzaat, R., Gallup, J.M., Larios-Mora, A., Crabbe, M., Huntjens, D., Raboisson, P., Langedijk, J.P., Ackermann, M.R., McLellan, J.S., Vendeville, S. and Koul, A. 2017. Therapeutic efficacy of a respiratory syncytial virus fusion inhibitor. *Nature communications*. **8**(1).

Russell, A.B., Trapnell, C. and Bloom, J.D. 2018. Extreme heterogeneity of influenza virus infection in single cells. *eLife*. **7**.

Rust, M.J., Lakadamyali, M., Zhang, F. and Zhuang, X. 2004. Assembly of endocytic machinery around individual influenza viruses during viral entry. *Nature Structural & Molecular Biology*. **11**(6), pp.567–573.

Sakai, T., Nishimura, S.I., Naito, T. and Saito, M. 2017. Influenza A virus hemagglutinin and neuraminidase act as novel motile machinery. *Scientific Reports*. **7**(1), pp.1–11.

San-Juan-Vergara, H., Sampayo-Escobar, V., Reyes, N., Cha, B., Pacheco-Lugo, L., Wong, T., Peeples, M.E., Collins, P.L., Castano, M.E. and Mohapatra, S.S. 2012. Cholesterol-Rich Microdomains as Docking Platforms for Respiratory Syncytial Virus in Normal Human Bronchial Epithelial Cells. *Journal of Virology*. **86**(3), pp.1832–1843.

Savolainen-Kopra, C. and Blomqvist, S. 2010. Mechanisms of genetic variation in polioviruses. *Reviews in Medical Virology*. **20**(6), pp.358–371.

Schulman, J. and Kilbourne, E. 1965. Induction of Partial Specific Heterotypic Immunitv in Mice by a Single Infection with Influenza A Virus. *Journal of Bacteriology*. **89**(1), pp.170–174.

Seladi-Schulman, J., Campbell, P.J., Suppiah, S., Steel, J. and Lowen, A.C. 2014a. Filament-producing mutants of influenza A/Puerto Rico/ 8/1934 (H1N1) virus have higher neuraminidase activities than the spherical wild-type. *PLoS ONE*. **9**(11), p.112462.

Selvaraj, M., Yegambaram, K., Todd, E.J.A.A., Richard, C.A., Dods, R.L., Pangratiou, G.M., Trinh, C.H., Moul, S.L., Murphy, J.C., Mankouri, J., Éléouët, J.F., Barr, J.N. and Edwards, T.A. 2018. The structure of the human respiratory syncytial virus m2-1 protein bound to the interaction domain of the phosphoprotein p defines the orientation of the complex. *mBio*. **9**(6), pp.1–13.

Semple, M.G., Cowell, A., Dove, W., Greensill, J., McNamara, P.S., Halfhide, C., Shears, P., Smyth, R.L. and Hart, C.A. 2005. Dual infection of infants by human metapneumovirus and human respiratory syncytial virus is strongly associated with severe bronchiolitis. *The Journal of Infectious Diseases*. **191**(3), pp.382–386.

Shaikh, F.Y., Utley, T.J., Craven, R.E., Rogers, M.C., Lapierre, L.A., Goldenring, J.R. and Crowe, J.E. 2012. Respiratory Syncytial Virus Assembles into Structured Filamentous Virion Particles Independently of Host Cytoskeleton and Related Proteins R. J. Pickles, ed. *PLoS ONE*. **7**(7), p.e40826.

Shaw, M.L., Stone, K.L., Colangelo, C.M., Gulcicek, E.E. and Palese, P. 2008. Cellular Proteins in Influenza Virus Particles. *PLOS Pathogens*. **4**(6), p.e1000085.

Shi, T., McAllister, D.A., O'Brien, K.L., Simoes, E.A.F., Madhi, S.A., Gessner, B.D., Polack, F.P., Balsells, E., Acacio, S., Aguayo, C., Alassani, I., Ali, A., Antonio, M., Awasthi, S., Awori, J.O., Azziz-Baumgartner, E., Baggett, H.C., Baillie, V.L., Balmaseda, A., Barahona, A., Basnet, S., Bassat, Q., Basualdo, W., Bigogo, G., Bont, L., Breiman, R.F., Brooks, W.A., Broor, S., Bruce, N., Bruden, D., Buchy, P., Campbell, S., Carosone-Link, P., Chadha, M., Chipeta, J., Chou, M., Clara, W., Cohen, C., de Cuellar, E., Dang, D.A., Dash-yandag, B., Deloria-Knoll, M., Dherani, M., Eap, T., Ebruke, B.E., Echavarria, M., de Freitas Lázaro Emediato, C.C., Fasce, R.A., Feikin, D.R., Feng, L., Gentile, A., Gordon, A., Goswami, D., Goyet, S., Groome, M., Halasa, N., Hirve, S., Homaira, N., Howie, S.R.C., Jara, J., Jroundi, I., Kartasasmita, C.B., Khuri-Bulos, N., Kotloff, K.L., Krishnan, A., Libster, R., Lopez, O., Lucero, M.G., Lucion, F., Lupisan, S.P., Marcone, D.N., McCracken, J.P., Mejia, M., Moisi, J.C., Montgomery, J.M., Moore, D.P., Moraleda, C., Moyes, J., Munywoki, P., Mutyara, K., Nicol, M.P., Nokes, D.J., Nymadawa, P., da Costa Oliveira, M.T., Oshitani, H., Pandey, N., Paranhos-Baccalà, G., Phillips, L.N., Picot, V.S., Rahman, M., Rakoto-Andrianarivelo, M., Rasmussen, Z.A., Rath, B.A., Robinson, A., Romero, C., Russomando, G., Salimi, V., Sawatwong, P., Scheltema, N., Schweiger, B., Scott, J.A.G., Seidenberg, P., Shen, K., Singleton, R., Sotomayor, V., Strand, T.A., Sutanto, A., Sylla, M., Tapia, M.D., Thamthitiwat, S., Thomas, E.D., Tokarz, R., Turner, C., Venter, M., Waicharoen, S., Wang, J., Watthanaworawit, W., Yoshida, L.M., Yu, H., Zar,

H.J., Campbell, H. and Nair, H. 2017. Global, regional, and national disease burden estimates of acute lower respiratory infections due to respiratory syncytial virus in young children in 2015: a systematic review and modelling study. *The Lancet*. **390**(10098), pp.946–958.

Shigeta, S. 1968. The Cell to Cell Infection of Respiratory Syncytial Virus in HEp-2 Monolayer Cultures. *Journal of General Virology*. **3**, pp.129–131.

Shinjoh, M., Omoe, K., Saito, N., Matsuo, N. and Nerome, K. 2000. In vitro growth profiles of respiratory syncytial virus in the presence of influenza virus. *Acta virologica*. **44**(2), pp.91–7.

Shiraki, K. and Daikoku, T. 2020. Favipiravir, an anti-influenza drug against life-threatening RNA virus infections. *Pharmacology & Therapeutics*. **209**, p.107512.

Shirley, M. 2020. Baloxavir Marboxil: A Review in Acute Uncomplicated Influenza. *Drugs*. **80**(11), pp.1109–1118.

Short, K.R., Habets, M.N., Payne, J., Reading, P.C., Diavatopoulos, D.A. and Wijburg, O.L. 2013. Influenza A virus induced bacterial otitis media is independent of virus tropism for α2,6-linked sialic acid. *Virology*. **10**(1), pp.1–6.

Sieczkarski, S.B. and Whittaker, G.R. 2002. Influenza Virus Can Enter and Infect Cells in the Absence of Clathrin-Mediated Endocytosis. *Journal of Virology*. **76**(20), pp.10455–10464.

Slee, E.A., Adrain, C. and Martin, S.J. 2001. Executioner Caspase-3, -6, and -7 Perform Distinct, Non-redundant Roles during the Demolition Phase of Apoptosis. *Journal of Biological Chemistry*. **276**(10), pp.7320–7326.

Slütter, B., Braeckel-Budimir, N. Van, Abboud, G., Varga, S.M., Salek-Ardakani, S. and Harty, J.T. 2017. Dynamics of influenza-induced lung-resident memory T cells underlie waning heterosubtypic immunity. *Science Immunology*. **2**(7).

Smith, C.M., Do Hyang Lee, D., Kulkarni, H., Radhakrishnan, P., Hirst, R., Easton, A. and O'Callaghan, C. 2019. Influenza virus infection of well-differentiated human airway epithelial cells by infectious aerosols: insights into the earliest stages of infection. *F1000Research*. **8**, p.337.

Spann, K.M., Collins, P.L. and Teng, M.N. 2003. Genetic Recombination during Coinfection of Two Mutants of Human Respiratory Syncytial Virus. *Journal of Virology*. **77**(20), pp.11201–11211.

Stauffer, S., Feng, Y., Nebioglu, F., Heilig, R., Picotti, P. and Helenius, A. 2014. Stepwise Priming by Acidic pH and a High K+ Concentration Is Required for Efficient Uncoating of Influenza A Virus Cores after Penetration. *Journal of Virology*. **88**(22), pp.13029–13046.

Stempel, H.E., Martin, E.T., Kuypers, J., Englund, J.A. and Zerr, D.M. 2009. Multiple viral respiratory pathogens in children with bronchiolitis. *Acta Pædiatrica*. **98**(1), pp.123–126.

Stieneke-Grober, A., Vey, M., Angliker, H., Shaw, E., Thomas, G., Roberts, C., Klenk, H.D. and Garten, W. 1992. Influenza virus hemagglutinin with multibasic cleavage site is activated by furin, a subtilisin-like endoprotease. *The EMBO Journal*. **11**(7), pp.2407–2414.

Su, S., Wong, G., Shi, W., Liu, J., Lai, A., Zhou, J., Liu, W., Bi, Y. and Gao, G. 2016. Epidemiology, Genetic Recombination, and Pathogenesis of Coronaviruses. *Trends in microbiology*. **24**(6), pp.490–502.

Sun, J. and Brooke, C.B. 2018. Influenza A Virus Superinfection Potential Is Regulated by Viral Genomic Heterogeneity. *mBio*. **9**(5).

Sutto-Ortiz, P., Tcherniuk, S., Ysebaert, N., Abeywickrema, P., Noël, M., Decombe, A., Debart, F., Vasseur, J.J., Canard, B., Roymans, D., Rigaux, P., Eléouët, J.F. and Decroly, E. 2021. The methyltransferase domain of the Respiratory Syncytial Virus L protein catalyzes cap N7 and 2'-O-methylation. *PLoS Pathogens*. **17**(5), p.e1009562.

Swanson, K.A., Rainho-Tomko, J.N., Williams, Z.P., Lanza, L., Peredelchuk, M., Kishko, M., Pavot, V., Alamares-Sapuay, J., Adhikarla, H., Gupta, S., Chivukula, S., Gallichan, S., Zhang, L., Jackson, N., Yoon, H., Edwards, D., Wei, C.J. and Nabel, G.J. 2020. A respiratory syncytial virus (RSV) F protein nanoparticle vaccine focuses antibody responses to a conserved neutralization domain. *Science Immunology*. **5**(47).

Takemoto, D.K., Skehel, J.J. and Wiley, D.C. 1996. A Surface Plasmon Resonance Assay for the Binding of Influenza Virus Hemagglutinin to Its Sialic Acid Receptor. *Virology*. **217**(2), pp.452–458.

Tamerius, J., Nelson, M.I., Zhou, S.Z., Viboud, C., Miller, M.A. and Alonso, W.J. 2011. Global influenza seasonality: Reconciling patterns across temperate and tropical regions. *Environmental Health Perspectives*. **119**(4), pp.439–445.

Tang, Y., George, A., Nouvet, F., Sweet, S., Emeagwali, N., Taylor, H.E., Simmons, G. and Hildreth, J.E.K. 2014. Infection of Female Primary Lower Genital Tract Epithelial Cells after Natural Pseudotyping of HIV-1: Possible Implications for Sexual Transmission of HIV-1. *PLOS ONE*. **9**(7), p.e101367.

Tanner, H., Boxall, E. and Osman, H. 2012. Respiratory viral infections during the 2009-2010 winter season in Central England, UK: Incidence and patterns of multiple virus co-infections. *European Journal of Clinical Microbiology and Infectious Diseases*. **31**(11), pp.3001–3006.

Tarendeau, F., Boudet, J., Guilligay, D., Mas, P.J., Bougault, C.M., Boulo, S., Baudin, F., Ruigrok, R.W.H., Daigle, N., Ellenberg, J., Cusack, S., Simorre, J.P. and Hart, D.J. 2007. Structure and nuclear import function of the C-terminal domain of influenza virus polymerase PB2 subunit. *Nature Structural & Molecular Biology*. **14**(3), pp.229–233.

Tayyari, F., Marchant, D., Moraes, T.J., Duan, W., Mastrangelo, P. and Hegele, R.G. 2011. Identification of nucleolin as a cellular receptor for human respiratory syncytial virus. *Nature Medicine*. **17**(9), pp.1132–1135.

Tenforde, M.W., Garten Kondor, R.J., Chung, J.R., Zimmerman, R.K., Nowalk, M.P., Jackson, M.L., Jackson, L.A., Monto, A.S., Martin, E.T., Belongia, E.A., Mclean, H.Q., Gaglani, M., Rao, A., Kim, S.S., Stark, T.J., Barnes, J.R., Wentworth, D.E., Patel, M.M., Flannery, B., Scott, B. and Health, W. 2020. Effect of Antigenic Drift on Influenza Vaccine Effectiveness in the United States—2019–2020. *Clinical Infectious Diseases*.

Thomas, K.W., Monick, M.M., Staber, J.M., Yarovinsky, T., Brent Carter, A. and Hunninghake, G.W. 2002. Respiratory Syncytial Virus Inhibits Apoptosis and Induces NF-κB Activity through a Phosphatidylinositol 3-Kinase-dependent Pathway *. *Journal of Biological Chemistry*. **277**(1), pp.492–501.

Thompson, C.I., Barclay, W.S., Zambon, M.C. and Pickles, R.J. 2006. Infection of Human Airway Epithelium by Human and Avian Strains of Influenza A Virus. *Journal of Virology*. **80**(16), pp.8060–8068.

Thompson, W.W., Shay, D.K., Weintraub, E., Cox, N., Anderson, L.J. and Fukuda, K. 2003. Mortality associated with influenza and respiratory syncytial virus in the United States. *JAMA*. **289**(2), pp.179–186.

Thongpan, I., Vongpunsawad, S. and Poovorawan, Y. 2020. Respiratory syncytial virus infection trend is associated with meteorological factors. *Scientific Reports*. **10**(1), pp.1–7.

Thornhill, E.M. and Verhoeven, D. 2020. Respiratory Syncytial Virus's Non-structural Proteins: Masters of Interference. *Frontiers in cellular and infection microbiology*. **10**.

Tremaglio, C.Z., Noton, S.L., Deflubé, L.R. and Fearns, R. 2013. Respiratory Syncytial Virus Polymerase Can Initiate Transcription from Position 3 of the Leader Promoter. *Journal of Virology*. **87**(6), pp.3196–3207.

Triantafilou, K., Kar, S., Vakakis, E., Kotecha, S. and Triantafilou, M. 2013. Human respiratory syncytial virus viroporin SH: a viral recognition pathway used by the host to signal inflammasome activation. *Thorax*. **68**(1), pp.66–75.

Tripp, R.A., Jones, L.P., Haynes, L.M., Zheng, H.Q., Murphy, P.M. and Anderson, L.J. 2001. CX3C chemokine mimicry by respiratory syncytial virus G glycoprotein. *Nature Immunology*. **2**(8), pp.732–738.

Tristam, D., Hicks, W. and Hard, R. 1998. Respiratory syncytial virus and human bronchial epithelium. *Archives of Otolaryngology*. **124**(7), pp.777–783.

Tristram, D.A., Miller, R.W., Mcmillan, J.A. and Weiner, L.B. 1988. Simultaneous infection with respiratory syncytial virus and other respiratory pathogens. *American Journal of Diseases of*

Children. **142**(8), pp.834–836.

Trueman, D., Woodcock, F. and Hancock, E. 2014. *Estimating the economic burden of respiratory illness in the UK blf Estimating the economic burden of respiratory illness in the UK*.

Tscherne, D.M., Evans, M.J., von Hahn, T., Jones, C.T., Stamataki, Z., McKeating, J.A., Lindenbach, B.D. and Rice, C.M. 2007. Superinfection Exclusion in Cells Infected with Hepatitis C Virus. *Journal of Virology*. **81**(8), pp.3693–3703.

Tuijtel, M.W., Koster, A.J., Jakobs, S., Faas, F.G.A. and Sharp, T.H. 2019. Correlative cryo super-resolution light and electron microscopy on mammalian cells using fluorescent proteins. *Scientific Reports*. **9**(1), pp.1–11.

Turk, M. and Baumeister, W. 2020. The promise and the challenges of cryo-electron tomography. *FEBS Letters*. **594**(20), pp.3243–3261.

United Kingdom Cabinet Office 2019. *National Risk Register*.

Utley, T.J., Ducharme, N.A., Varthakavi, V., Shepherd, B.E., Santangelo, P.J., Lindquist, M.E., Goldenring, J.R. and Crowe, J.E. 2008. Respiratory syncytial virus uses a Vps4-independent budding mechanism controlled by Rab11-FIP2. *Proceedings of the National Academy of Sciences*. **105**(29), pp.10209–10214.

Vafadar, S., Shahdoust, M., Kalirad, A., Zakeri, P. and Sadeghi, M. 2021. Competitive exclusion during co-infection as a strategy to prevent the spread of a virus: A computational perspective. *PLOS ONE*. **16**(2), p.e0247200.

Vahey, M.D. and Fletcher, D.A. 2019. Influenza a virus surface proteins are organized to help penetrate host mucus. *eLife*. **8**.

Valdovinos, M. and Gómez, B. 2003. Establishment of respiratory syncytial virus persistence in cell lines: association with defective interfering particles. *Intervirology*. **46**(3), pp.190–198.

Vanover, D., Smith, D. V., Blanchard, E.L., Alonas, E., Kirschman, J.L., Lifland, A.W., Zurla, C. and Santangelo, P.J. 2017. RSV glycoprotein and genomic RNA dynamics reveal filament assembly prior to the plasma membrane. *Nature Communications*. **8**(1), pp.1–15.

Vekemans, J., Moorthy, V., Giersing, B., Friede, M., Hombach, J., Arora, N., Modjarrad, K., Smith, P.G., Karron, R., Graham, B. and Kaslow, D.C. 2019. Respiratory syncytial virus vaccine research and development: World Health Organization technological roadmap and preferred product characteristics. *Vaccine*. **37**(50), pp.7394–7395.

te Velthuis, A.J.W., Grimes, J.M. and Fodor, E. 2021. Structural insights into RNA polymerases of negative-sense RNA viruses. *Nature Reviews Microbiology*. **19**(5), pp.303–318.

Verhelst, J., Hulpiau, P. and Saelens, X. 2013. Mx Proteins: Antiviral Gatekeepers That Restrain the Uninvited. *Microbiology and Molecular Biology Reviews*. **77**(4), p.551.

Vijayakrishnan, S., Loney, C., Jackson, D., Suphamungmee, W., Rixon, F.J. and Bhella, D. 2013. Cryotomography of Budding Influenza A Virus Reveals Filaments with Diverse Morphologies that Mostly Do Not Bear a Genome at Their Distal End. *PLOS Pathogens*. **9**(6), p.e1003413.

Villenave, R., Thavagnanam, S., Sarlang, S., Parker, J., Douglas, I., Skibinski, G., Heaney, L.G., McKaigue, J.P., Coyle, P. V., Shields, M.D. and Power, U.F. 2012. In vitro modeling of respiratory syncytial virus infection of pediatric bronchial epithelium, the primary target of infection in vivo. *Proceedings of the National Academy of Sciences of the United States of America*. **109**(13), pp.5040–5045.

de Vries, E., Tscherne, D.M., Wienholts, M.J., Cobos-Jiménez, V., Scholte, F., García-Sastre, A., Rottier, P.J.M. and de Haan, C.A.M. 2011. Dissection of the Influenza A Virus Endocytic Routes Reveals Macropinocytosis as an Alternative Entry Pathway. *PLOS Pathogens*. **7**(3), p.e1001329.

Walsh, E.E., McConnochie, K.M., Long, C.E. and Hall, C.B. 1997. Severity of respiratory syncytial virus infection is related to virus strain. *The Journal of infectious diseases*. **175**(4), pp.814–820.

Walzl, G., Tafuro, S., Moss, P., Openshaw, P.J.M. and Hussell, T. 2000. Influenza virus lung

infection protects from respiratory syncytial virus-induced immunopathology. *The Journal of experimental medicine*. **192**(9), pp.1317–1326.

Wang, G., Deval, J., Hong, J., Dyatkina, N., Prhavc, M., Taylor, J., Fung, A., Jin, Z., Stevens, S.K., Serebryany, V., Liu, J., Zhang, Q., Tam, Y., Chanda, S.M., Smith, D.B., Symons, J.A., Blatt, L.M. and Beigelman, L. 2015. Discovery of 4'-chloromethyl-2'-deoxy-3',5'-di-O-isobutyryl-2'-fluorocytidine (ALS-8176), a first-in-class RSV polymerase inhibitor for treatment of human respiratory syncytial virus infection. *Journal of Medicinal Chemistry*. **58**(4), pp.1862–1878.

Wang, X., Li, Y., O'Brien, K.L., Madhi, S.A., Widdowson, M.A., Byass, P., Omer, S.B., Abbas, Q., Ali, A., Amu, A., Azziz-Baumgartner, E., Bassat, Q., Abdullah Brooks, W., Chaves, S.S., Chung, A., Cohen, C., Echavarria, M., Fasce, R.A., Gentile, A., Gordon, A., Groome, M., Heikkinen, T., Hirve, S., Jara, J.H., Katz, M.A., Khuri-Bulos, N., Krishnan, A., de Leon, O., Lucero, M.G., McCracken, J.P., Mira-Iglesias, A., Moïsi, J.C., Munywoki, P.K., Ourohiré, M., Polack, F.P., Rahi, M., Rasmussen, Z.A., Rath, B.A., Saha, S.K., Simões, E.A., Sotomayor, V., Thamthitiwat, S., Treurnicht, F.K., Wamukoya, M., Yoshida, L.M., Zar, H.J., Campbell, H. and Nair, H. 2020. Global burden of respiratory infections associated with seasonal influenza in children under 5 years in 2018: a systematic review and modelling study. *The Lancet Global Health*. **8**(4), pp.e497–e510.

Watson, A. and Wilkinson, T.M.A. 2021. Respiratory viral infections in the elderly. *Therapeutic Advances in Respiratory Disease*. **15**.

Weis, W., Brown, J.H., Cusack, S., Paulson, J.C., Skehel, J.J. and Wiley, D.C. 1988. Structure of the influenza virus haemagglutinin complexed with its receptor, sialic acid. *Nature*. **333**(6172), pp.426–431.

Welliver, T.P., Garofalo, R.P., Hosakote, Y., Hintz, K.H., Avendano, L., Sanchez, K., Velozo, L., Jafri, H., Chavez-Bueno, S., Ogra, P.L., McKinney, L., Reed, J.L. and Welliver, R.C. 2007. Severe Human Lower Respiratory Tract Illness Caused by Respiratory Syncytial Virus and Influenza Virus Is Characterized by the Absence of Pulmonary Cytotoxic Lymphocyte Responses. *The Journal of Infectious Diseases*. **195**(8), pp.1126–1136.

Williams, K., Bastian, A.R., Feldman, R.A., Omoruyi, E., de Paepe, E., Hendriks, J., van Zeeburg, H., Godeaux, O., Langedijk, J.P.M., Schuitemaker, H., Sadoff, J. and Callendret, B. 2020. Phase 1 Safety and Immunogenicity Study of a Respiratory Syncytial Virus Vaccine With an Adenovirus 26 Vector Encoding Prefusion F (Ad26.RSV.preF) in Adults Aged ≥60 Years. *The Journal of Infectious Diseases*. **222**(6), pp.979–988.

Wu, A., Mihaylova, V.T., Landry, M.L. and Foxman, E.F. 2020. Interference between rhinovirus and influenza A virus: a clinical data analysis and experimental infection study. *The Lancet Microbe*. **1**(6), pp.e254–e262.

Wu, N.-H., Yang, W., Beineke, A., Dijkman, R., Matrosovich, M., Baumgärtner, W., Thiel, V., Valentin-Weigand, P., Meng, F. and Herrler, G. 2016. The differentiated airway epithelium infected by influenza viruses maintains the barrier function despite a dramatic loss of ciliated cells. *Scientific Reports*. **6**.

Xiao, H., Killip, M.J., Staeheli, P., Randall, R.E. and Jackson, D. 2013. The Human Interferon-Induced MxA Protein Inhibits Early Stages of Influenza A Virus Infection by Retaining the Incoming Viral Genome in the Cytoplasm. *Journal of Virology*. **87**(23), pp.13053–13058.

Xu, X., Qiao, D., Mann, M., Garofalo, R.P. and Brasier, A.R. 2020. Respiratory Syncytial Virus Infection Induces Chromatin Remodeling to Activate Growth Factor and Extracellular Matrix Secretion Pathways. *Viruses*. **12**(8), p.804.

Yang, L., Chan, K.H., Suen, Lorna K.P., Chan, K.P., Wang, X., Cao, P., He, D., Peiris, J.S.M. and Wong, C.M. 2015. Age-specific epidemic waves of influenza and respiratory syncytial virus in a subtropical city. *Scientific Reports*. **5**(1), pp.1–8.

Yang, L., Chan, K.H., Suen, Lorna K. P., Chan, K.P., Wang, X., Cao, P., He, D., Peiris, J.S.M. and Wong, C.M. 2015. Impact of the 2009 H1N1 Pandemic on Age-Specific Epidemic Curves of Other Respiratory Viruses: A Comparison of Pre-Pandemic, Pandemic and Post-Pandemic Periods in a Subtropical City E. Goldstein, ed. *PLOS ONE*. **10**(4), p.e0125447.

Yang, W. and Marr, L.C. 2011. Dynamics of Airborne Influenza A Viruses Indoors and Dependence on Humidity. *PLOS ONE*. **6**(6), p.e21481.

Yaqinuddin, A. 2020. Cross-immunity between respiratory coronaviruses may limit COVID-19 fatalities. *Medical Hypotheses*. **144**, p.110049.

Ye, Z., Liu, T., Offringa, D.P., McInnis, J. and Levandowski, R.A. 1999. Association of Influenza Virus Matrix Protein with Ribonucleoproteins. *Journal of Virology*. **73**(9), pp.7467–7473.

Yu, Q., Hardy, R.W. and Wertz, G.W. 1995. Functional cDNA clones of the human respiratory syncytial (RS) virus N, P, and L proteins support replication of RS virus genomic RNA analogs and define minimal trans-acting requirements for RNA replication. *Journal of Virology*. **69**(4), pp.2412–2419.

Zavada, J. 1982. The Pseudotypic Paradox. *Journal of General Virology*. **63**, pp.15–24.

Zebedee, S.L. and Lamb, R.A. 1988. Influenza A virus M2 protein: monoclonal antibody restriction of virus growth and detection of M2 in virions. *Journal of virology*. **62**(8), pp.2762–2772.

Zhang, D., He, Z., Xu, L., Zhu, X., Wu, J., Wen, W., Zheng, Y., Deng, Y., Chen, J., Hu, Y., Li, M. and Cao, K. 2014. Epidemiology characteristics of respiratory viruses found in children and adults with respiratory tract infections in southern China. *International Journal of Infectious Diseases*. **25**, pp.159–164.

Zhang, J. and Lamb, R.A. 1996. Characterization of the membrane association of the influenza virus matrix protein in living cells. *Virology*. **225**(2), pp.255–266.

Zhang, J., Pekosz, A. and Lamb, R.A. 2000. Influenza Virus Assembly and Lipid Raft Microdomains: a Role for the Cytoplasmic Tails of the Spike Glycoproteins. *Journal of Virology*. **74**(10), pp.4634–4644.

Zhang, L., Bukreyev, A., Thompson, C.I., Watson, B., Peeples, M.E., Collins, P.L. and Pickles, R.J. 2005. Infection of Ciliated Cells by Human Parainfluenza Virus Type 3 in an In Vitro Model of Human Airway Epithelium. *Journal of Virology*. **79**(2), pp.1113–1124.

Zhang, L., Collins, P.L., Lamb, R.A. and Pickles, R.J. 2011. Comparison of differing cytopathic effects in human airway epithelium of parainfluenza virus 5 (W3A), parainfluenza virus type 3, and respiratory syncytial virus. *Virology*. **421**(1), pp.67–77.

Zhang, L., Peeples, M.E., Boucher, R.C., Collins, P.L. and Pickles, R.J. 2002. Respiratory Syncytial Virus Infection of Human Airway Epithelial Cells Is Polarized, Specific to Ciliated Cells, and without Obvious Cytopathology. *Journal of Virology*. **76**(11), p.5654.

Zhang, Y., Yang, L., Wang, H., Zhang, G. and Sun, X. 2016. Respiratory syncytial virus non-structural protein 1 facilitates virus replication through miR-29a-mediated inhibition of interferon-α receptor. *Biochemical and biophysical research communications*. **478**(3), pp.1436–1441.

Zhang, Y., Zhao, J., Zou, X., Fan, Y., Xiong, Z., Li, B., Wang, C., Li, H., Han, J., Liu, X., Xia, Y., Lu, B. and Cao, B. 2020. Severity of influenza virus and respiratory syncytial virus coinfections in hospitalized adult patients. *Journal of Clinical Virology*. **133**.

Zhao, X., Singh, M., Malashkevich, V. and Kim, P. 2000. Structural characterization of the human respiratory syncytial virus fusion protein core. *Proceedings of the National Academy of Sciences of the United States of America*. **97**(26), pp.14172–14177.

Zhirnov, O.P. and Klenk, H.D. 2007. Control of apoptosis in influenza virus-infected cells by up-regulation of Akt and p53 signaling. *Apoptosis*. **12**(8), pp.1419–1432.